Cr (VI)-CONTAINING ELECTRIC FURNACE DUST AND FILTER CAKE: CHARACTERISTICS, FORMATION, LEACHABILITY AND STABILISATION

by

Guojun Ma

Submitted in partial fulfilment of the requirements for the degree

Philosophiae Doctor

(Metallurgical Engineering)

in the Faculty of Engineering, Built Environment and Information Technology,
University of Pretoria, Pretoria

12 December 2005

To my lovely wife Yinhua,

my son, Junteng and

my parents

Acknowledgements

The thesis has been carried out at Department of Materials Science and Metallurgical Engineering, University of Pretoria. I would like to express my sincere gratitude to my supervisor Prof. A.M. Garbers-Craig for her valuable suggestions, discussions and continuous encouragement during the past three years.

I also wish to thank Profs. P.C. Pistoruis and J.M.A. Geldenhuis for their invitation to join in the interesting project and their fruitful discussions. Special thanks are also given to China Scholarship Council (CSC) and Wuhan University of Science and Technology (WUST, P. R. China) as well as Mr. Yanggeng Wei from the education section of Chinese embassy in South Africa for their understanding, help and support during the study period.

The Technology and Human Recourses for Industry Program (THRIP) are greatly acknowledged for the financial support of the project. Thanks are also due to Messrs. Johan Ackeman, Peter Scurr and Nathan Antony from Columbus stainless and Dewald van Niekerk from Middleburg Ferrochrome (MFC) for their discussions and supplying the samples.

I am also greatly indebted to all the personnel and postgraduates at Department of Materials Science and Metallurgical Engineering, especially Mrs Sarah Havenga and Mr Johann Borman (deceased) for their help, and Industrial Metals and Minerals Research Institute (IMMRI) for their friendly support, specifically Prof. Tom von Moltke (XPS), Mr. Carl Coetzee (SEM) and Ms. Junior Mogwaneng (FT-IR) for their help on the relative experimental works and discussions.

Thanks also extend to Dr. Sabine M.C. Verryn (XRD) (Department of Geology), Mrs Maggi Loubser (XRF) (Department of Geology) and Mrs Mila Maksa (TG/DTA) (Department of Chemistry) for their help on the X-ray and thermal analytical experiments,

University of Pretoria etd – Ma, G (2006)

and Mr. Vusi Mulaudzi (Department of Chemistry) for his discussion on the analysis of Cr (VI).

Finally, I wish to thank my parents (Mr. Anlan Ma and Mrs Anxiang He), my wife (Mrs Yinhua Zhou) for their endless love and unconditional support.

Guojun Ma

12 December 2005

Pretoria, South Africa

Cr (VI)-CONTAINING ELECTRIC FURNACE DUST AND FILTER CAKE: CHARACTERISTICS, FORMATION, LEACHABILITY AND STABILISATION

Candidate: Guojun Ma

Supervisor: Prof. A.M. Garbers-Craig

Department: Department of Materials Science and Metallurgical Engineering

Degree: Philosophiae Doctor

Abstract

In South Africa, the ferrochromium industry produces approximately 100,000 t bag house filter dust and slurry, while the stainless steel industry produces 24,000 t of dust annually [17,39]. The toxic substances in these wastes potentially pose a threat to the environment and human health, especially Cr (VI) due to its toxic, carcinogenic, highly soluble and strongly oxidizing properties. Therefore, the existence and treatment of wastes from stainless steel and ferrochrome production remain a challenge and an issue of concern. The increase of environmental legislation globally and the trend towards sustainable development are drives for alternatives to landfill.

In the present thesis, the characteristics, formation mechanisms, leachability and stabilisation of the Cr (VI)-containing electric furnace dust and filter cake were investigated using various techniques such as XRD, XRF, TG/DTA, XPS, SEM-EDS, FT-IR, Raman spectrometer and UV/Vis spectrometer.

The study on the characteristics of these wastes showed that the electric furnace dust and filter cake are very fine particles. The electric furnace dust has bulk densities that vary between 0.49 and 2.42gcm^{-3}, and has low moisture contents. The main phases that are present in the stainless steel plant dust are the $(Mg,Fe,Mn,Cr)_3O_4$ spinel phase, quartz, $Ca(OH)_2$ and nickel. The dominant phases of the coarse fraction of ferrochrome plant dust are chromite, partly altered chromite, quartz and carbon, while the main components

of the fine fractions include chromite, SiO_2, ZnO, NaCl and Mg_2SiO_4. The major phase present in the filter cake is CaF_2. It is assumed that Cr (VI)-containing species in ferrochrome dust are generated at the top of the SAF or in the off-gas duct, as Cr (VI) is found on the surface of the dust.

Stainless steel dust forms by the entrainment of charge materials, evaporation or volatilisation of elements and ejection of slag and metal by spitting or the bursting of gas bubbles. It was found that ferrochrome dust is formed by the ejection of slag and metals droplets from the electrode hole, the entrainment of charge materials, vaporisation as well as the formation and precipitation of compounds from vaporised species in the off-gas duct. Filter cake contains crystal phases (CaF_2 and $CaSO_4$) and metal rich amorphous phases. It is formed due to super saturation and precipitation.

Leaching experiments on the wastes showed that Cr (VI) rapidly leaches out by distilled water. The aging experiment of the stainless steel plant dust and filter cake shows that the Cr (III) species in these wastes can be oxidised into Cr (VI) in the presence of lime at room temperature. Increasing the molar ratio of CaO to Cr_2O_3 and increasing temperature promotes the oxidation of Cr (III) into Cr (VI). Cr (VI) in the wastes can also be reduced into Cr (III) possibly by Fe (II).

Bricks were produced by mixing wastes (stainless steel plant dust, ferrochrome dust and filter cake) and clay. The optimum sinter parameter was found to be 1100^{o}C and 5 hours for a 50wt% SPD-50wt% AS mixture in the brick. Decreasing sinter temperature, increasing waste content in the brick and reducing sinter time increase the Cr (VI) leachability. The leachability of Cr(VI) is strongly influenced by the mass%CaO/mass%SiO_2 ratio and alkali metal oxides content in the wastes. Ferrochrome dust and filter cake that were sintered with 50% AS clay at 1000^{o}C for 5 hours could not be stabilised as the concentrations of zinc and/or Cr (VI) from the stabilised wastes in the modified TCLP and ASTM D 3987-85-tests exceed the regulation limits. The emission factors from the stabilised wastes (SPD, FCD1, FCD2 and FC) are similar to those reported for the cement industry.

Semi-dynamic leaching tests indicated that the predominant leaching mechanisms of chromium species are initial surface wash-off followed by matrix diffusion. The cumulative release fractions of chromium from the solidified wastes are lower than 2% over a period of approximately 5 months. More than 80% of the leachable chromium from the stabilised products is Cr (VI) species.

Keywords: Cr (VI), dust, filter cake, waste management, leachability, stabilisation, sintering, stainless steel, ferrochrome, electric furnace

Contents

List of Figures

University of Pretoria etd – Ma, G (2006)

List of Tables

Chapter 1 Introduction

1.1 Background

Stainless steel is typically smelted in an electric arc furnace (EAF) from scrap, molten or lump ferrochrome and slag formers (lime, fluorspar and dolomite), after which it is refined in an argon oxygen decarburisation (AOD) or Creusot-Loire Uddeholm (CLU) converter. Ferrochrome however, is produced by the carbothermic reduction of chromite ore in a submerged-arc furnace (SAF) or direct current furnace (DC).

The emissions from these pyrometallurgical plants, which consist of NO_x, CO_x, SO_x, organic compounds and particulate dust, pose a potential threat to human health and the environment. The particulate furnace dust contains valuable components (e.g. chromium, zinc and iron) as well as significant toxic substances [e.g. chromium (VI), lead], which can leach into the groundwater when stockpiled or land filled. Of these toxic substances, chromium (VI) is both toxic and carcinogenic and exceeds the regulation thresholds in many countries [1]. According to Cox et al. [2], about 20% of the total chromium in the ferrochrome dust is present as Cr (VI), which is leachable. The US Environmental Protection Agency (US EPA) has classified the electric arc furnace dust as hazardous material (K061) as it exceeds the Toxicity Characteristics Leaching Procedure (TCLP) test limits for Pb, Cd and Cr [3]. Typically, approximately 18 to 25kg of dust or slurry per ton of ferrochrome produced is collected by the abatement systems in ferrochromium plants, and approximately 18 to 33 kg bag house filter dust is generated per ton of stainless steel produced [4-8].

Filter cake, which is the precipitate after the treatment of waste pickling acid (classified as K062 by the US EPA) in stainless steel plants, also contains significant Cr (VI) species and inorganic salts [9]. It is also potentially harmful to the environment.

Currently, there are two possible methods by which this electric furnace dust and filter cake can be managed: Landfilling or stockpiling in the waste site is the simplest and easiest method. However, this could lead to the contamination of the soil and

groundwater by toxic substances. The maximum acceptable concentrations of chromium species, zinc and lead in the leachate from these wastes, as specified by different countries, are listed in Table 1.1 [10-15]. It shows that the limits and test methods vary from country to country. However, the Cr (VI) species has the lowest limits (0.02~1.5mg/l) and is considered to be the most harmful species in the dust due to its high solubility in water and carcinogenic properties. These wastes therefore cannot be disposed without prior treatment. Thus, the existence and treatment of wastes from stainless steel and ferrochrome production remain a challenge and an issue of concern. The increase of environmental legislation globally and the trend towards sustainable development are drives for alternatives to landfill.

Table 1.1 The maximum acceptable concentrations of Cr species, Zn and Pb in leachate from the wastes specified by different countries [10-15]

Country	Leachate	Regulation limits (mg/l)				References
		Cr (III)	Cr (VI)	Zn	Pb	
Spain	DIN[a] leachate	4	0.5	20	0.5	10
Germany	Leachate	-	0.5	-	-	11
Japan	Leachate	-	1.5(0.5[b])	-	-	
Italy	TCLP leachate	2[c]	0.2	2	0.2	12,13
USA	TCLP leachate	5[c]	-	10	5	11,14
South Africa	ARL[d]	4.7	0.02	0.7	0.1	15

[a]Deutsches Institut fűr Normung; [b]The maximum concentration for ocean disposal;
[c]Cr total; [d]Acceptable risk levels.

Various alternative methods have been developed to manage these wastes. Figure 1.1 shows the waste minimisation techniques that can be used to manage the Cr (VI)-containing pyrometallurgical wastes. It shows that waste can be minimised through source reduction (i.e. waste prevention) as well as recycling (on site and off site). The choice of input materials, products, and technology changes, as well as good operational practices can also efficiently reduce the generation of wastes. Recovery is another method whereby the problem of wastes can be minimised. In South Africa, the

ferrochromium industry produces approximately 68,000 t bag house filter dust and 28 000 t slurry, while the stainless steel industry produces 24 000 t of dust annually [5,16,17]. A very strong need therefore exists to investigate the problem comprehensively and develop an appropriate treatment process.

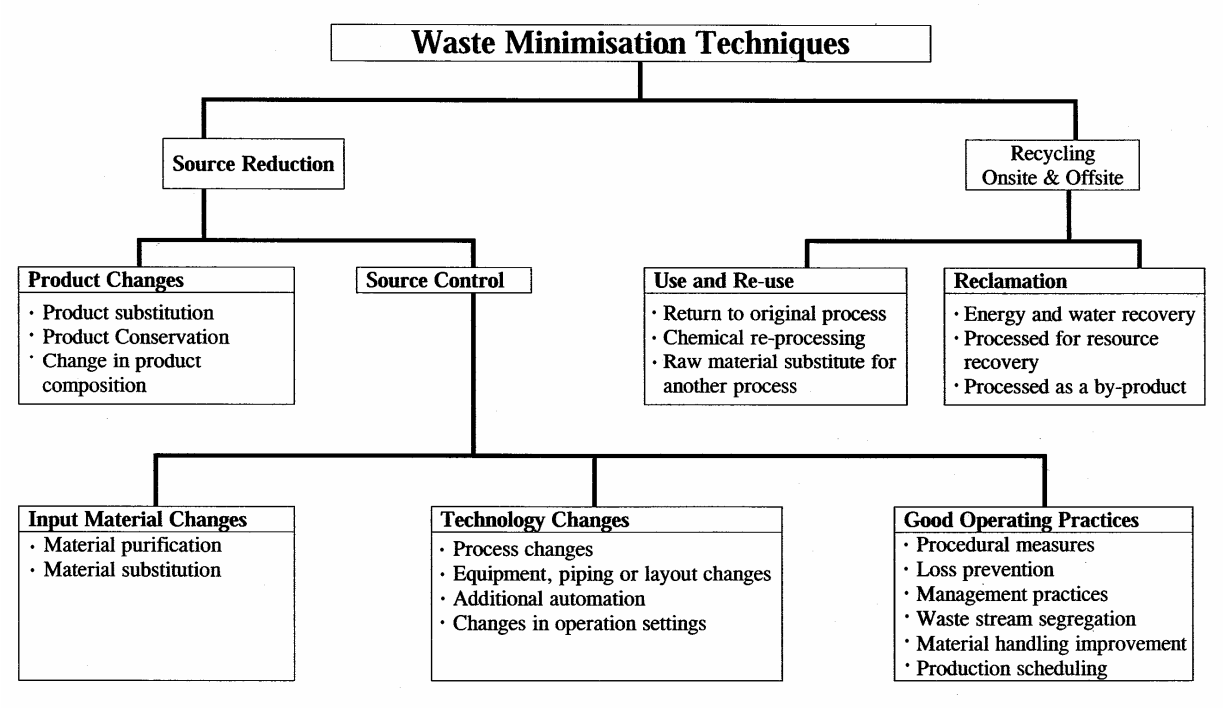

Figure 1.1 Various waste minimisation techniques that can be used to manage the Cr (VI)-containing pyrometallurgical wastes [15]

1.2 Objectives of this project

The aim of this project was to minimise the generation of the Cr (VI)-containing electric furnace dust and filter cake and develop an appropriate method to treat these wastes. This was done by studying the -

- characteristics of the wastes,
- formation mechanisms of the wastes,
- leachability of the wastes,
- aging behaviour of Cr (VI)-containing electric furnace dust and filter cake,
- stabilisation of Cr (VI) by silica-rich clay, and

- leaching mechanisms of chromium species from the stabilised wastes.

1.3 Structure of the thesis

The dissertation starts with a review chapter (Chapter 2) in which previous work on electric furnace dust and waste pickling acid are discussed. It reviews the characteristics, formation mechanisms and treatment processes of Cr (VI)-containing pyrometallurgical wastes (stainless steel plant dust, ferrochrome dust and filter cake).

Chapter 3 focuses on the investigation of the characteristics of the electric furnace dust and filter cake samples collected from a South African stainless steel plant and ferrochrome plant. The particle size distribution, bulk density, moisture content, pH, chemical composition and phase composition of the wastes were studied. TG/DTA analysis, Raman spectrometry and X-ray photoelectron spectrometry (XPS) were also used to further understand the basic properties of these wastes.

The microstructures and formation mechanisms of the wastes are presented in Chapter 4. In this Chapter, the formation mechanisms of these wastes are postulated from the observed microstructures and the production processes of stainless steel, high-carbon ferrochromium and filter cake. Chapter 5 describes the leachability of the wastes based on the TCLP test, ASTM D 3987-85 test and static leaching test results. Chapter 6 deals with the aging behaviour of Cr (VI)-containing stainless steel plant dust and filter cake. Chapters 7 and 8 investigate the stabilisation of Cr (VI) by silica-rich clay, using synthetic and electric furnace dust and filter cake samples. The leaching mechanisms of the chromium species from the wastes that were stabilised with clay were also studied using a semi-dynamic test, and are presented in Chapter 9. Finally, a summary of the results are given and conclusions are drawn in Chapter 10. Recommendations for future work are also made in Chapter 10.

Chapter 2 The characteristics, formation mechanisms and treatment processes of Cr (VI)-containing pyrometallurgical wastes: a review

2.1 Introduction

Cr(VI)-containing wastes are produced by stainless steel and ferrochrome plants. These wastes include dust, sludge and waste acid from stainless steel pickling plants. Stainless steel plant dust contains significant levels of valuable elements such as chromium, nickel and iron [4], while the electric furnace dust generated by ferrochrome plants typically consists of coarse dust, which is collected by the cyclone separators, and fine dust that is captured by the bag house filters. The ferrochrome coarse dust mostly consists of chromite ore, silica particles, carbon-bearing particles and ejected slag particles. The ferrochrome fine dust is however mainly associated with vaporised substances such as zinc oxide [9].

The stainless steel waste pickling acid, which contains Cr (VI), iron and nickel salts and waste nitric and hydrofluoric acid, is treated by either recycling or precipitation. The waste acid recycling processes include the diffusion dialysis separation process [18], the distillation-crystallisation process [19], the solvent extraction process [19] and the ion exchange process [20]. In the precipitation process lime is typically used to precipitate the metal ions as metal hydroxides under alkaline conditions, whereby a filter cake is formed. All these pyrometallurgical wastes contain leachable Cr(VI) salts and other toxic substances, which can potentially pollute the ground water and soil when stockpiled or land filled [9].

The potential leachability of the toxic substances from these wastes into the ground water is often evaluated by the Toxic Characteristics Leaching Procedure (TCLP) test that was developed by the US Environmental Protection Agency (US EPA) [21]. In South Africa, the treatment policy of these wastes is guided by the minimum requirements for the handling, classification and disposal of hazardous waste that was published by the Department of Water Affairs and Forestry (DWAF) in 1998 [15]. Of all the leachable

toxic substances, Cr (VI) has the strictest limits with an acceptable environmental risk concentration of 0.02 ppm [15]. The limits that were set by different countries on Cr (VI) species for different water sources are shown in Table 2.1 [13,17,22]. It shows that the limits for Cr (VI) are between 0.005 and 0.1 mg/l for different kinds of water, while the total chromium limits vary from 0.0031 to 2 mg/l.

Table 2.1 The regulation limits of Cr species for different water sources specified by different countries [13,17,22]

Country	Type of water	Concentration, mg/l	
		Cr (VI)	Cr (Tot)
France	General water	0.1	0.5
Germany	Drinking water	nr*	0.05
	Metal/chemical industry	0.1	0.5
Japan	Drinking water	0.05	nr
	Public water systems	0.5	2
Kazakhstan	Drinking water	nr	0.0031
	Liquid effluent emissions	0.005-0.03	nr
South Africa	Effluent discharge	nr	0.5
	Drinking water	0.05 [17]	0.1
USA	Drinking water	0.1 [22]	0.1
UK	Drinking water	nr	0.05

*nr: not reported

In order to understand the properties of the wastes, minimise waste formation and develop an appropriate process to treat them, the characteristics and formation mechanisms of the wastes have been investigated by numerous researchers [23-37]. Over the past decades, different treatment processes have also been developed to treat these wastes. This chapter subsequently reviews the properties and formation mechanisms of Cr(VI)-containing pyrometallurgical wastes. The present treatment processes of the wastes are also summarised and the solidification/stabilisation processes of the wastes are highlighted.

2.2 The characterisation of electric furnace dust and filter cake

The treatment policy of wastes is closely associated with the characteristics of the wastes. It is therefore important to know the physical and chemical properties of the wastes before a treatment method is developed or chosen.

2.2.1 Electric furnace dust

2.2.1.1 Macro and microstructure

The stainless steel dust is typically chocolate-brown in colour, and emits foul gases (possibly acetylene) [38], especially when coming in contact with water. The high carbon ferrochrome fine dust however, is grey, while the coarse dust appears black in colour due to the significant levels of chromite ore particles and carbon-bearing materials [9].

The micrographs of electric furnace dust from a South African stainless steel plant and ferrochrome plant are shown in Figure 2.1 [39,40]. The electric furnace dust includes metal and oxide particles that are present in either spherical or angular shape [4,38,39,41,42]. The stainless steel plant dust contains very small spherical particles, slag spheres, metal particles that are coated with a slag layer, as well as oxide particles that contain dendritic crystals [4,38,39,41]. The ferrochrome bag house filter dust is very fine and is constituted of agglomerated particles. It consists of chromite ore, char particles (phase A in Figure 2.1), ferrochrome particles (phase C in Figure 2.1) and particles with significant levels of Mg, Si, Cr and Zn (phase B in Figure 2.1) [2,40].

2.2.1.2 Physical properties

The particle size distribution of the stainless steel plant dust ranges from sub-micron to 200μm [41]. The mean particle diameters (d_{50}) range from 0.7 to 21.52 μm for the stainless steel dust, and between 0.71 and 13.23 μm for the ferrochrome bag house filter dust (Table 2.2). The electric furnace dust has low moisture contents (0.19-0.63 wt%) and high specific surface areas (4.09-13.2 m^2/g).

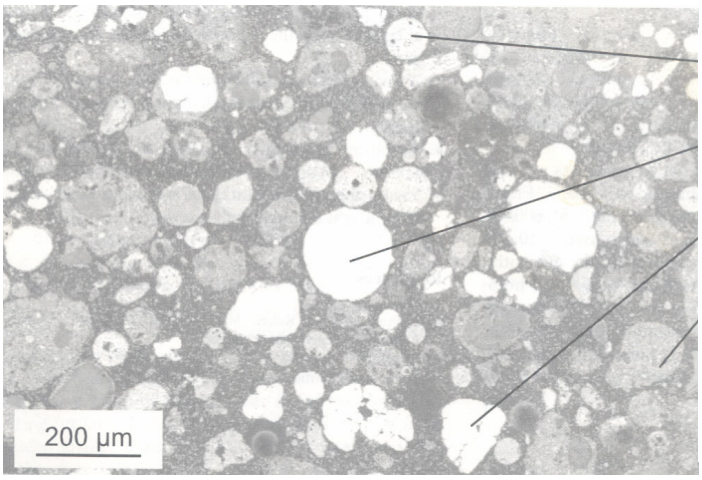

(a)

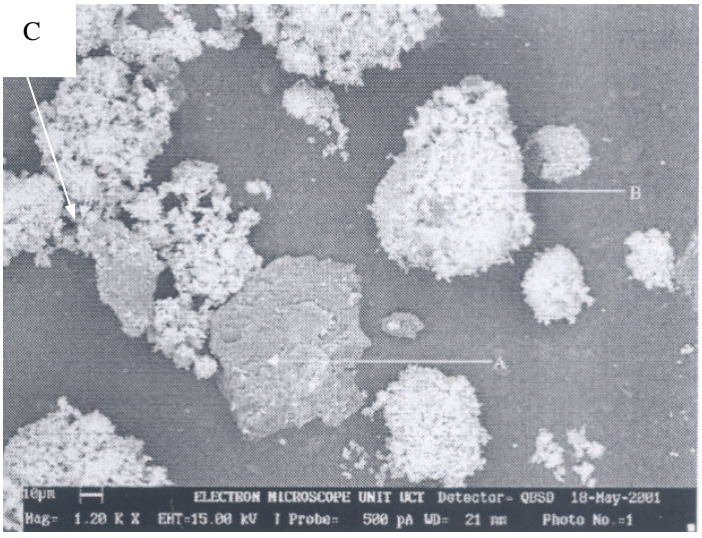

(b)

Figure 2.1 Micrographs of electric furnace dust from a South African stainless steel plant (a) [39] and ferrochrome plant (b) [40]

The bulk densities of the stainless steel dust range from 0.90 to 2.53 g/cm^3, while the true densities of the dust range from 3.01 to 5.22 g/cm^3. This implies that many voids exist inside the dusts, and that they would require big storage and transportation volumes.

The stainless steel dust generates a basic solution with a pH of about 12 when leached in water [12,38,43]. It is believed that this is due to the presence of the lime in the dust. The

Table 2.2 Physical properties of electric furnace dust [2,4,6,9,12,14,17,38-51]

	Stainless steel dust	**Ferrochrome dust**
Particle size, d_{50}, (μm)	0.7-21.52	0.71-13.23
Moisture (wt%)	0.19-0.62	nr*
Specific surface area (m^2/g)	4.09-5.73	5.31-13.2
Bulk density (g/cm^3)	0.90-2.53	nr
Density (g/cm^3)	3.01-5.22	nr
Water soluble fraction (wt%)	6.7	3.34-11.86
pH	11.96-12.4	nr

*nr: not reported

soluble fraction, due to the presence of salts in the dust, is 6.7 wt% for the stainless steel dust, whereas for the ferrochrome dust it ranges between 3.34 and 11.86 wt% [17,42].

2.2.1.3 Chemical composition and phases

Compared to carbon steel plant dust, stainless steel plant dust has a low zinc concentration, but is enriched in metallic components, since high alloy scrap is used in the production of stainless steel [4,39]. The chemical composition of and crystalline phases present in the dust vary considerably, depending on the steel grade produced, raw materials used, operational parameters, furnace type and heats. Due to the same reasons, the compositions of ferrochrome dust as well as the crystalline phases present in them vary. The typical compositional ranges and crystalline phases that are present in the stainless steel plant dust, ferrochrome coarse dust and ferrochrome fine dust are shown in Table 2.3. It shows that stainless steel dust consists mainly of oxide phases that are rich in Ca, Cr, Fe, Ni, Mn, Zn and Mg, with minor amounts of Si, Al, Mo, Pb, Ti, Cu, P, S, alkaline metals (K, Na) and halogens (Cl, F) [2,4,6,9,14,17,38-53]. The ferrochrome coarse dust from the cyclone separators is also oxide-based and contains significant levels of Si (9.15-13.86wt.%), Al (5.61-6.62wt.%), Cr (13.14-17.11wt.%), Fe (5.37-10.58wt.%), Mg (4.14-5.4wt.%) and C (9.97-15.5wt.%), while the oxide-based ferrochrome fine dust

from the baghouse filter is relatively high in Si, Zn, Na, K, Mg, Cl and S, but lower in Cr, Fe and C concentrations [9,16,17,54-58]. Chromium and iron oxides (CrO and Fe_2O_3) as well as spinel phases, such as $FeCr_2O_4$, Fe_3O_4, $MnFe_2O_4$ and $ZnFe_2O_4$, and their solid solutions are the major crystalline phases present in the stainless steel plant dust, while the minor phases are pure metallic particles (iron, zinc and nickel), oxide phases (NiO, MgO, PbO, SiO_2 and ZnO), halogens ($PbCl_2$, $ZnCl_2$, KCl and NaCl), indialite ($Mg_2Al_4Si_5O_{18}$), mullite ($3Al_2O_3{\cdot}2SiO_2$), SiC, fayalite (Fe_2SiO_4), sulphates, hydrates ($ZnCl_2{\cdot}4Zn(OH)_2$, $Ca(OH)_2$) and some raw material particles (CaO, CaF_2 and $CaCO_3$) [4,6,14,38-53].

No data, to the author's knowledge, have been published on the phase compositions of ferrochrome dust. The characterisation of ferrochrome dust was therefore an important part of this study because it is essential to know the phase compositions before a method can be developed to treat it.

The Cr (VI) concentrations (0.035-0.6wt%) in the stainless steel plant dust and ferrochrome fine dusts are enough to be harmful to human health and the environment (Table 2.3). Cox et al. reported that Cr (VI) exists in the form of $Cr_2O_7^{2-}$ or CrO_4^{2-} on the surface of ferrochrome dust particles, and indicated that more than 75% of the Cr (VI) originates from particles that are less than 10μm in diameter [2]. These particles constitute approximately 28 % of the dust by mass.

The concentrations of sodium, potassium and zinc are extremely high in the TCLP leachate of the ferrochrome dusts (Na 2848-22400 mg/l, K 632-1919 mg/l, Zn 65.3-1109mg/l) [9,17,55,56]. This further increases the treatment difficulties of these wastes [58]. Since the sulphur content in the ferrochrome dust ranges from 0.28 to 3.4wt% [9], it would not be viable to recycle it directly to the furnace due to the harmful impact, which it would have on the quality of the metal products.

Table 2.3 Typical elemental compositions and crystalline phases present in the stainless steel plant dust and ferrochrome dust [2,4,6,9,14,17,38-58]

Element [a]	Composition range of element, wt.%			Phases that contain the element
	Stainless steel dust	FeCr coarse dust	FeCr fine dust	Stainless steel dust
Cr	0.28-16.5 (69)	13.14-17.11 (0.4) [b]	1.92-7.4 (21)	Chromite ($FeCr_2O_4$), chromium oxide (CrO), $(Mg,Fe,Mn,Cr)_3O_4$ spinel and $MgCr_2O_4$
Cr (VI)	0.14-0.6	0.0005-0.0017	0.035-0.122	-
Si	0.09-4.51	9.15-13.86	16.45-34.2 (298.5)	Quartz (SiO_2)[d], indialite ($Mg_2Al_4Si_5O_{18}$), Mullite ($3Al_2O_3{\cdot}2SiO_2$), SiC and fayalite (Fe_2SiO_4)
Al	0.16-0.81	5.61-6.64	1.06-5.62	Alumina (Al_2O_3), indialite ($Mg_2Al_4Si_5O_{18}$), Mullite ($3Al_2O_3{\cdot}2SiO_2$) or substitute for spinel phase
Ca	0.83-14.78 (716)	0.71-1.72	0.14-0.57(65.6)	Lime (CaO), fluorite (CaF_2) and $CaCO_3$, $Ca(OH)_2$
Zn	0.04-12.76 (311)	0.59-0.64 (0.1)	1.37-12.13 (65.3-1109)	Zincite (ZnO), zinc ferrite ($ZnFe_2O_4$), zinc metal, $ZnCl_2$ and $ZnCl_2{\cdot}4Zn(OH)_2$
Fe	14.77-53.50 (0.3)	5.37-10.58	0.61-3.01 (1.0)	Magnetite (Fe_3O_4), zinc ferrite ($ZnFe_2O_4$), jacobite ($MnFe_2O_4$), fayalite (Fe_2SiO_4), chromite ($FeCr_2O_4$) hematite (Fe_2O_3), $(Mg,Fe,Mn,Cr)_3O_4$ spinel and iron
Mn	0.30-7.65	0.11-0.18 (0.2)	0.23-0.58(12-17)	Jacobite ($MnFe_2O_4$) and $(Mg,Fe,Mn,Cr)_3O_4$ spinel
Mg	0.042-10.2 (452)	4.14-7.16	1.01-13.92 (434)	Indialite ($Mg_2Al_4Si_5O_{18}$), $MgCr_2O_4$, $(Mg,Fe,Mn,Cr)_3O_4$ spinel and periclase (MgO)
Mo	0.18-1.30 (8)	-	0.008(12)	-
Pb	0.03-1.9 (0.06)	0.007-0.009 (0.3)	0.06-0.123 (0.01-0.03)	Lead oxide (PbO), lead chloride ($PbCl_2$) and lead sulphate ($PbSO_4$)
Ni	0.045-5.42	0.062-0.079	0.0053-0.1	Bunsenite (NiO) and nickel metal
S	0.19-1.65	0.28-0.76	0.96-3.4	Sulfates
Cl	0.5-5.20	0.89	0.95-3.32	Potassium chloride (KCl), sodium chloride (NaCl) and $ZnCl_2$ and $ZnCl_2{\cdot}4Zn(OH)_2$
Na	<0.07-4.91 (320)	1.32-1.89	1.71-5.94 (2848-22400)	Sodium chloride (NaCl)
K	0.08-2.99 (650)	0.84-0.91	1.0-7.58 (632-1919)	Potassium chloride (KCl)
Ti	0.03-0.21	0.31-0.4	0.03-0.12	-
P	0.02-0.82	0.013-0.044	0.013-0.044	-
C	0.0-1.3	9.97-15.5	1.1-1.58	Graphite, SiC and $CaCO_3$
Cu	0.11-0.65	0.024	0.008-0.018	-
F	0.012-0.016	0.01	0.04-0.9	Fluorite (CaF_2)
Ga	-	0.015	0.026-0.39	-

Note: [a] :The elements such as Cr, Si, Al, Ca, Fe, Mn, Mg, Na, K and Ti can also exist in the glassy slag phase that is present in the dust.

[b] :Values in brackets are the elemental concentrations in ppm in the TCLP leachate.

2.2.2 Filter cake from the waste pickling acid treatment plant

In order to improve the surface quality of stainless steel three different methods are used, namely acid pickling, fused salt bath conditioning followed by the acid pickling and acid pickling following electrolytic neutral pickling [59]. The acid pickling following electrolytic neutral pickling is displacing the two former conventional processes due to the good condition of the pickled strip surface, the lower operation and maintenance cost [59]. The typical electrolytic neutral pickling solution is sodium sulphate, while the pickling acids are nitric, hydrofluoric, sulphuric and hydrochloric acids [20,59]. The waste pickling acids are acidic with a typical pH of 1 and contain significant concentrations of fluorine, iron, nickel and chromium [9]. The typical composition range of the spent HNO_3/HF pickling acid is shown in Table 2.4 [19]. The standard treatment process for the waste pickling acid includes three steps, i.e. the neutralisation of the waste acid through the addition of lime, the reduction process of Cr (VI) with ferrous sulphate and the precipitation of metallic species with lime. The last step of the process is the collection of the precipitate, whereby the filter cake is produced [9].

Table 2.4 The typical compositions of the stainless steel pickling acid wastes [19]

Acids or elements	Composition range, kg/m^3
HNO_3	100-200
HF	10-80
Fe	30-70
Ni	3-10
Cr	3-12
Mo	0-0.5

The original filter cake is constituted of very fine particles with a d_{50} of approximately 3.7 um [60]. It mainly contains calcium, fluorine and iron which amount to approximately 49 wt% to 64 wt% of the filter cake [60]. The remainder are nickel (approximately 1-3 wt%), chromium (approximately 2-3 %), sulphur (approximately 3 wt%) and oxygen [60]. After being heated up to 1000^{o}C, the total weight loss of the filter cake is between 10 to 15 wt% due to the dehydration of the metal hydroxides [60].

The X-ray diffraction analysis shows that the filter cake contains high proportions of amorphous phases that include metal ions such as Cr, Fe and Ni [60]. It also contains the crystalline phases calcium fluoride (CaF_2) [60,61] and calcium sulphate ($CaSO_4$) [61], and stainless steel scale which include the phases Cr_2O_3 and $FeCr_2O_4$ [62]. The high fluorite and sulphate contents in the filter cake seem to restrict the reuse of the filter cake in the steelmaking plant. It is therefore suggested that the wastes from the pickling bath and the neolyte tank should be treated separately [63].

2.3 Formation mechanisms of electric furnace dust and filter cake

2.3.1 Dust formation in the stainless steel plant

The formation of stainless steel plant dust includes in general two steps, i.e., emission of dust from the electric arc furnace or converter, followed by escape from the furnace to the bag house filters. In the first step, the dust is carried off by the off-gas, whereas the chemical and physical transformation of the particulate matter, such as chemical reactions between gaseous, liquid and solid phases and the agglomeration of fine particles, occur during the second step [23].

The formation mechanisms of dust in the electric arc furnace are shown schematically in Figure 2.2 [23-37]. The following mechanisms contribute to dust formation in electric arc furnaces:

1) Vaporisation of the elements or compounds from the high temperature zones, i.e. arc zone (1), oxygen blowing zone (1') and the reaction zone of decarburisation. Zinc, lead and cadmium as well as alkaline metals and oxides can vaporise in these areas in the furnace. Metal oxides phases such as ZnO are then the oxidation products in the off-gas duct [29].
2) Ejection of slag and metal, by CO gas bubble bursting due to decarburisation (3), oxygen blowing (2'), the force of the arc (2) and the ejection of the bursting droplets (4) when the burst metal droplets (3) decarburise in contact with the oxidised atmosphere.

.

University of Pretoria etd – Ma, G (2006)

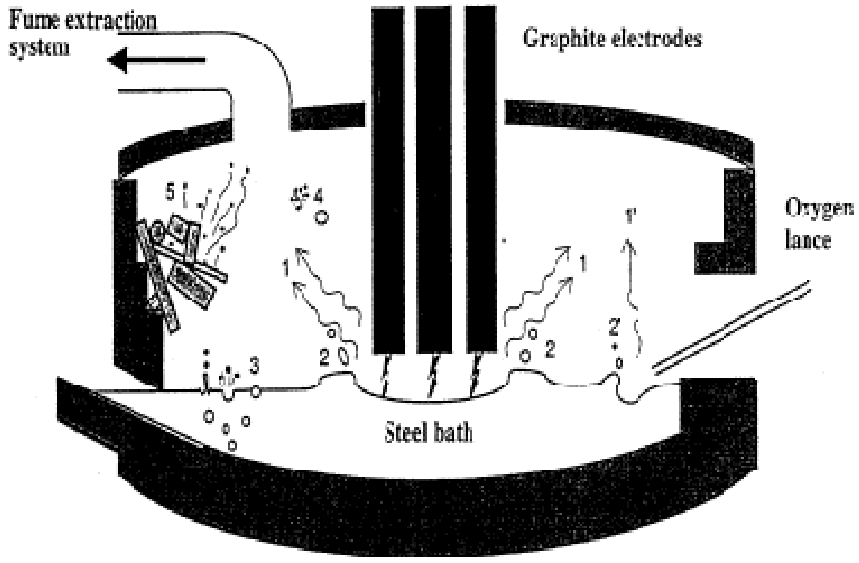

Figure 2.2 Formation mechanisms of dust in the EAF [23]

The formation mechanisms of fine droplets due to bubble bursting in the melt bath is shown in Figure 2.3. The CO gas bubbles formed by the decarburisation reaction enter the slag layer with a thin steel film (a). The dust droplets can form through fragmentation of the bubble film cap, whereby small film droplets form (b and c). The remaining crater would close up and form jet droplets (d, e, f and g). However, these droplets do not have enough kinetic energy to carry them out of the furnace and are often captured by the off-gas [64]. Huber et al. concluded that the formation of film droplets is the major dust formation mechanism, while the jet droplets are larger in size and therefore drop down to the bath [23].

3) Direct capturing of charged fines such as lime, quartz and ferroalloy particles (5, Figure 2.2) by the off-gas. Quartz, lime, fluorite, calcite, nickel metal and graphite in the dust are directly captured by the off-gas during the course of charging. $Ca(OH)_2$ forms in the off-gas duct due to the hydration of lime.

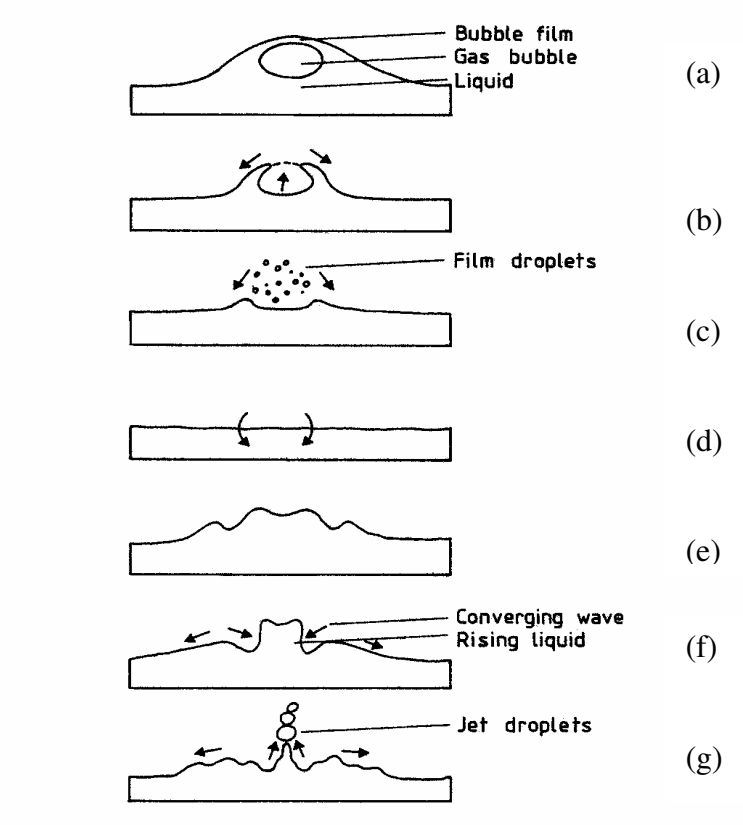

Figure 2.3 Formation mechanisms of fine droplets due to bubble bursting [24]

Different authors reported that the respective formation mechanisms contribute to different extents to dust formation: Huber et al. reported that approximately 60 wt% of the total dust are metal and slag droplets, while volatiles in the dust contribute about 27 wt% [23]. It is also found that dust emission is closely associated with the emission of CO gas [23]. Dalhaes et al. however showed that about 3 wt% of the total dust formed through vaporisation in the AOD converter, while the ejection of metal and slag by the bursting of gas bubbles is the main dust forming mechanism (about 91 wt% of the total dust) [24]. Ohno et al. found that most of the dust is less that 5 μm in diameter and caused by the bursting of gas bubbles [25]. There is general agreement however that the ejection of slag and metal by gas bubble bursting is the major mechanism of dust formation in the steelmaking plant.

In order to minimise dust formation, it is suggested that:

University of Pretoria etd – Ma, G (2006)

a. The size of the bubbles is reduced by controlling the decarburisation reaction in the EAF [23];
b. Operational issues such as the foamy slag practice, the pre-heating of the scrap, slopping, the position of the oxygen lance and the bottom injection of additives or fluxes should be optimised [23-27];
c. The energy input (electrical and chemical) should be optimised [23,27].

2.3.2 Dust formation in the ferrochrome plant

Ferrochrome dust formation mechanisms in submerged arc furnaces (SAFs) has not been reported in the literature. It is suggested that the vaporisation of elements or compounds from high temperature zones of the SAF and the charge materials that are directly captured in the off-gas could be involved in dust formation [40]. Carbon-bearing particles, quartz and chromite particles that are angular in shape present in the dust presumably originated from charge fines that were entrained in the off-gas.

The reported leachable Cr(VI) concentration of ferrochrome bag house dust range between 0.035 and 0.122 ppm [17,55,56]. Beukes reported that chromium (III)-containing particulate substances can be oxidised into Cr (VI) by flare in the off-gas duct [65]. Maine et al. also assumed that Cr (VI) formation is interrelated with the alkali metals in the charge [17]. Moreover, lower temperatures and higher lime contents are conducive to the formation of Cr (VI) species [65]. The presence of alkaline bearing materials therefore impacts strongly on Cr (VI) formation, and should be reduced in the charge [65].

2.3.3 The formation of filter cake in the waste acid treatment plant

The scale of the hot rolled or annealed stainless steel strip predominantly contains Fe_xO (x=0.67, 0.75 and 1), Cr_2O_3, NiO, SiO_2, $NiCr_2O_4$ and $FeCr_2O_4$ [66]. The formation mechanisms of the filter cake vary according to the treatment process. For the traditional three step treatment process, the filter cake contains amorphous phases which consist of metal ions such as Cr, Fe, Ca and Ni, crystalline phases such as calcium fluoride (CaF_2) [60,61], calcium sulphate ($CaSO_4$) [61], Cr_2O_3 and spinel phase ($FeCr_2O_4$) [62]. Based on

an analysis of the production process, the amorphous phases are mixtures of the metal hydroxides that precipitated from the alkaline solution. CaF_2 and $CaSO_4$ however might precipitate due to their low solubilities (solubility limits of 0.016g/l and 2.09g/l respectively [67]). Cr_2O_3 and the spinel phases (e.g. $FeCr_2O_4$) are associated with stainless steel scale that remained after pickling.

2.4 Treatment processes of electric furnace dust and filter cake

A number of problems currently hamper the treatment of Cr(VI)-containing electric furnace dust and filter cake: (a) The variation in composition of the dusts (as shown in Table 2.3) due to changes in heats, raw materials, grade and operational parameters which require that the technology can treat all kinds of dusts; (b) Volatile substances in the dusts can impact on the normal operation of the furnace if it is simply charged back to the furnace; (c) Leachates from the electric furnace dusts are highly basic, and therefore require large volumes of acid in order to adjust the pH [68]; (d) the high sulphur content in the filter cake makes it difficult to recycle back to the steelmaking plant [63]. (e) Cr (VI) is highly soluble, and has very low regulation limits. As an alternative to land filling or stockpiling, different methods have been developed to deal with these wastes:

1) Minimisation of the wastes at source by optimising the operational parameters;
2) Direct recycling of the dust back to the electric furnace by injection with air [69-73];
3) Recovery processes, which include hydrometallurgical methods [68,74-89] and pyrometallurgical methods [90-112];
4) Solidification/stabilisation methods, for instance, cementation and vitrification or glassification processes [3,5,113-123]; and
5) Use as a raw material for fertiliser, glass and pigment plants [124,125].

2.4.1 Recycling

Direct recycling of electric furnace dust back to the blast furnace and electric furnace typically use agglomeration or pneumatic injection technologies [69-73]. In the pneumatic injection technologies the dust is either injected on its own, or together with

coal or coke [69-73]. Figure 2.4 shows the typical direct injection process. The dust is pelletised and screened, and then injected into the furnace. The powder mixture of dust and/or carbon is used to foam the slag, but in the process the zinc content of the resultant electric furnace dust is increased by up to more than 30 wt%, which then needs to be recovered [70]. The disadvantage of recycling back to the blast furnace is that if the dust contains significant concentrations of vaporised species such as zinc, cadmium, lead and alkaline metals (Na and K), these species circulate in the blast furnace and induce blockages [86]. For EAF operation, it would increase the energy consumption. In a trial at one of the local ferrochrome plants, pelletised ferrochrome bag house dust was charged back to the SAF [9]. However, it induced blockages and corrosion of the off-gas duct due to the high temperatures employed and enrichment of chemicals in the off-gas.

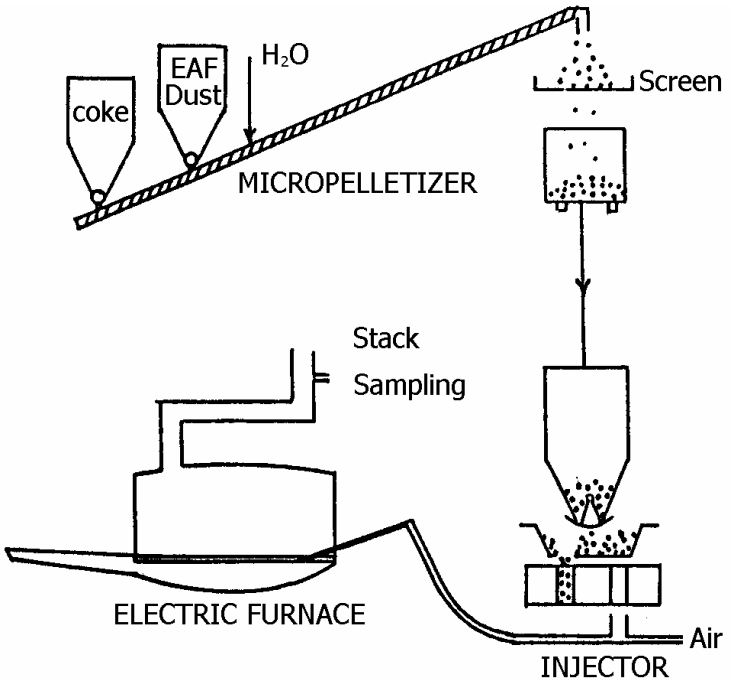

Figure 2.4 The direct recycling process [70]

2.4.2 Recovery

In the past decades, a number of methods have been developed to recover EAF dusts. It includes pyrometallurgical methods such as the Waltz and Enviroplas processes,

hydrometallurgical methods such as the ZINCEX and EZINEX processes, and combinations of hydro and pyrometallurgical methods (MRT and IBDR-ZIPP processes). Table 2.5 shows the available recovery processes and the main products formed in these processes. It shows that most of them are pyrometallurgical methods, in which mainly Zn and Fe bearing products are formed.

In hydrometallurgical recovery processes leaching solutions such as caustic soda, sulphuric acid, mononitrilotriacetate anion (NTA^{3-}) and hexahydrated ferric chloride ($FeCl_3 \cdot 6H_2O$), hydrochloride, acetic acid as well as NH_3-$(NH_4)_2CO_3$ solutions are used, depending on the variation of the chemical compositions and crystalline phases present in the electric furnace dust [74-89]. Microwave and ultra sound wave technology can be used to improve the reaction rates in these processes [68,76]. The major product of these recovery processes is zinc metal. However, the main problem associated with these processes is the detoxicification of the leach residues [87].

In the pyrometallurgical treatment processes, electric furnace dust is refined or reduced by a gaseous (methane, hydrogen) or solid (coke, coal, iron powder) reductant to produce a crude Zn, Cd, Pb, Cr and Ni bearing ferroalloy at high temperatures [90-112]. Power is supplied by either plasma arc, electricity, solar or microwave heat energy. The disadvantages of these pyrometallurgical methods are the high energy consumptions and investment costs, as well as the molten slag and off-gas that are generated as secondary waste, which need to be treated further.

2.4.3Solidification/stabilisation

In solidification / stabilisation processes the hazardous wastes can either be chemically transformed into a non-toxic form or additives can bond with the waste, whereby the mobility of the toxic substances are reduced and value added to the waste [113]. The solidification/stabilisation processes are, from an environmental and economic viewpoint,

Table 2.5 Electric furnace dust management methods [3,114]

Process name	Process type	Zn-bearing product	Fe-bearing product	Other products
Waelz kiln (2-stage)	Pyro	ZnO	Iron oxide/metallized iron	$PbCl_2/CdCl_2$ fume
Waelz kiln (1-stage)	Pyro	ZnO	Iron oxide/metallized iron	-
Flame reactor	Pyro	ZnO	Slag	-
ZTT Ferrolime	Pyro	ZnO	Ferrolime	Salt mixture
MR/Electrothermic	Pryo	ZnO	Slag/residue	-
MRT	Hydro/pyro	High purity ZnO	Iron oxide/metallized iron	Pb/Cd metals
Laclede Steel	Pyro	Zn metal	Slag	-
EZINEX	Hydro	Zn metal	Iron oxide	Salt mixture
Ausmelt	Pyro	ZnO	Slag	-
MetWool	Pyro	ZnO	Pig iron	Mineral wool
Enviroplas	Pyro	Zn metal or ZnO	Slag	-
AllMet	Pyro	Zn metal	Fe/Fe_3C	Salt mixture
IBDR-ZIPP	Pyro/Hydro	ZnO	Pig iron	Salt mixture
ZINCEX	Hydro	Zn metal	Residue	Pb/Cd cement
Rezada	Hydro	Zn metal	Iron oxide	Salt mixture, Pb/Cd cement
Cashman	Hydro	High purity ZnO	Iron oxide/metallized iron	Salt mixture, Pb/Cd cement
Terra Gala	Hydro	ZnS	Iron oxide	$PbCl_2$, Pb/Cd cement
Elkem	Pyro	Zn metal	Iron oxide slag	-
IMS	Pyro	Zn metal	Iron oxide slag	-
Hi-Plas	Pyro	Zn metal	Pig iron	-

the most promising methods to treat electric furnace dust and filter cake. It can use clay and waste that are generated by other industries (such as incinerator fly ash, coal fly ash and blast furnace slag) to stabilise or solidify the toxic substances in the electric furnace dust and filter cake [3,113-121]. The resultant waste mixture is a non-toxic material, which can be used by the building and glass industries. The solidification/stabilisation treatment processes of the electric furnace dust and filter cake can typically be divided into cementation, vitrification or glassification processes:

2.4.3.1 Cementation process

The Super Detox process, which was marketed by EnviroSource and commercialised since 1989, was developed by Bethlehem Steel Corporation [3,114]. In this process, the electric furnace dust, lime, aluminosilicates and other additives are well mixed into the concrete-like material. The toxic substances in the dust are either precipitated or oxidised/reduced into the least soluble components and thereafter immobilised by the alumino-silicate matrix. Both wet and dry electric furnace dusts can be treated. The product is very impermeable.

Another commercial solidification process successfully treats carbon steel and alloy steel electric furnace dust as well as waste pickling acid at Atlas Steels [115,116]. It uses spent pickling acid, slag and lime to treat electric furnace dust. The treatment process is schematically shown in Figure 2.5. It includes (a) the acidification of waste with iron and silicon containing materials (slag) and (b) using lime to adjust the pH in order to solidify the metal silicates. The laboratory, pilot and industrial tests show that the leachable concentrations of lead, cadmium and chromium (VI) from this precipitate are below the limits of the Ontario drinking water standard and the US EPA. It is an economic and safe way to treat electric furnace dust and spent pickling acid.

The production of cement blocks that use ferrochrome dust as raw material have been studied by Giesekke et al. [16]. The mixtures consisted of ferrochrome dust and electric arc furnace slag with different ratios of ordinary Portland cement (OPC), which were cured for 56 days. The German DIN 38414 procedure was used to evaluate the

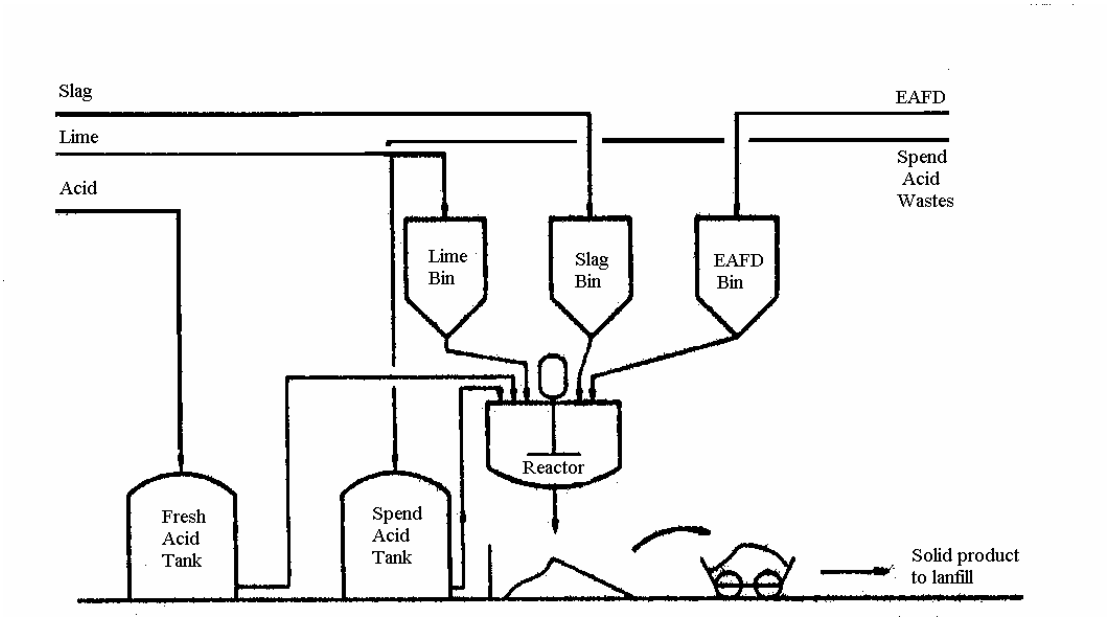

Figure 2.5 The solidification process for treating EF dust with spent acid [115]

leachability of these cement blocks after it was crushed to less than 10 mm. The results show that about 95% of the Cr (VI) and 30-55% of the salts (Na, K, SO_4 and Cl) were stabilised. The addition of $FeCl_2$ and electric arc furnace slag improved the stabilisation ratio of Cr (VI). However, the Cr (VI) concentration in the leachate was higher than the regulation limits (0.05 mg/l) set for drinking water in South Africa [17].

2.4.3.2 Vitrification or Glassification processes

The Inorganic Recycling Corporation (IRC) developed a process that can completely transform EAF dusts into commercial products [117,118]. This process (Figure 2.6) includes three parts, i.e., mixing, vitrification and off-gas treatment. The electric furnace dusts are first mixed with I/R chemicals and silicates such as silica sand, clay and cullet. The mixture is then melted in the vitrification furnace at 816-1371 ^{o}C (1500-2500 ^{o}F), poured into a mould or quenched into particulate materials. Particulate material in the off-gas is fed back to the mixer. The products, which are environmentally friendly, can be used in architectural applications or in abrasive applications. The water waste is also recycled back to the mixing step, thereby creating a zero-waste process.

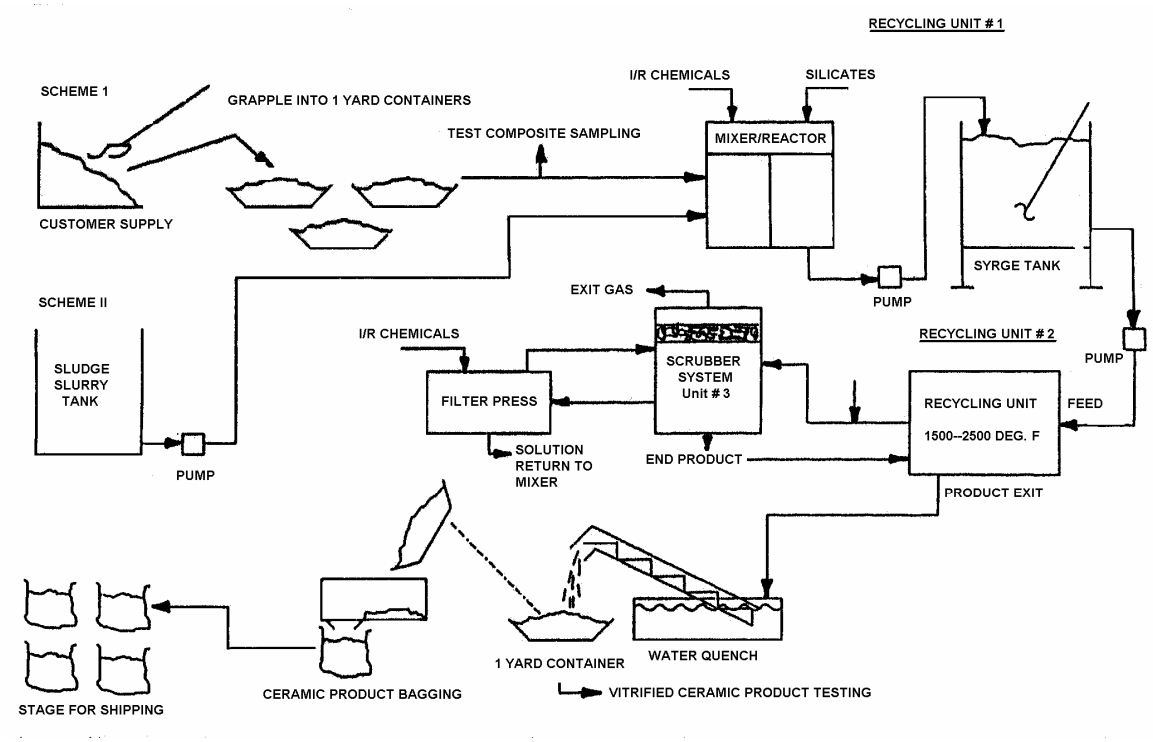

Figure 2.6 Inorganic Recycling Corporation process in which electric furnace dust is treated [118]

The Glassification process [119], which was developed by Glassification International, use pyrometallurgical wastes, such as electric furnace dust, slag, spent refractory and mill scale, to produce a non-hazardous product. In this process, the waste and glass forming materials are blended and melted at approximately 1371°C (2500 ^{o}F). Vaporised species are condensed and charged back to the furnace in order to prevent air pollution. The glassy product can be either quenched into granules or cast into different kinds of products such as tiles and sheets for architectural purposes.

The stabilisation of Cr (VI) in stainless steel plant dust by clay has also been investigated [5]. Bricks were prepared by mixing different mass ratios of dust to clay (5:5, 4:6 and 3:7), followed by drying at 110^{o}C and sintering between 1000 and 1200^{o}C for different time periods (1, 2, 3 and 5 hours). Cr (VI) in the stainless steel dust was effectively stabilised with a mass ratio of clay to stainless steel dust of 5:5 at 1200^{o}C. The Cr (VI)

University of Pretoria etd – Ma, G (2006)

concentration in the sintered brick decreased with an increase in sintering time and sintering temperature, while it increased with increasing clay:dust ratio. It was assumed that the Cr (VI) concentration decreased due to the redox reaction during the sintering period, when Cr (VI) was reduced into Cr (III), presumably by iron oxide. Peng et al. also used clay as additive to vitrify stainless steel flue dust in order to stabilise the toxic substances [44]. The softening temperature of the mixture decreased to 1200^{o}C when a 1:1 mass ratio of clay to dust was used. TCLP tests on the vitrification product indicated that the concentrations of toxic substances in the leachate are lower than the US EPA limits. TG/DTA and FT-IR analysis showed that the vitrification product is very stable, with only a 0.3% weight loss when heated to 1000^{o}C. Gericke reported that heavy metals in ferrochrome dust can be immobilised through mixing 20% of ferrochrome dust with 80% of clay or 50% clay with 30% ferrochrome dust and 20% ferrochrome slag [57]. TCLP tests indicated that Cr (VI) concentrations in the leachate are less than 0.03 ppm. Maine et al. also used 50% of clay and 50% ferrochrome bag house filter dust, and sintered it at 1200^{o}C to stabilise the Cr (VI) and salts in the ferrochrome dusts [17]. The results showed that more than 99% of Cr (VI) and 90% of salt in the ferrochrome dusts were stabilised. The Cr (VI) concentration also decreased with an increase in sinter temperature.

2.5 Conclusions

This chapter has shown that electric furnace dust and filter cake that are produced by ferrochrome and stainless steel plants contain significant amounts of Cr(VI), which is both toxic and carcinogenic. Since unacceptable levels of Cr(VI) can leach from these wastes into the groundwater, they first need to be treated before being stockpiled or land filled.

The electric furnace dust and original filter cake are very fine particles that contain valuable elements such as Fe, Cr and Ni. The stainless steel dust is formed by the vaporisation of the elements or compounds at the high temperature zones, by the direct capturing of charge fines by the off-gas and by ejection of slag and metal through the bursting of gas bubbles, which is the major mechanism of dust formation in the

steelmaking plant. Vaporisation and direct capturing of charge materials are two mechanisms whereby dust forms during ferrochrome production. Filter cake is formed due to the precipitation of metal hydroxides, and super saturated salts and from remnants of stainless steel scale.

These wastes can be either minimised at source by optimising the operation parameters or be detoxified by the proper treatment methods. Direct recycling of electric furnace dust back to the ironmaking and steelmaking plant is the easiest way to treat these wastes, whereas the disadvantages of this process are blockage and corrosion of the off-gas duct and an increase in the energy consumption. Pyrometallurgical, hydrometallurgical and combinations of hydro and pyrometallurgical processes can be used to recover the valuables in the electric furnace dust. However, the main problems associated with these processes are the detoxicification of the leach residues, the high energy consumptions and investment costs, as well as the molten slag and off-gas that are generated as secondary waste, which need to be treated further. Solidification/stabilisation processes are effective ways to treat these pyrometallurgical wastes. The electric furnace dusts can be cemented, glassified and sintered into value added products with other pyrometallurgical wastes such as slag, spent refractory, mill scale and spent acid. The advantages of the solidification/stabilisation process include low investment costs, operational simplicity and the minimization of secondary waste residues.

Chapter 3 The characteristics of the Cr (VI)-containing electric furnace dust and filter cake from a stainless steel waste treatment plant

3.1 Introduction

Particular dust emissions from the electric furnaces of stainless steelmaking plants and ferrochrome plants are cooled down in the off-gas duct and gathered by cyclones and bag house filters. Figure 3.1 schematically shows the dust treatment systems of the ferrochromium and stainless steel plants. In the ferrochromium plant (Figure 3.1a), the coarse dust is collected by a cyclone separator, while the bag house filters gather the fine dusts. The particulate matter from the EAF and refining converter are also collected by the bag house filter in the stainless steel plant (Figure 3.1b). The electric furnace (EF) dust contains valuable components (e.g. chromium, zinc, iron) as well as significant levels of toxic substances (e.g. chromium (VI), lead), which can leach into the groundwater when stockpiled or land filled. Of these toxic substances, chromium (VI) is both toxic and carcinogenic, and exceeds the regulation thresholds in many countries [4,17]. The EF dusts are therefore considered to be hazardous materials and need to be treated.

Stainless steel plants also produce filter cake that contains significant amounts of Cr (VI) and fluoride, which is also potentially harmful to human health and the environment. This filter cake is produced in the waste pickling acid treatment plant from a neutral solution of sodium sulphate as well as a mixture of nitric acid and hydrofluoric acid, that are used to dissolve the oxide scale on the surface of the stainless steel by electrochemical and chemical ways in order to improve the surface quality of the stainless steel (Figure 3.2). These waste solutions are treated through neutralisation with lime, followed by iron sulphate addition to reduce Cr (VI) species to Cr (III), and then the precipitation of metals by lime (typically at pH ≈ 9.5). Finally, the precipitate is pressed into a filter cake [9].

Worldwide the existence and treatment of these wastes remain very concerning issues in stainless steel and ferrochrome production, due to environmental legislation. In order to

University of Pretoria etd – Ma, G (2006)

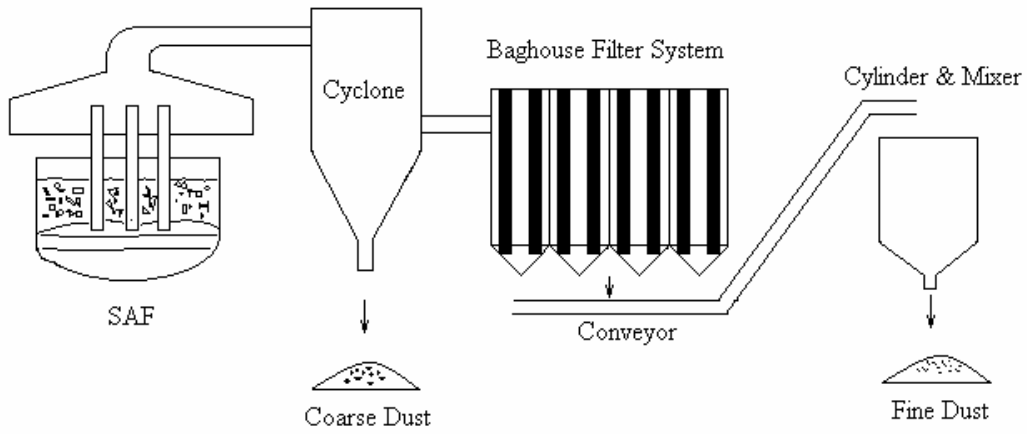

(a)

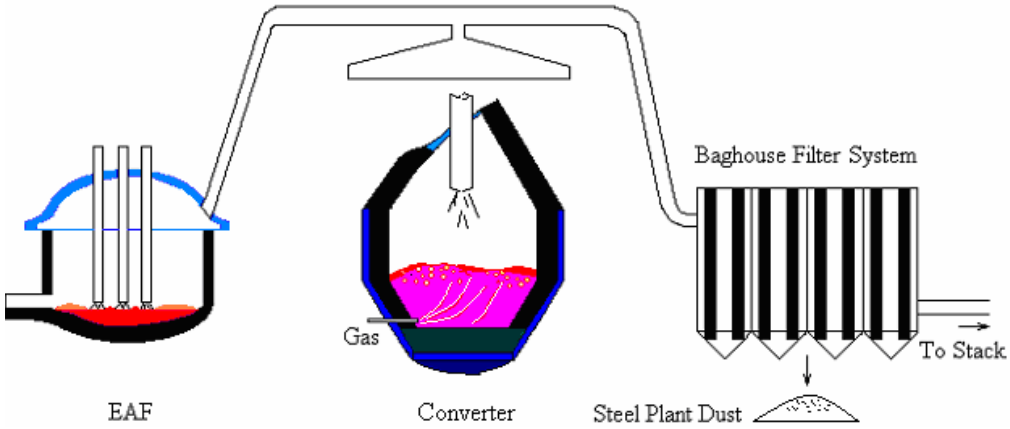

(b)

Figure 3.1 Schematic diagrams of dust treatment systems in the ferrochrome plant (a) and the stainless steel plant (b) from which the waste samples were taken

develop a technique whereby the Cr(VI)-containing EF dust and filter cake can successfully be treated, it is important to first comprehensively characterise these waste materials. In this chapter, various techniques such as TG/DTA, XRF, XRD, SEM-EDS, FT-IR, XPS and Raman spectrometer, were used to characterise the Cr(VI)-containing EF dust and filter cake from a South African stainless steel and ferrochromium plant.

University of Pretoria etd – Ma, G (2006)

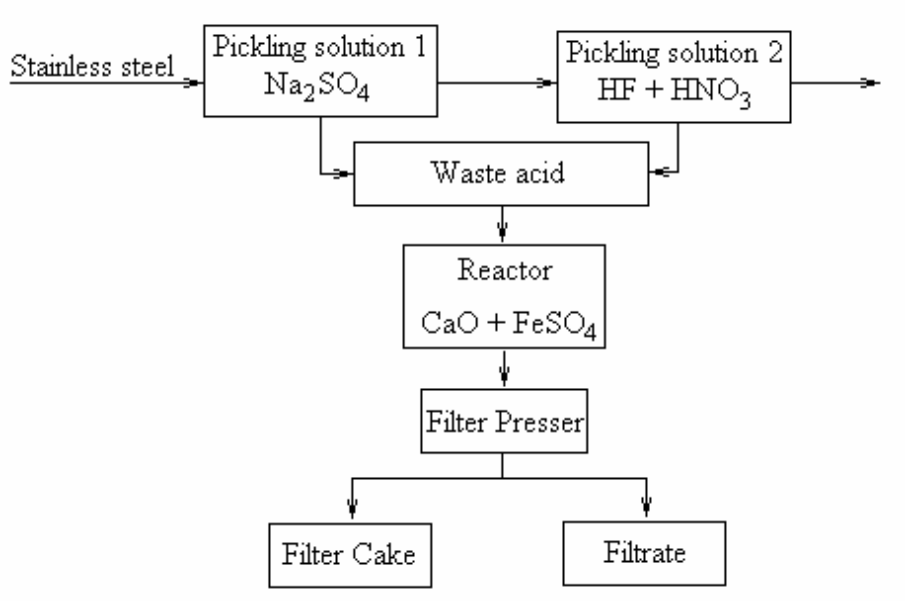

Figure 3.2 The production process of filter cake in the stainless steel pickling waste treatment plant

3.2 Experimental

3.2.1 Waste materials and sample preparation

A stainless steel plant and a ferrochrome plant supplied the EF dust samples. The dust sample from the stainless steel plant (SPD) was collected from the bag house filter system, and consists of a mixture of EAF and converter dust. Two fine fractions and one coarse fraction of ferrochrome dust were gathered from the dust treatment system of two semi-closed SAFs of the ferrochrome plant, which produces up to 150t of fine dust and 4t of coarse dust per month. The fine fractions were collected from the bag house filter system of the F2 dust plant (FCD1) and the F1 dust plant (FCD2) respectively, while the coarse fraction was taken from the cyclone separator of the F1 dust plant (FCD3) [9].

The sample of filter cake (FC) is the precipitate from the waste pickling acid treatment plant of the stainless steel plant. The original filter cake typically has a moisture content of 50 wt%. The waste treatment plant generates about 750 t of filter cake per month [9].

Representative sub-samples from the EF dust were obtained through riffling as well as splitting, in which the cone method was used. The filter cake was first dried at 110°C, crushed and ground, before representative sub-samples were taken.

3.2.2 Analytical procedures

Representative sub-samples were used for the determination of the particle size distribution, bulk density, moisture content, pH, thermal properties, chemical composition, phase chemical composition and microstructure of the dust and filter cake.

3.2.2.1 Physical and thermal properties

The particle size distributions of the EF dusts were analysed with a Malvern Mastersizer 2000 (UK). A Mettler Toledo HR73 moisture analyser was used to determine the moisture content of the samples. The bulk densities as well as the pH of the wastes were determined by the American Society for Testing and Materials (ASTM) D 5057-90 [126] and ASTM D 4980-89 methods [127], respectively.

The thermal properties of the samples were examined by simultaneous thermogravimetry (TG) and differential thermal analysis (DTA), using a Mettler Toledo TGA/SDTA851^{e} Module. 30mg samples were heated in dry air at a flow rate of 50ml/min at 20°C/min from room temperature up to 1300°C. The sintered products were examined by scanning electron microscopy (SEM) (JSM-6300), using energy dispersive X-ray spectrometry (EDS). The evolved gas species from the TG/DTA experiments were analysed with an off-line Perkin Elmer Fourier Transform Infrared (FT-IR) Spectrometer. Reaction products which condensed on the inside of the alumina lid during the TG/DTA experiments were analysed with a Perkin Elmer X-ray photoelectron spectrometer (Mode 5400), using a Mg Kα X-ray (1253.6eV) source. A FT-IR Spectrometer was also used to analyse the samples in the band regions of 400-3800 cm^{-1} with a background of dried potassium bromide. Raman analysis was conducted with a Dilor XY multi-channel Raman spectrometer with an Olympus microscope and a charge-coupled detector. The sample was excited with the 514.5 nm line of an argon ion laser with a power of 100mW.

University of Pretoria etd – Ma, G (2006)

3.2.2.2 Chemical composition and microstructure

The wastes were chemically analysed by X-ray fluorescence (XRF). The received waste samples were ground to <75μm in a Tungsten Carbide milling vessel, roasted at 1000 ^{o}C to determine Loss On Ignition (LOI) and fused into a glass bead after adding 1g of sample to 6g $Li_2B_4O_7$. Major element contents in the wastes were analysed on the fused bead using a ARL9400XP+ spectrometer, while the trace element analyses were determined after pressing the sample into a powder briquette [1)]. The carbon contents were determined with a LECO CS400 instrument and the oxidation states of iron by a redox titration method with potassium dichromate. The detection limit of this latter method is 0.01%.

A Siemens D-501 X-ray diffraction (XRD) instrument (Cu *K*α radiation, 40kV and 40mA) was used to identify the crystalline phases in these wastes. The phase compositions of the dust and filter cake samples were also examined by SEM-EDS. The elemental composition on the surface of the dust samples were analysed with a Perkin Elmer X-ray photoelectron spectrometer. The samples were prepared by pressing it into Indium foil. The C1s (284.6eV) binding energy was chosen as the reference to calibrate the binding energy curve. The oxidation states of chromium were identified by using the NIST XPS binding energy database [128].

3.3 Results

3.3.1 Particle Size Distribution, Bulk Density, Moisture Content and pH

The stainless steel dust and ferrochrome fine dusts are very fine particles, and easy to agglomerate into micro-pellets. The particle size distributions of the dust and original filter cake are shown in Figure 3.3. The mean particle diameter values are 6.54, 3.19, 2.92, 5.49 and 79.76 micron for samples FC, SPD, FCD1, FCD2 and FCD3, respectively. Figure 3.3 also indicates that almost 90% of filter cake particles are less than 50 μm in diameter. More than 85% dust particles are smaller than 40 micron in the SPD. About 90%, 75% and 20% particles are less than 40μm for FCD1, 2 and 3, respectively.

[1)] Sample FCD3 could not be fused into a glass bead due to the high concentrations of chromium, and was therefore analysed using a powder briquette.

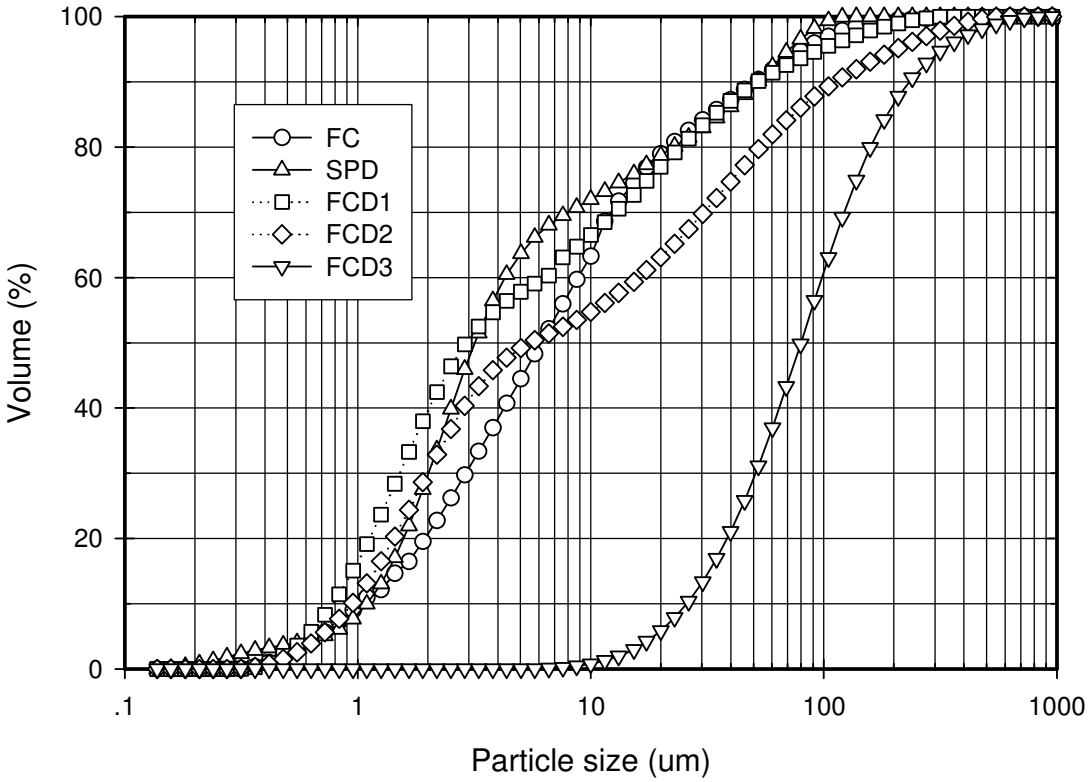

Figure 3.3 The particle size distributions of the original FC, SPD, FCD1, 2 and 3

The bulk density, moisture content and pH of these wastes are presented in Table 3.1. It can be seen from Table 3.1 that sample FCD3 has the highest bulk density (2.42 gcm^{-3}) while sample FCD1 (0.49 gcm^{-3}) has the lowest bulk density of the examined waste materials. The moisture contents of the dust range between 0.4 and 1.06%. It was also found that the EF dust and filter cake all generate basic solutions (pH>8) when leached in water.

Table 3.1 Physical properties of the EF dust and filter cake

	SPD	FCD1	FCD2	FCD3	FC
Bulk density (g/cm^3)	1.39±0.1	0.49±0.2	0.93±0.2	2.42±0.1	1.18±0.2
Moisture content (%)	0.40±0.01	1.06±0.02	0.93±0.06	0.48±0.03	nd*
pH value (in H_2O)	11.96±0.02	8.08±0.01	8.48±0.03	11.18±0.02	10.02±0.00

*nd-not determined

3.3.2 Chemical Composition and Phase Composition of the EF Dusts and FC

The chemical compositions of the EF dust and filter cake are given in Table 3.2. The SPD is iron oxide, chromium oxide and CaO rich, but also contains some MgO, MnO, SiO_2, ZnO and nickel. The FCD1 and 2 contain significant concentrations of SiO_2, ZnO, MgO and alkali metal oxides, but also some sulphur and chlorine, while FCD3 is SiO_2-chromium oxide-iron oxide-Al_2O_3-MgO-C-based. The concentrations of calcium, fluorine, iron and sulphur are high in the filter cake.

Table 3.2 Chemical analysis of the EF dusts and filter cake [2)]

%	SPD	FCD 1	FCD 2	FCD 3	FC
SiO_2	4.81	35.25	40.31	26.60	1.74
TiO_2	0.08	0.09	0.08	0.67	0.05
Al_2O_3	0.40	5.01	3.92	12.55	0.62
Fe_2O_3	43.4	2.82	2.21	15.23	20.0
MnO	5.08	0.43	0.53	0.22	0.98
MgO	5.44	11.85	19.09	11.93	1.21
CaO	12.9	0.52	0.38	2.41	39.6
Na_2O	0.60	10.21	6.54	1.78	0.35
K_2O	0.97	2.63	3.92	1.01	0.03
P_2O_5	0.04	0.03	0.03	0.03	0.04
Cr_2O_3	14.6	3.26	3.42	23.34	3.15
NiO	2.79	0.02	0.02	0.10	1.50
V_2O_5	0.09	0.02	0.02	0.23	0.03
ZnO	4.49	15.10	9.58	0.73	0.40
MoO_3	1.35	nd	nd	nd	0.08
Ga_2O_3	nd*	0.52	0.20	0.02	nd
PbO	0.39	0.10	0.07	0.01	nd
SO_3	0.47	3.38	2.37	1.89	7.25
F	nd	0.81	0.04	0.01	22.5
Cl	0.86	3.32	0.95	0.89	0.06
LOI	-0.21	8.12	6.48	nd	13.90
Total	98.55	103.49	100.16	99.65	113.49
C	0.68	1.58	1.17	9.97	1.01
Fe (T)	31.6	1.69	1.50	12.0	12.40
Fe (0)	1.13	<0.01	<0.01	0.07	ud**
Fe (II)	5.49	0.56	0.16	0.65	ud
Fe (III)	24.98	1.12	1.33	11.28	12.40

*nd-not determined **ud-undetectable

[2)] Any metallic particles present (stainless steel, ferrochrome or nickel) have been converted into oxide species during the sample preparation procedure for XRF analysis. Distinction is only made between the oxidation states of iron.

Table 3.2 also shows that SPD contains approximately 5.5 wt % ferrous components, while the Fe (II) content is less than 0.65 wt % in the ferrochrome dust. In filter cake, the concentration of Fe (II) is undetectable, and it is believed that it is lower than 100 ppm.

XRD (Figure 3.4) and EDS analyses indicate that the SPD mainly contains a $(Mg,Fe,Mn,Cr)_3O_4$ spinel phase, quartz, CaF_2, pure Ni particles, stainless steel particles, $Ca(OH)_2$ and a glassy slag phase. The major phases that are present in dust samples FCD1 and FCD2 include NaCl, ZnO, MgO, Mg_2SiO_4, chromite particles, cristobalite, ferrochrome particles and a glassy slag phase. Small amounts of zinc hydroxy-chlorosulphate hydrate $[NaZn_4(SO_4)Cl(OH)_6{\cdot}6H_2O]$ and zinc sulphate hydroxide hydrate $[Zn_4SO_4(OH)_6{\cdot}5H_2O]$ could also be detected by XRD. Moreover, an amorphous phase was identified in the ferrochrome fine dusts, which is presumably associated with carbon and silica in the dusts. The coarse ferrochrome dust sample (FCD3) contains chromite and partially altered chromite (PAC) particles, carbon, quartz, $(Ca,Mg)(CO_3)_2$ and a glassy slag phase from which anorthite $[(Ca,Na)(Si,Al)_4O_8]$ precipitated.

Fluorite (CaF_2) is the major phase in the filter cake, while $CaSO_4$, $CaCO_3$, an amorphous metal oxide rich phase, a few lime particles and undissolved stainless steel scale are also present.

Raman analysis was used to confirm the crystalline information in the ferrochrome fine dust. A typical Raman spectrum for FCD 2 is shown in Figure 3.5. It shows the existence of Raman bands at 453, 551, 691, 854, 986, 1346, 1394 and 1595 cm^{-1}. The bands at 1346, 1394 and 1595 cm^{-1} can be attributed to amorphous carbon materials [129]. The bands at 551 and 691 cm^{-1} are associated with chromite particles, of which the major peaks shift towards 680~770cm^{-1} with a change in (Cr+Fe)/(Cr+Fe+Al) ratio [130]. The remainding bands at 453, 854, 986 cm^{-1} can possibly be attributed to Mg_2SiO_4 [131].

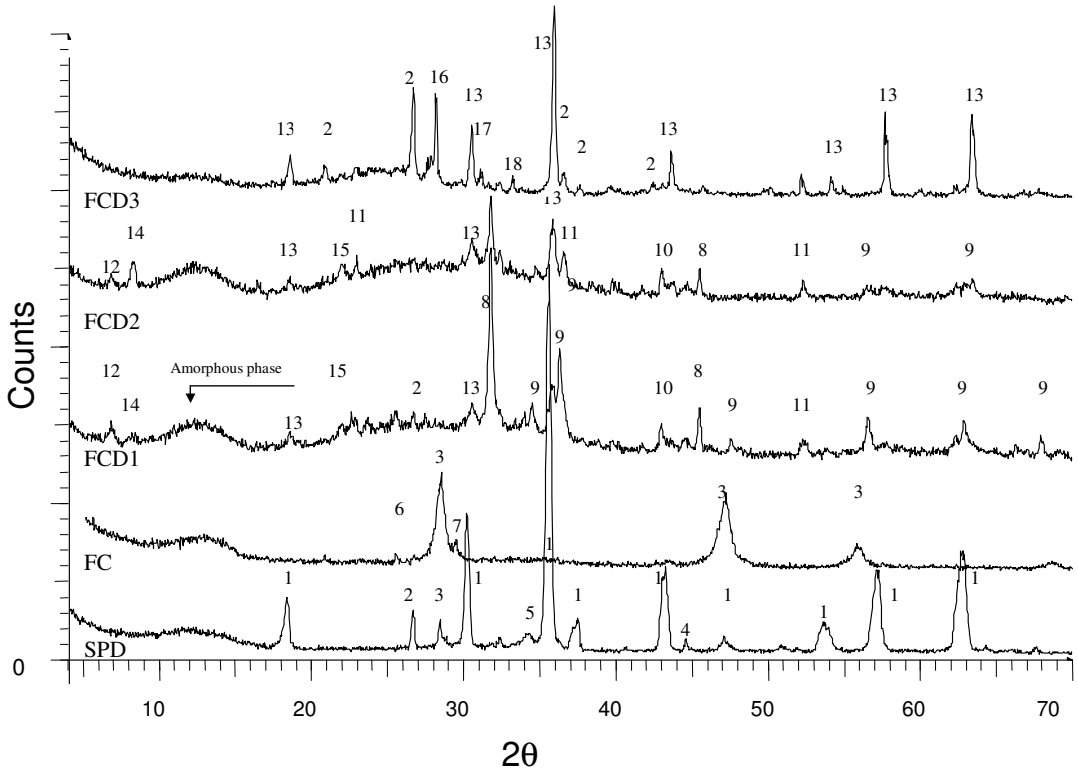

1-$(Mg,Fe,Mn,Al,Cr)_3O_4$ 2-Quartz SiO_2 3-CaF_2 4-Ni 5-$Ca(OH)_2$ 6-$CaSO_4$ 7-$CaCO_3$ 8-NaCl 9-ZnO 10-MgO 11-Mg_2SiO_4 12- $NaZn_4(SO_4)Cl(OH)_6{\cdot}6H_2O$ 13-$(Fe,Mg)(Cr,Fe,Al)_2O_4$ 14-$Zn_4SO_4(OH)_6{\cdot}5H_2O$ 15-Cristabolite SiO_2 16-$(Ca,Na)(Si,Al)_4O_8$ 17-$CaMg(CO_3)_2$ 18-Fe_2O_3

Figure 3.4 XRD patterns of the EF dusts and filter cake

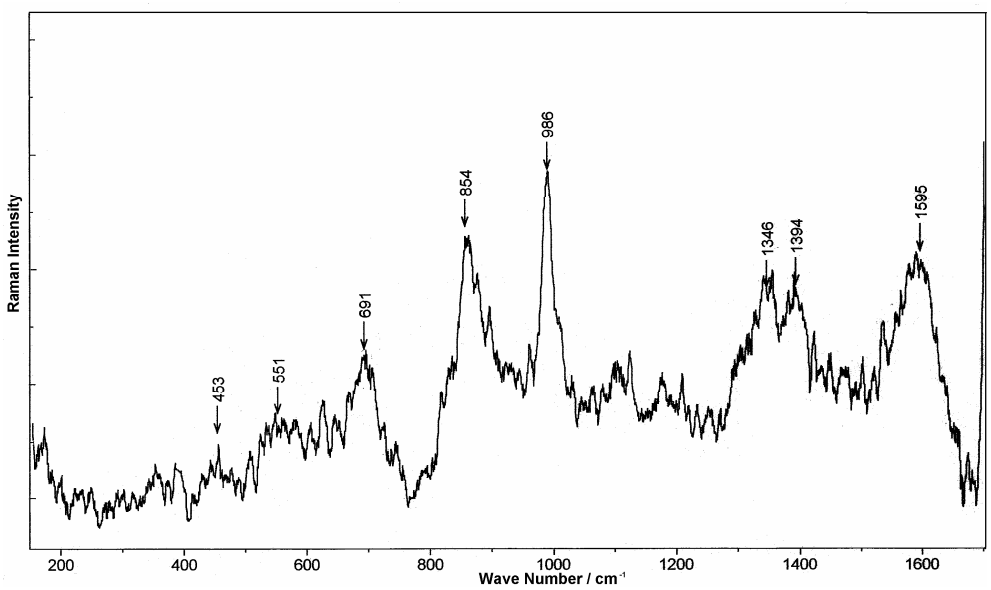

Figure 3.5 Typical Raman spectrum obtained for the ferrochrome fine dust (FCD2)

FT-IR spectroscopy was also used to identify the crystalline phases in the waste samples, specifically the crystalline hydrate phases. Zinc oxide, silica, cristabolite, magnesium oxide, forsterite (Mg_2SiO_4) and halite have strong peaks at 400~500 cm^{-1}, 1100 cm^{-1}, 1100 cm^{-1}, 550 cm^{-1}, 1100 cm^{-1} and 200 cm^{-1}, respectively [132]. The hydrate crystal $NaZn_4(SO_4)Cl(OH)_6{\cdot}6H_2O$ has bands at 3342, 3401, 3442 and 3507 cm^{-1} for the O-H stretching and, 1639 and 1672 cm^{-1} in the HOH bending vibration region as well as 1116, 988, 784 and 603 cm^{-1} for the SO_4 and Zn-OH vibrations [133]. The absorbance FT-IR spectra of the ferrochromium fine dust and the synthetic $ZnSO_4{\cdot}Zn(OH)_3{\cdot}5H_2O$ is shown in Figure 3.6a. It shows that FCD1 and 2 have bands at approximately 3549, 3476, 3414, 1639, 1620, 1110, 1030, 618 and 475 cm^{-1}. Synthetic $ZnSO_4{\cdot}Zn(OH)_3{\cdot}5H_2O$ with minor amounts of $ZnSO_4{\cdot}6H_2O$ crystals has peaks at 3510, 3409, 3338, 1670, 1639, 1119, 989, 798, 610, 508 and 434 cm^{-1} (Figure 3.6b) [3)]. Therefore, it can be concluded that small amounts of hydrate crystalline phases exist in the ferrochrome fine dust.

3.3.3 TG/DTA Analysis

The TG curve for SPD shows a total weight loss of 2.75% (Figure 3.7a). The initial weight loss originated from the loss of absorbed water. The calcium hydroxide dehydrates between 380°C and 480°C with an endothermic peak in the DTA curve. Furthermore, two marked increases in mass occur in the temperature range of 480°C-640°C and 740°C-940 °C. The first increase in mass is associated with the oxidation of the Fe (II) and Fe (0) species to Fe (III) [134]. The second mass gain can be associated with the oxidation of nickel [135]. Between the two mass gain stages a 1.25% weight loss is associated with the decomposition of carbonates, as FTIR analysis indicated that carbon dioxide was expelled from the sample. SEM analysis (Figure 3.8) indicated that the SPD sample that was heated to 1300°C, contained a substantial portion of a liquid phase, which caused the sample to sinter.

The mass losses of the ferrochrome dust samples FCD1, FCD2 and FCD3 are respectively 9.7%, 7.4% and 14.5%, in the 25-1300°C temperature range (Figures 3.7b-

[3)] The method whereby synthetic $ZnSO_4{\cdot}Zn(OH)_3{\cdot}5H_2O$ crystals was produced is described in Chapter 4.

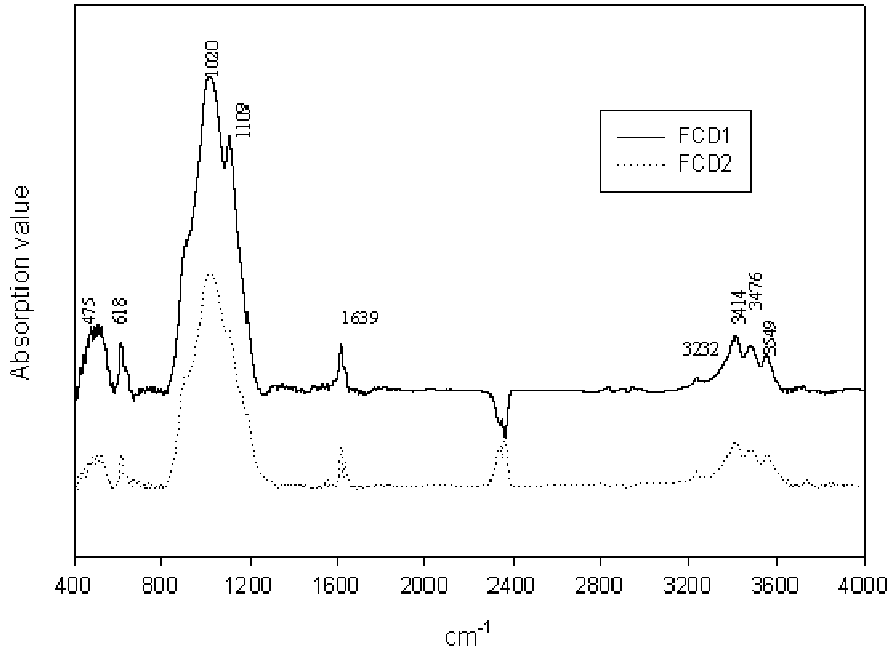

(a) FCD1 and FCD2

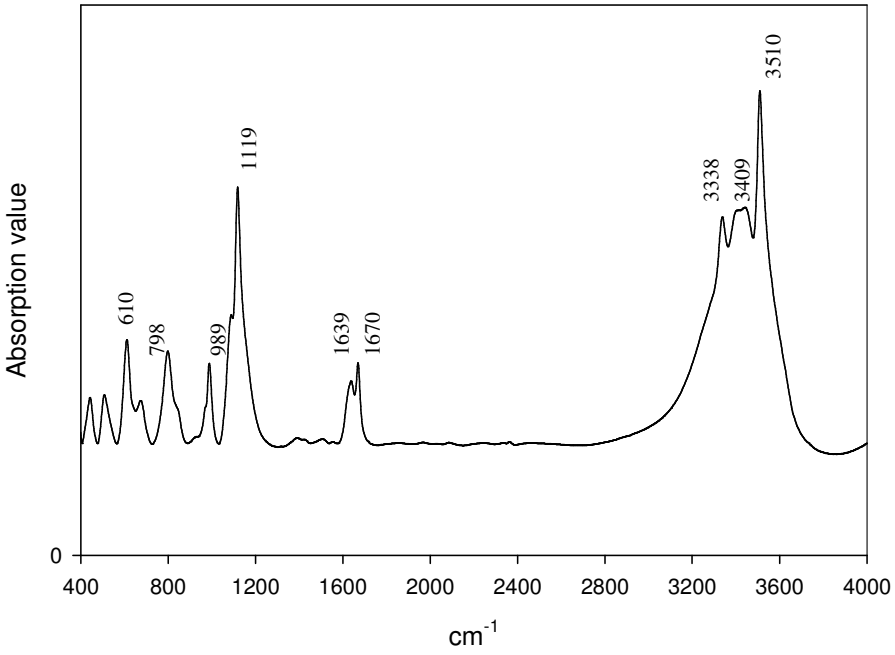

(b) Synthetic $ZnSO_4 \cdot Zn(OH)_3 \cdot 5H_2O$

Figure 3.6 Absorbance FT-IR spectra of FCD1 and FCD2 (a), and synthetic basic zinc sulphate hydrate (b)

d). The coarse dust (FCD3) did not lose any mass at temperatures above 900°C, and remained thermally stable up to the maximum test temperature of 1300°C. The larger mass loss of FCD3 can be attributed to the combustion of carbon with an exothermic peak at 600°C [136] and the decomposition of carbonates. The TG/DTA curves of the FCD1 and FCD2 samples show similar trends. The absorbed water is vaporised at ~100°C. An endothermic peak at ~220°C is believed to be associated with the dehydration of zinc hydroxide layer in the zinc hydroxy-chlorosulphate hydrate [$NaZn_4(SO_4)Cl(OH)_6 \cdot 6H_2O$] [133] and zinc sulphate hydroxide hydrate [$Zn_4SO_4(OH)_6 \cdot 5H_2O$]. More than half of the weight loss occurs at temperatures above 800°C. Small quantities of carbon dioxide were detected by FTIR in all three ferrochrome dust samples. This is presumably due to the decomposition of the carbonates and the oxidation of carbon. SEM-EDS analysis (Figure 3.9) of the residue of FCD2 indicated that chromite particles remained in the sample at 1300°C.

Figure 3.7e depicts the high temperature behaviour of the filter cake. A mass loss of approximately 15% was observed over the 25-1300°C temperature range. XPS analysis of the inside surface of the alumina lid of the crucible used in the TG/DTA analysis, indicated that fluorine, calcium, oxygen, sulphur and silicon containing compounds condensed on the lid. This can be interpreted as the loss of moisture at 100°C, dehydration up to 270°C, and the reaction of sulphates whereby $SO_2(g)$ and $SO_3(g)$ are driven off at temperatures above 600°C [137].

Figure 3.10 shows the DTG curves for the ferrochrome fine dust (FCD1 and FCD2). It shows that there is a peak below 100ºC due to the loss of absorbed water. A mass loss at approximately 220ºC is possibly associated with the dehydration of zinc hydroxide from Gordaite [$NaZn_4(SO_4)Cl(OH)_6 \cdot 6H_2O$] [133]. The DTA curves also show an endothermic peak at the same position. As Bear et al [138] reported, the zinc sulphate hydroxide hydrate would change into an anhydrate product $ZnSO_4 \cdot Zn(OH)_3$ after heating up to 175ºC. The DTG curve of $ZnSO_4 \cdot Zn(OH)_3 \cdot 5H_2O$ has a peak at approximately 290ºC. For

(a) TG/DTA curve of SPD

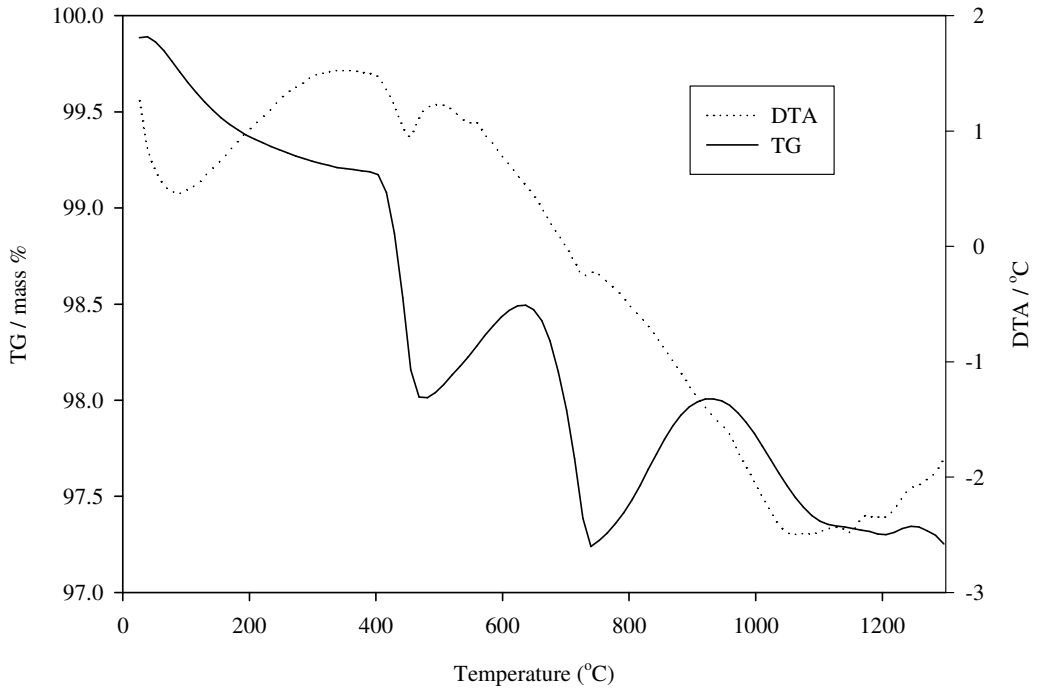

(b) TG/DTA curve of FCD1

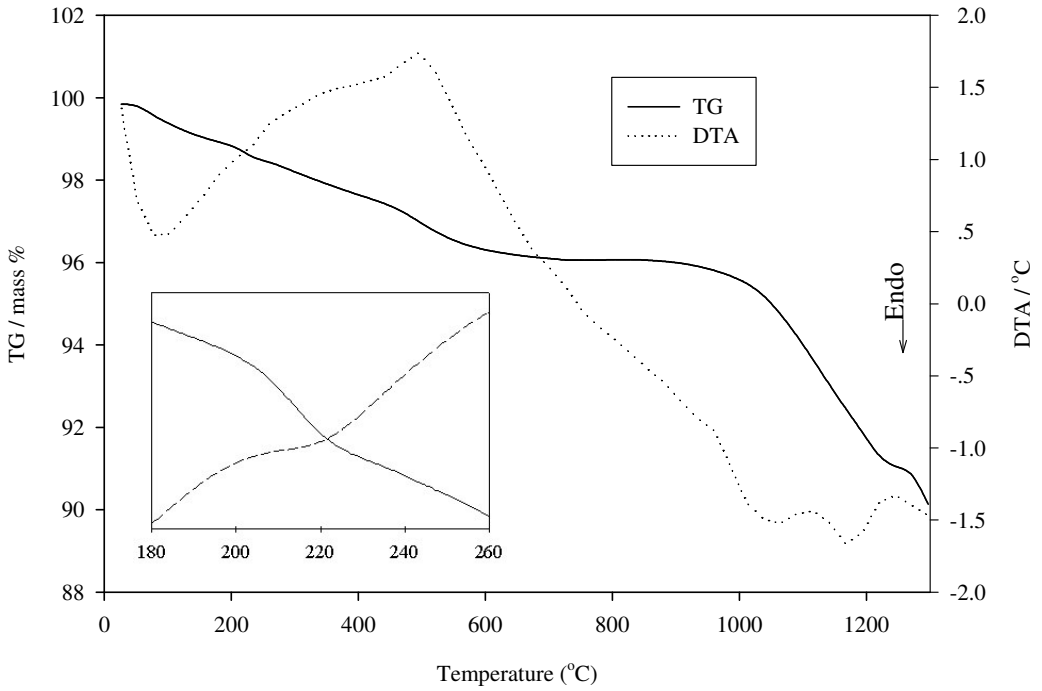

(C) TG/DTA curve of FCD2

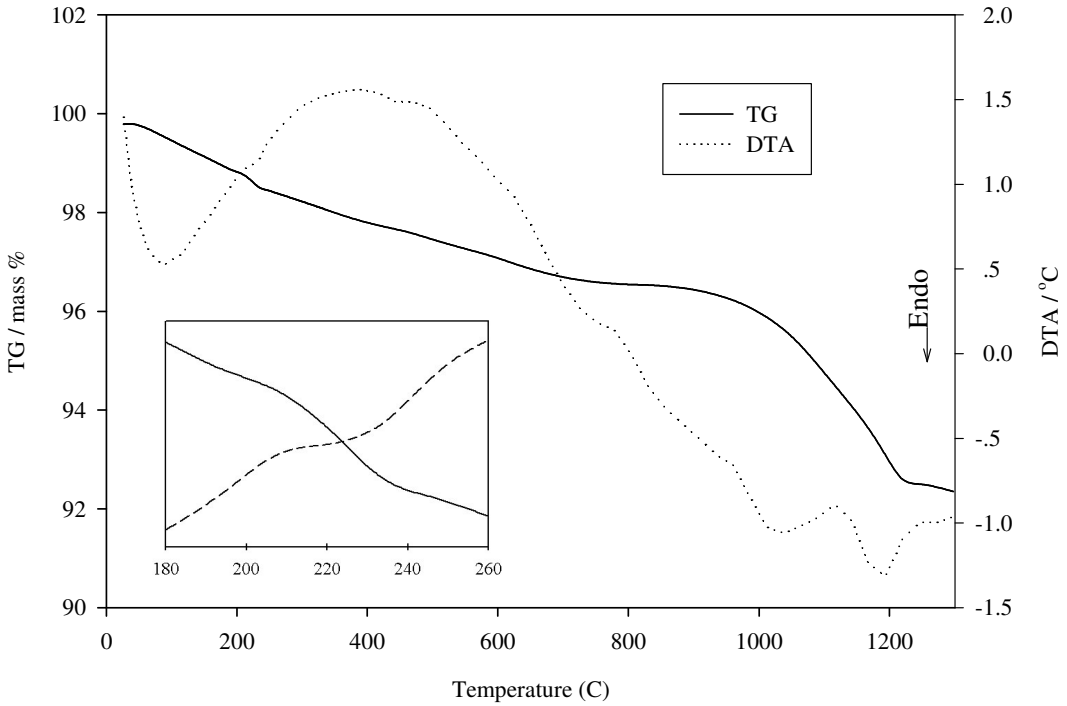

(d) TG/DTA curve of FCD3

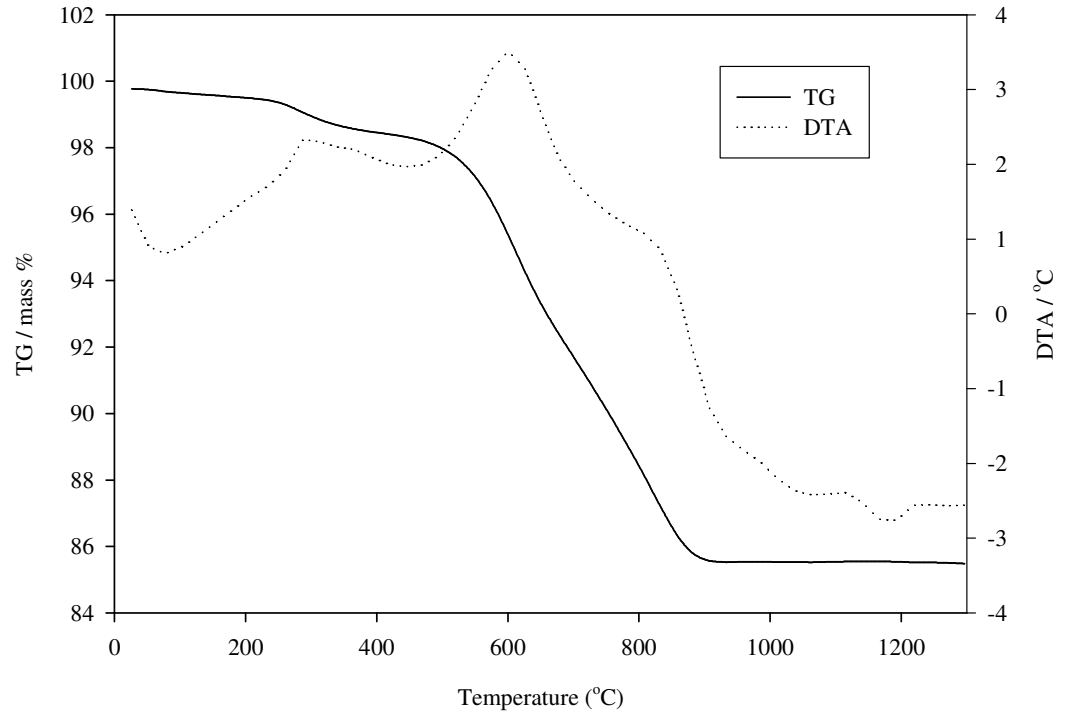

(e) TG/DTA curve of FC

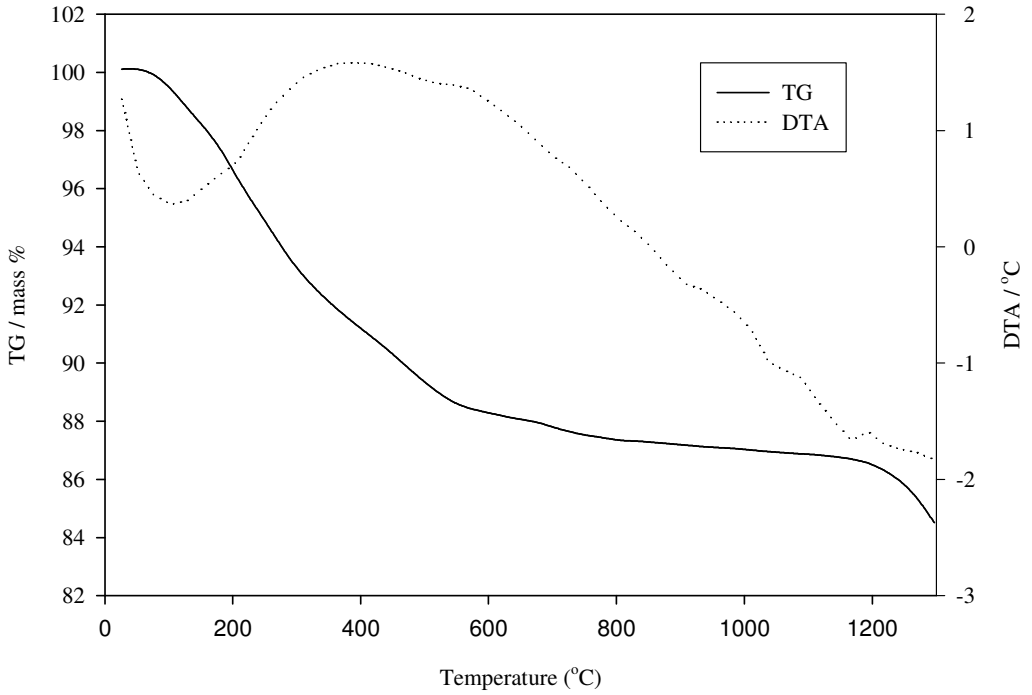

Figure 3.7 The TG/DTA curves of the EF dusts and filter cake

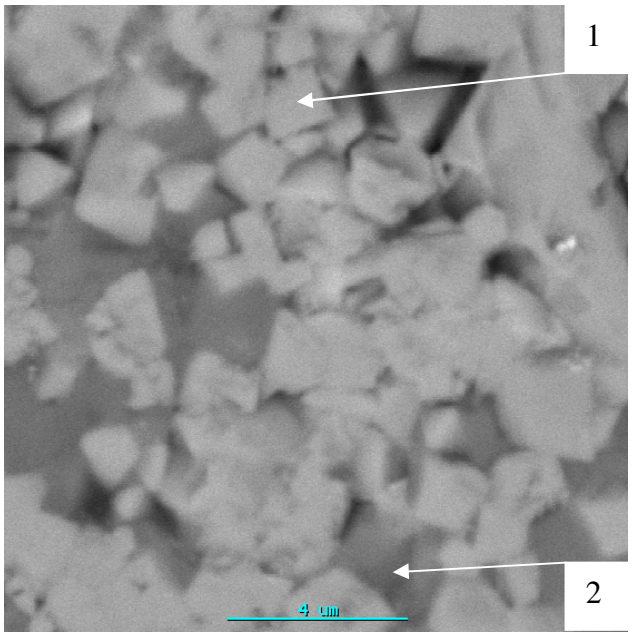

Figure 3.8 Backscatter electron image of the SPD after TG/DTA experiment (1-spinel; 2-glassy phase)

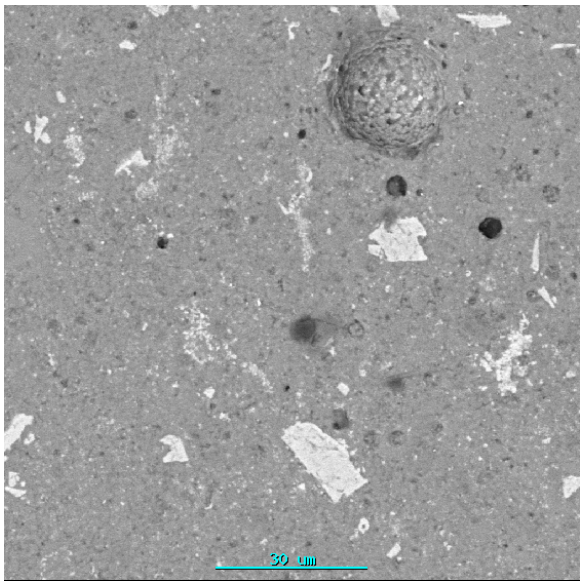

Figure 3.9 SEM image of the TG/DTA residue (FCD2)

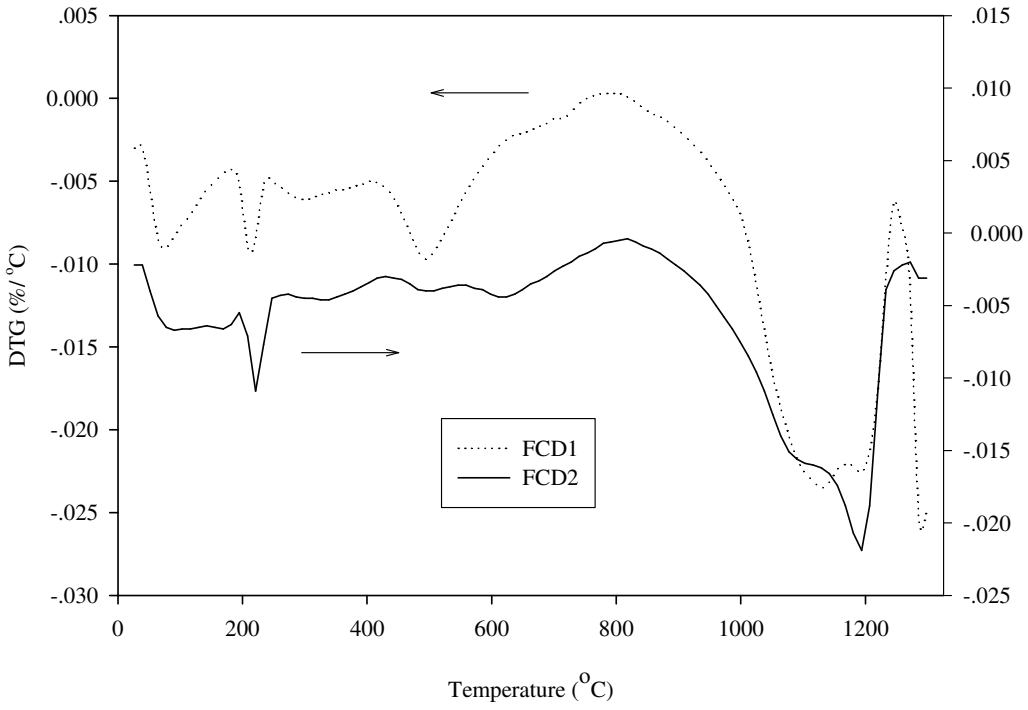

Figure 3.10 The DTG curves for the ferrochrome fine dusts

FCD1, the DTG curve shows a small peak at 299ºC. It is possibly associated with the decomposition of the anhydrate $ZnSO_4 \cdot Zn(OH)_3$. This confirms the presence of zinc sulfate hydroxide hydrate. There is no evidence from the DTG curve of the FCD2 which can confirm the existence of $ZnSO_4 \cdot Zn\ (OH)_3 \cdot 5H_2O$, possibly due to the lower concentration in the sample.

3.3.4 XPS analysis of the EF dust

The electric furnace dust samples were also characterized by XPS. Figure 3.11 shows the surface elements survey of the dusts by XPS. It shows that zinc, halogens (F, Cl), alkali metals (K, Na) and the elements O, Cr, S and Si are present on the surface of the ferrochrome dust. The major elements on the surface of the SPD are Zn, O, Si and Mg, while Na, F, Cr, K, C, Cl, Ca and Fe are present in minor amounts.

The elements that exist on the surface of the electric furnace dust are shown in Table 3.3. It indicates that oxides and elements, which vaporise at high temperatures, are the major components on the surface of FCD1 and FCD2 particles. On the surface of the ferrochrome coarse dust, carbon and silicon oxides are the major substances. It also shows that the Na, Zn, K, total Cr and Cl concentrations on the surface of the ferrochrome fine dusts are higher than those on the surface of the ferrochrome coarse dusts.

The chromium species on the surface of the FCD2 particles were specifically considered. A mathematical curve fit procedure of the Cr $2p_{3/2}$ photoelectron peak was performed in order to identify peak positions that are associated with binding energies of 574.28eV, 576.07eV, 577.62eV and 579.76eV (Figure 3.12). By comparing these binding energies with standard spectra of various chromium species [128], it can be assumed that the lowest binding energy (574.28±0.2eV) is associated with chromium (0) and that the binding energies of 576.07±0.2eV and 577.62±0.3eV are associated with Cr_2O_3 and $Cr(OH)_3$ respectively. The highest binding energy (579.76±0.2eV) is associated with CrO_3, CrO_4^{2-} or $Cr_2O_7^{2-}$. Chromium present in oxidation states (0), (III) and (VI) are therefore associated with the surface layers of fine dust particles of FCD2.

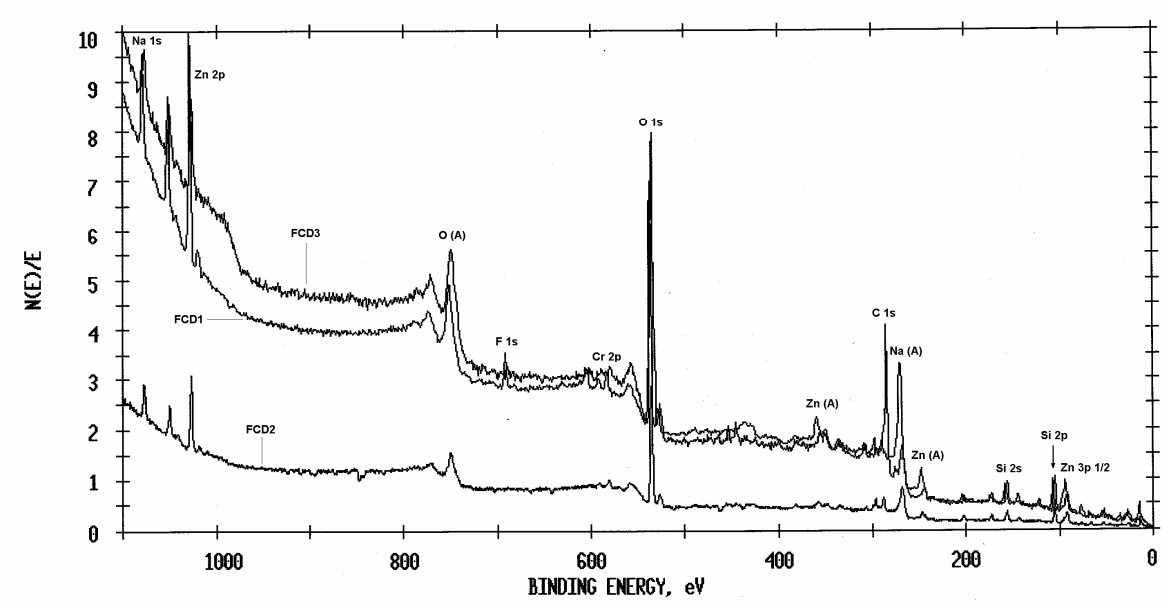

(a) Ferrochrome dust

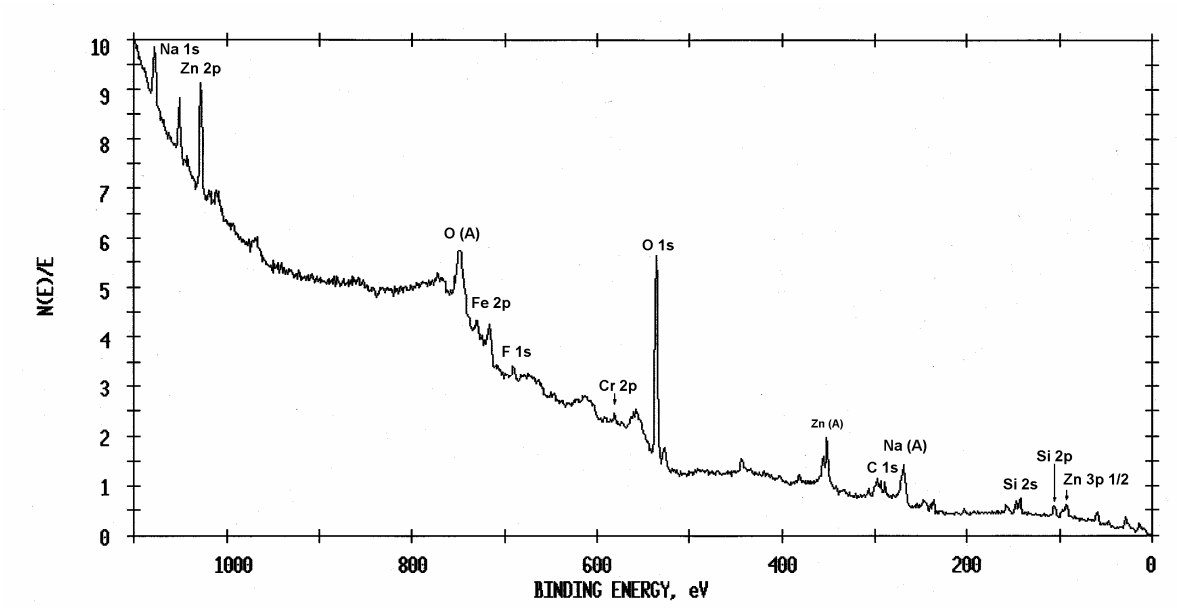

(b) SPD

Figure 3.11 Surface elemental survey of the ferrochrome dust (a) and SPD (b)

Table 3.3 Surface element analysis of the dusts by XPS (atomic%)

Element	Chemical state	FCD1	FCD2	FCD3	SPD
Na	Na^{+}	7.21	5.80	1.63	4.47
Zn	Zn^{2+}	9.74	6.38	2.63	5.19
F	F^{-}	5.18	0.49	0.34	2.35
Cr	Cr, Cr^{3+}, Cr^{6+}	1.52	1.37	0.81	0.89
O	Oxides	53.07	54.98	44.53	55.10
K	K^{+}	1.49	2.12	0.32	1.00
C	C, CO_3^{2-}	5.93	9.86	37.53	3.98
Cl	Cl^{-}	1.46	2.13	0.81	0.95
S	SO_4^{2-}	1.32	2.61	1.32	0.09
Si	Si^{4+}	13.09	14.27	10.06	6.24
Ca	Ca^{2+}	nd*	nd	nd	3.08
Mg	Mg^{2+}	nd	nd	nd	12.05
Fe	Fe^{2+}, Fe^{3+}	nd	nd	nd	2.96

*nd - not determined.

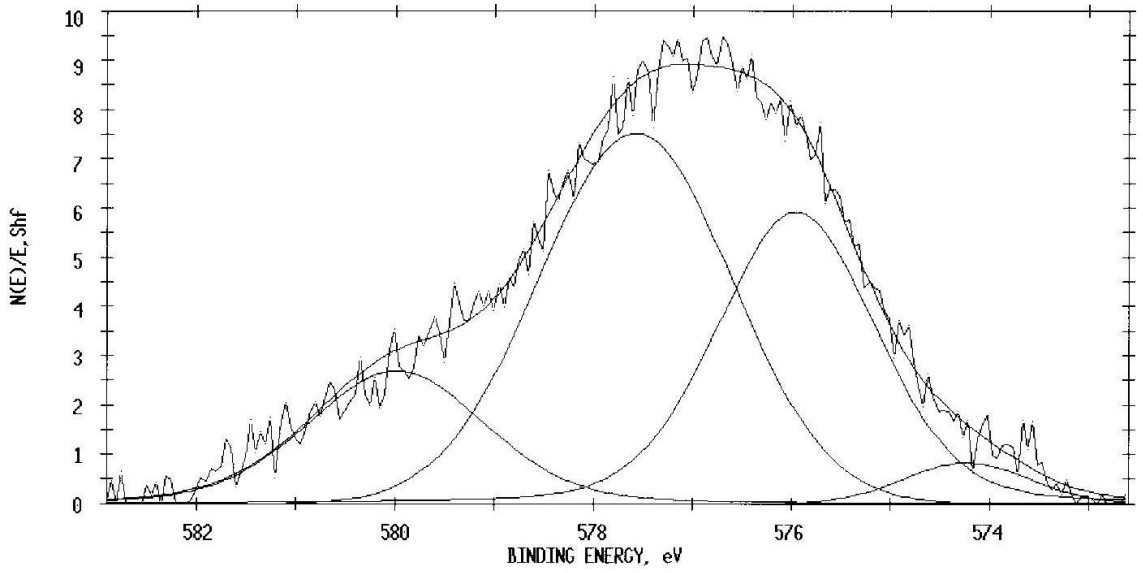

Figure 3.12 Mathematical curve fit of the Cr $2p_{3/2}$ photoelectron peak for sample FCD2

It is assumed that the presence of chromium (0) refers to the ferrochrome particles that are present in the dust, while the presence of chromium (III) species refers to the chromite ore. Chromium (VI) species, however, could not form in the furnace due to the reducing atmosphere that prevails during ferrochrome production. It can therefore be assumed that chromium (VI) species are formed at the top of the furnace or in the off-gas duct, where higher oxygen potentials exist. XPS analysis also indicated that chromium in the FCD2 sample is mainly present as chromium (III).

3.4 Discussion

As is shown in Figure 3.1, the EF dust samples have very small particle diameters. This would induce air-borne pollution when transported to stockpile at the waste site. It also makes it difficult to directly recycle it back to the furnace due to the small particles [139].

The leaching behaviour of chromium species by ground water is related to the pH of the environment and the redox potential of the aqueous solution [140]. In natural groundwater chromium has two stable oxidation states, i.e., Cr (III) and Cr(VI). Cr(VI) is the stable species under oxidising conditions that is found in shallow ground waters, whereas Cr(III) is thermodynamically stable under reducing conditions in deeper ground waters [140]. The dominant species of Cr(VI) are highly soluble $HCrO_4^-$ and CrO_4^{2-}. Under oxidizing conditions, in natural groundwater with a pH value between 6 and 8, the predominant species is CrO_4^{2-} [140]. In addition, CrO_4^{2-} prevails at high pH. It was also found that the EF dust samples and filter cake all generate basic solutions when leached in water (Table 3.1). The CrO_4^{2-} species can therefore potentially be leached from these materials in shallow groundwater. Moreover, the SPD generates the strongest alkaline solution, and therefore requires a large amount of acid for neutralisation before being disposed.

According to the "Minimum requirements for the handling, classification and disposal of hazardous wastes" [15], recycling or recovering of the valuables in the wastes back to the production process is the best way to treat it. However, one has to consider the

environmental and economic factors of the process besides resource utilization. The basic concept of developing a process to treat wastes is shown in Figure 3.13. It shows that the developed process should consider all three of these aspects. It is acceptable only in the shaded area (Figure 3.13).

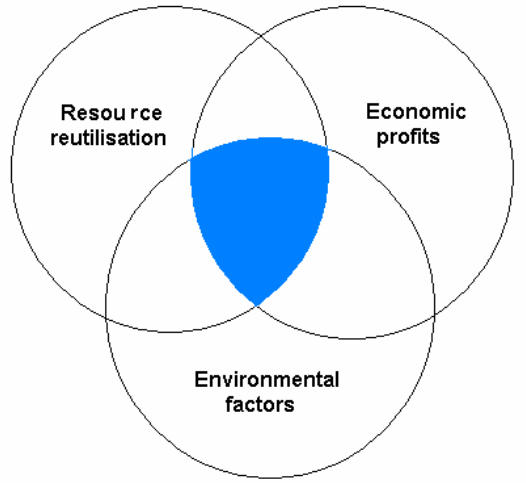

Figure 3.13 The waste treatment process by considering resource utilization, environmental and economic factors

The SPD contains large amounts of alloying elements such as Fe, Cr, Ni and Mo which are in the form of pure nickel, spinel phase and metal droplets. It also contains minor amounts of valuable components that vaporize such as Zn. Recovery of these valuables can therefore potentially be performed by minerals processing methods (gravity separation and magnetic separation) due to the different densities and magnetic properties of the particles [39]. However, the toxic substances such as Cr (VI) can leach out during the minerals processing and hydrometallurgical operations, the wastewater of the processes therefore require further treatment.

The ferrochrome fine dust contains significant levels of SiO_2, ZnO, MgO and alkali metal oxides. It also contains small amounts of Fe, Cr and Ga. It seems that zinc is the most valuable substance in the ferrochrome dust which could be recovered. Alkali metal containing components can be expected to vaporise with Zn if pyrometallurgical recovery methods are employed, and would therefore influence the quality of the Zn-bearing

products. The Cr (VI) and soluble salts can leach out as a secondary waste if hydrometallurgical methods are used.

Filter cake contains Fe, Cr and Ni in the amorphous phase and crystalline phases such as CaF_2 and $CaSO_4$. The disadvantage of recycling the valuables in the filter cake (Fe, Cr and Ni) back to the steelmaking process is high concentrations of fluorite and sulphate, which will impact on the quality of the stainless steel.

The solidification/stabilisation processes are therefore widely considered to be an effective method that can encapsulate, glassify or combine the toxic elements, and simultaneously add value to these wastes. The secondary wastes are also minimised in these processes.

3.5 Conclusions

The size distribution, bulk density, moisture content, pH, thermal properties, chemical composition, phase composition and microstructure of Cr (VI)-containing EF dusts and filter cake were characterized. The following conclusions can be drawn:

1) The EF dusts are very fine particles, have bulk densities that vary between 0.49 and 2.42gcm^{-3}, and have low moisture contents.
2) On leaching in water the examined EF dusts and filter cake produce alkaline solutions. Since water-soluble Cr(VI) species are the stable species in alkaline solutions under oxidization conditions, it can be expected that Cr(VI) species will leach from these materials.
3) The main phases that are present in the SPD are the $(Mg,Fe,Mn,Cr)_3O_4$ spinel phase, quartz, $Ca(OH)_2$ and nickel. The dominant phases of the coarse fraction of ferrochrome plant dust are chromite, partly altered chromite, quartz and carbon, while the main components of the fine fractions include chromite, SiO_2, ZnO, NaCl and Mg_2SiO_4. The major phase present in the filter cake is CaF_2.
4) TG/DTA analysis in air indicated that mass losses and gains occur during heating of these waste materials due to reactions in which H_2O, CO_2, SO_2, SO_3, fluorine, calcium and silicon are driven off, and metallic particles oxidize.

5) It is assumed that Cr (VI)-containing species in ferrochrome dust are generated at the top of the SAF or in the off-gas duct, as Cr (VI) is found on the surface of the dust.
6) A stabilisation/solidification process is likely the best method whereby these wastes can be treated.

Chapter 4 The formation mechanisms of Cr(VI)-containing electric furnace dust and filter cake from a stainless steel waste treatment plant

In order to minimise the generation of these wastes, the microstructures and formation mechanisms of the wastes first need to be understood. This chapter subsequently describes the microstructures and formation mechanisms of the dust and filter cake in order to provide suggestions on how to reduce the amounts of these wastes.

4.1 Experimental

4.1.1 Sample Preparation

Three ferrochrome dusts samples (FCD1, FCD2 and FCD3), one stainless steel plant dust sample (SPD) and a filter cake sample (FC) were obtained from the same ferrochromium and stainless steel plants as discussed in Chapter 3. Representative sub-samples were produced from each of these samples for analysis.

4.1.2 Analytical Methods

Polished sections of the electric furnace dust and filter cake as well as the unmounted samples of waste were examined by scanning electron microscopy (JSM-6300), using energy dispersive X-ray spectrometry (EDS). The crystalline phases present in the samples were identified by X-ray diffraction (XRD) (Siemens D-501, Cu *K*α radiation, 40kV and 40mA).

4.2 Results

4.2.1 Steel plant dust

Stainless steel plant dust particles are of varying microstructure, and can be divided into three categories: (1) particles that are irregular in shape, (2) spherical or near spherical particles and (3) particles coated with slag or oxides. The particles that are spherical or near spherical, as well as the spherical particles that are coated with slag or oxides, are the most abundant in the SPD sample.

The particles that are irregular in shape include pure nickel (Figure 4.1), quartz, lime, fluorspar and ferrochrome particles. It is clear that these particles were captured by the off-gas during charging.

The spherical or near spherical particles include metal particles (Figure 4.2) and slag particles. These particles range from submicron to more than 200µm in diameter. The slag particles are either hollow (Figure 4.3) or consist of a glassy silicate-based matrix that contains oxide crystals (Figures 4.4-4.6) and metal droplets (Figure 4.7). The oxide crystals are either cubic (Figure 4.4), dendritic (Figure 4.5) or needle-like (Figure 4.6). EDS analysis indicated that the cubic and dendritic crystals are $(Mg,Fe,Mn)(Cr,Al)_2O_4$ spinel crystals, while the needles are $CaCr_2O_4$. Spherical stainless steel particles (Fe-3.0 wt% Cr-7.2 wt% Ni-3.9wt% Mo) that are coated with slag were also found (Figure 4.7). Slag particles that are covered with an oxide layer, which is of different chemical composition to the centre of the particle, could also be distinguished. Such slag particles are shown in Figures 4.8 and 4.9. X-ray mapping indicated that the centres of these types of particle are enriched in Cr, Ca and Al, while the rim is rich in Zn and Fe (Figure 4.9).

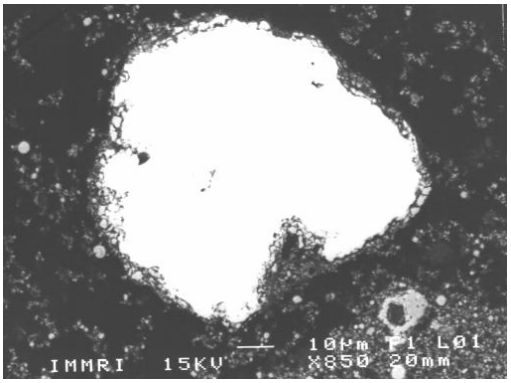

Figure 4.1 A nickel particle (SPD).

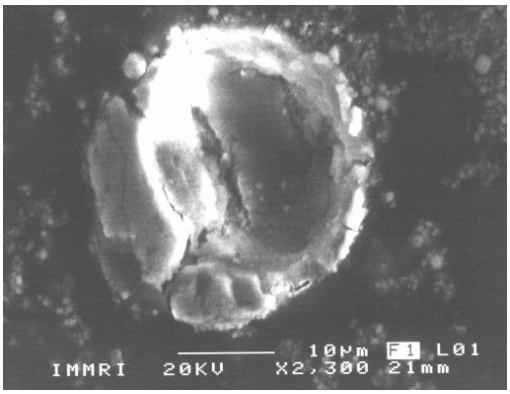

Figure 4.2 A hollow spherical metal particle (SPD).

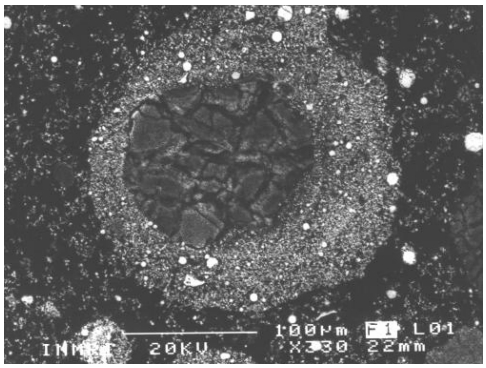

Figure 4.3 A hollow slag particle (SPD).

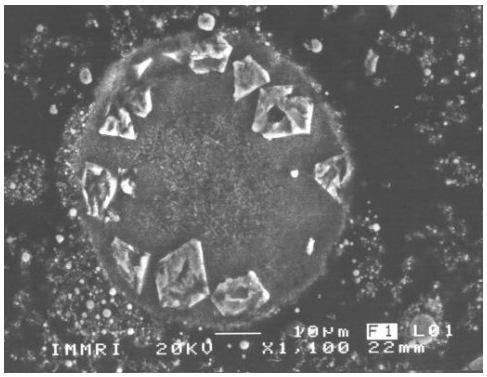

Figure 4.4 A spherical slag particle with cubic spinel crystals (SPD).

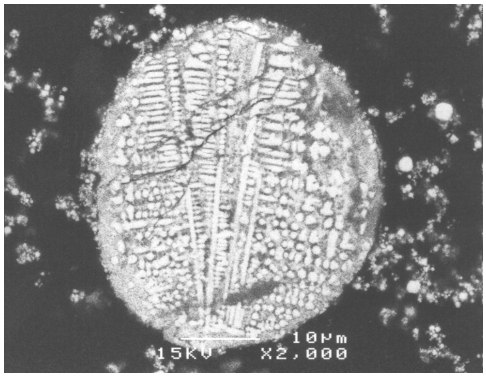

Figure 4.5 A spherical particle with dendritically precipitated crystals (SPD).

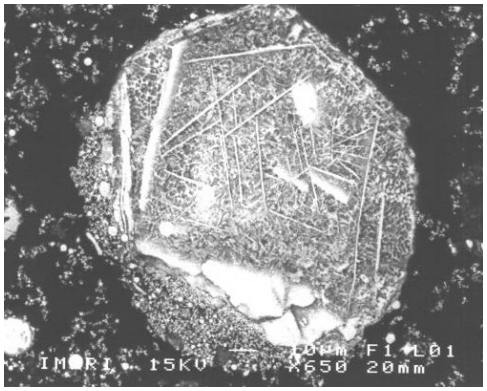

Figure 4.6 A spherical particle with precipitated $CaCr_2O_4$ needles (SPD).

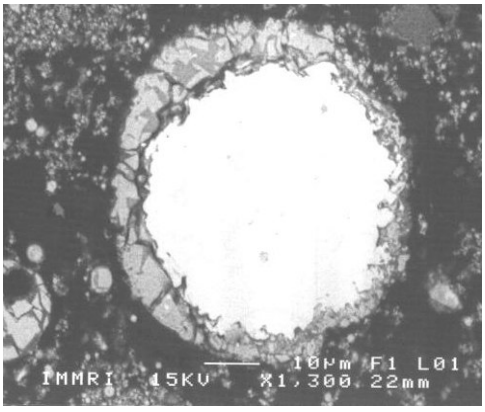

Figure 4.7 A stainless steel droplet, coated with slag (SPD).

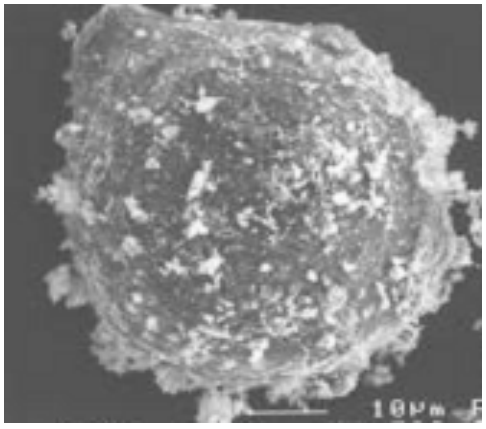

Figure 4.8 Slag droplet with a rim of small particles (SPD).

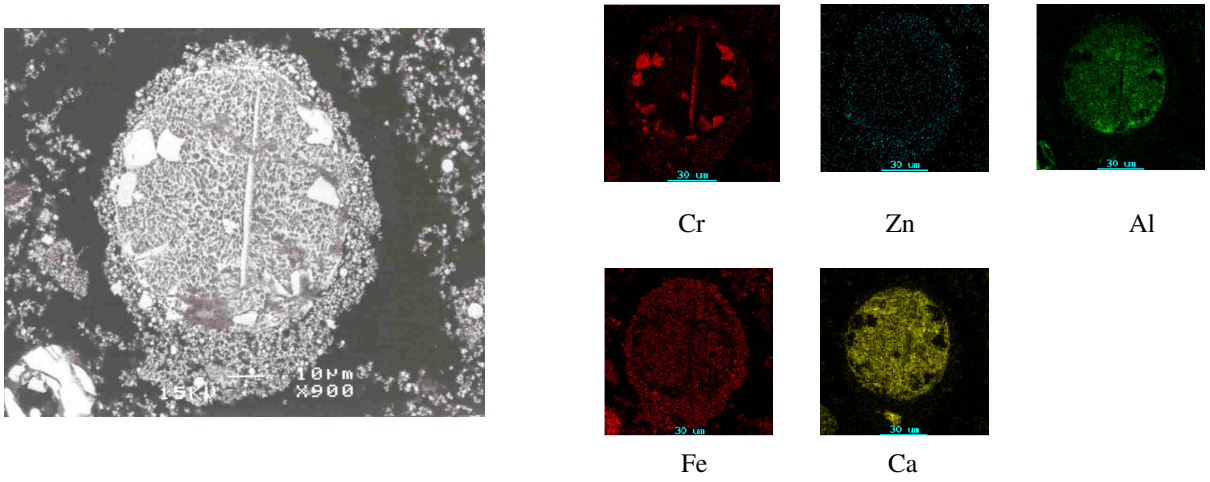

Figure 4.9 Backscattered electron image and X-ray map of a slag particle coated with a Fe-Zn-rich oxide layer (SPD)

4.2.2 Ferrochrome plant dust

The fine fractions of ferrochrome dusts (FCD1 and FCD2) mostly consist of agglomerated particles that formed clusters (Figures 4.10 and 4.11). Such clusters typically contain chromite and partly altered chromite (PAC) particles, reductant (C-based particles), metallic ferrochrome droplets, flux (quartz) and SiO_2-based slag droplets that are embedded in a matrix of very fine particles. This matrix is mainly SiO_2-MgO-ZnO-$(Na,K)_2O$ based.

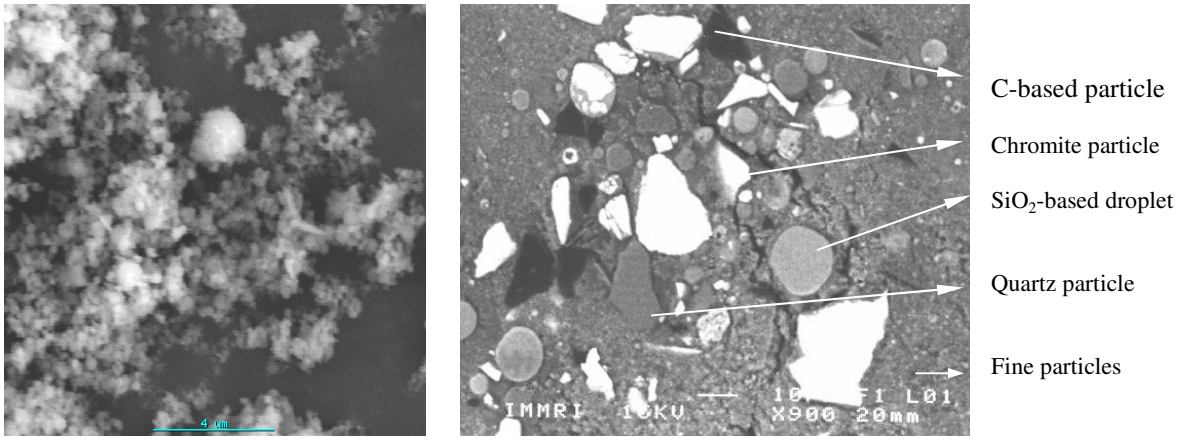

Figure 4.10 The FCD2 ferrochrome dust sample: (a) Agglomerated fine dusts; (b) Backscattered electron image of the typical microstructure.

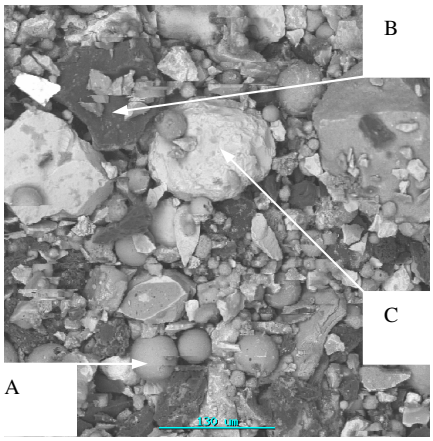

Figure 4.11 Microstructure of the FCD3 ferrochromium EF dust. (A): Slag droplet, (B) carbon-bearing material; (C) chromite ore.

The coarse fraction (FCD3) mostly contains particles that are irregular in shape, but also spherical or near spherical particles and particles coated with a slag layer. The particles that are irregular in shape include chromite ore particles, quartz particles and carbon-based particles. The spherical particles include metal particles, Si-Ca-Mg-Fe based slag particles, particles that contain spinel crystals and ferrochrome droplets that are embedded in a porous sodium-rich silicate slag layer (Figure 4.12), as well as chromite particles that are surrounded with a porous layer that contains some very small Cr-Fe-based metal droplets, followed by a more solid layer of Mg_2SiO_4 (Figure 4.13).

4.2.3 Filter Cake

The filter cake consists of very finely intergrown light grey areas that are Ca-F-S-O based, and dark areas that contain high concentrations of metal oxides of iron, chromium and nickel (Figure 4.14). XRD analysis indicated that the Ca-F-S-O-based areas consist of a mixture of CaF_2 and $CaSO_4$ while the metal-rich oxide phase is amorphous. The Ca-F-S-O based precipitate presumably formed due to super-saturation of the waste acid with respect to CaF_2 and $CaSO_4$ (solubility limits of 0.016g/l and 2.09g/l respectively [67]) in the neutralisation and reduction steps. It is assumed that the metal oxide-rich precipitate is the reaction product between the metal ions and the lime particles during the final

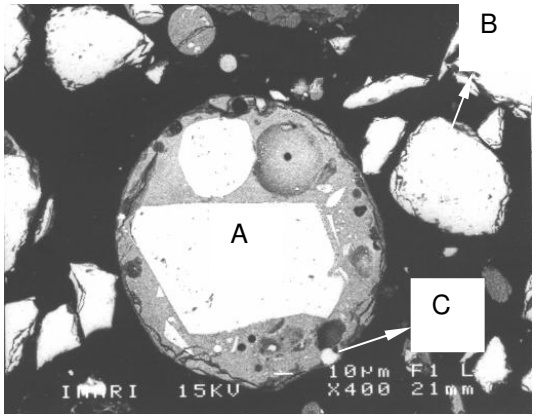

Figure 4.12 Spinel crystal in a sodium-rich silicate slag matrix (FCD3). [A=spinel crystal; B=PAC; C=FeCr droplet]

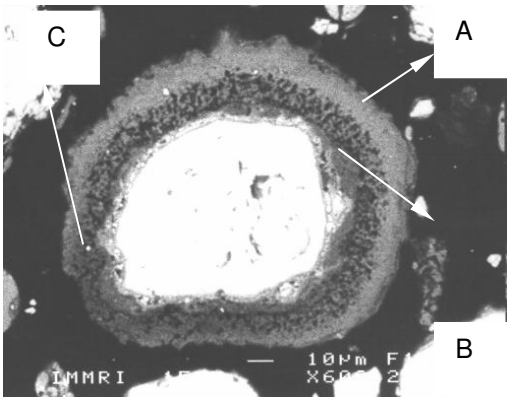

Figure 4.13 PAC particle with a Mg_2SiO_4-based rim (FCD3). [A=Mg_2SiO_4 rim; B=porous layer; C=FeCr droplets]

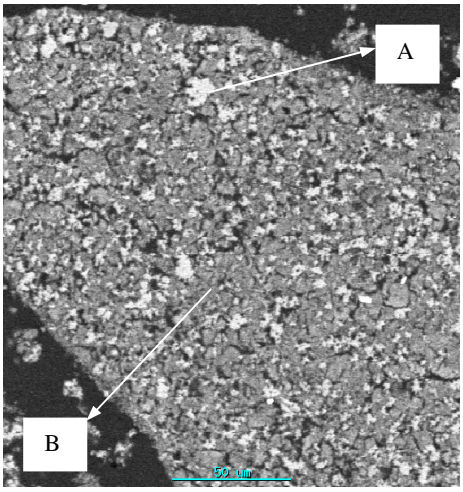

Figure 4.14 Typical SEM image of FC[A=Ca-S-F-O rich phase; B=Metal rich phase]

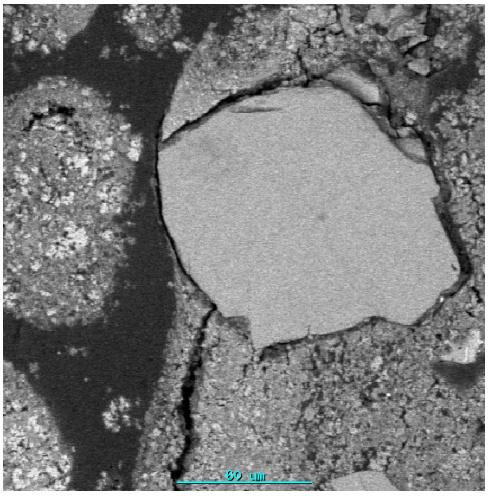

Figure 4.15 An un-reacted lime particle in the FC

precipitation step. Free lime particles (Figure 4.15) and undissolved stainless steel scale could also be distinguished in the filter cake.

4.3 Discussion

4.3.1 The formation mechanisms of stainless steel plant dust

Three different dust formation mechanisms have been reported to contribute to dust generation in the EAF and refining converter of stainless steel plants [23-37], i.e.,

(1) direct entrainment of the charged materials in the off-gas;

(2) evaporation or volatilisation of elements in the melting bath or high temperature zone of the furnace and later, oxidization or solidification of these elements in the off-gas duct and;

(3) ejection of slag and metal by spitting or bursting of gas bubbles such as carbon monoxide and argon gas. In the EAF and refining converter, the gas bubbles could entrain a thin layer of steel, enter the molten slag layer, and then burst into very fine metal droplets. When the gases escape the gas-slag interface, the film would break up on top of the bath. The falling slag can then generate waves on the surface of the molten bath whereby film droplets and jet drops can form. Moreover, the metal and slag droplets could also be ejected in the arc and oxygen-blowing zones.

In this study, the formation mechanisms of the wastes were determined from analyses of the processes and microstructures of the wastes. Fluorite (CaF_2), quartz (SiO_2) and nickel particles that were found in the examined SPD entered the bag house system through the entrainment of the charge materials in the off-gas. The $Ca(OH)_2$ formed through the hydration of lime particles which are also carried off by off-gas. These particles are all irregular in shape. Zinc is found on the surface of the dust particles (Figure 4.9). It seems that zinc is first vaporised and later condensed.

The spherical particles consist of metallic and slag particles which come from the melting bath. Spinel crystals and metallic droplets could also be found in the slag particles. These particles enter the off-gas duct by the bursting of gas bubbles. Primary spinel crystals could be found in certain of the slag particles, while in other slag particles the spinels crystallised on cooling.

4.3.2 The formation mechanisms of the ferrochrome dust

FACT Sage 5.1 was used in the theoretical prediction of the reactions that can contribute to dust formation during the production of ferrochrome in submerged arc furnaces (SAFs) (Figure 4.16) [141].

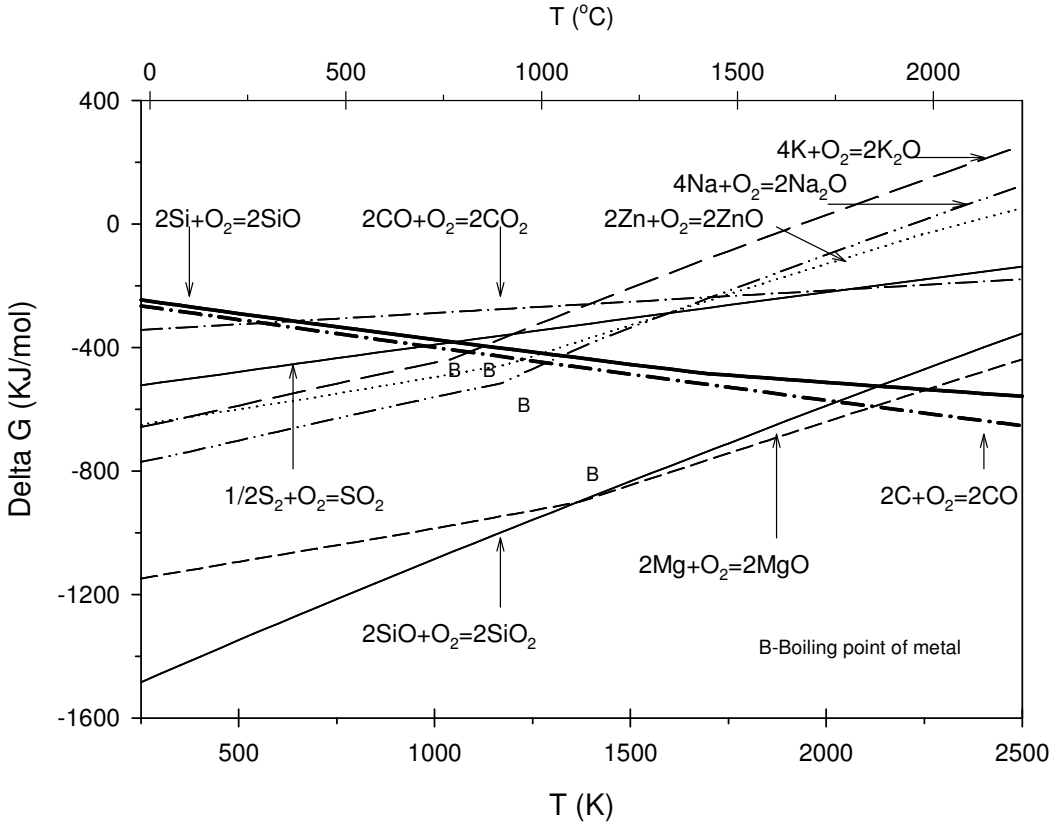

Figure 4.16 ΔG vs. temperature calculations for reactions that can contribute to dust formation during ferrochromium production, using FACT Sage 5.1

In the production of ferrochrome low oxygen partial pressures ($<10^{-8}$ atm [40]) prevail, during which the off-gas typically contains about 90% CO [8]. Under these conditions zinc, potassium and sodium in the charge can be reduced by carbon or CO gas at low temperatures (approximately 800-1100°C), after which they vaporise. These species can re-oxidise by the leakage of air or CO_2 gas and can then condense on other particles in the off-gas duct. SiO_2, which is either in the charge as quartz or in the slag, can also be reduced by carbon into SiO(g). Similarly magnesium oxide in the slag phase can be converted into Mg(g). These reactions can occur in the elevated temperature zone of the

SAF, especially near the electrode (>2000°C [142]). The SiO(g) and Mg(g) can easily re-oxidise into SiO_2 and MgO when the oxygen potential of the gas phase increases.

The moisture in the charge is also vaporised into the off-gas at high temperatures. Some inorganic components such as chlorine and sulphur from the carbon-based reductant would vaporise together with other metal elements or decompose. Coal, which contains volatile organic and inorganic substances, as well as volatile metals such as K and Na, is often used as a substitute for coke in the production of ferrochrome in order to reduce cost. The chlorine in coal typically ranges between 50-2000ppm in concentration, and vaporise at high temperatures in the form of HCl, NaCl and KCl [143,144]. Coal, coke and charcoal also contain significant levels of sulphur and heavy metals such as As, Cd and Pb. Sulphur is released into the off-gas through the formation of SO_2(g) and SO_3(g).

Gas species such as SiO, Mg, SO_2, SO_3, O_2, CO, CO_2, H_2O, Zn and NaCl, or reaction products between them, can therefore exist in the off-gas duct of the SAF. NaCl, Mg, SiO and Zn gases could first be oxidised by the off-gas and then condense. Mg_2SiO_4 can form through the reduction of chromite ore by the carbon-bearing reductant (Figure 4.13) or the reaction of SiO, Mg and oxygen in the off-gas duct. ZnO can react with SO_3 to form $ZnSO_4$ due to the oxidising atmosphere in the duct. XPS results showed that the major elements on the surface of these dusts are elements that vaporised (Chapter 3).

The synthetic hydrate samples were used to verify the possible formation of $NaZn_4(SO_4)Cl(OH)_6{\cdot}6H_2O$ and zinc sulfate hydroxide hydrate crystals in the ferrochrome fine dusts. Two mixtures were prepared from different molar ratios of ZnO, $ZnSO_4{\cdot}7H_2O$ and NaCl (AR grade), i.e. ZnO: $ZnSO_4{\cdot}7H_2O$ =3:1 and ZnO: $ZnSO_4{\cdot}7H_2O$: NaCl = 3:1:1, since ZnO, $ZnSO_4$, H_2O and NaCl possibly exist in the off-gas duct. These mixtures were placed in desiccators of which the bottoms were filled with water. The lid was closed with vacuum grease for approximately one week. The XRD patterns and SEM images of the reaction products are shown in Figure 4.17 and Figure 4.18. XRD and EDS analyse indicated that the main synthetic products are $Zn_4SO_4(OH)_6{\cdot}5H_2O$ and $NaZn_4(SO_4)Cl(OH)_6{\cdot}6H_2O$.

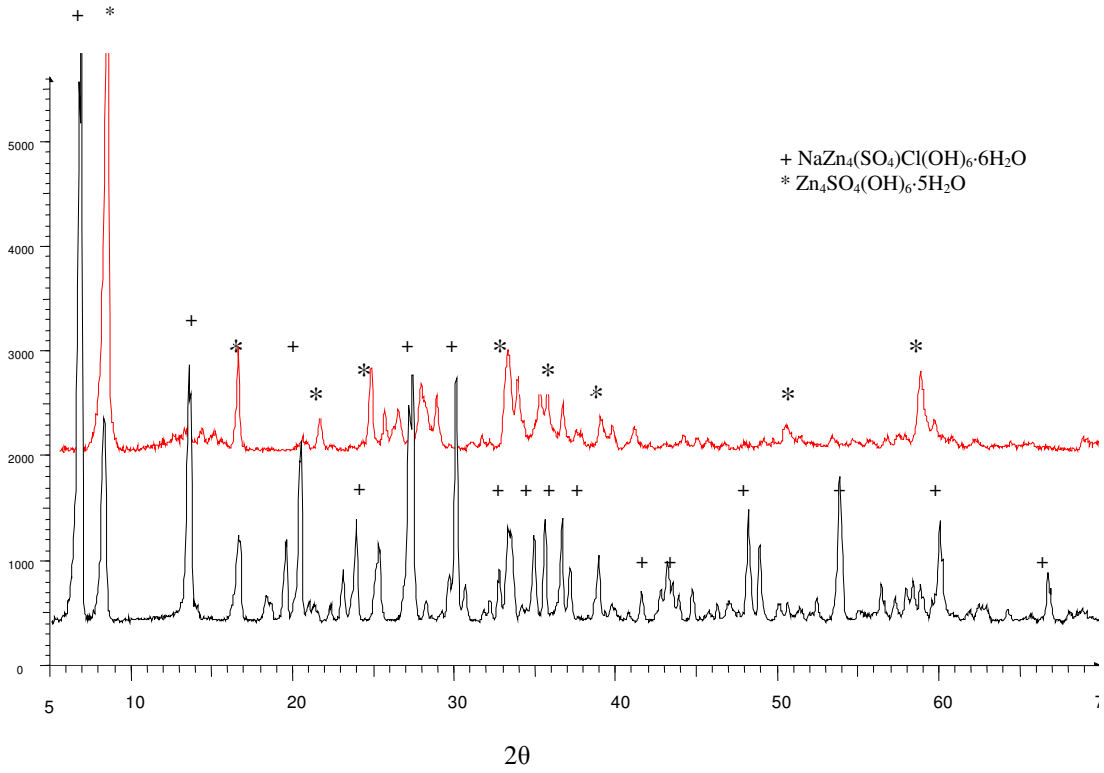

Figure 4.17 XRD patterns of $Zn_4SO_4(OH)_6{\cdot}5H_2O$ and $NaZn_4(SO_4)Cl(OH)_6{\cdot}6H_2O$

These phases can therefore form in the off-gas duct from ZnO, $ZnSO_4$, H_2O and NaCl. Hence the overall reactions can be written as:

$$ZnO + C/CO \leftrightarrow Zn + CO/CO_2$$

$$2SO_2 + O_2 \rightarrow 2SO_3$$

$$ZnO + SO_3 \rightarrow ZnSO_4$$

$$ZnSO_4 + 3ZnO + 8H_2O \rightarrow Zn_4SO_4(OH)_6{\cdot}5H_2O$$

$$ZnSO_4 + 3ZnO + NaCl + 9H_2O \rightarrow NaZn_4(SO_4)Cl(OH)_6{\cdot}6H_2O$$

Figure 4.19 schematically shows the dust formation mechanisms in semi-closed SAFs. It can be divided into four categories:

a. Vaporisation of elements or compounds from high temperature zones (1): Halite (NaCl) in the ferrochrome dust is a vaporisation product when the

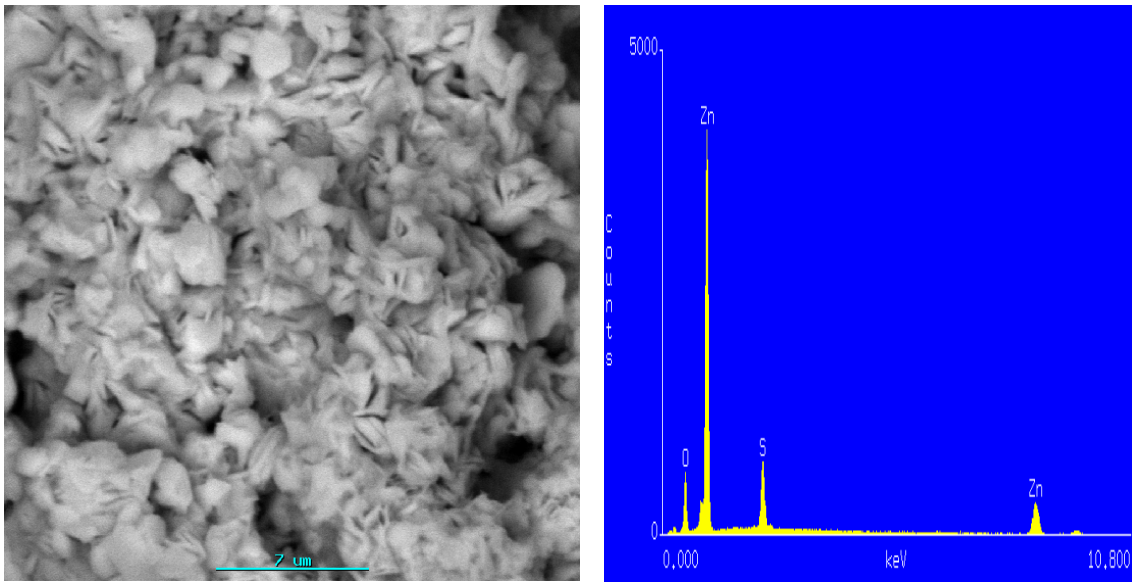

(a) $Zn_4SO_4(OH)_6{\cdot}5H_2O$

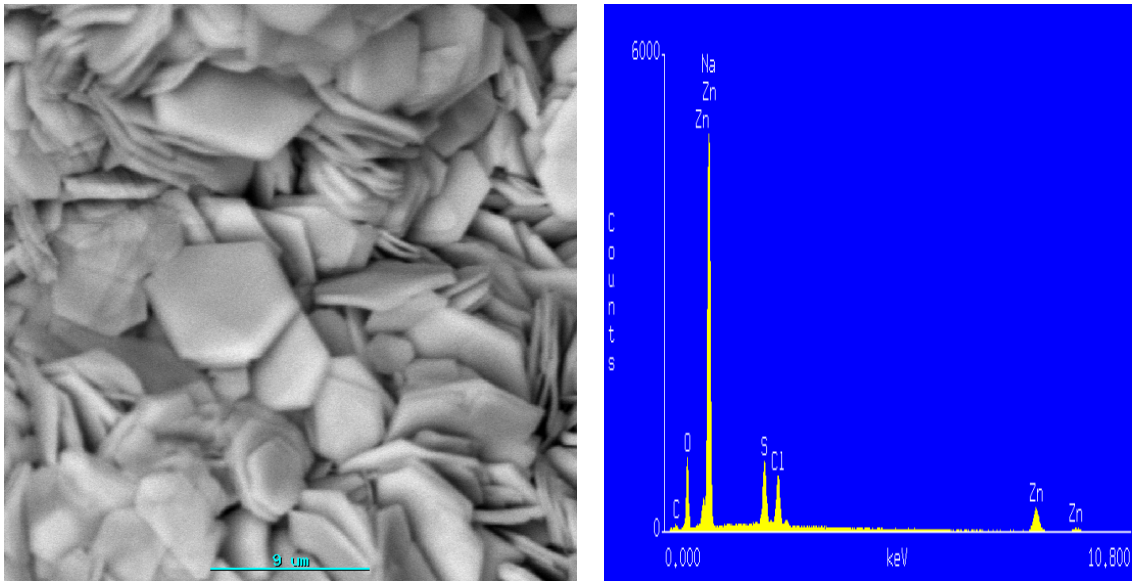

(b) $NaZn_4(SO_4)Cl(OH)_6{\cdot}6H_2O$

Figure 4.18 Secondary electron image and EDS spectrum of the synthetic crystals (a) $Zn_4SO_4(OH)_6{\cdot}5H_2O$ and (b) $NaZn_4(SO_4)Cl(OH)_6{\cdot}6H_2O$

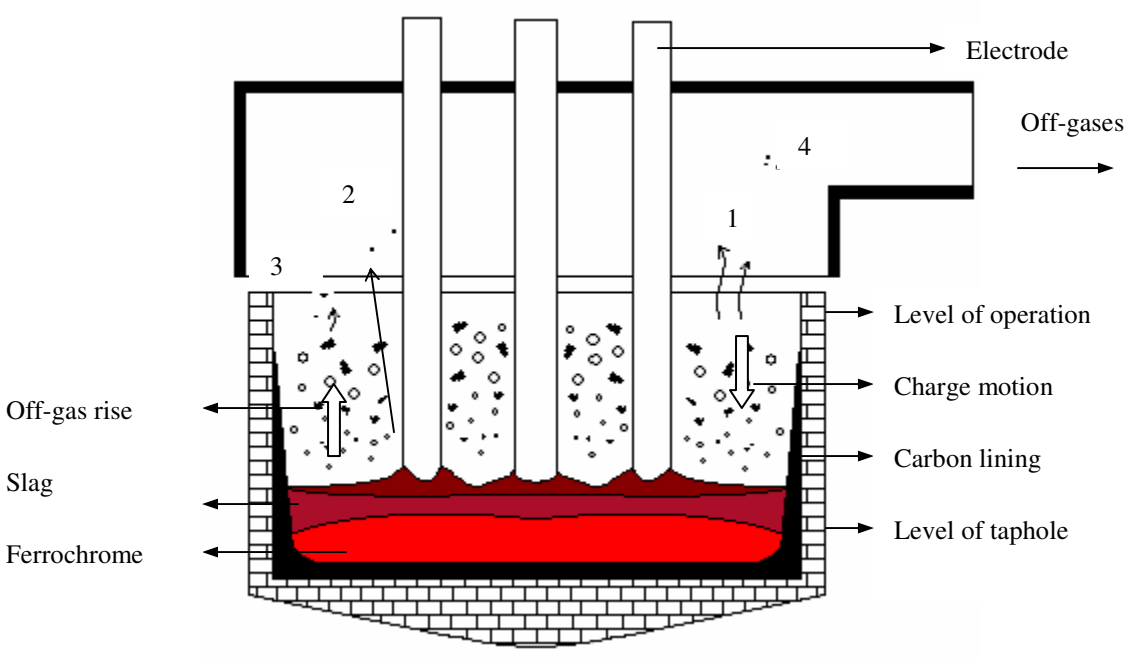

Figure 4.19 Dust formation mechanisms in semi-closed SAF

charge enters the high temperature zone of the SAF. Cristobalite (SiO_2), periclase (MgO) and ZnO are the oxidation products of oxide species that were fumed through a reduction reaction with carbon or carbon monoxide.

b. Ejection of slag and metal via the holes of the electrodes (2):
c. Charge materials that are directly captured in the off-gas (3):
   Carbon-bearing particles, quartz and chromite particles in angular shape present in the dust originate from the charge fines that were entrained in the off-gas.
d. Phases and reaction products that form in the off-gas duct from species in the off-gas (4):

The carbon-bearing particles, quartz and chromite particles present in the dusts originate from the charge fines, which were entrained in the off-gas. NaCl and ZnO are vaporisation products that formed during production. The metal and slag droplets were presumably ejected from the holes of the electrodes, while forsterite (Mg_2SiO_4) and the small amount of hydrate crystals [$Zn_4SO_4(OH)_6{\cdot}5H_2O$ and $NaZn_4(SO_4)Cl(OH)_6{\cdot}6H_2O$] formed in the off-gas duct via chemical reactions. Anorthite [$(Ca,Na)(Si,Al)O_8$] that is

present in the ferrochrome coarse dust, precipitated from the slag droplets during cooling in the off-gas duct.

4.3.3 The formation mechanisms of filter cake

The filter cake contains crystalline CaF_2, $CaSO_4$ and $CaCO_3$, as well as amorphous metal hydroxides. By considering the waste acid treatment process, it can be concluded that the crystalline phases (CaF_2 and $CaSO_4$) are generated in the neutralisation and reduction steps, $CaCO_3$ is the reaction product of the remnant lime particles with the carbon dioxide in the atmosphere, while the amorphous phases are generated in the precipitation step.

The overall reactions of the pickling acid treatment process can be summarised as follows:

Neutralisation step: $CaO + H_2O \longrightarrow Ca(OH)_2$ and $Ca^{2+} + SO_4^{2-} \longrightarrow CaSO_4$

$H^+ + OH^- \longrightarrow H_2O$ and $Ca^{2+} + 2\,F^- \longrightarrow CaF_2$

Reduction step: $3Fe^{2+} + Cr^{6+} \longrightarrow 3Fe^{3+} + Cr^{3+}$ and $Ca^{2+} + SO_4^{2-} \longrightarrow CaSO_4$

Precipitation step: $CaO + H_2O \longrightarrow Ca(OH)_2$ and $M^{n+} + n\,OH^- \longrightarrow M(OH)_n \downarrow$

(M represents metal cations such as Cr^{3+}, Fe^{3+} and Ni^{2+}).

4.3.4 Measures to reduce waste generation

Table 4.1 shows the process parameters that possibly influence dust formation during stainless steelmaking and ferrochrome production. Since ejection of slag or metal due to the bursting of the bubbles is the major dust formation mechanism in the stainless steel plant, measures should be taken to control the decarburisation reaction by changing the blowing (O_2 or Ar/O_2) time and rate as well as the position of the lance in the EF and converter. Slopping should also be minimised. To avoid vaporisation from the molten bath, the concentrations of volatile components in the scrap and molten ferrochrome should also be controlled. Moreover, the time of addition, method of addition (top charging or bottom injection), quantity and quality of charge materials influence the quantity of the dust particles that are directly captured in the off-gas.

Table 4.1 Parameters that possibly affect EF dust formation

Formation mechanisms	EAF smelting	AOD or CLU converter	Ferrochrome production
Vaporisation	Properties of charge (scrap and molten ferrochrome)	-	Raw materials properties
Directly captured during charging	The time of addition, type of addition (top charging or injection), quantity and quality of charge		Particle size distribution of charge
Ejection or bursting of bubbles	Oxygen blowing volume and time	Ar/O_2 ratio	Arc fluctuating
	Slag or non-slag operation	Blowing time, rate and temperature of gas mixture	Furnace type (open, semi-open or closed)

The output of ferrochrome fine dust is approximately 40 times by mass that of the ferrochrome coarse dust in a semi-closed SAF. It is therefore more important to reduce the formation of ferrochrome fine dusts than it is to reduce the amount of ferrochrome coarse dust. However, the volatile substances are the main components in the ferrochrome fine dusts. The volatile components (Na_2O + K_2O + ZnO + SO_3 + F + Cl + LOI) constitute up to ~ 44 wt % and ~ 30 wt% of FCD1 and 2, respectively (Table 3.2). Thus, controlling the quality of the raw materials, especially the volatile components in the coal, coke and charcoal, is a major task in reducing the amount of dust formed during ferrochrome production. Furthermore, small particles of raw materials should be avoided during charging in order to directly reduce the amount of dust that is carried off in the off-gas. It can be first agglomerated after which it is charged into the SAF.

Regarding the reduction of Cr (VI) formation during the production of ferrochrome: The temperature profiles, chemical compositions of the off gases and dusts, and the crystalline phases that are present in the dusts at different positions in the off gas duct, i.e., from the gas extraction hood to the bag house filters, need to be comprehensively investigated. The modelling of the behaviour of the off gas and dust in the duct is also very important. This can reduce the degree of Cr (VI) generation from the furnace to the bag house filter dust plant. A reduction in Cr (VI) generation in the furnace can be achieved by using

closed SAF operation, which will create more reducing conditions at the top of the furnace [145].

4.4 Conclusions

In the present chapter, the formation mechanisms of Cr(VI)-containing EF dust and filter cake were studied based on a microstructural investigation and FACTSage calculations. The following conclusions can be drawn:

1) Stainless steel dust contains particles that are irregular in shape, spherical or near spherical particles and particles coated with slag or oxides.
2) Stainless steel dust is formed by the entrainment of charge materials, evaporation or volatilisation of elements and ejection of slag and metal by spitting or the bursting of gas bubbles.
3) Ferrochrome fine dusts consist mainly of clusters which contain charge materials, slag droplets as well as very fine SiO_2-MgO-ZnO-$(Na,K)_2O$ based particles. The coarse particles consist of reductant, slag droplets and chromite particles.
4) Ferrochrome dusts are formed by the ejection of slag and metals droplets from the electrode hole, the entrainment of charge materials, vaporisation as well as the formation and precipitation of compounds from vaporised species in the off-gas duct.
5) Filter cake contains crystalline phases (CaF_2, $CaSO_4$ and $CaCO_3$) and metal rich amorphous phases. The crystalline phases (CaF_2 and $CaSO_4$) are generated in the neutralisation and reduction steps due to super saturation, while the metal rich amorphous phases are generated in the precipitation step.

Chapter 5 The leachability of the Cr (VI)-containing electric furnace dust and filter cake from a stainless steel waste treatment plant

5.1 Introduction

The leachability of toxic substances from waste materials directly influences the treatment policy of the wastes. TCLP and ASTM D 3987-85 tests [21,146], which were respectively developed by the Environmental Protection Agency (US EPA) and American Standards Tests for Materials (ASTM), are widely used to understand the leachability of toxic substances from wastes. The TCLP test is also used to evaluate the risk of wastes to groundwater.

The TCLP and ASTM D 3987-85 tests, however, address neither the leachability of toxic substances over time, nor the leaching kinetics of the toxic substances. The shrinking core model can be used to understand the leaching mechanisms of toxic substances from wastes (Figure 5.1) [147,148]. According to this leaching model, the leaching steps can be divided into the following [147,148]:

1) Diffusion step of the leachant to the surface of the solid particle through the boundary layer.
2) Diffusion of the leachant to the leaching reaction interface.
3) Reaction step which can remove the toxic substances from the interface into the leachate via a set of physical and/or chemical processes such as dissolution, de-absorption and ion-exchange.
4) Diffusion step inside the leached layer of the particle which can transport the toxic substances to the surface of the particles through the matrix inside the particles.
5) Diffusion step in the aqueous boundary layer which can move the species into the bulk solution.
6) Bulk aqueous transport via diffusion or advective transport.

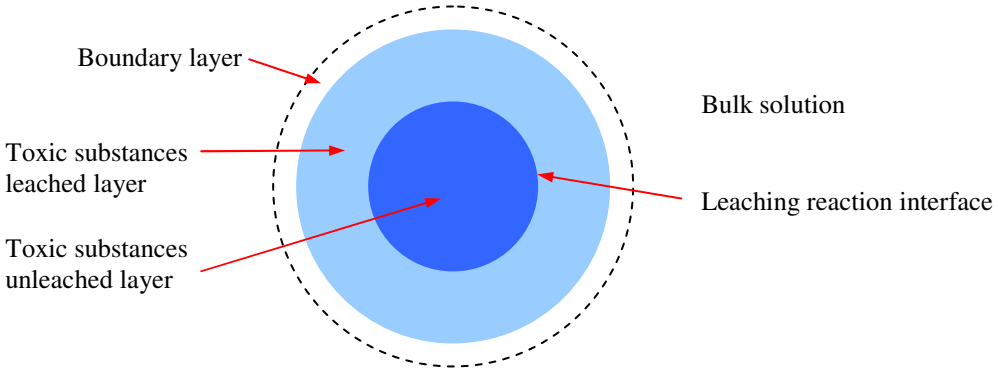

Figure 5.1 Leaching model of the toxic substances from the waste particles

The rate controlling step of the overall leaching reaction is the slowest step of the leaching process. However, the rate of steps (1) to (6) can be altered by changing the leaching parameters. For example, reducing the particles size of the wastes increases the surface areas of the wastes, and therefore increases the interface of the leaching reaction and the rate of step (1), while the temperature or pressure of the leaching system and the presence of a catalyst can change the rate of reaction (3). To change the rate of step (4), one can change the temperature, pH and the concentration of the leachant. Increasing the agitating speed of the impellers increases the rates of step (5) and step (6) [147,148].

In the present chapter, the leachability of Cr (VI) from the wastes was investigated using the TCLP and ASTM D 3987-85 tests. Distilled water and nitric acid leaching tests were also used to further understand the leaching behaviour of Cr (VI) from these wastes.

5.2 Experimental

5.2.1 Sample preparation

The samples used in this study and the methods of sample preparation are the same as that described in Chapter 3.

5.2.2 Experiment methods

5.2.2.1 TCLP test and ASTM D 3987-85 test

The TCLP test was used to evaluate the leachability of the toxic substances from the wastes. In the preliminary evaluation of the TCLP test, 5.0 g of waste was added to 96.5 ml of distilled water (DW) and stirred with a magnetic stirrer. It was found that the pH values of the solutions are all larger than 5. After the addition of 3.5 ml of 1N HCl, the solutions were heated up to 50^{o}C and kept at 50^{o}C for 10 minutes. The pH values of the resultant solutions of FCD1, FCD2, FCD3, SPD and FC were found to be 6.99, 6.76, 3.15 12.17 and 7.56, respectively. This confirmed that TCLP solution 2 (pH=2.88±0.05) is the appropriate test solution for SPD, FCD1, FCD2 and FC, whereas TCLP solution 1 (pH=4.93±0.05) should be used to test FCD3. In the extraction step, 100g samples (in triplicate) were added to 2 l of the appropriate TCLP solution, contained in borosilicate glass bottles. These bottles were then continuously rotated at 30 rpm for 20 hours, after which the slurries were filtered (using a glass fibre filter) and the pH of the leachate measured.

The ASTM D 3987-85 test was employed in this study to further understand the leachability of the wastes. 70 g samples (in triplicate) were added to 1400ml of distilled water and agitated continuously for 18 hours at 23^{o}C. The mixtures were filtered with a glass fibre filter by vacuum, and the pH of the leachate determined.

The Cr (VI) concentrations of the leachates from the TCLP and ASTM D 3987-85 tests were measured by the colorimetric method with a S20D spectrophotometer. The total chromium concentrations were also analysed after Cr (III) was oxidised to Cr (VI) by potassium permanganate in an acid solution. The analytical method is attached in Appendix I. The concentrations of zinc and lead were measured with a GBC909 flame atomic absorption spectrometer (AAS), by respectively using US EPA methods 7950 and 7420 [149].

5.2.2.2 Nitric acid and distilled water leaching

Static distilled water (DW) and nitric acid (NA) leaching tests were also conducted in order to study the surface composition of the particles. In these tests, 50g of dust was added to 1l of distilled water or nitric acid (to obtain a solid:liquid ratio of 1:20), for 2 hours at 25±1^{o}C. The slurries were then filtered and dried. The crystalline phases in the residues were identified with a Siemens D-501 X-ray diffraction (XRD) instrument and the atomic concentrations on the surfaces of the leaching residues were determined with a X-ray photoelectron spectrometer.

The leachability of Cr (VI) was also determined at different stirring speeds and temperatures (Table 5.1). The effect of stirring speed was studied at 600, 800 and 1000 rpm, while the effect of temperature at 25, 40 and 55^{o}C was studied at a stirring speed of 800 rpm. The effect of pH was investigated by using pH buffer solutions of 5 and 9 at a stirring speed of 800rpm. In these experiments a 50 g sample was again added to 1l of distilled water. Approximately 2~3 ml leachate was sampled at different intervals and filtered using a 0.22 µm membrane filter. Thereafter, the same amount of distilled water was added back to the solution. The leachate samples were immediately analysed. Zinc concentrations in the leachate of FCD2 were also determined using the US EPA method 7950 [149].

Table 5.1 Experimental conditions of the Cr (VI) leaching tests

Parameters	SPD	FCD1, 2, 3 and FC
Stirring speed (rpm)	600, 800, 1000	800
pH of the leach solutions	5, Distilled water, 9	Distilled water
Leaching temperature (^{o}C)	25, 40, 55	25
Total leach time (hours)	24	168
Solid waste/leach solution (g/ml)	1/20	1/20

5.3 Results and discussion

5.3.1 TCLP and ASTM D 3987-85 tests

The results of the TCLP and ASTM D 3987-85 tests of the wastes are shown in Figures 5.2a and 5.2b, respectively. It shows that all the wastes are hazardous materials

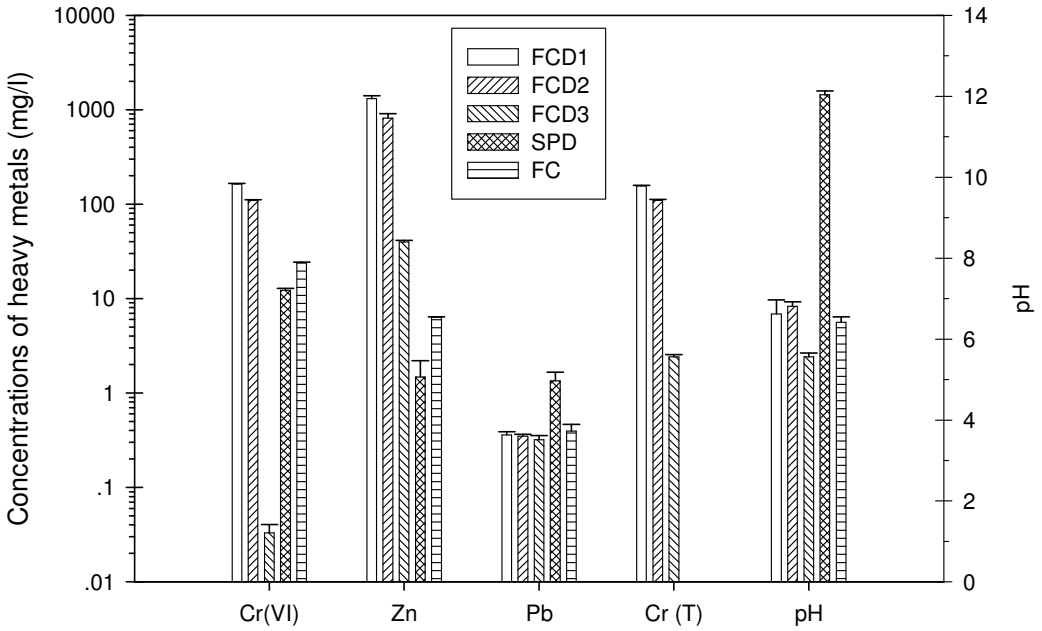

(a) TCLP test

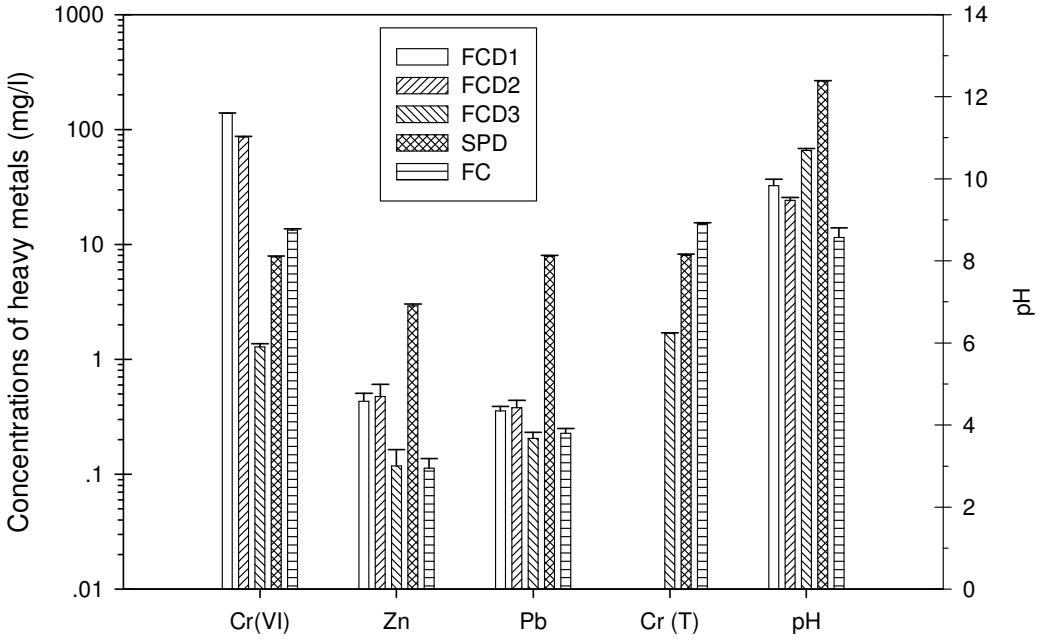

(b) ASTM D3987-85 test

Figure 5.2 The concentrations of toxic substances in TCLP test(a) and ASTM D3987-85 test(b)

according to South African legislation. It also shows that most of the leachable chromium exists in the form of Cr (VI). High levels of chromium are present in the TCLP leachate of FCD3 although the concentration of Cr (VI) is substantially lower than that determined by the ASTM D 3987-85 test. This is possibly due to the reduction of Cr (VI) by metal ions such as Fe^{2+} that are present in the TCLP leachate (pH<6), while it is precipitated at a pH of approximately 11 during the ASTM D 3987-85 test [150]. The zinc concentrations in the TCLP leachate of FCD1, 2 and 3 (approximately 1314, 810 and 40 mg/l, respectively) are much higher than those of the ASTM D 3987-85 test (less than 0.5 mg/l), since zinc is mostly present as zinc oxide, which cannot be extracted by distilled water, but by glacial acetic acid.

All the leachates from the ASTM D 3987-85 tests form basic solutions, while the TCLP leachates are acidic except for the SPD (pH≈12). The high pH value of the TCLP leachate from the SPD is due to the existence of $Ca(OH)_2$ in the dust.

5.3.2 Static distilled water and nitric acid leaching tests

The static distilled water and nitric acid leaching tests were only conducted on the EF dusts. After leaching these dusts with either 1M HNO_3 or distilled water for 2 hours, the dusts were examined by XRD (Figures 5.3 and 5.4). XRD analyses of the leaching residues of the ferrochrome dust show that chromite particles, quartz, cristobalite, ZnO, MgO, Mg_2SiO_4 and ferrochrome particles still exist after the 2h distilled water leaching test, while $NaZn_4(SO_4)Cl(OH)_6 \cdot 6H_2O$ and $Zn_4SO_4(OH)_6 \cdot 5H_2O$ as well as NaCl dissolved (Figure 5.3). Only chromite particles, quartz, cristobalite, Mg_2SiO_4 and ferrochrome particles are present in the nitric acid leach residue of the ferrochrome fine dust. It indicates that the nitric acid leach dissolves $Ca(OH)_2$ and oxidises parts of the nickel particles from the SPD (Figure 5.4). Spinel phases, fluorite and silica still exist. Small gas bubbles are liberated from the stainless steel plant dust during the nitric acid leach. This is possibly hydrogen. The nitric acid leachate is light brown in colour (possibly due to Fe^{3+} species), while the distilled water leachate is light yellow in colour (presumably Cr^{6+} species). The analysis results show that the Cr (VI) concentration in the NA leachate (0.13mg/l) is lower than that in the DW leachate (6.4mg/l).

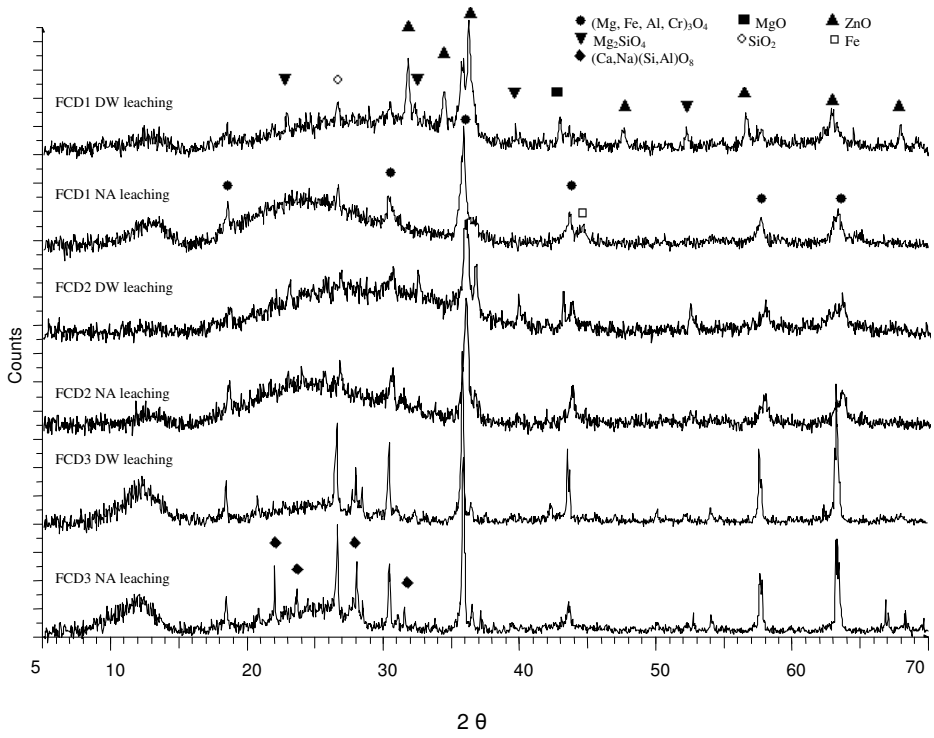

Figure 5.3 XRD patterns of FCD 1,2 and 3 after DW and NA leach for 2 h

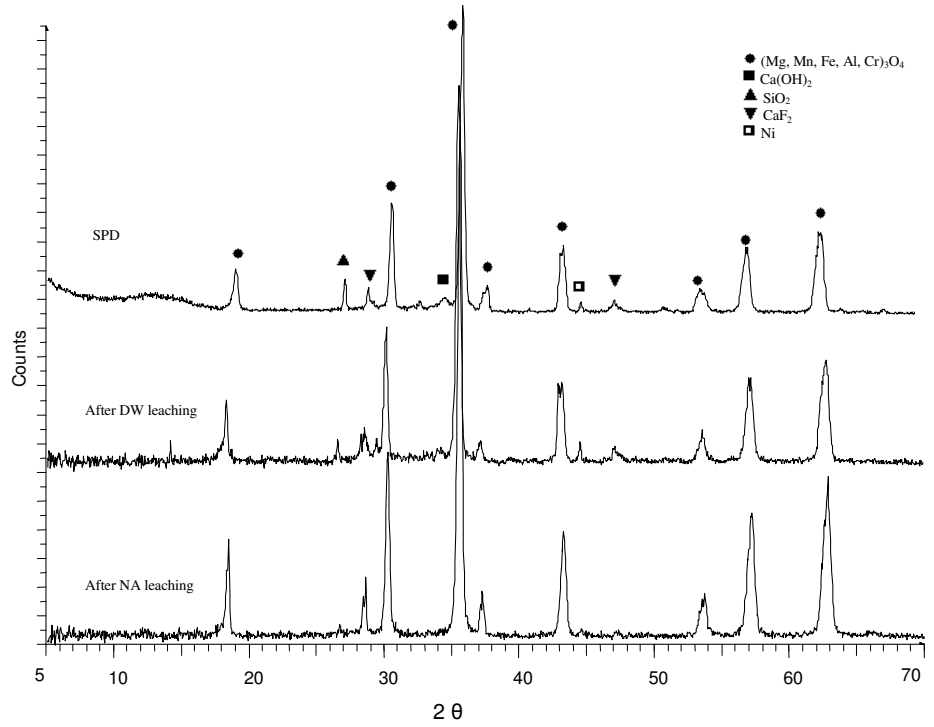

Figure 5.4 XRD patterns of SPD before and after DW and NA leach for 2 h

The elements that exist on the surface of the electric furnace dust and the residue of the distilled water and nitric acid leaching tests of ferrochrome dust are shown in Table 5.2. The major elements on the surface of the SPD are Zn, O, Si and Mg, while Na, F, Cr, K, C, Cl, Ca and Fe are present in minor amounts. Before the leaching experiments, zinc, halogens (F, Cl), alkali metals (K, Na) and the elements O, Cr, S and Si are present on the surface of the ferrochrome dust. It shows that the elements that can easily vaporise are the major components on the surface of the dust particles.

Table 5.2 XPS analysis of the EF dusts (atomic%)

Element	Chemical state	FCD1	FCD2	FCD3	FCD1 (DW)*	FCD1 (NA)**	SPD
Na	Na^{+}	7.21	5.80	1.63	2.33	0.86	4.47
Zn	Zn^{2+}	9.74	6.38	2.63	9.24	0.75	5.19
F	F^{-}	5.18	0.49	0.34	4.03	0.39	2.35
Cr	Cr, Cr^{3+}, Cr^{6+}	1.52	1.37	0.81	1.27	0.62	0.89
O	Oxides	53.07	54.98	44.53	60.64	64.54	55.10
K	K^{+}	1.49	2.12	0.32	0.45	0.16	1.00
C	C, CO_3^{2-}	5.93	9.86	37.53	5.35	3.76	3.98
Cl	Cl^{-}	1.46	2.13	0.81	0.32	0.15	0.95
S	SO_4^{2-}	1.32	2.61	1.32	0.46	Nd	0.09
Si	Si^{4+}	13.09	14.27	10.06	15.91	28.53	6.24
Ca	Ca^{2+}	nd***	nd	nd	nd	nd	3.08
Mg	Mg^{2+}	nd	nd	nd	nd	nd	12.05
Fe	Fe^{2+}, Fe^{3+}	nd	nd	nd	nd	nd	2.96

*distilled water leach residue; **nitric acid leach residue; ***not determined.

The Na, Zn, K, total Cr and Cl concentrations are higher on the surface of the ferrochrome fine dusts, than those of the ferrochrome coarse dusts. After distilled water leaching of FCD1 the concentrations of sodium and chlorine decrease noticeably, while

after leaching with nitric acid the atomic concentrations of Na, Cl, Zn and F on the surface are reduced. Tables 3 also shows that the most abundant elements are Si and O with a ratio of 1:2 after nitric acid leaching. It confirms that some of the ferrochrome dust particles have a core of SiO_2 with an out layer of vaporised substances such as ZnO and NaCl. In contrast to the XRD results, it shows that most of the NaCl condensed on the surface of the particles and are easy to leach out, while zinc is present in the form of zinc oxide.

5.3.3 Effect of stirring speed on the leachability of Cr (VI) from stainless steel dust

The effect of the stirring speed on the leachability of Cr (VI) is shown in Figure 5.5. It shows that approximately 65% Cr (VI) (7.8mg/l) leached out in 5 min, and that stirring speed has no effect on the leaching of Cr (VI). This indicates that most of Cr (VI) exists on the surface or near the surface of the dust particles, and that it will easily leach out when it rains or snows. It cannot simply be stockpiled at the waste site, since Cr (VI) can leach out and thereby contaminate surface water, ground water and soil. It also means that the leaching of Cr (VI) is not controlled by either step (4) or step (5) of the described leaching model, since agitation does not have an effect on the leaching rate of Cr (VI) from the waste particles. In addition, it shows that the Cr(VI) content of the stainless steel plant dust can substantially be reduced in a simple washing process.

Figure 5.5 also shows that the Cr (VI) concentration firstly increases and reaches a maximum after 1 hour of leaching. Then the Cr (VI) concentration starts to decrease, which can be explained by the transformation of Cr (VI) to Cr (III). It seems that the Cr (VI) concentration remains stable after 9 hours of leaching.

5.3.4 Effect of temperature on the leachability of Cr (VI) from stainless steel dust

The effect of temperature on the leachability of Cr (VI) from SPD is shown in Figure 5.6. It was found that Cr (VI) dissolution increases with an increase in temperature of the leachate. At 55ºC, with a stirring speed of 800 rpm, approximately all of the Cr (VI) leached out within 24 hours. It is therefore believed that the Cr (VI) leaching reaction is controlled by either diffusion of Cr (VI) inside the Cr (VI) leached layer and/or chemical

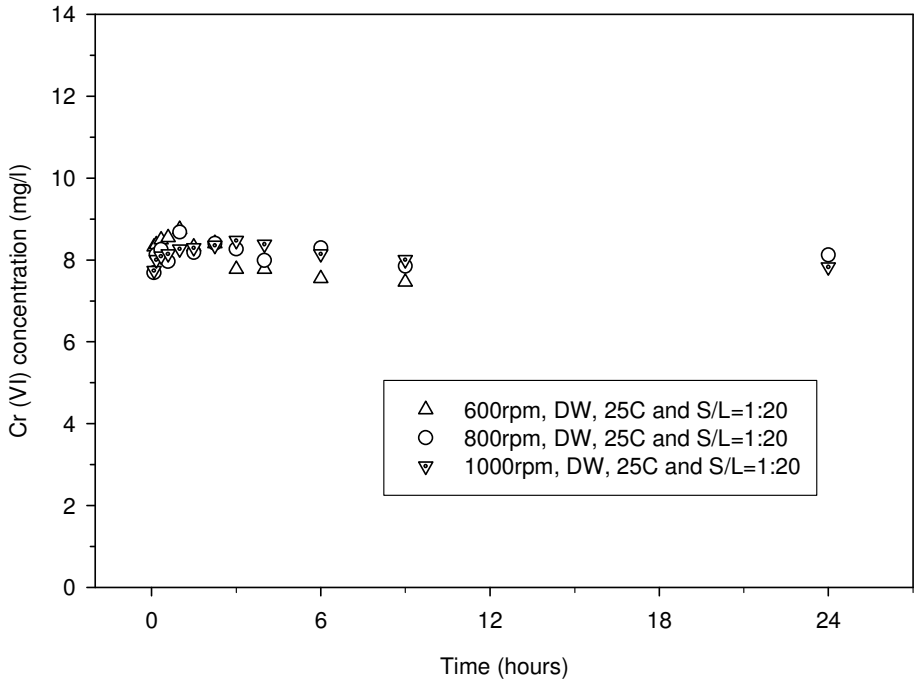

Figure 5.5 Effect of stirring speed on the leachability of Cr (VI) from SPD

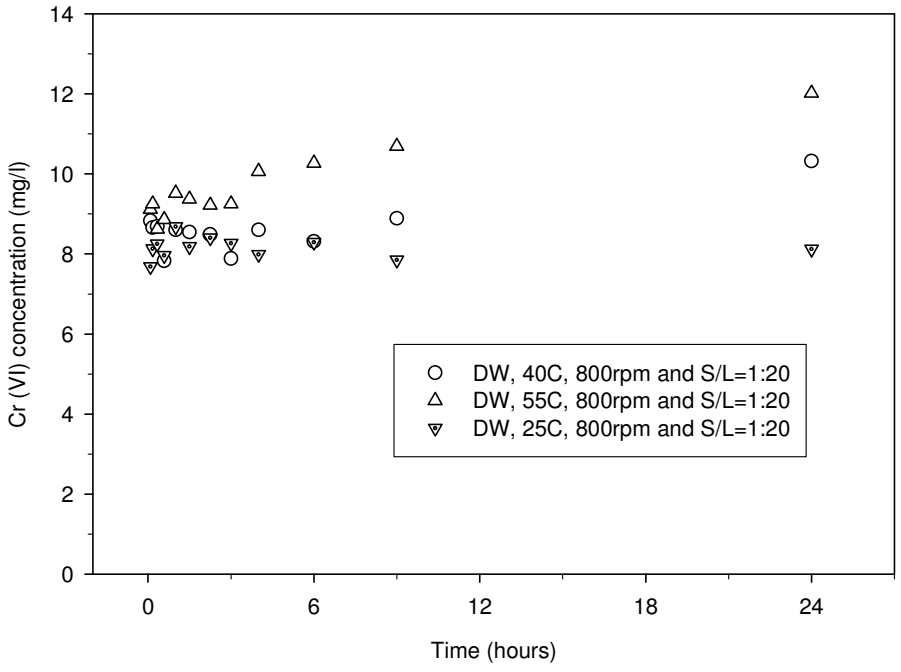

Figure 5.6 Effect of temperature on the leachability of Cr (VI) from SPD

reactions whereby Cr (III) is transformed into Cr (VI). The latter reactions are influenced by the pH of the aqueous solution and redox potential.

Since the chemical and phase composition of the stainless steel dust is complex, it is difficult to fully understand the leaching mechanisms of Cr (VI) from the waste. Certain components in the dust can influence the Cr (VI) concentration in the leachate. These include reducing agents, such as Fe (II), which can influence the redox potential of the solution, and lime which can change the pH of the solution. These components can over time change the Cr (VI) concentration in the leaching solution, and therefore make the leaching mechanisms of Cr (VI) complicated to understand.

5.3.5 Effect of pH on the leachability of Cr (VI) from stainless steel dust

The leachability of Cr (VI) from SPD, using solutions of different pH, is shown in Figure 5.7. At 25ºC and a stirring speed of 800rpm more Cr (VI) is leached from acidic and basic solutions than from distilled water with a pH of approximately 6.5. Under the current experimental conditions more Cr (VI) is leached from basic solutions than from acidic solutions.

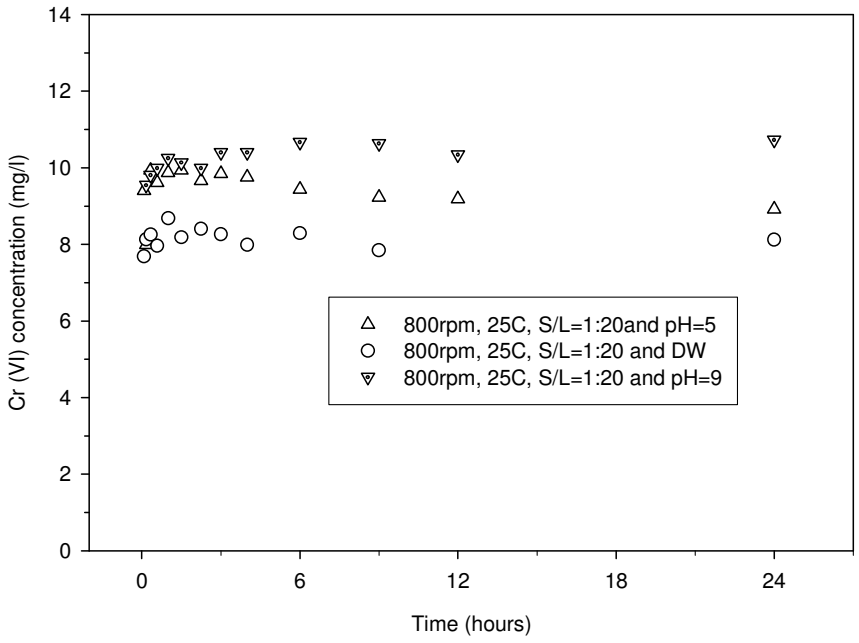

Figure 5.7 Effect of pH on the leachability of Cr (VI) from SPD

5.3.6 The leachability of Cr (VI) from ferrochrome dusts and filter cake

In order to understand the leaching behaviour of Cr (VI) from ferrochrome dust and filter cake, a seven day leaching test was performed with distilled water at 25ºC. The results are shown in Figures 5.8 and 5.9. It shows that approximately 72% and 62% of Cr (VI), present respectively in dust samples FCD1 and FCD 2, were leached out by distilled water under 1 min. This is presumably due to "wash-off" of Cr (VI) from the surface of the dust particles. The maximum Cr (VI) concentration (~132mg/l) was reached after 24 hours for sample FCD1, while the peak value of ~73mg/l Cr (VI) was reached within an hour for sample FCD2. Ferrochrome fine dusts are therefore very harmful to the environment, and should not come in contact with water before being processed. The Cr (VI) in the ferrochrome fine dust can also be lowered by washing the dusts. However, the wastewater needs to be treated further due to the significant levels of Cr(VI).

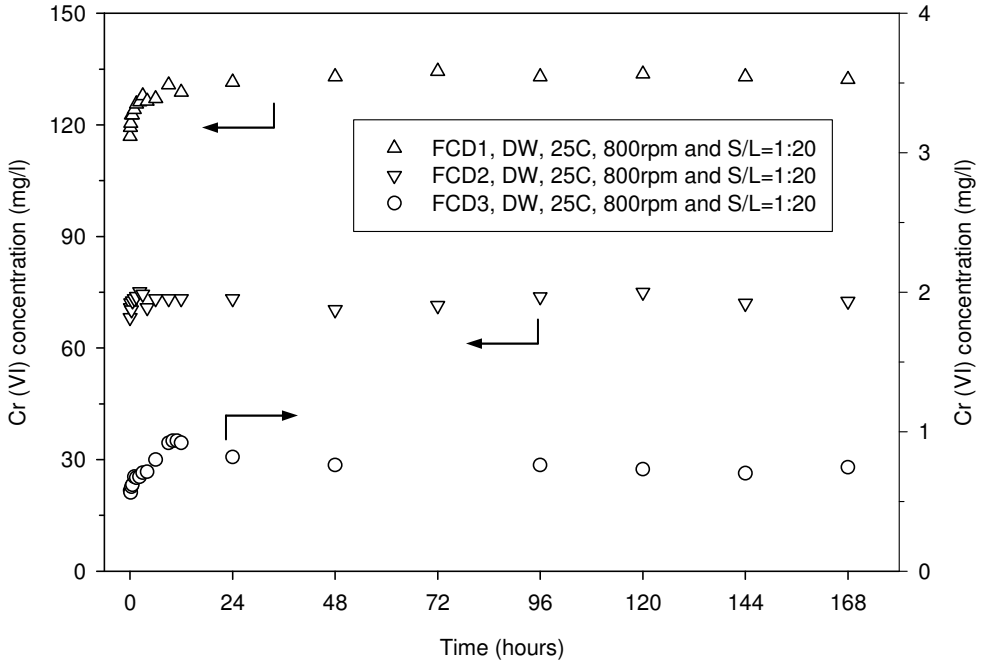

Figure 5.8 The leachability of Cr (VI) from ferrochrome dust, using distilled water

The amount of Cr (VI) that was leached from sample FCD3 was below 1 mg/l Cr(VI), and increased with time up to 9 hours, after which it slightly decreased when the leaching

time exceeded 9 hours. It is assumed that this is due to the reduction of Cr (VI) by Fe^{2+} in the leachate. Since the ferrochrome coarse dust (sample FCD3) contains low concentrations of volatile substances and hazardous Cr (VI), but also exploitable quartz and chromite, it is suitable to be recycled back to the furnace after being agglomerated by briquetting or pelletising using binders.

Figure 5.9 shows that approximately 25 mg/l Cr (VI) would leach out in 1 min from the FC. A maximum amount of approximately 44mg/l Cr (VI) was leached from the FC within 3 hours. It also shows that Cr (VI) is rapidly leached out.

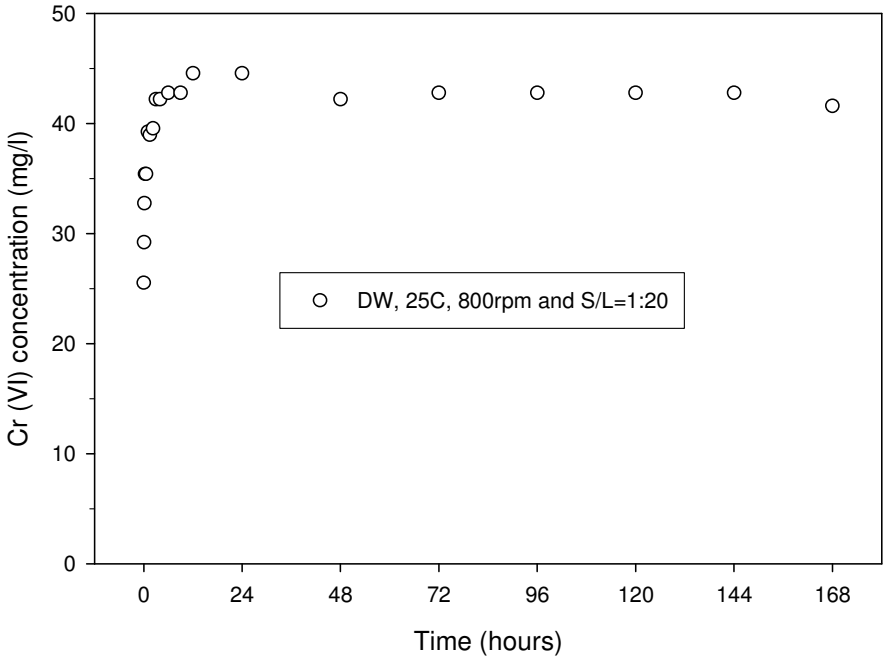

Figure 5.9 The leachability of Cr (VI) from FC

The change in zinc concentration and pH of the FCD2 leachate with time are shown in Figure 5.10. It was observed that the pH of the leachate did not change significantly during the leaching period. The zinc concentration in the leachate however, reached a maximum value after approximately 4 hours, after which it then decreased over time, possibly due to the precipitation of zinc in alkaline solutions (pH ≈ 9) [150]. Most of the zinc in the dust remained unaffected during the distilled water leach. If zinc would

therefore be recovered from ferrochrome fine dust, using a hydrometallurgical route, an acidic leach solution should be used.

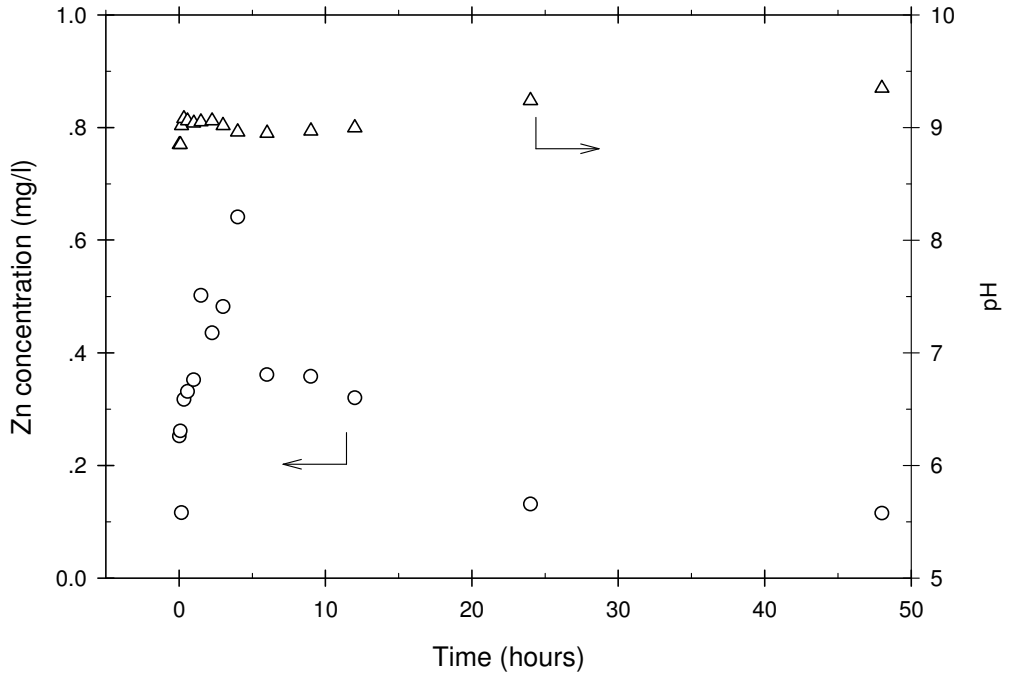

Figure 5.10 Zinc concentration and pH in FCD2 leachate versus time (DW, 800rpm, 25^{o}C and S/L=1/20)

5.4 Conclusions

In the present study, the leachability of Cr(VI)-containing EF dust and filter cake were studied. The following conclusions can be drawn:

1) TCLP and ASTM 3987-85 tests show that stainless steel plant dust, ferrochrome fine dust and filter cake are hazardous materials according to South African legislation. They therefore pose a potential threat to the environment.
2) Static distilled water and nitric acid leaching experiments show that the ferrochrome fine dust particles have a core of SiO_2 with an outer layer that consists of vaporised substances such as ZnO and NaCl.
3) Leaching experiments on the stainless steel plant dust show that approximately 65% of the Cr (VI) leaches out within 5 min under the current experimental

conditions, but that the Cr (VI) leach out more easily in acidic and basic solutions than in distilled water.

4) Since the leaching behaviour of Cr (VI) does not change with stirring speed but with temperature, it can be concluded that the Cr (VI) leaching reaction is most probably controlled by the diffusion of Cr(VI) inside the Cr (VI) leached layer and the rate of the chemical reaction whereby Cr (III) is transformated into Cr (VI).

5) Distilled water leaching experiments on ferrochrome dusts and filter cake show that Cr (VI) is easily leached by distilled water. Due to the high Cr(VI) concentration of the ferrochrome fine dust, it should not come in contact with water before being processed. The coarse ferrochrome dust is suitable to be recycled back to the SAF, as it contains low concentrations of volatile substances, but also usable carbon, quartz and chromite particles.

Chapter 6 The aging behaviour of Cr (VI)-containing Electric furnace dust and filter cake from a stainless steel waste treatment plant

6.1 Introduction

Chromium exists in various oxidation states, the most stable ones being Cr (III) and Cr (VI). In soil and aqueous solutions, numerous authors reported that Cr (VI) can easily be reduced into Cr (III) by Fe (II) via reaction 6.1, S^{2-} or organic components at room temperature [151,152].

$$4H_2O + CrO_4^{2-} + 3Fe^{2+} + 4\ OH^- \rightarrow 4Fe_{0.75}Cr_{0.25}(OH)_3\ (s) \qquad (6.1)$$

Peterson et al. reported that Cr (VI) in the contaminated soil samples can be reduced into Cr (III) by Fe^{2+}-bearing slag or minerals, such as magnetite (Fe_3O_4), ferrous containing goethite [FeO(OH)], biotite [$K(Mg,Fe^{2+})_3(Al,Fe^{3+})Si_3O_{10}(OH,F)_2$] and pyrite ($FeS_2$) [153-156].

On the other hand, Cr (III) can also be oxidised into Cr (VI) by either MnO_2, or in the presence of lime and oxygen either at ambient or high temperatures according to reaction (6.2) [38,157,158].

$$Cr_2O_3 + 2CaO + 1.5O_2 \rightarrow 2CaCrO_4 \qquad (6.2)$$

The oxidation mechanism of Cr_2O_3 by lime particles is schematically shown in Figure 6.1 [158]. It shows that the oxidation reaction occurs on the boundary between Cr_2O_3 and lime particles. The Cr (III) oxidation reaction can be restricted by minimising the total exposure grain area and oxygen diffusion [158].

As discussed in the previous chapter, the electric furnace dust and filter cake are classified as hazardous wastes based on the significant Cr (VI) in the leachates from the TCLP and ASTM D3987-85 tests. However, these Cr (VI)-containing wastes contain free lime particles as well as Fe^{2+}-bearing components. Since the leachability of Cr (VI) from these wastes influences its treatment policy, it is very important to study the aging behaviour of Cr (VI) in these wastes. Moreover, the experimental results can also serve as

guidelines on the management of other Cr-containing pyrometallurgical wastes, such as ferrous slag and waste refractories.

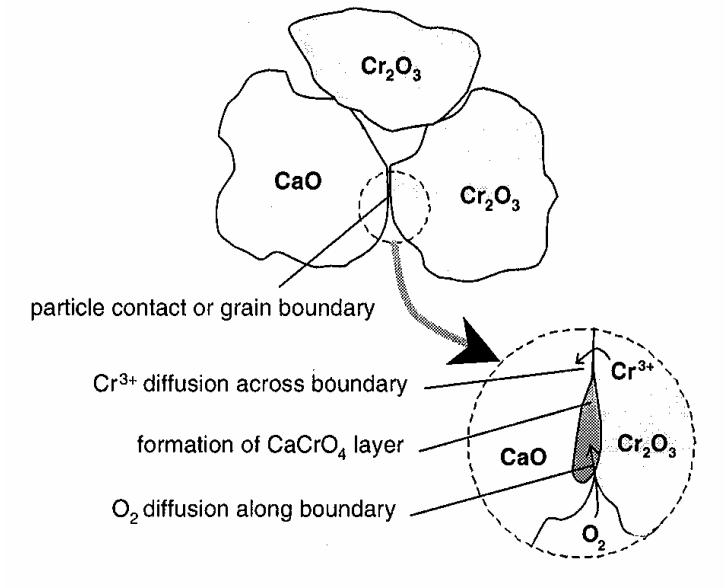

Figure 6.1 Oxidation mechanism of Cr_2O_3 by CaO in air [158]

In this chapter, the leaching behaviour of Cr (VI) from the electric furnace dust and filter cake over 4 months is discussed. The synthetic mixtures of Cr_2O_3 and CaO were also prepared to confirm the oxidation of Cr (III) into Cr (VI) in the presence of lime at ambient atmosphere and temperature.

6.2 Experimental

6.2.1 Sample preparation

Two pyrometallurgical wastes were used in this study, i.e., stainless steel plant dust (SPD) and filter cake (FC). The original filter cake contains significant moisture (typically 50%). It was dried at 110°C, crushed and ground. Representive waste powder samples were taken using a splitter. Approximately 25 g sub-samples were then taken and contained in a plastic boat. These samples were then stored in a room with a controlled temperature of 20±2 ^{o}C. The influence of several parameters on the oxidation or reduction of chromium were examined: (1) pellets vs. powdered samples, (2) temperature, (3) particle size of the wastes, and (4) atmosphere (the contents of water vapour and oxygen).

The pellets were prepared from the powdered wastes using a stainless steel die with a diameter of 40 mm at 5 kN force using a hydraulic press for 5 minutes.

Two temperatures were examined in this study, i.e. 20±2^{o}C and 30±1^{o}C. For the aging experiment at 30±1^{o}C, the powdered samples were contained in plastic boats. They were then put on a water bath which was controlled at 30±1^{o}C during the aging experiment.

To study the effect of particle size on the leaching behaviour of Cr (VI), three ranges of particles sizes were selected, i.e., -53um, +53um-106um and +106um. The powdered waste samples were sieved and splitted into small batches which served as representive samples for the aging experiments.

The effect of atmospheric conditions on the leaching behaviour of Cr (VI) at 20±2 ^{o}C was also examined. This was done by storing several sets of samples under dry air, water-saturated air, dry Ar gas and water-saturated Ar gas. Under conditions of a "dry air atmosphere", the waste samples were stored inside desiccators that contained silica gel at the bottom of the desiccators. If distilled water was contained at the bottom of the desiccators, the condition of so-called water-saturated air was created. For the dry Ar gas environment, silica gel was put into the bottom of the desiccators, after which they were sealed with high vacuum grease and dry argon gas with a purity of 99.999% purged through the desiccators. If distilled water was contained at the bottom of the desiccators, the environment was the so-called water-saturated argon gas.

In order to better understand the effect of lime on the oxidation behaviour of Cr (III) in the wastes, the synthetic powder mixtures of Cr_2O_3 and CaO were prepared. The Cr_2O_3 was first washed with a 1 mol/l NaOH solution for 4 hours and twice filtered by distilled water in order to reduce the residual Cr (VI) in the Cr_2O_3 powder. The molar ratios of Cr_2O_3 to CaO were chosen to be the same as the ratio in the filter cake and steel plant dust.

6.2.2 Leaching experiment and analysis methods

All the waste samples were analysed, using a modified TCLP test. This "modified" TCLP test differs from the standard TCLP test in that approximately 25 g samples were used, instead of 100 g samples. Some of the analyses were duplicated. Cr (VI) in the waste samples were extracted with glacial acetic acid solution (TCLP solution 2) using a 1:20 ratio of solid to leachant, and an end-over-end rotator at 30 rpm (Figure 6.2) at 20±2 ^{o}C. The leachants were subsequently sampled and filtered using a Millipore membrane filter with a pore size of 0.22um.

Figure 6.2 Experimental setup of the modified TCLP test

The extractable Cr (VI) was determined with a Perkin Elmer Lambda 25 UV/Vis Spectrometer at a wavelength of 542nm (The analytical method is given in Appendix I). Calcium containing phases in samples of different particles size fractions were semi-quantitatively determined using a Siemens D-501 XRD.

6.3 Results

6.3.1 Effects of temperature and time on the aging behaviour of Cr (VI)

Increasing temperature promotes the extraction of Cr (VI) (Figure 6.3a and 6.3b). This agrees with data from the literature [38,159]. The amount of extractable Cr (VI) is higher when the SPD is pelletised, than when it remains in powder form. The same trend was

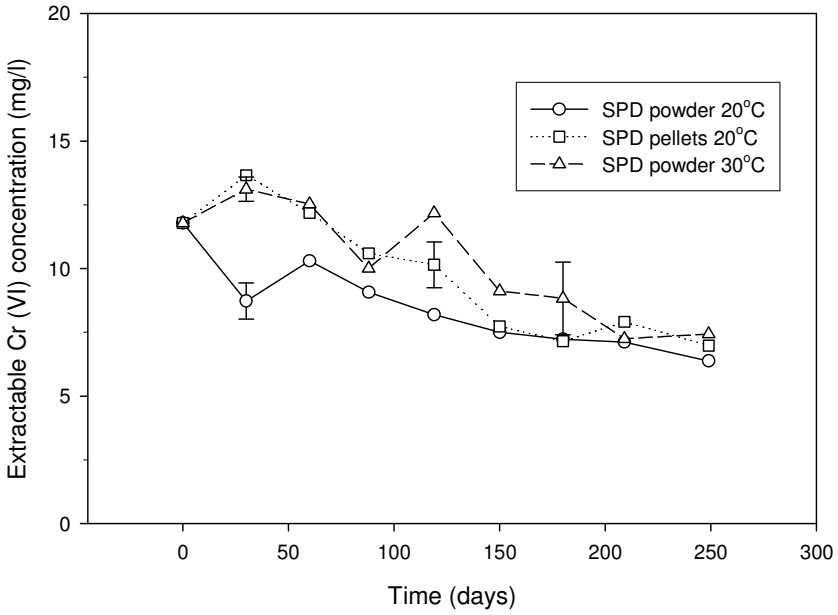

(a) SPD

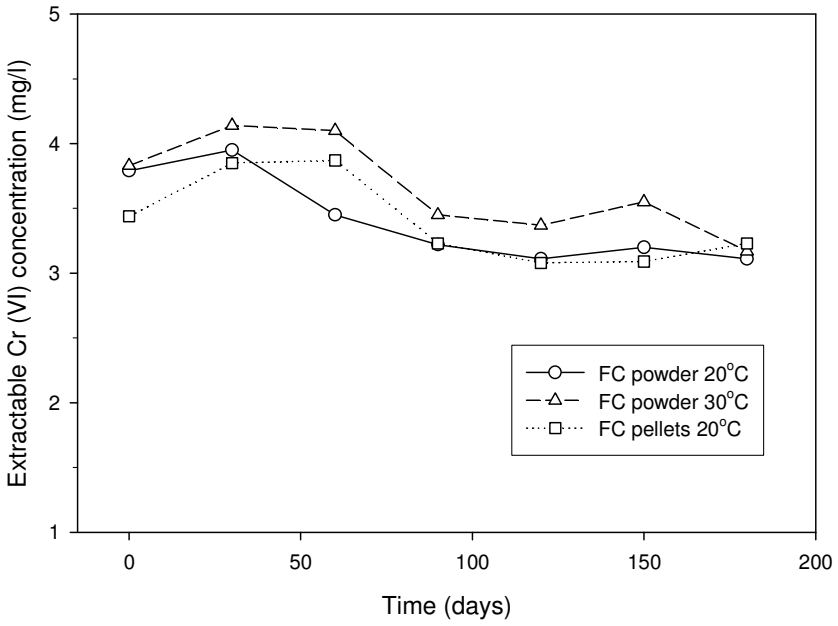

(b) FC

Figure 6.3 Effects of temperature and aging time on the leaching behaviour of Cr (VI)

not observed for the FC. It is also noted that the extractable Cr (VI) in the wastes decreases with increasing aging time, possibly due to the reducing reaction 6.1.

6.3.2 Effect of particle size of the wastes on the aging behaviour of Cr (VI)

The effect of particle size of the waste on the extractable Cr (VI) concentration is shown in Figure 6.4. It shows that the extractable Cr (VI) content increases with decreasing particle size in the SPD, while it increases with increasing particles size of the FC. The Cr (VI) which is extractable from the stainless steel plant dust and filter cake seems to remain constant after 5 months (150 days) and 3 months (90 days), respectively.

Figure 6.4 also shows that most of the extractable Cr (VI) comes from particles smaller than 53 μm in the SPD, while particles larger than 106 μm in the FC shares about 66 wt% of the leachable Cr (VI) in FC. It is also found that the extractable Cr (VI) in the wastes decreases with increasing aging time. After 8 months (approximately 240 days), approximately 44 %, 51% and 51 % of the extractable Cr (VI) in the SPD were decreased in the particles larger than 106 μm, the particles between 53 μm and 106 μm and the particles smaller than 53 μm, respectively. However, the reduction in the amount of extractable Cr (VI) in the FC was less (approximately 20%), presumably due to the relative low concentrations of Fe (II) in the FC.

6.3.3 Effect of atmosphere on the aging behaviour of Cr (VI)

The results are shown in Figure 6.5. The error bars are due to the increasing of the samples mass which absorbed water vapour during the aging experiment. It indicates that the extractable Cr (VI) from the SPD samples that were stored under the water-saturated conditions is higher than that of the samples that were stored under dry conditions, whereas the extractable Cr (VI) from the SPD samples that were stored in dry air is lower than that of the samples that were stored in dry Ar (Figure 6.5a). The extractable Cr (VI) from the SPD samples that were stored in water-saturated air is similar to that of the samples that were stored in water-saturated Ar (Figure 6.5a). Furthermore, it seems that there is no significant difference for the FC samples under different partial pressure and different water vapour content during the aging experiment (Figure 6.5b). The influence

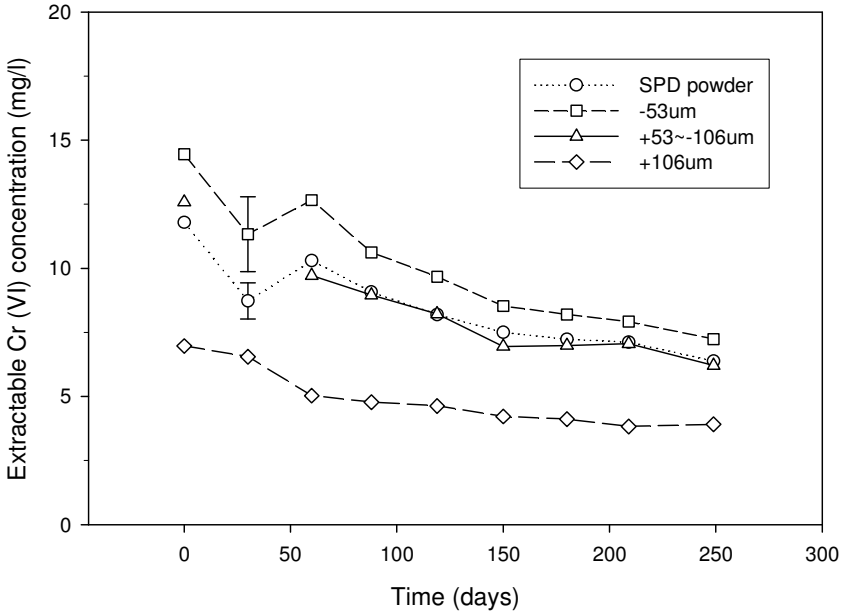

(a) SPD

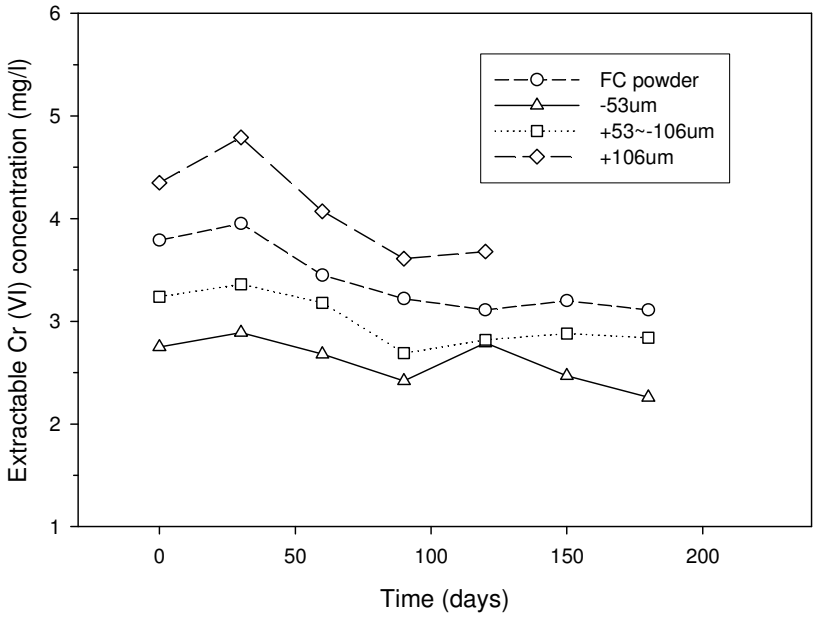

(b) FC

Figure 6.4 Effect of particle size of the wastes on the Cr (VI) aging behaviour

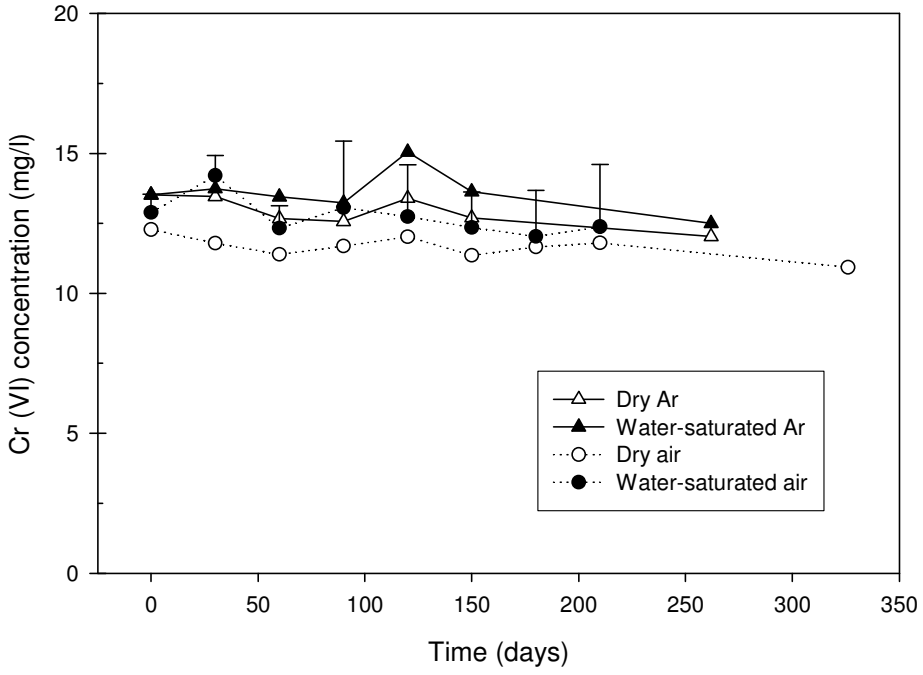
Cr (VI) concentration (mg/l)
Time (days)
Dry Ar
Water-saturated Ar
Dry air
Water-saturated air
0
5
10
15
20
0
50
100
150
200
250
300
350

(a) SPD

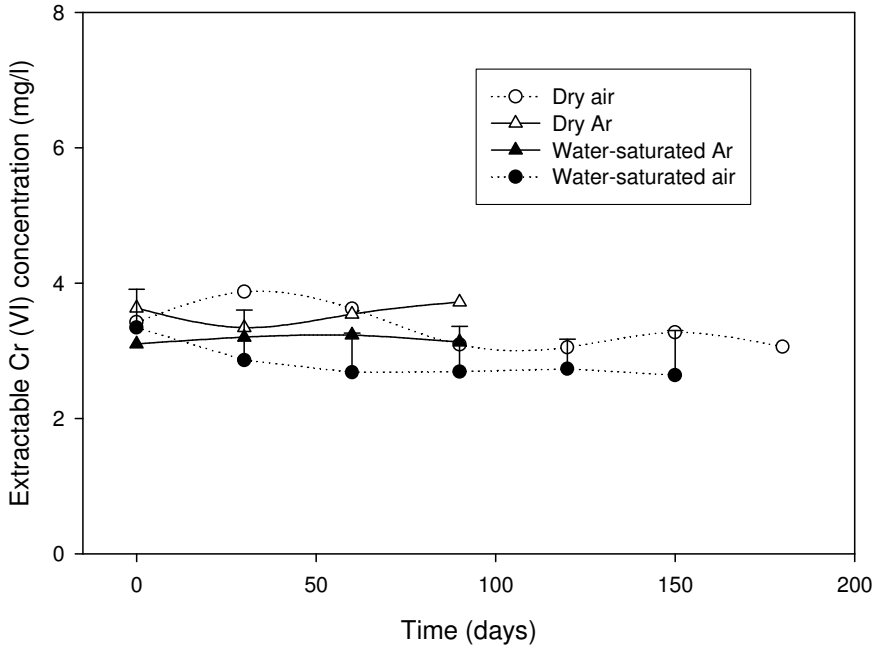
Extractable Cr (VI) concentration (mg/l)
Time (days)
Dry air
Dry Ar
Water-saturated Ar
Water-saturated air
0
2
4
6
8
0
50
100
150
200

(b) FC

Figure 6.5 Effect of atmosphere on the Cr (VI) aging behaviour

of partial oxygen pressure and water vapour content on the extractable amount of Cr(VI) from the FC could not unequivocally be determined, presumably due to the low concentrations of chromium in the FC.

6.4 Discussion

Both reactions 6.1 and 6.2 can possibly happen during the aging period since both SPD and FC contain Fe^{2+} and calcium bearing phases (calcium hydroxide and calcium fluorite in the case of SPD and free lime particles and calcium fluorite in the case of FC, Chapter 3). Chemical analysis also showed that 5.49 wt% Fe(II) is present in the SPD, possibly in the spinel phases [$(Fe,Mg,Mn)(Fe,Cr)_2O_4$]. It is also believed that trace amounts of Fe (II) (below 0.01%) are present in the FC. In this study, calcium containing phases, such as CaO, $CaCO_3$, CaF_2 and $Ca(OH)_2$, and Fe^{2+} bearing components are considered to play significant roles in the aging behaviour of Cr (VI). However, the reported rates of these two reactions are significantly different. Cr (III) can slowly be oxidised into Cr (VI) in the present of lime at ambient conditions [38], while it is fast for Fe (II) to reduce Cr (VI) at room temperature to Cr (III), especially in aqueous solution [152].

In order to confirm the conversion of Cr (III) by lime in the wastes under oxidising atmospheres, two synthetic mixtures of Cr_2O_3 and CaO were prepared, one with a CaO mol%/ Cr_2O_3 mol% ratio of 2.40 (similar to the SPD) and one with a CaO mol%/ Cr_2O_3 mol% ratio of 1.18 (similar to the FC). Figure 6.6a shows the results of the aging experiment for the synthetic samples. It clearly shows that the extractable Cr (VI) concentration increases with time. It is further confirmed that Cr (III) can be oxidised into Cr (VI) in the presence of lime. The linear regression analysis of the experimental data shows that the slope of the extractable Cr (VI) versus time curve for the synthetic SPD is higher than that of the synthetic FC. It therefore indicates that Cr (III) is more easily oxidised in the samples with the higher molar ratio of CaO to Cr_2O_3, for the same oxidation period. It means that the CaO/Cr_2O_3 molar ratio has a significant influence on the oxidation of Cr (III) to Cr (VI) in the presence of lime. The results are very similar to

the results of Pillay et al. who respectively used mixtures of 50 wt% CaO and 20wt% CaO and Cr_2O_3 in air (Figure 6.4b) [158].

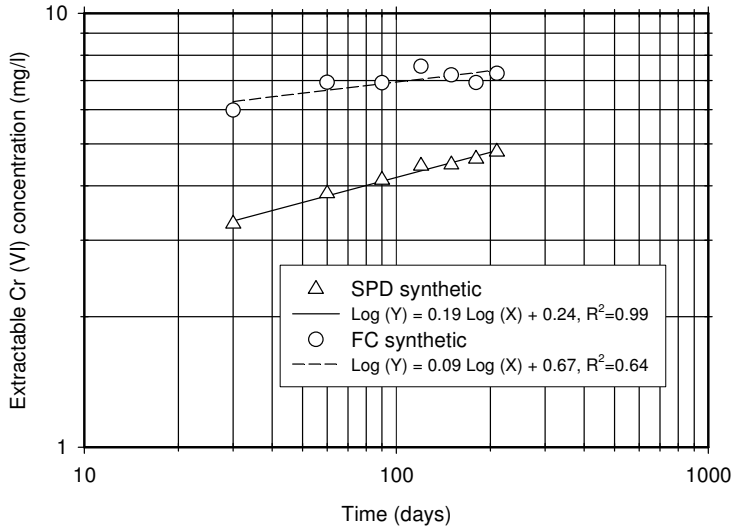

(a) The oxidation of Cr_2O_3 by CaO in air at 20°C (synthetic samples)

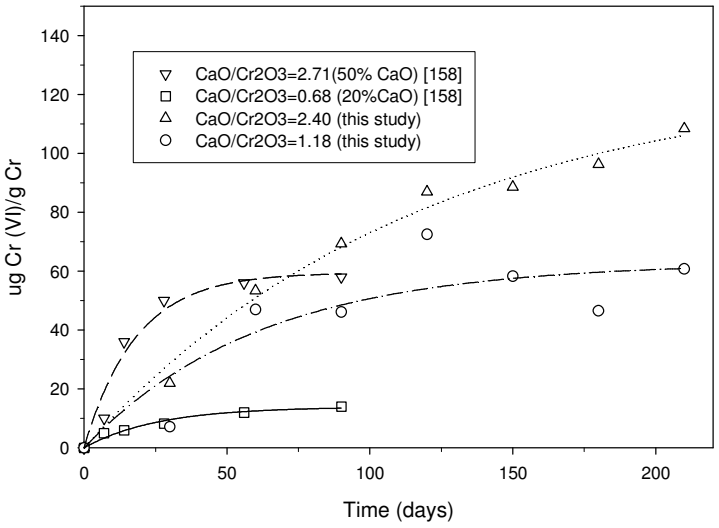

(b) Effects of CaO/Cr_2O_3 mole ratio on the oxidation of Cr_2O_3

Figure 6.6 The oxidation of Cr_2O_3 by CaO particles in air at 20°C (synthetic samples)

(a) and effects of CaO/Cr_2O_3 mole ratio on the oxidation of Cr_2O_3 (b)

If it is assumed that the reaction between CaO and Cr_2O_3 particles proceed as is shown in Figure 6.1 [158], it can be expected that this reaction would slow down as time

progresses. This can explain why the extractable Cr (VI) from SPD and FC remain constant after 5 months (150 days) and 3 months (90 days), respectively. Moreover, larger reaction surfaces are present in the pellets and therefore, more extractable Cr (VI) should exist. Increasing temperature promotes the diffusion of the reactants and the rates of the chemical reactions, and should therefore increase the formation of Cr (VI). This is in agreement with the experimental results (Figure 6.3).

The synthetic experiments suggest that Cr (III) species in the SPD and FC would be oxidised into Cr (VI), since they contain $CaO/CaCO_3$ or $Ca(OH)_2$. In addition, fluorite (CaF_2) also plays a role in the formation of Cr (VI) which is similar to CaO [160]. It is therefore expected that the extractable Cr (VI) concentration should increase during the aging experiment. However, the effects of $CaO/CaCO_3$ or $Ca(OH)_2$ and CaF_2 cannot only be considered because the SPD and FC are complex systems. Figures 6.3a and 6.3b show that the extractable Cr (VI) in the SPD and FC decrease with increasing aging time. It implies that a reduction reaction occurs during the aging experiment. It is believed that Fe (II)-containing phases, such as spinel phases in the SPD and trace amounts of ferrous bearing components in the FC, play significant roles in reducing the amount of Cr (VI) from the SPD and FC during the aging experiment. However, no efforts were made to confirm this assumption.

As shown in Figure 6.4, most of the extractable Cr (VI) comes from particles smaller than 53 μm in the SPD, while particles larger than 106 μm in the FC shares about 66 wt% of the leachable Cr (VI) in FC. This is possibly due to the different distribution of Cr(VI) in these wastes. For SPD, Cr(VI) was formed due to the change of oxygen potential in the off-gas duct, flaring of the dust particles and the presence of alkali elements [65]. It is expected that more Cr(VI) can be formed in the smaller fractions of SPD due to the better kinetics conditions for the smaller particles of SPD, such as larger surface area, and higher concentrations of alkali metals than the larger fractions of SPD (7.1% in -53μm of SPD vs. 3.8% and 3.5% in 53-106μm and +106μm of SPD, respectively) (Table 6.1). Therefore, it leaches more Cr(VI) in the small fractions of SPD than the other two fractions of SPD. This is agreement with the results (Figure 6.4). However, the leachable

Cr(VI) is mainly influenced by the ratio of Ca-containing phases to Cr_2O_3 and Fe(II)-bearing species during the aging experiment. It can be expected that more Cr(VI) can be formed in the +106μm fractions in SPD during the aging experiment due to the higher ratio of Ca-containing phases to Cr_2O_3 in the +106μm of SPD (0.41 in +106μm of SPD vs. 0.16 and 0.14 in +53-106μm and -53μm of SPD, respectively) (Table 6.2). Considering the role of Fe(II) species, it means that less decease of the leachable Cr(VI) in +106 μm of SPD during the aging experiment (3.0mg/l in +106 μm of SPD vs. 6.4mg/l and 7.2mg/l in +53-106μm and -53μm of SPD, respectively).

Table 6.1 Chemical analysis of different size fractions of SPD and FC (wt%)

%	SPD			FC		
	+106 μm	53-106 μm	-53 μm	+106 μm	53-106 μm	-53 μm
SiO_2	4.21	4.50	3.98	1.74	1.70	1.67
TiO_2	0.11	0.07	0.07	0.05	0.03	0.04
Al_2O_3	0.26	0.28	0.31	0.40	0.42	0.44
Fe_2O_3	41.95	41.52	39.97	18.57	18.48	17.94
MnO	5.00	4.90	4.52	0.98	0.86	0.89
MgO	5.67	4.77	4.36	1.05	1.31	1.26
CaO	12.12	13.26	11.43	39.33	39.65	38.99
Na_2O	1.00	1.04	0.76	0.33	0.23	0.27
K_2O	2.46	2.79	6.31	0.05	0.05	0.05
P_2O_5	0.02	0.03	0.05	0.05	0.05	0.05
Cr_2O_3	14.92	14.48	13.78	2.84	2.93	2.91
NiO	3.16	2.96	2.53	1.39	1.53	1.41
ZnO	4.58	4.59	4.28	0.31	0.39	0.42
MoO_3	1.18	1.31	1.18	0.08	0.09	0.08
SO_3	0.45	0.39	0.62	5.03	6.11	5.76
F	nd*	nd	nd	27.72	26.05	27.70
Cl	2.04	2.33	5.13	0.03	0.05	0.05
Total	99.11	99.19	99.28	99.95	99.92	99.94

*nd-not determined

For FC, it is the precipitate from the waste solution. After it was dried, crushed and ground, the major parameter which can influence the leachability of Cr(VI) is the ratio of Ca-containing phases to Cr_2O_3. Table 6.1 indicates that the ratio of Ca-containing phases to Cr_2O_3 in +106μm of FC is larger than the other two fractions of FC (13.85 in +106μm of FC vs. 13.53 and 13.40 in 53-106μm and -53μm of FC, respectively). Therefore, more leachable Cr(VI) would be detected. However, the reduction of the leachable Cr(VI) in different size fractions of FC has no significant change, presumably due to the low contents of chromium in FC (~3%).

Table 6.2 Semi-quantitative XRD analysis of different size fractions of SPD and FC

Samples*	SPD			FC**		
	+106 μm	53-106 μm	-53 μm	+106 μm	53-106 μm	-53 μm
$CaCO_3$ (%)	19.90±3.90	3.68±1.53	2.45±1.53	20.79±2.97	5.60±3.30	5.40±3.30
$Ca(OH)_2$(%)	ud***	7.70±1.35	6.82±1.32	ud	ud	ud
CaF_2 (%)	3.29±1.98	1.68±0.90	2.72±1.02	78.00±3.60	88.60±4.20	87.90±3.60
Sieve analysis (%)	2.1	25.1	72.8	56.1	18.3	25.6

*: The Ca-containing crystalline phases are different to the phases which are described in Chapter 3, due to the fact that the present analysis was performed approximately 2 years later than the previous one, and some of the calcium hydroxide reacted with carbon dioxide in the air to form calcite.
**: It is only indicated that the ratio of calcite and fluorite in the crystalline phases.
***: undetectable

The extractable Cr (VI) from the SPD samples under water-saturated conditions is higher than that under dry conditions. This suggests that water vapour in the atmosphere enhances the oxidation of Cr (VI). It is expected that more leachable Cr (VI) will form in air than in argon, due to the associated higher oxygen potential. However, it was found that the amount of extractable Cr (VI) is higher in Ar than in air. The reason for this is still not clear.

6.5 Conclusions

The aging behaviour of Cr (VI) in the stainless steel plant dust and filter cake were studied and reported on in this chapter. The results show that:

(1) The Cr (III) species can be oxidised into Cr (VI) in the presence of lime at 20°C. Increasing the molar ratio of CaO to Cr_2O_3 promote the oxidation of Cr (III).

(2) Increasing temperature favours the oxidation of Cr(III) into Cr(VI) in the wastes.

(3) The extractable amount of Cr (VI) from the SPD and FC decreases with increasing aging time, possibly due to the reduction reaction of Cr (VI) into Cr (III) by Fe (II)-containing phases.

(4) The highest amount of Cr (VI) is extracted from the –53 μm size fraction of SPD, while in the case of the FC it is extracted from +106 μm size fraction.

(5) Water vapour enhances the formation of Cr (VI) in the SPD, but not in the case of FC.

Chapter 7 Stabilisation of Cr (VI) through sintering using silica-rich clay, Part I: Synthetic samples

7.1 Introduction

Cr (VI) is toxic, carcinogenic, highly soluble and strongly oxidizing [13]. The Cr (VI)-containing wastes can be treated by different methods, such as high temperature recovery processes, conventional chemical precipitation processes [161], carbon absorption processes [161] and stabilisation/solidification processes [5,44,56,157,162]. Stabilisation/solidification processes are effective technologies whereby Cr (VI)-containing pyrometallurgical wastes can be treated. The wastes can be cemented, glassified and sintered into value added products such as bricks, cement and glass during the processes. Furthermore, it requires low investment costs and is easy to operate. Only small amounts of secondary waste residues emit from these processes.

Recently, Hattori et al. reported that Cr (VI)-containing sludge wastes can be immobilised by silica-rich clay at 1000^{o}C [157]. Thermodynamic calculations and experimental work revealed that chromium (VI) species react with silica to form the less soluble chromic oxide (Cr_2O_3) and uvarovite ($Ca_3Cr_2Si_3O_{12}$) at high temperatures and therefore reduce the leachability of Cr (VI) [157]. Huang et al. studied the incorporation of Cr (III) and Cr (VI) in a simulated basaltic industrial waste (40.5%SiO_2-11.5Al_2O_3-23%Fe_2O_3-11.5%CaO-10.0%MgO-3.5%Na_2O) [162]. It was found that chromium is stabilised by being crystallised as Cr-rich primary spinel phases at high temperatures and secondary spinel during cooling [162]. Furthermore, the stabilised waste product can be used as a medium-grade abrasive, whereby the wastes are transformed into commercial products. Maine et al. proposed that chromium in fired mixtures of 50% clay-50% ferrochrome dust is stabilised in the amorphous glassy phase (Mg-Al-Fe-Si rich) [17].

More recently, several workers have used sinter operations to stabilise Cr (VI) and soluble salts in the stainless steel plant dust and ferrochrome dust [5,16,44,58]. However, the mechanisms whereby Cr (VI) in these wastes are stabilised and the leaching

mechanisms of chromium species from the stabilised wastes forms using clay are not clear. In addition, identifying the optimum sinter parameters remain a challenge due to the variation of the characteristics of the stainless steel plant dust, ferrochrome dusts and filter cake from the waste acid treatment plant.

This chapter investigates the effects of sinter temperature, sinter time, clay type, CaO content and sinter atmosphere on the leachability of Cr (VI) from synthetic CrO_3-clay mixtures, the possible mechanisms whereby Cr (VI) is stabilised using silica-rich clay, were also studied.

7.2 Experimental

7.2.1 Materials

Three clay samples (AS, AC and MR) were collected from a local brick plant. The as-received clays were sieved manually using a screen with a pore size of 1mm. The particle size distributions of the clays of the –1mm fraction were determined with a Malvern Mastersizer 2000. The thermal characteristics of the clays were examined by the same TG/DTA instrument as described in Chapter 3. Approximately 30mg ground clay samples were heated in dry air at a flow rate of 50ml/min at 20°C/min from room temperature up to 1300°C.

Representive clay samples of approximately 135g were mixed with analytical reagent grade CrO_3 to attain the same Cr (VI) concentration as is found in the stainless steel plant dust (245mg/kg). The minimum amount of distilled water (approximately 15ml) was added to each sample. The mixture was pressed in a mould (28mm×20mm×100mm) using a hydraulic press at 50 kN force. The samples were then dried at 110^{o}C for 48 hours after which they were reacted in a tube furnace. Figure 7.1 schematically shows a cross section of the furnace. In this set of experiments, the sinter temperature, sinter time, sinter atmosphere, initial Cr (VI) concentration and the influence of lime addition were investigated. The experimental parameters are shown in Table 7.1. The sinter temperatures ranged from 1150^{o}C to 1250^{o}C. The sinter time ranged from 3 to 7 hours. Reagent grade CaO was added to the clays in order to obtain mass %CaO/mass %SiO_2

(in the clay) ratios of 0.05, 0.1 and 0.2. Different initial amounts of CrO_3 and different atmospheres (air and argon) in the brick were also considered (Table 7.1). The samples that were spiked with 245 mg/kg CrO_3 and sintered at 1200°C for 5 h were duplicated.

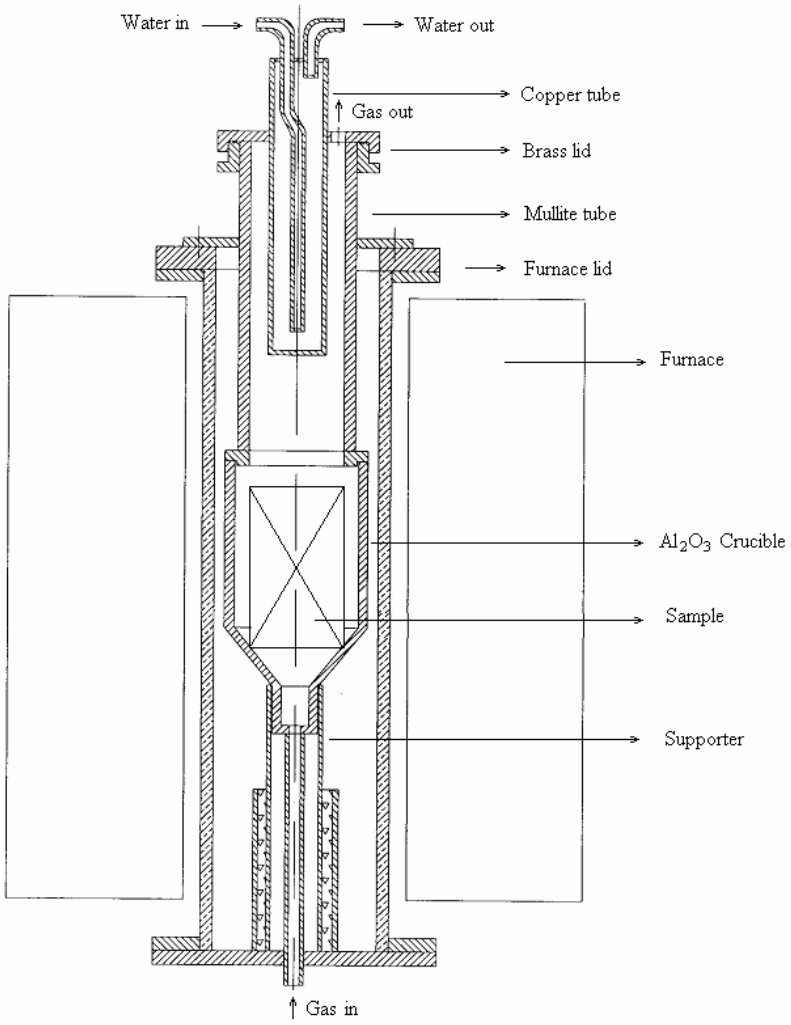

Figure 7.1 The furnace set-up

Table 7.1 Experimental conditions

Clay	AS, MR, AC
Sinter temperature (°C)	1150, 1200, 1250
Sinter time (hours)	3, 5, 7
CaO/SiO_2 mass ratio	0, 0.05, 0.1, 0.2
Initial Cr (VI) concentration (mg/kg)	0, 245, 2450
Atmosphere	Dry air and argon

The heating and cooling rates during the experiments were ~1.5^{o}C/min. The temperature profile of the tube furnace was measured with a calibrated type-B thermocouple with an error of ±1^{o}C.

In order to examine chromium losses during the sintering process, and therefore potential secondary pollution, a water-cooled copper finger was set inside the tube furnace to condense any volatile Cr-containing species. The condensate was dissolved in 50ml nitric acid solution (1mol/l). The total chromium concentration was determined using a UV/Vis spectrophotometer.

7.2.2 Analytical techniques

X-ray diffraction (XRD), X-ray fluorescence (XRF) and scanning electron microscopy (SEM-EDS) were used to examine the phase compositions, chemical compositions and microstructures of the sintered samples (described in Chapter 3). Cr (VI) in the sintered brick was digested in a sodium carbonate/sodium hydroxide solution and photometrically determined using an Inductively Coupled Plasma Optical Emission Spectrometer (ICP-OES).

The sintered clay products were ground and the leachability of Cr (VI) was evaluated with the modified TCLP and modified ASTM D 3987-85 tests. The Cr (VI) concentration in the leachate was determined (see Appendix I). The detection limit of Cr (VI) using this method is approximately 0.004 mg/l, while it is reliable when Cr (VI) concentrations are higher than 0.01 mg/l [163,164].

7.3 Results and discussion

7.3.1 Characteristics of the clays

7.3.1.1 Particle size distribution, chemical composition, phase composition and microstructure

Clays AS and AC are grayish in colour, while MR is brownish. The particle size distributions of the sieved clays are shown in Figure 7.2. It shows that the mean size of

clays AS, MR and AC are approximately 52, 34 and 22 μm, respectively. The chemical compositions of the clay samples are shown in Table 7.2. Approximately 93 wt% of clay AS consists of SiO_2 and Al_2O_3, while clay MR contains less silica but more iron oxide, alumina and alkali metal oxides than clay AS. Clay AC has the highest Al_2O_3 and TiO_2 contents and loss on ignition (LOI) at 1000°C.

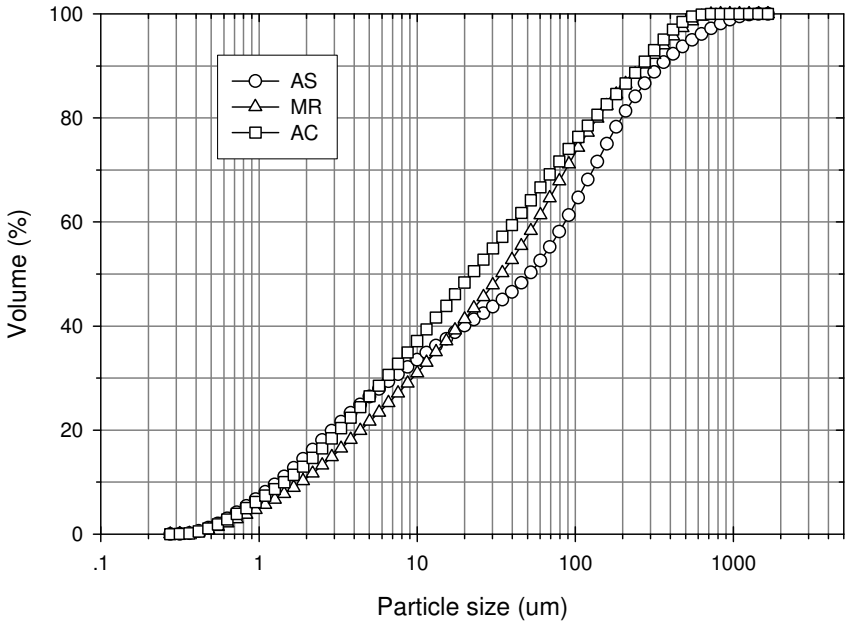

Figure 7.2 The particle size distribution of the clays

Table 7.2 The chemical compositions of the clays (wt.%)

Clay	SiO_2	TiO_2	Al_2O_3	Fe_2O_3	MnO	MgO	CaO	Na_2O	K_2O	Cr_2O_3	LOI	Total
AS	80.68	0.78	12.20	0.99	0.02	0.06	0.00	0.06	0.87	0.02	3.84	99.45
MR	67.33	0.82	16.06	6.49	0.18	0.86	0.04	0.16	4.18	0.03	3.45	99.60
AC	57.03	1.40	27.18	3.04	0.02	0.19	0.07	0.05	0.53	0.03	9.46	99.00

The XRD patterns of the clays are shown in Figure 7.3. Clay AS contains the crystalline phases quartz (SiO_2), kaolinite ($Al_2Si_2O_5(OH)_4$), microcline ($KAlSi_3O_8$) and small amounts of rutile (TiO_2) and $(Al,Fe,Ti)_3O_5$. Clays MR and AC contain muscovite ($(K,Na)(Al,Mg,Fe)_2(Si_{3.1}Al_{0.9})O_{10}(OH)_2$) besides the above phases. Iron is incorporated in

the muscovite phase structure and exists in $(Al,Fe,Ti)_3O_5$. Trace amounts of $ZrSiO_4$ particles also exist in clay AS.

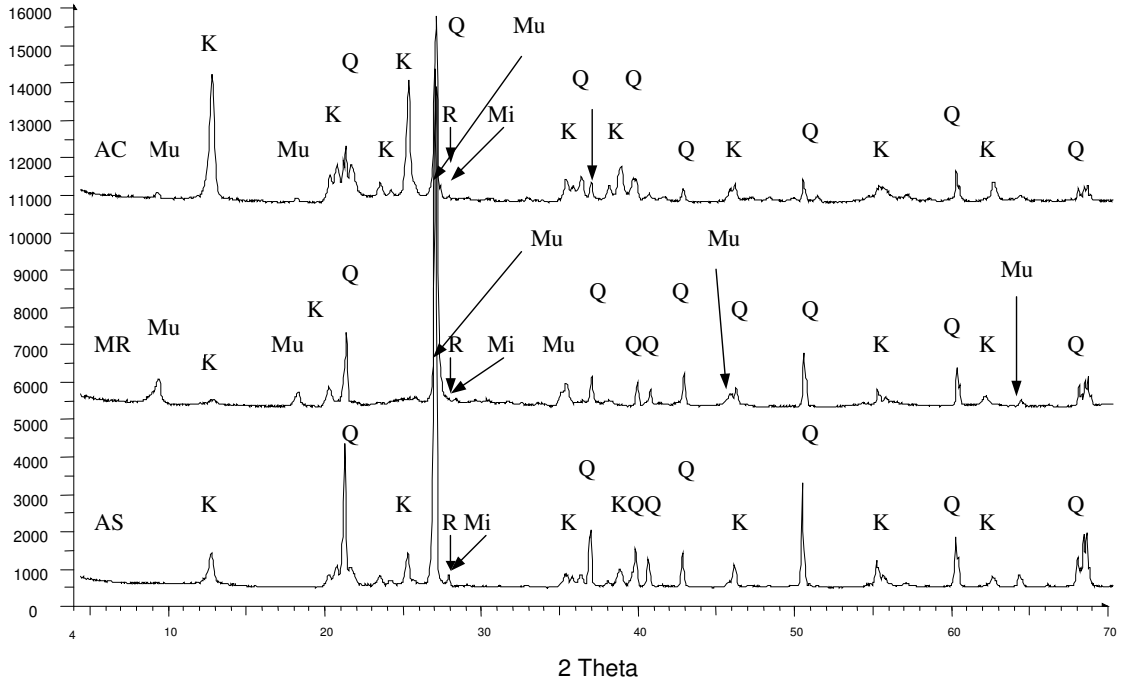

Figure 7.3 The crystalline phases present in the clays (Q-quartz, K-kaolinite, Mi-Microcline, Mu-Muscovite, R-Rutile)

The semi-quantitative XRD analysis of the clays is shown in Table 7.3. It indicates that quartz and kaolinite are the major phases in clay AS. Clay MR contains large portions of quartz and muscovite (about 92 wt%), while quartz, kaolinite and muscovite comprises about 95 wt% of the crystalline phases in clay AC. It further confirms that clay AC should have the highest loss on ignition due to the high content of kaolinite and muscovite (approximately 72 wt% in clay AC vs. 31 wt% and 46 wt% for clays AS and MR, respectively). Most of the potassium in clay MR is in muscovite.

Table 7.3 Semi-quantitative XRD analysis

Clay	Q	K	Mi	Mu	R
AS	64.5	31.4	2.4	nd*	1.7
MR	50.5	4.7	1.4	41.3	2.1
AC	22.4	62.3	2.4	10.1	2.8

Note: Q-quartz, K-kaolinite, Mi-Microcline, Mu-Muscovite, R-Rutile. *nd-not determined

The thermal characteristics of clays have extensively been investigated [165-169]. It was also examined in this study and is reported on in Appendix II.

7.3.2 Leaching behaviour of Cr(VI) from the sintered brick

7.3.2.1 Effect of temperature on the leachability of Cr (VI)

Cr (VI) leachability from the sintered clay which was spiked with Cr (VI), as a function of sinter temperature, is shown in Figure 7.4. Both the modified TCLP and ASTM D 3987-85 tests indicate that the Cr (VI) concentration decreases with increasing sintering temperature. The Cr (VI) concentration becomes less than 0.015 mg/l after sintering at 1200°C and 5 hours (duplicated), which is below the acceptable environmental risk concentration of Cr (VI) of 20 ppb. Cr (VI) concentration in the leachate from the sintered brick (AS, 1250°C, 5 hours and dry air) is less than the detection limit (0.004 mg/l).

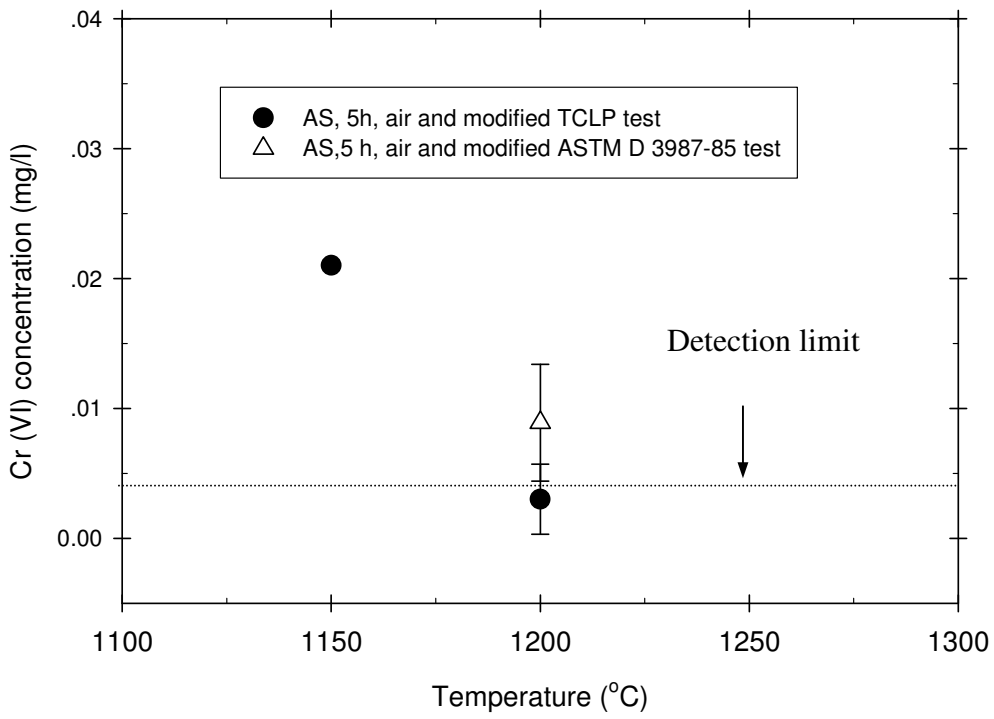

Figure 7.4 The effect of temperature on the leachability of Cr (VI)

The Cr (VI) stabilisation ratio when clay AS is used can be calculated using the following equation:

$$\text{Cr (VI) stabilisation ratio (\%)} = \frac{\text{Cr (VI)}_{\text{spiked}} - \text{Cr (VI)}_{\text{in the sintered brick}}}{\text{Cr (VI)}_{\text{spiked}}} * 100 \qquad (7.1)$$

Where Cr (VI) $_{\text{spiked}}$ is the total amount of Cr (VI) which was spiked into the clay brick, and Cr (VI) $_{\text{in the sintered brick}}$ is the Cr (VI) content of the sintered brick.

The mass of the green brick, which was spiked with CrO_3 and sintered at 1250°C for 5 hours using clay AS, is 133.6g, while the mass of the brick after being sintered is 127.9 g. The Cr (VI) concentration in the sintered brick is 1.15 ppm (as determined by ICP-OES). Hence, the stabilisation ratio can be calculated as:

$$\text{Cr (VI) stabilisation ratio (\%)} = \frac{245mg/kg * 0.1336kg - 1.15mg/kg * 0.1279kg}{245mg/kg * 0.1336kg} * 100$$

$$= 99.6$$

This indicates that sintering is an effective method whereby Cr (VI)-containing wastes can be treated.

The XRD results show that the major phases present in the sintered brick are quartz, mullite ($3Al_2O_3 \cdot 2SiO_2$) and cristobalite (Figure 7.5). The microstructure of the brick after it has been sintered at 1200°C for 5 hours is shown in Figures 7.6 and 7.7. It indicates that a glassy phase, small quartz particles and rutile or $(Al,Fe,Ti)_3O_5$ are sintered together to form the major matrix of the brick (Figure 7.6). In addition, the glassy phases (Al-Si-K-Fe based) exist between the quartz particles. The typical EDS analysis of the different phases is shown in Table 7.4 (average value obtained from 5 analyses at different positions in the brick). Mullite crystals are too fine, and could not be analysed without picking up from the surroundings.

The mass balance of the sample which was spiked with CrO_3 and sintered at 1200°C for 5 hours are attached in Appendix III. It shows that chromium is stabilised in the brick, probably in the mullite phase and glassy phases.

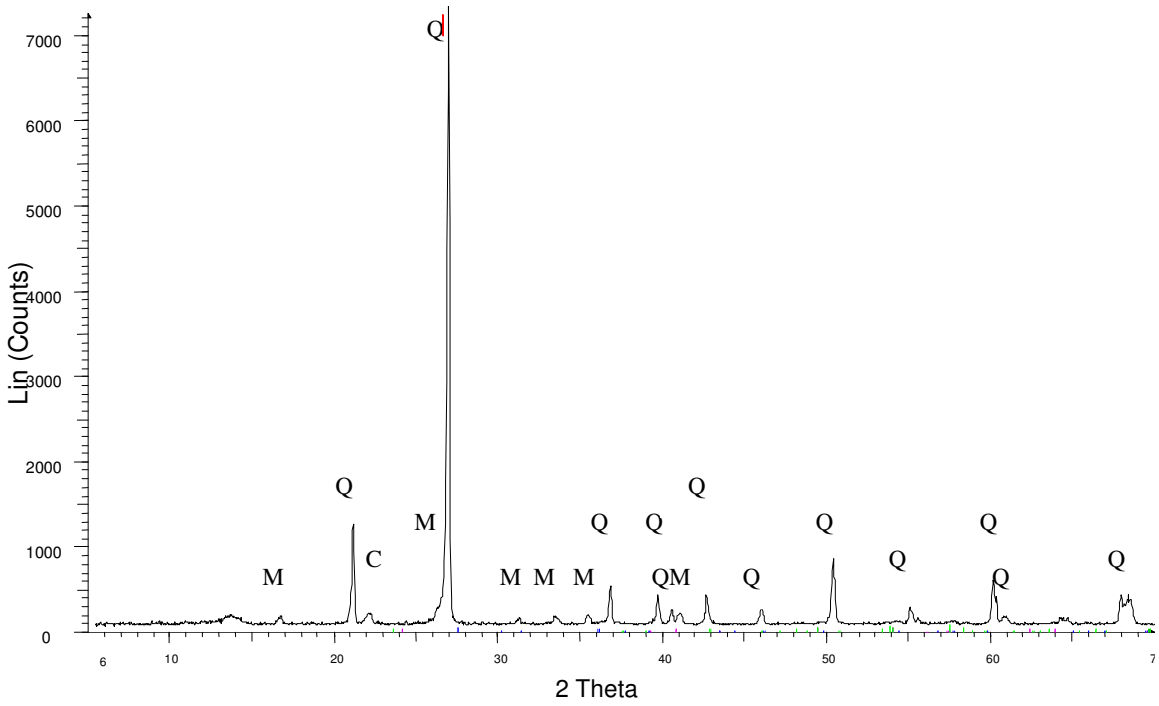

Figure 7.5 XRD Pattern of the sintered brick (1200°C, 5h, AS+CrO_3) (Q-quartz, M-Mullite, C-Cristobalite, R-Rutile)

Table 7.4 Typical EDS analysis of different phases (wt%)

Phases	SiO_2	Al_2O_3	K_2O	TiO_2	Fe_2O_3
Silica	100	0	0	0	0
Mullite+ silica	60.9	35.9	0	0	3.2
Rutile	0	0	0	100	0
$(Al,Fe,Ti)_3O_5$	0	11.2	0	48.8	40.0
Glassy phase	53.7	39.8	1.5	0	5.0

7.3.2.2 Effect of sintering time on the leachability of Cr (VI)

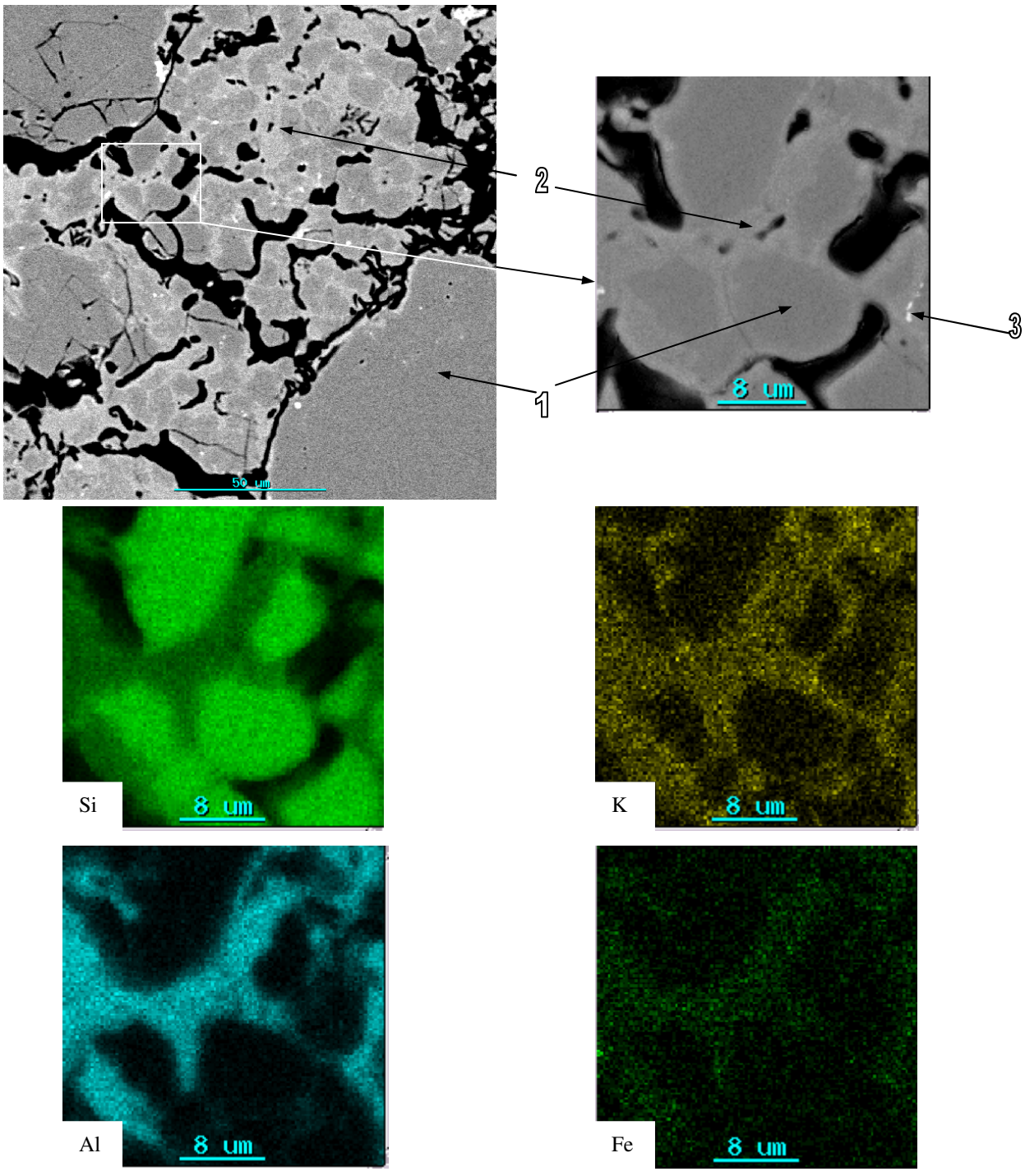

Figure 7.6 Typical microstructure and X-ray map of the sintered clay brick (1200^{o}C and 5h) (1-Quartz, 2-Glassy phase (Si-Al-K-Fe), 3-Rutile)

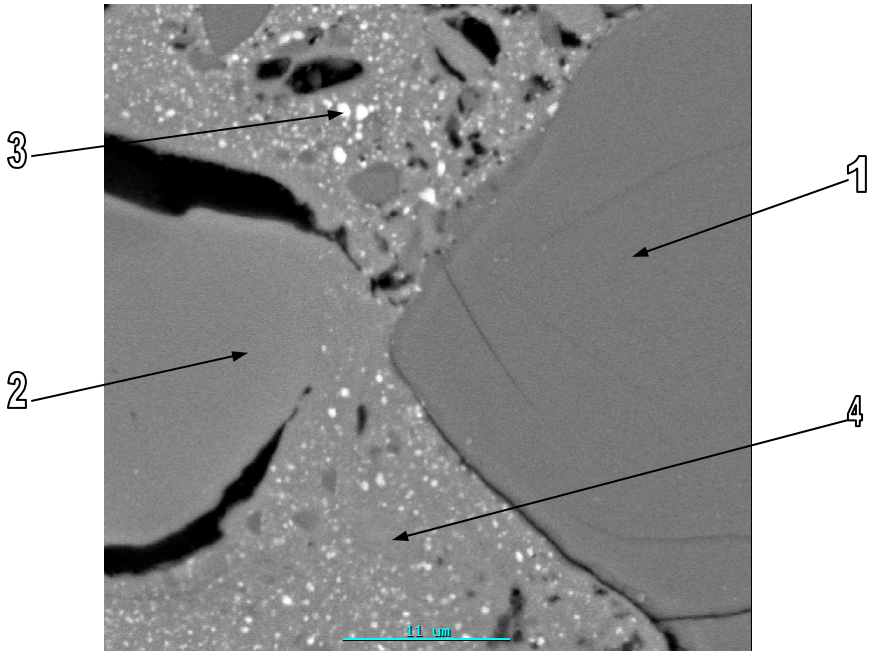

Figure 7.7 Typical microstructure of the sintered clay brick (1200^{o}C and 5h)(1-Quartz, 2-Mullite+ silica, 3-$(Al,Fe,Ti)_3O_5$, 4-Glassy phase (Si-Al-K-Fe based))

The effect of sintering time on the leachability of Cr (VI) is shown in Figure 7.8. According to the modified TCLP test, the leachability of Cr (VI) decreases with increasing of sintering time, while the modified ASTM D 3987-85 test indicated that the leachable Cr (VI) remains constant. The leachable Cr (VI) concentrations are in both instances however, in compliance with the regulatory limits of South Africa (the acceptable environmental risk concentration of Cr (VI) is 20 ppb). The difference in leachability of Cr (VI) between these two leaching tests is due to the fact that leach solutions of different pH were used [170-172]. Figure 7.8 also indicates that Cr (VI) can be stabilised with clay AS by sintering it at 1200^{o}C over 3 hours.

7.3.2.3 Effect of clay on the leachablity of Cr (VI)

The effect of different clays on the leachability of Cr (VI) from the sintered bricks is shown in Figure 7.9. It shows that there is no significant difference between the amounts of Cr (VI) that leached when the three different types of clay were used. In addition,

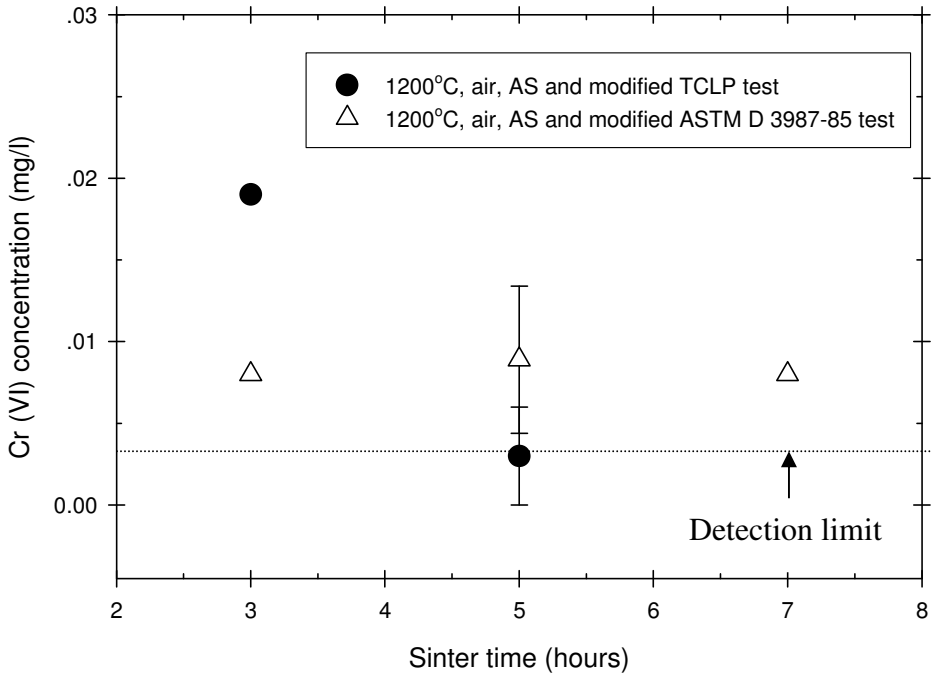

Figure 7.8 The effect of sintering time on the leachability of Cr (VI)

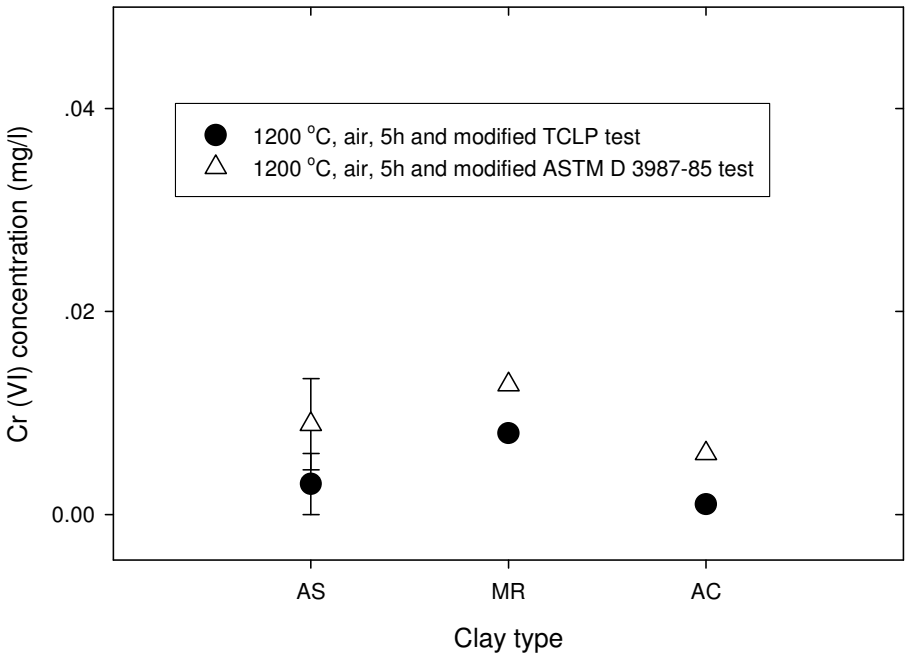

Figure 7.9 The effect of clays on the leachability of Cr (VI)

Figure 7.9 indicates that all the clays have enough capacity to stabilise such lower amounts of Cr (VI) in the clay (approximately 245 mg/kg).

7.3.2.4 Effect of CaO content on the leachability of Cr (VI)

The effect of the basicity ratio of the clay-CrO_3 samples (expressed as mass %CaO/mass %SiO_2) on the leachability of Cr (VI) is shown in Figure 7.10. The modified ASTM D 3987-85 test indicates that the addition of lime increases the leachability of Cr (VI), while the modified TCLP tests indicates that the leachability of Cr (VI) is not affected by the basicity ratio. The Cr (VI) concentration in the leachate from the modified ASTM D 3987-85 test on the brick with a mass %CaO/mass %SiO_2 ratio of 0.05 and the modified TCLP test on the bricks with a mass %CaO/mass %SiO_2 ratio of 0.1 and 0.2, is below the detection limit. It is, therefore, very important to keep the CaO content in the sintered brick as low as possible (0.05 under current experimental conditions) when Cr (VI) in the wastes is stabilised using clay. By only considering the effect of CaO, it can therefore be expected that the extractable Cr(VI) content from the mixture of AC-CrO_3 is higher than that from the mixtures of clays MR/AS-CrO_3, since it has the highest mass %CaO/mass %SiO_2 ratio in the mixture.

7.3.2.5 Effect of initial Cr (VI) content on the leachability of Cr (VI)

The effect of initial Cr (VI) content on the leachability of the Cr (VI) is shown in Figure 7.11. It shows that the leachability of Cr (VI) remains below 0.01 mg/l although the initial Cr (VI) content in the green brick can be as high as approximately 2450 mg/kg. Cr (VI) can therefore be effectively stabilised by clay.

7.3.2.6 Effect of sinter atmosphere on the leachability of Cr (VI)

The effect of sinter atmosphere on the leachability of Cr (VI) from the sintered bricks is shown in Figure 7.12. It indicates that sinter atmosphere has no significant influence on the leachability of Cr (VI).

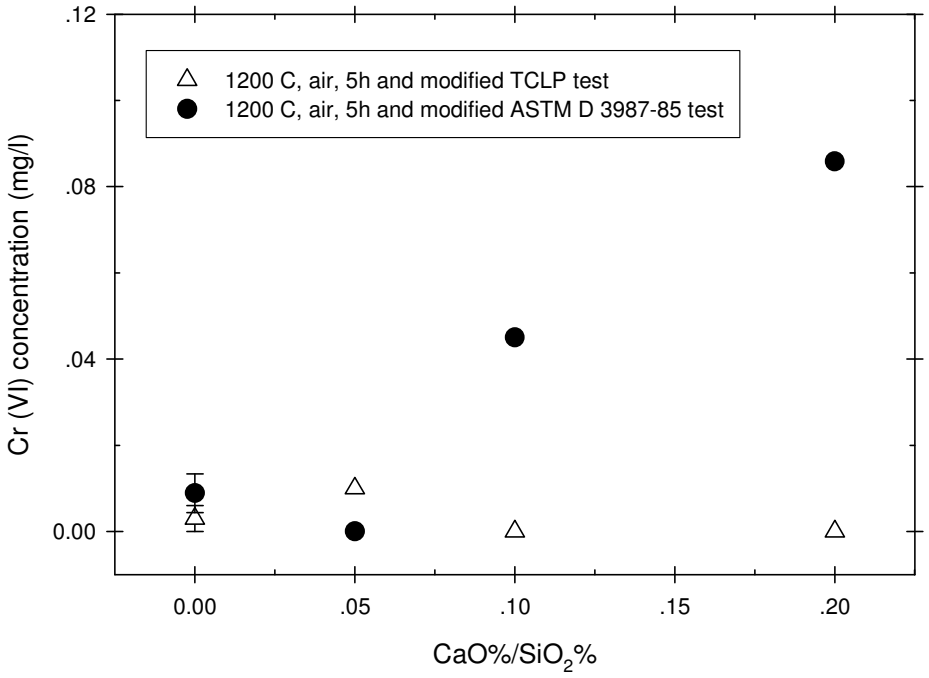

Figure 7.10 The effect of mass %CaO/ mass %SiO_2 on the leachability of Cr (VI)

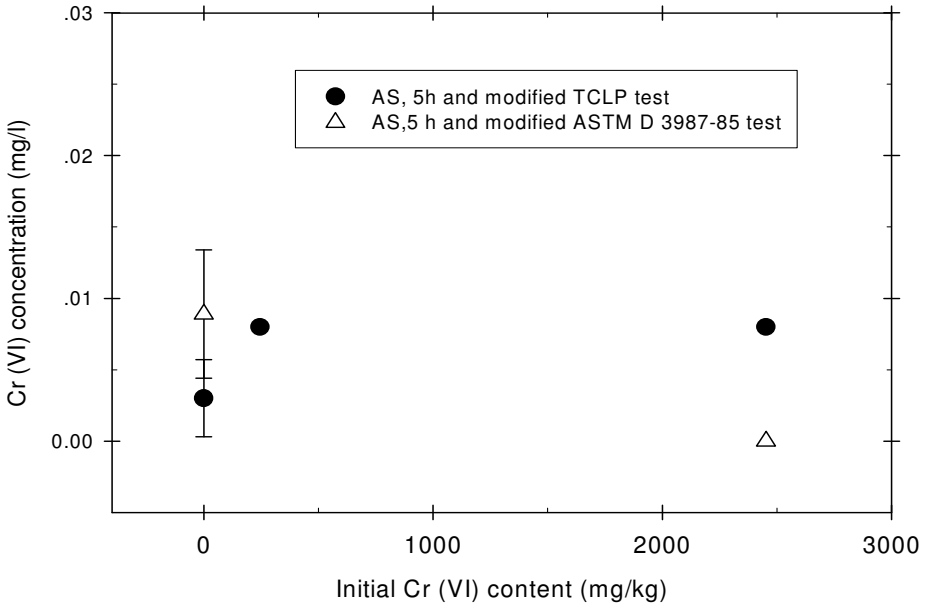

Figure 7.11 The effect of initial Cr (VI) content on the leachability of the Cr (VI)

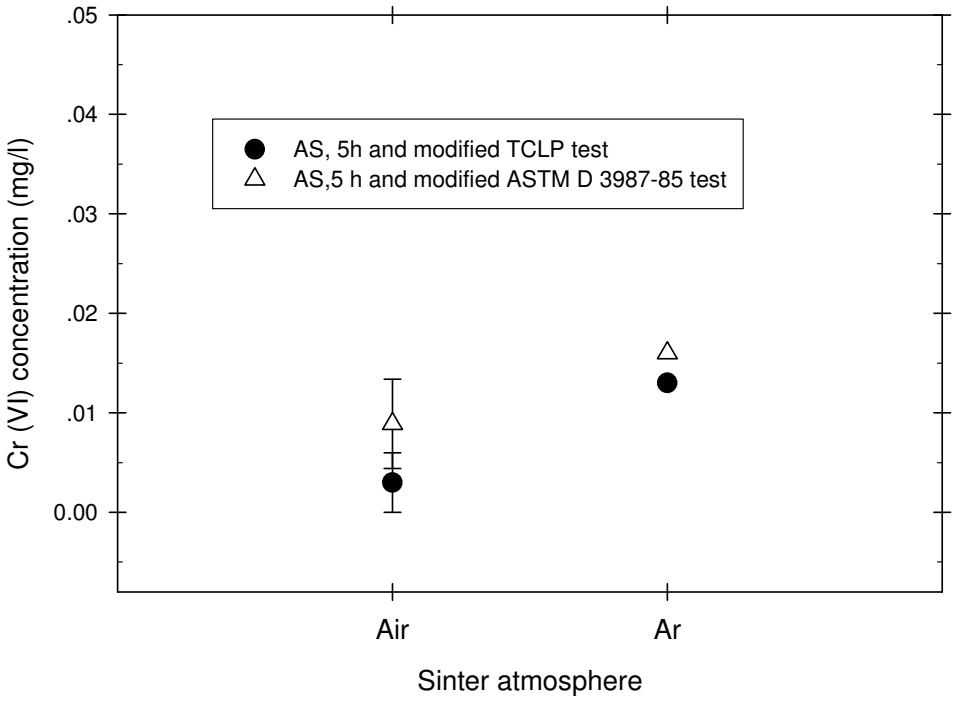

Figure 7.12 The effect of sinter atmosphere on the leachability of the Cr (VI)

7.3.3 Chromium emissions during sintering process

Chromium emissions were very low in all the experiments although detectable (Figure 7.13). It is assumed that all the collected chromium on the copper tube is Cr (VI)-containing components due to the high vaporization tendency of Cr (VI) [173-175]. It shows that increasing sinter temperature and initial chromium content increase the chromium that is released into the atmosphere. The type of clay used has no significant influence on the chromium emission. On the other hand, the chromium emission factors during the sintering process are quite low compared to other industrial sources (Table 7.5 [176,177]). It also shows that Cr (VI) species are easier to vaporise in an atmosphere of high Po_2 (dry air) than in an atmosphere of low Po_2 (argon). The chromium emissions vary from 10.6 mg/t brick to 43.7 mg/t brick under different sinter conditions. However, chromium emissions could be potentially higher if higher concentrations of chromium are present in the wastes.

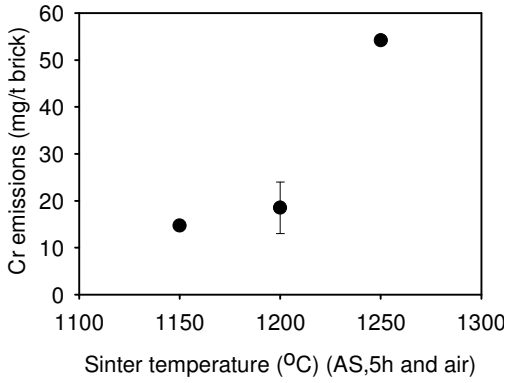

(a)

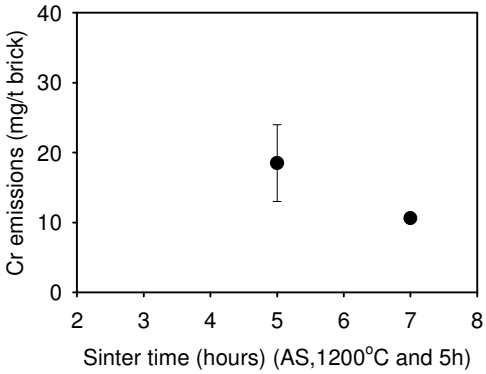

(b)

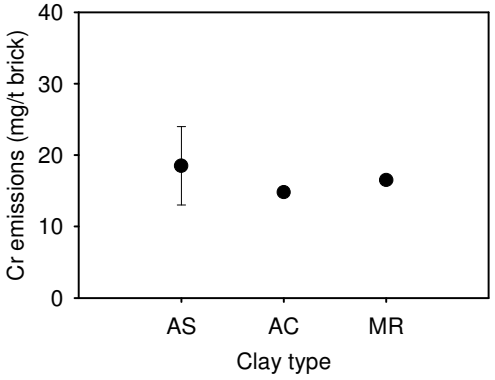

(c)

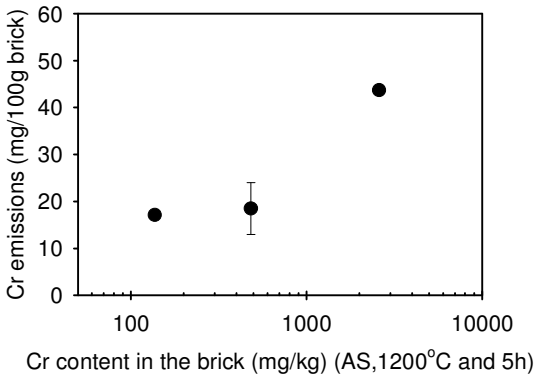

(d)

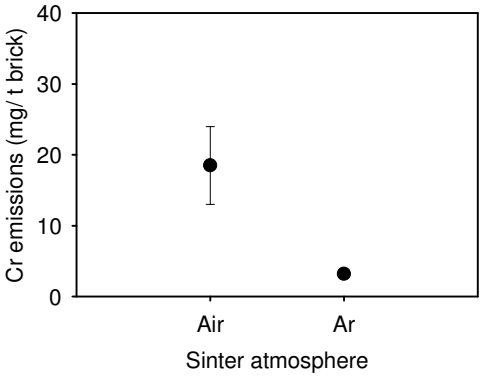

(e)

Figure 7.13 Chromium emissions during the sintering experiments

Table 7.5 Emission factors of chromium in various industries [177,178]

Coal-fired industrial boiler (g/t)	Oil-fired industrial boiler(g/1000l)	Steel works (g/t steel)			Municipal incinerator (g/t)	Sewage sludge incineration (g/t)	Cement Industry (g/t)
		VS	EP	BF			
1.7	2.2	9.0	13.5-36.1	4.0	1.10	10	1.6

Note: VS-Venturi Scrubber; EP-Electrostatic Precipitator; BF-Baghouse filter.

7.4 Conclusions

The stabilisation of synthetically prepared Cr (VI)-clay mixtures was investigated in this chapter. The leachability of Cr (VI) from the sintered clay bricks was evaluated through the use of the modified TCLP and ASTM D 3987-85 tests. The following conclusions can be drawn:

1) Silica-rich clay can be used to stabilise Cr (VI). The stabilisation ratio of Cr (VI) can be as high as 99.6% when the brick is sintered at 1250^{o}C for 5 hours.
2) Increasing sintering temperature and time, and keeping the CaO/SiO_2 ratio content below 0.05 reduce the leachability of Cr (VI), while the type of clay does not seem to significantly influence the leachability of Cr (VI).
3) The leachability of Cr (VI) remains below 0.01 mg/l although the initial content of Cr (VI) in the green brick is approximately 2450 ppm. It is efficient to stabilise Cr (VI) by sintering at 1200^{o}C over 3 hours using any of the examined clays.
4) The chromium emission during the sintering process is low and varies from 10.6 mg/t brick to 54.2 mg/t brick in this study.

Chapter 8 Stabilisation of Cr (VI) through sintering using silica-rich clay, Part II: Electric furnace dust and filter cake

8.1 Introduction

The Estimated Environmental Concentration (EEC) and the acceptable risk level ($0.1 \times LC_{50}$[1)]) are often used to evaluate whether the hazardous wastes are acceptable in South Africa [15]. Therefore, bricks that are constituted from electric furnace dust and filter cake and clay can only be used in the construction industry when the EEC of Cr(VI) is lower than 0.02 ppm (acceptable risk level). The acceptable concentration of Cr(VI) in the leachates of the modified TCLP or the modified ASTM D3987-85 tests should be less than 0.013 mg/l (calculation details are given in Appendix IV). This value was used in this chapter to evaluate whether the stabilised products are environmentally acceptable.

In Chapter 7, it is proven that Cr (VI) can be stabilised through sintering using silica-rich clay. However, the optimum parameters of the sintering process and the Cr (VI) stabilisation in the wastes need to be studied when electric furnace dust and filter cake are used to substitute parts of the clay. This chapter subsequently describes (1) the optimum sinter parameters when Cr (VI) is stabilised (sinter time, temperature and the ratio of clay to dust) in stainless steel plant dust that was produced in South Africa and (2) the Cr (VI) stabilisation in the dust and filter cake using clay.

8.2 Experimental

8.2.1 Sample preparation

Approximately 125g mixtures of clay and electric furnace dust and filter cake samples were pressed into small bricks with cross sections of 28mm×100mm using a hydraulic press at 50 kN force for 5 minutes. The minimum amounts of distilled water (about 12 wt%) were added to the mixture. The green samples were then dried at 110°C for 48 hours, after which they were weighed and sintered in a tube furnace.

[1)] Acute ecotoxicity of substances in waste, which can kill 50% of the aquatic animals tested, mg/kg [15].

8.2.2 Experimental methods

The furnace set up is similar to the one shown in Figure 7.1. In this set of experiments, different types of clays, sinter temperatures, ratios of clay to waste and sinter times were investigated in order to find the optimum sintering parameters. The extent to which these parameters, were varied in the experiments, are listed in Table 8.1. It is shown that three clays (AS, MR and AC) were used in this study. The sinter temperatures ranged from 1000°C to 1150°C and the sinter time from 1 hour to 5 hours. In order to find the optimum ratio of waste to clay, different mixtures were made, ranging from 0 to 100wt%. Furthermore, lime was added to the mixture to confirm the effect of basicity (mass %CaO/mass % SiO_2) on the leachability of Cr (VI) from the stabilised wastes.

Table 8.1 The process parameters of the experiments

Waste materials	**SPD**	**FCD1, 2 and FC**
Clay type	AS, MR, AC	AS
Sinter temperature (°C)	1000, 1050, 1100, 1150	1000
Sinter time (hours)	1, 3, 5	5
Amount of waste materials (wt%)	0, 40, 50, 60, 70, 100	50
Spiked agent (50%AS+50%SPD)	CrO_3, $K_2Cr_2O_7$, K_2CrO_4, $CaCrO_4$ and K_2O	-

Since the Cr (VI) concentration in the sintered brick is very low (possibly in the ppb range), it is impossible to directly determine the stabilisation behaviour of Cr (VI) using the available analytical methods such as SEM-EDS and XRD. Therefore, large amounts of Cr (VI) were spiked into the mixture in order to identify where Cr (VI) is and how it is stabilised in the sintering process. In these experiments, reagent grade CrO_3 (1 wt% and 10 wt%), $K_2Cr_2O_7$, K_2CrO_4 as well as synthetic $CaCrO_4$[2)] (the same amount of Cr (VI) as in 1 wt%CrO_3), were spiked into the mixture of 50 wt% AS and 50 wt% waste to study the stabilisation of Cr (VI). K_2O (2.07 wt% and 4.07 wt%) was also spiked into the

[2)] The process whereby $CaCrO_4$ was prepared is given in Appendix V.

50%AS-50%SPD mixtures (added as K_2CO_3) to study the influence of alkaline metals on the leachability of Cr (VI).

Dry air was purged through the furnace in the experiments. Both heating and cooling rates of the furnace were ~1.5^{o}C/min.

8.2.3 Analytical methods

The modified TCLP and modified ASTM D 3987-85 tests were used to evaluate the leachability of Cr (VI) from the sintered product. Two TCLP solutions were prepared for the modified TCLP tests: TCLP solution 1 had a pH of approximately 4.93, and was prepared by diluting a mixture of 11.4ml analytical reagent glacial acetic acid and 128.6 ml 1 M NaOH solution in 2 l with distilled water. TCLP solution 2 was prepared by diluting 11.4ml analytical reagent glacial acetic acid in 2 l solution with distilled water. TCLP solution 2 was only used for the sintered pure SPD brick and the lime spiked brick. TCLP solution 1 was used for the remainder of sintered samples. The modified ASTM D 3987-85 leaching solution consists of distilled water with a pH of approximately 6.

The Cr (VI) concentration in the leachate was determined photometrically using a UV-Vis spectrophotometer. Due to the fact that the concentrations of toxic substances [except Cr (VI)] which leached from the sintered bricks in the modified TCLP test are higher than that in the modified ASTM D 3987-85 test, the leachable toxic substances [except Cr (VI)] in the modified TCLP leachate from the selected samples were measured using an ICP-OES. The redox potential of the leachate was determined using a Thermo Model 97-78-00 Platinum Redox Electrode. XRD, SEM-EDS and XRF were used to analyse the sintered bricks with respect to the crystalline phases present, microstructure and chemical composition.

8.3 Results and discussion

8.3.1 Effect of clay type on the leachability of Cr (VI)

The effect of different types of clays on the leachability of Cr (VI) from the sintered brick is shown in Figure 8.1. The results indicate that the Cr (VI) concentration in the leachate

of the modified TCLP tests are below the detection limit of the spectrophotometer, while the Cr (VI) concentrations from the modified ASTM D 3987-85 test are significantly higher and can therefore be determined.

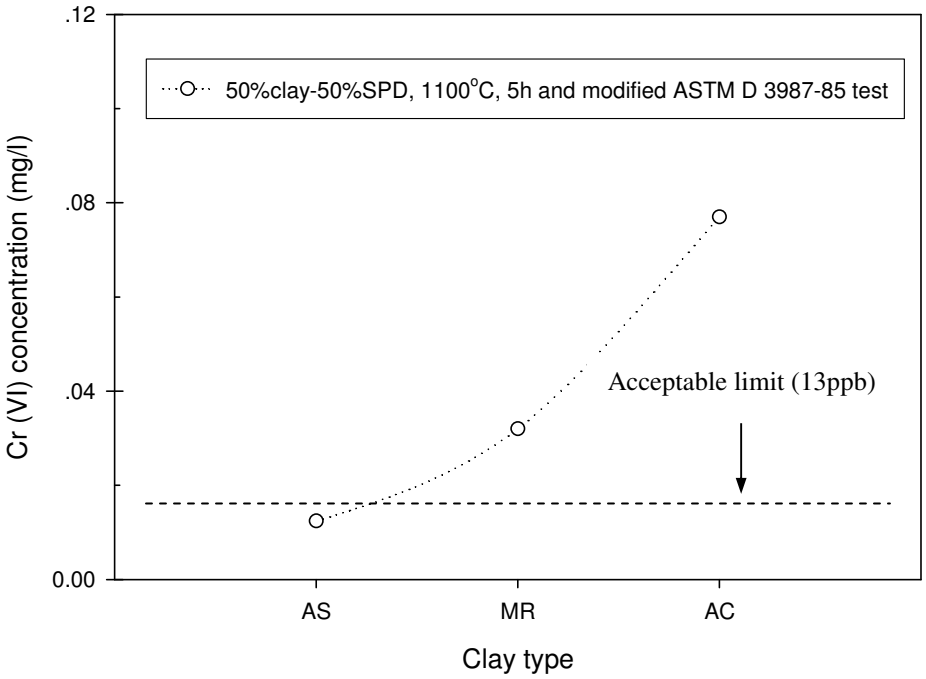

Figure 8.1 The influence of different types of clays on the leachability of Cr (VI)

This is due to the fact that in the modified TCLP tests, the leaching buffer solution has a pH of approximately 4.93, while the modified ASTM D 3987-85 leaching solution has a pH of approximately 6. When the sintered product is added to the leachant, it can change the redox potential of the leachate and therefore possibly transform extracted Cr (III) species into Cr (VI) species. On the other hand, the extraction of other species, such as Fe^{2+} and organic components, can potentially reduce Cr (VI) species into Cr (III) species [178-180], thereby changing the Cr (VI) concentration in the leachate.

Figure 8.1 also shows that clay AS has the best stabilisation capacity of Cr (VI), while clay AC has the worst. It could be due to the different mass % CaO/mass %SiO_2 ratios in the sintered bricks (0.15, 0.18, 0.21 for AS, MR and AC containing bricks, respectively). In order to examine this hypothesis, synthetic sample with a mass %CaO/mass %SiO_2

ratio of 0.5 was prepared by adding CaO to the 50wt% SPD-50wt% AS mixture. The sample was also sintered at 1100°C for 5 hours in the tube furnace. The results from the modified TCLP and modified ASTM D 3987-85 tests are plotted in Figure 8.2. It is important to note that the Cr (VI) concentrations from the leachates of the modified TCLP and the modified ASTM D 3987-85 tests increased to more than 7.6 mg/l when the mass %CaO/mass %SiO_2 ratio increased from 0.15 to 0.5. It shows that the mass %CaO/mass %SiO_2 ratio has a significant influence on the leachability of Cr (VI), and confirms that an increase in the basicity of the mixture increases the leachability of Cr (VI). This is similar to what was reported for the refractories industry [160].

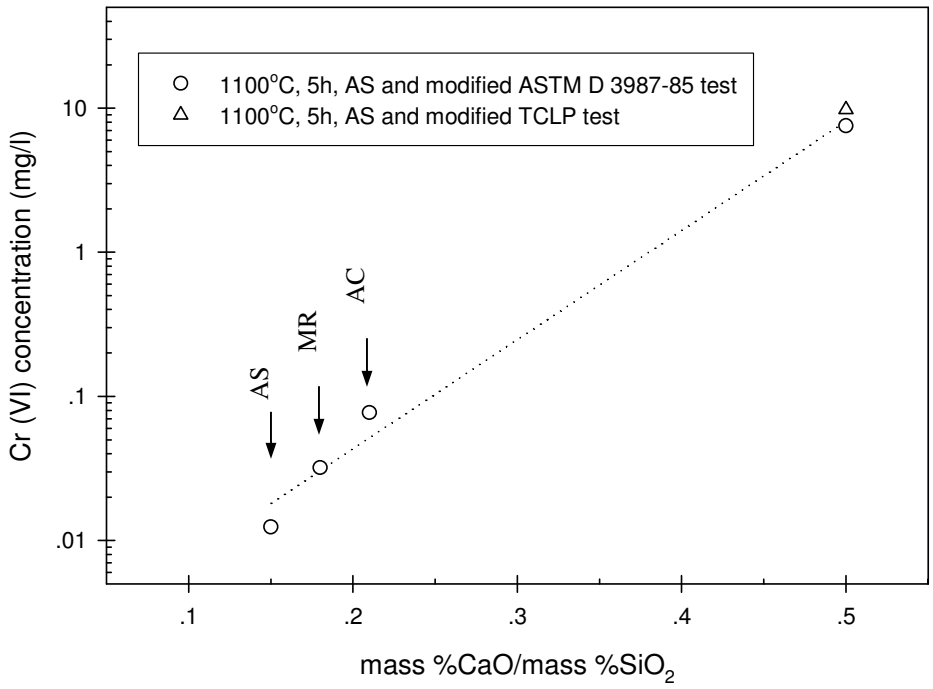

Figure 8.2 The influence of mass %CaO/mass %SiO_2 ratio on the leachability of Cr (VI) from the stabilised wastes (SPD, 1100°C and 5 hours)

8.3.2 Effect of leach time on the leachability of Cr (VI) in the modified TCLP test

The effect of leach time on the leachability of Cr (VI) in the modified TCLP test after spiking 2mg/l Cr (VI) into the TCLP leachate of sample 40%AS-60%SPD that was sintered at 1100°C for 5h is shown in Figure 8.3. It is clearly shown that Cr (VI) recovery

decreases with increasing leaching time, which means that the spiked Cr (VI) was reduced or transformed into Cr (III) during the leaching period. This ties up with reports from the literature which indicate that the extracted Cr (VI) is influenced by the potential of the leaching solution, pH and/or the reductant in the solution [170-172].

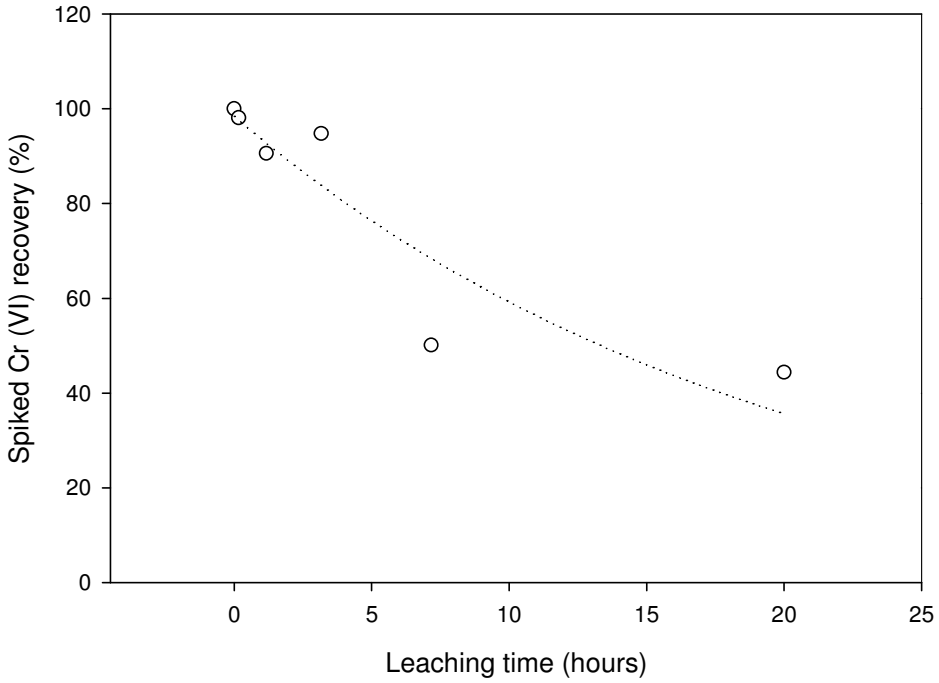

Figure 8.3 The Cr (VI) concentration in the modified TCLP leachate as a function of time (spiked with 2mg/l Cr (VI) in leachate from 40%AS-60%SPD sample @ 1100^{o}C for 5h)

The Eh-pH diagram for chromium species is shown in Figure 8.4. It indicates that the stable Cr-containing ion is Cr (III) during the TCLP leaching period (in the pH range of 4.66-5.36 and Eh range of 0.425-0.537 V), while Cr (III) can transform into Cr (VI) species with an increase in pH as is associated with the ASTM D 3987-85 leachate (in the pH range of 6.08-8.66 and Eh range of 0.311-0.412 V). It possibly contributes some Cr (VI) to the final leachate. In addition, organic compounds and iron (II) in the leachate can potentially reduce Cr (VI) components to Cr (III) [151].

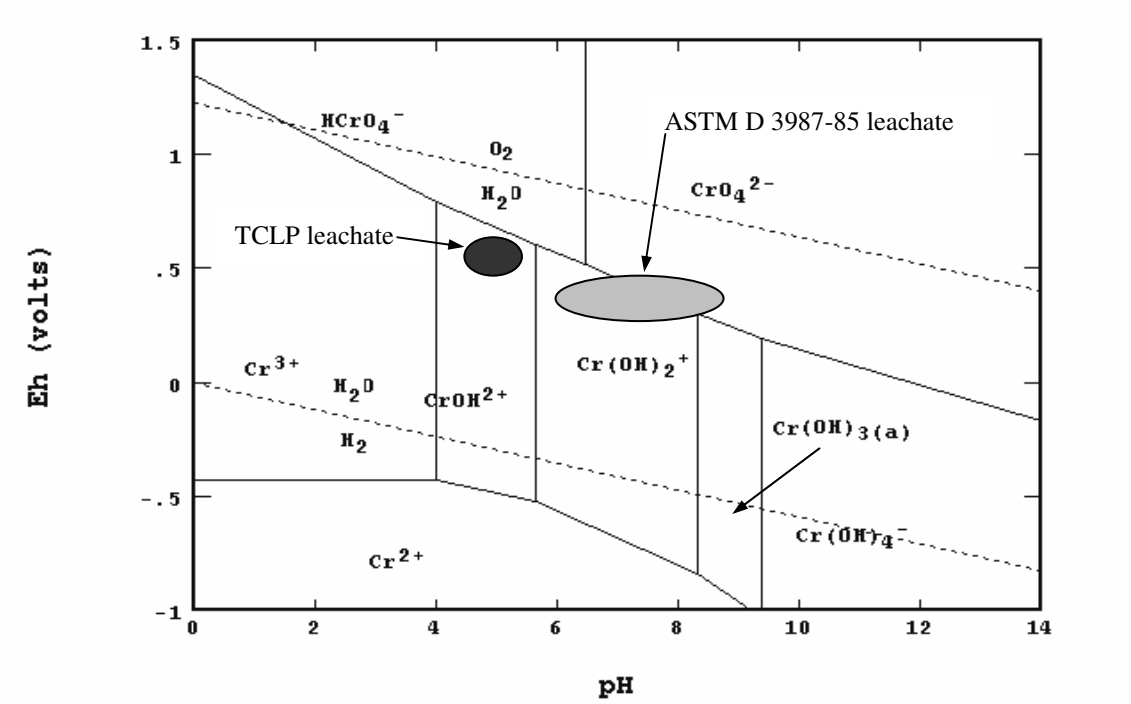

Figure 8.4 The Eh-pH diagram for Cr species calculated using STABCAL with 10^{-6}mol/l chromium concentration at 25°C [181]

8.3.3 Influence of sinter temperature on the leachability of Cr (VI)

The effect of sinter temperature on the leachability of Cr (VI) from 50%AS-50%SPD mixtures that were reacted for 5 hours is shown in Figure 8.5. It shows that increasing sinter temperature promotes the stabilisation of Cr (VI). The modified TCLP test indicated that the Cr (VI) concentration in the leachate is under the detection limit of the spectrophotometer when the brick was sintered at temperatures of 1050°C and higher for 5 hours. However, the Cr (VI) concentration was detectable in the leachate from the modified ASTM D 3987-85 test. Cr (VI) concentrations in the leachates of the modified ASTM D 3987-85 test from the bricks, which were sintered at 1000 °C and 1050°C, are higher than the acceptable limit, while when the brick was sintered at 1100°C for 5 hours, Cr (VI) was stabilised according to both the modified TCLP test and the modified ASTM D 3987-85 test [Cr (VI) concentration < 13 ppb].

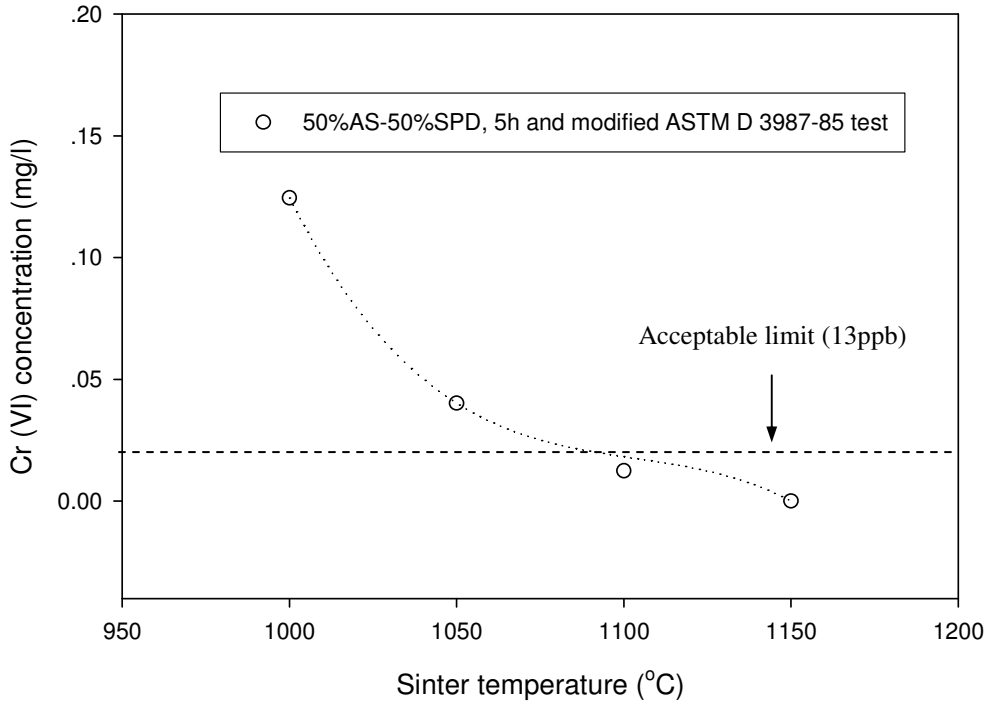

Figure 8.5 The influence of sinter temperature on the leachability of Cr (VI)

In South Africa, the TCLP test is generally used to evaluate whether hazardous wastes are environmentally acceptable. In this study, the Cr (VI) concentrations in the leachate when the sintered bricks were examined with the modified TCLP test are below 10 ppb, which is environmentally acceptable in South Africa. However, the leachable Cr (VI) in certain of the leachates of the modified ASTM D 3987-85 test is above 13 ppb and is still considered to be a potential threat to the environment and human health. It is therefore recommended that the modified ASTM D 3987-85 test is used to evaluate the degree of toxicity of the sintered bricks.

The physical appearance of the bricks (50%AS-50%SPD), which were sintered at different temperatures are shown in Figure 8.6. It shows that the brick that was sintered at 1000°C remained brown (the original colour of the stainless steel plant dust), while it changed into dark grey with an increase in sinter temperature. The brick shrank

significantly at sintering temperatures above 1100°C for 5 hours. For a 50%AS-50%SPD mixture, the optimum sintering temperature is therefore 1100°C.

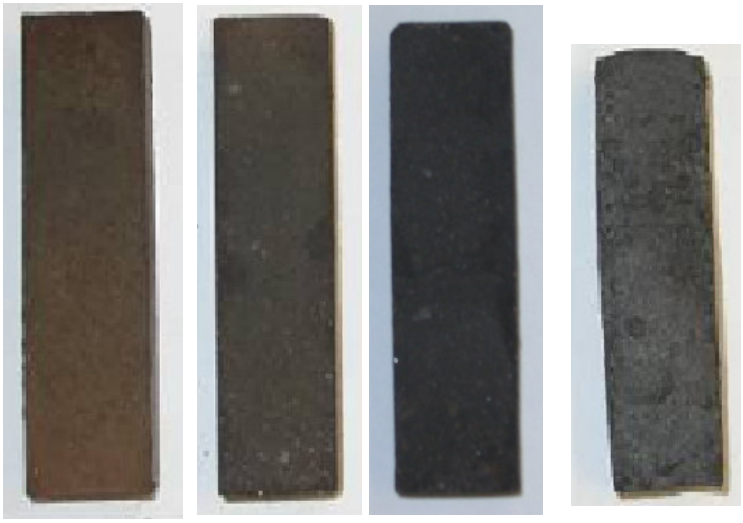

1000°C 1050°C 1100°C 1150°C

Figure 8.6 Bricks (constituted of 50%clay/50%dust) sintered at different temperatures

8.3.4 Influence of the SPD content of the brick on the leachability of Cr (VI)

The influence of the SPD content of the brick on the leachability of Cr (VI) is shown in Figure 8.7. These bricks contain clay AS and were sintered at 1100°C for 5 hours. It can be seen that the leachability of Cr (VI) increases with increasing stainless steel plant dust content of the sintered brick. Increasing SPD ratio increases the initial Cr (VI) concentration in the mixture, which can potentially increase the leachable Cr (VI). In addition, the silica content of the brick decrease with a reduction in the clay content of the mixture, and therefore increases the mass %CaO/mass %SiO_2 ratio in the mixture.

Two reference samples, i.e., pure AS clay and pure stainless steel plant dust samples, were also sintered under the same conditions (Figure 8.7). It was found that 4×10^3 mg Cr (VI) per kg SPD leached from the pure sintered stainless steel plant dust, which is considerably more than the amount that leached from the original stainless steel plant dust (approximately 2.5×10^2 mg Cr (VI) /kg stainless steel plant dust). This indicates that

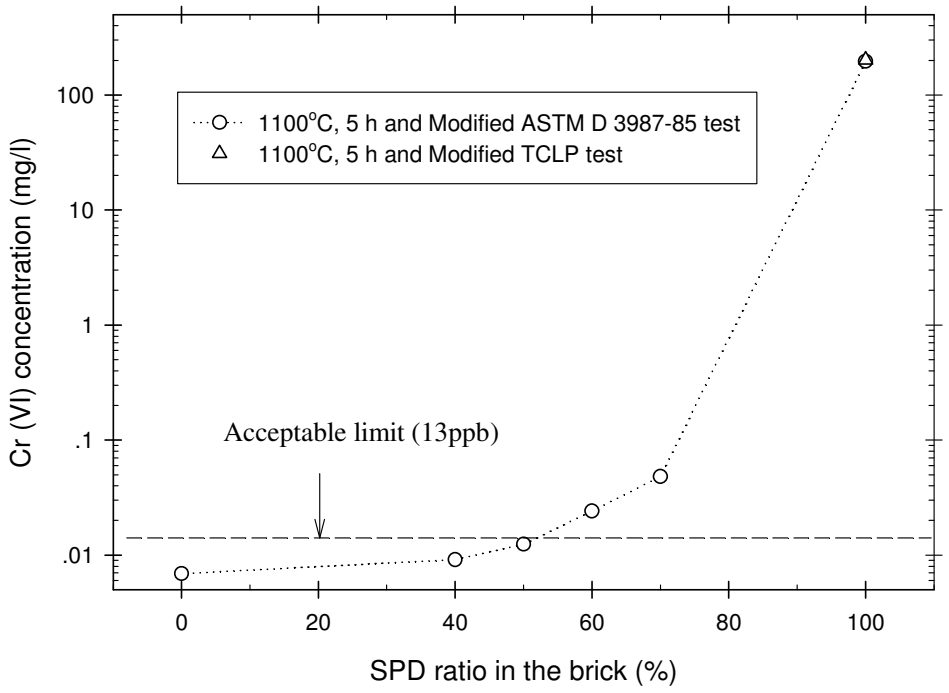

Figure 8.7 The influence of the ratio of SPD in the brick on the leachability of Cr (VI)

Cr (VI) must have formed during the sinter process either by oxidisation or through both oxidation and reaction with CaO or alkali oxides to form Cr (VI)-containing components via the following reactions [174,182,183]:

$$2Cr_2O_3\ (s) + 3O_2 \rightarrow 4CrO_3\ (s) \quad (8.4)$$

$$4CaO\ (s) + 3O_2 + 2Cr_2O_3\ (s) \rightarrow 4CaCrO_4\ (s) \quad (8.5)$$

$$1/2FeCr_2O_4+Na_2CO_3/K_2CO_3+7/8O_2 \rightarrow Na_2CrO_4/K_2CrO_4+1/4Fe_2O_3+CO_2 \quad (8.6)$$

For the AS-SPD mixture, the leachability of Cr (VI) from the bricks, which were sintered at 1100°C for 5 hours, are below the acceptable limit of South Africa (13 ppb in this study) when it contained 50 wt% SPD or less. Judging from both the regulatory limits on Cr (VI) and using as much stainless steel plant dust as possible in the sinter process, the optimum stainless steel plant dust content in the brick is 50 mass %.

8.3.5 Influence of sinter time on the leachability of Cr (VI)

The effect of sinter time on the leachability of Cr (VI) was studied by sintering 50%AS-50%SPD mixtures at 1100°C for 1, 3 and 5 hours. The results are shown in Figure 8.8. It shows that increasing sinter time increases the stabilisation of Cr (VI). The leachability of Cr (VI) from the bricks, which were sintered at 1100°C for 5 hours, is below the acceptable limit of 13 ppb. A 50%AS-50%SPD mixture that is sintered at 1100°C, should therefore at least be reacted for 5 hours in order to sufficiently stabilise the Cr (VI).

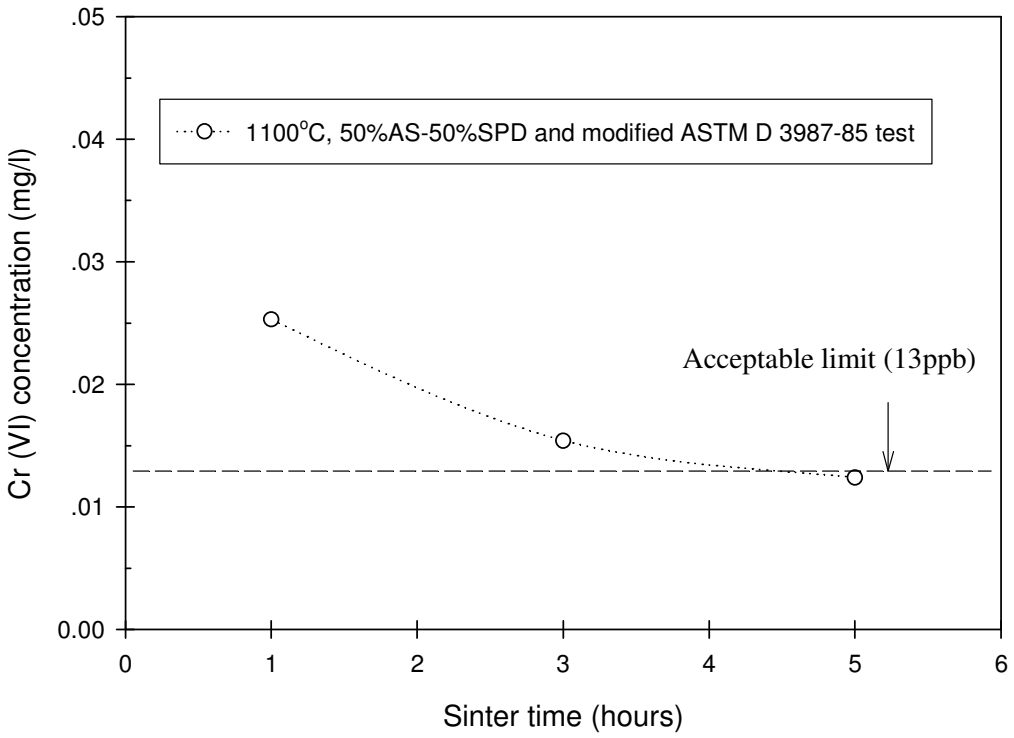

Figure 8.8 The influence of sinter time on the leachability of Cr (VI)

8.3.6 The leachability of other toxic substances from the stabilised wastes

The leachability of selected toxic substances from the stabilised SPD (sintered with 50% clay AS at 1100°C for 5 hours) is shown in Table 8.2. It shows that the concentrations of all of these leachable toxic substances are below the acceptable risk levels of South Africa, except for possibly cadmium. It confirms that when Cr (VI) is stabilised with clay in a sinter process, other toxic substances such as arsenic, zinc and lead are also

stabilised. Sintering is therefore considered to be an effective process to stabilise stainless steel plant dust.

Table 8.2 Concentrations of toxic substances in the modified TCLP leachates from the stabilised 50%AS-50%SPD mixture that was sintered at 1100°C for 5 hours.

Elements	As	Al	Ca	Cd	Cr	Fe	Mg	Mn	Ni	Pb	Si	V	Zn
Conc. (ppm)	<0.1	1.3	5.56	<0.05	0.16	5.27	1.60	0.29	0.38	<0.05	2.24	<0.05	0.21
ARL *[15]	0.43	na	na	0.031	4.7**	na	na	0.3	1.14	0.1	na	1.3	0.7

Note: *: Acceptable Risk Level; **: ARL of Cr (III); na-not available.

8.3.7Crystalline phases present in and microstructure of the sintered brick

The XRD pattern of the brick which was sintered at 1100°C for 5 hours indicates the brick consist of quartz, cristobalite, anorthite ($CaAl_2Si_2O_8$), hematite (Fe_2O_3), augite [$Ca(Mg,Fe,Al)(Si,Al)_2O_6$] and spinel phase [$(Fe,Zn,Ni,Mg,Mn)(Fe,Cr,Al)_2O_4$] (Figure 8.9). The peaks of hematite have slightly shifted, presumably due to Cr_2O_3, Al_2O_3 and Mn_2O_3 being taken into solid solution with Fe_2O_3. SEM-EDS results confirmed the existence of these phases.

The microstructures of selected sintered brick samples are shown in Figures 8.10-8.13. It indicates that the sintered bricks, which were made at 1050, 1100 and 1150°C, consist of un-reacted big quartz particles, crystals (spinel and hematite), silicate phases (anorthite and augite), pores and un-reacted metal particles (Figure 8.10). The spinel phases are either dendritic or cubic (Figure 8.11). Large amounts of small pores remain in the sintered wastes. Columnar hematite crystals, which contain small amounts of Cr, Mn and Al in solid solution were found in the sintered brick (Figure 8.12). Precipitated augite crystals were dendritic or needle-like in shape (Figure 8.13), while anorthite crystals were very fine and very difficult to identify. It was also found that larger quantities of augite and a glassy phase were formed during the sintering process of mixtures 50%AS-50%SPD and 50%MR-50%SPD than in mixture of 50%AC-50%SPD, while less anorthite were found.

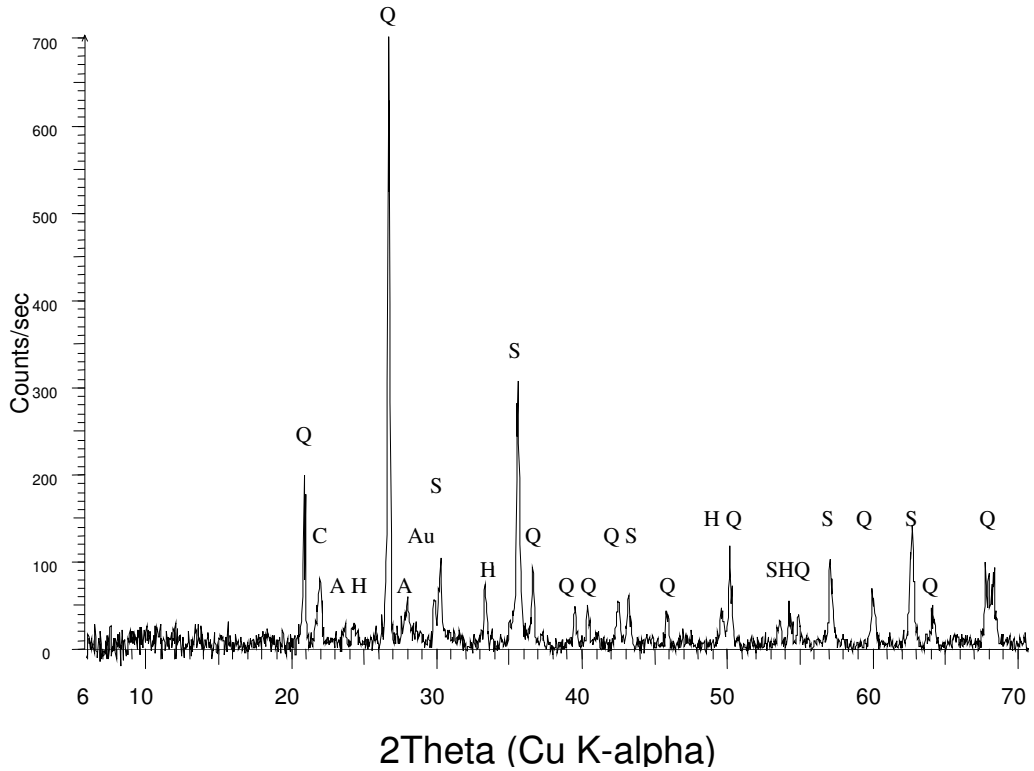

Figure 8.9 The XRD pattern of the sintered brick 50%AS-50% SPD at 1100°C for 5h (Q-quartz; C-cristobalite; A-anorthite; H-hematite; Au-augite and S-spinel)

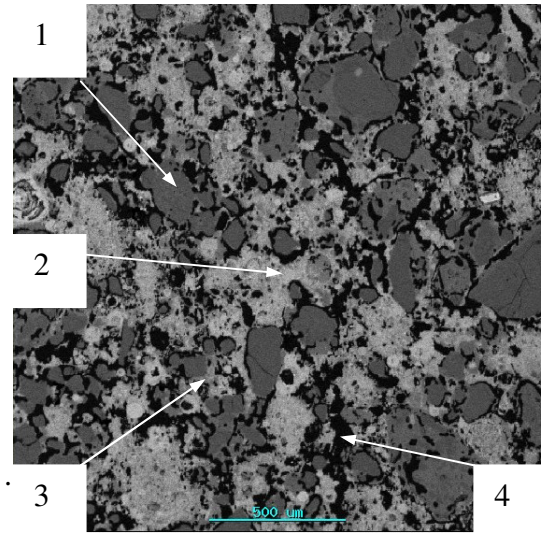

(a) AS, 1100°C and 1 hour

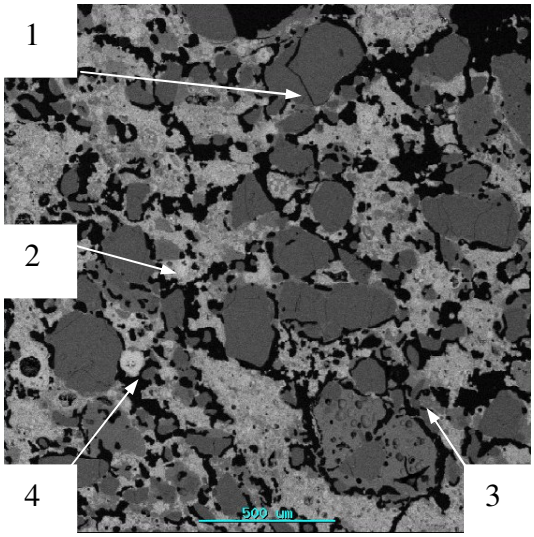

(b) AS, 1100°C and 3 hours

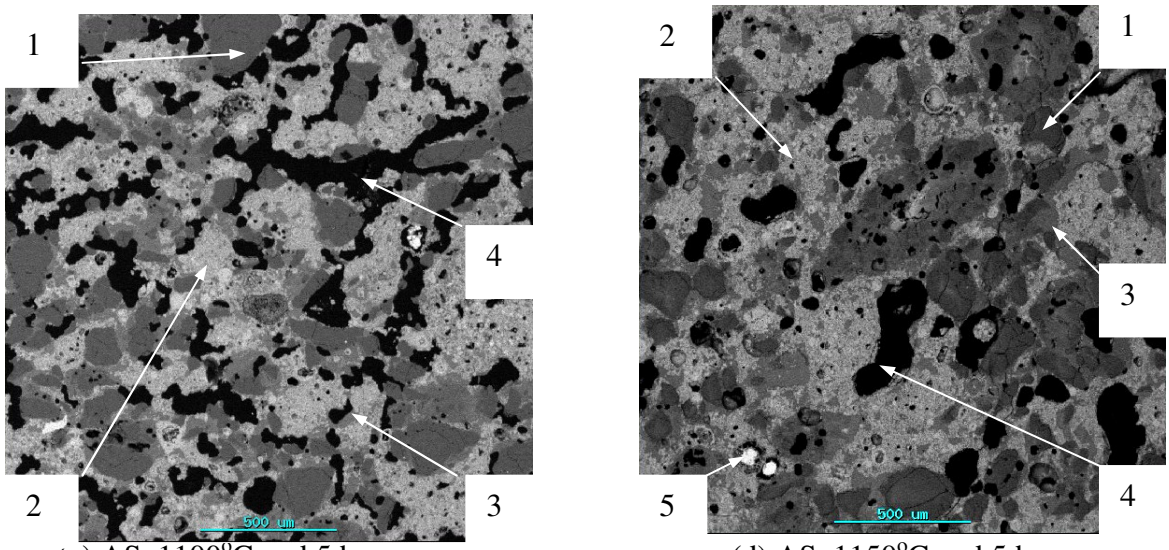

(c) AS, 1100°C and 5 hours (d) AS, 1150°C and 5 hours

Figure 8.10 Microstructure of the 50%AS-50%SPD sintered brick (1-unmelted quartz; 2-hematite and spinels; 3-anorthite and augite; 4-pores; 5-unreacted metal particles)

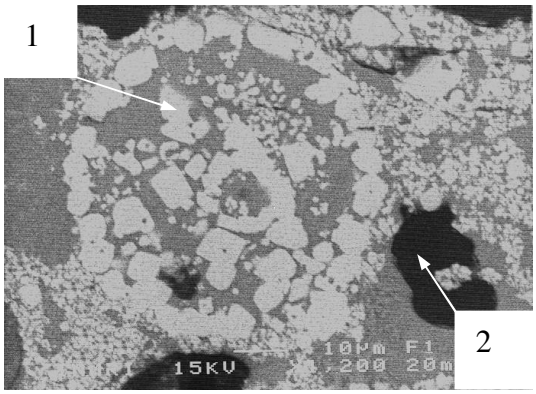

Figure 8.11 Microstructure of the 50%AS-50%SPD brick that was sintered at 1100°C for 5 h (1-spinel; 2-pore)

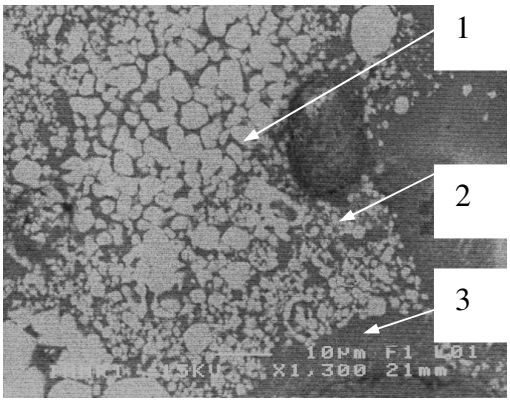

Figure 8.12 Columnar hematite crystals (1), spinels (2) and anorthite (3) in the 50%AS-50%SPD brick sintered at 1100°C for 5 h

The elemental X-ray maps indicate that the spinels mainly contain iron and chromium but also small amounts of Al, Mg, Mn, Zn and Ni. It includes larger Cr-rich spinel crystals and very fine Fe-rich spinel crystals.

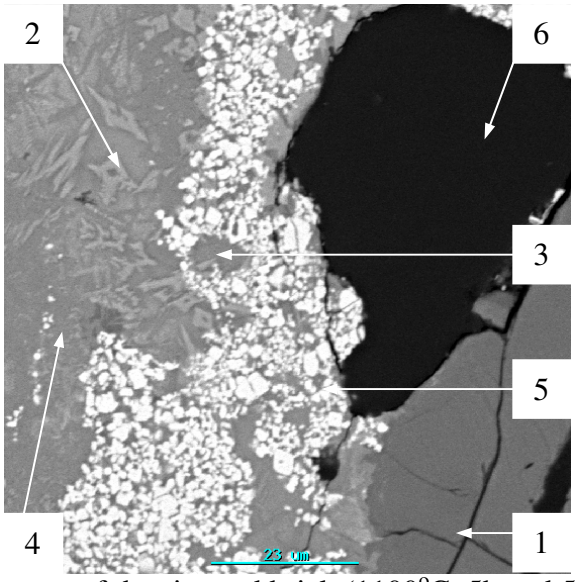

Figure 8.13 The X-ray map of the sintered brick (1100°C, 5h and 50%AS-50% SPD) (1-Quartz; 2-Augite; 3- Glassy phase; 4- Anorthite; 5- Spinel; 6-Pore)

Hematite contains Fe, Cr, Al and Mn. Augite contains calcium, silicon, aluminium, iron and magnesium, while anorthite is Ca-Al-Si-Fe-O based (Figure 8.14). Typical EDS analyses of these phases indicated that the spinel and hematite phases contain chromium (average of 8 different analyses) (Table 8.3). The Cr_2O_3 content in the spinel and hematite ranged from approximately 8 to 54wt%. It is assumed that hematite crystals formed due to the oxidation of spinel particles. In addition, augite crystals also contain small amounts of chromium. Calcium is present in the augite, anorthite and glassy phases.

Table 8.3 Typical EDS analyses of the phases present in the brick (50%AS-50%SPD, sintered at 1100°C for 5h) (mass%)

Phases	Fe_2O_3	Cr_2O_3	CaO	Al_2O_3	SiO_2	MgO	MnO	ZnO	NiO	K_2O
Cr-rich spinel	17.5	53.4	0	2.3	0	5.7	8.7	10.9	1.5	0
Fe-rich spinel	45.2	29.1	0	2.5	0	3.5	8.5	5.2	6.0	0
Hematite	88.1	8.1	0	1.6	0	0	2.2	0	0	0
Augite	15.5	1.4	23.2	7.6	44.0	7.6	2.5	0	0	0
Anorthite	3.3	0	19.3	29.0	48.4	0	0	0	0	0
Quartz	0	0	0	0	100	0	0	0	0	0
Glassy phase	5.0	0	18.3	12.2	62.3	0	0	0	0	2.2

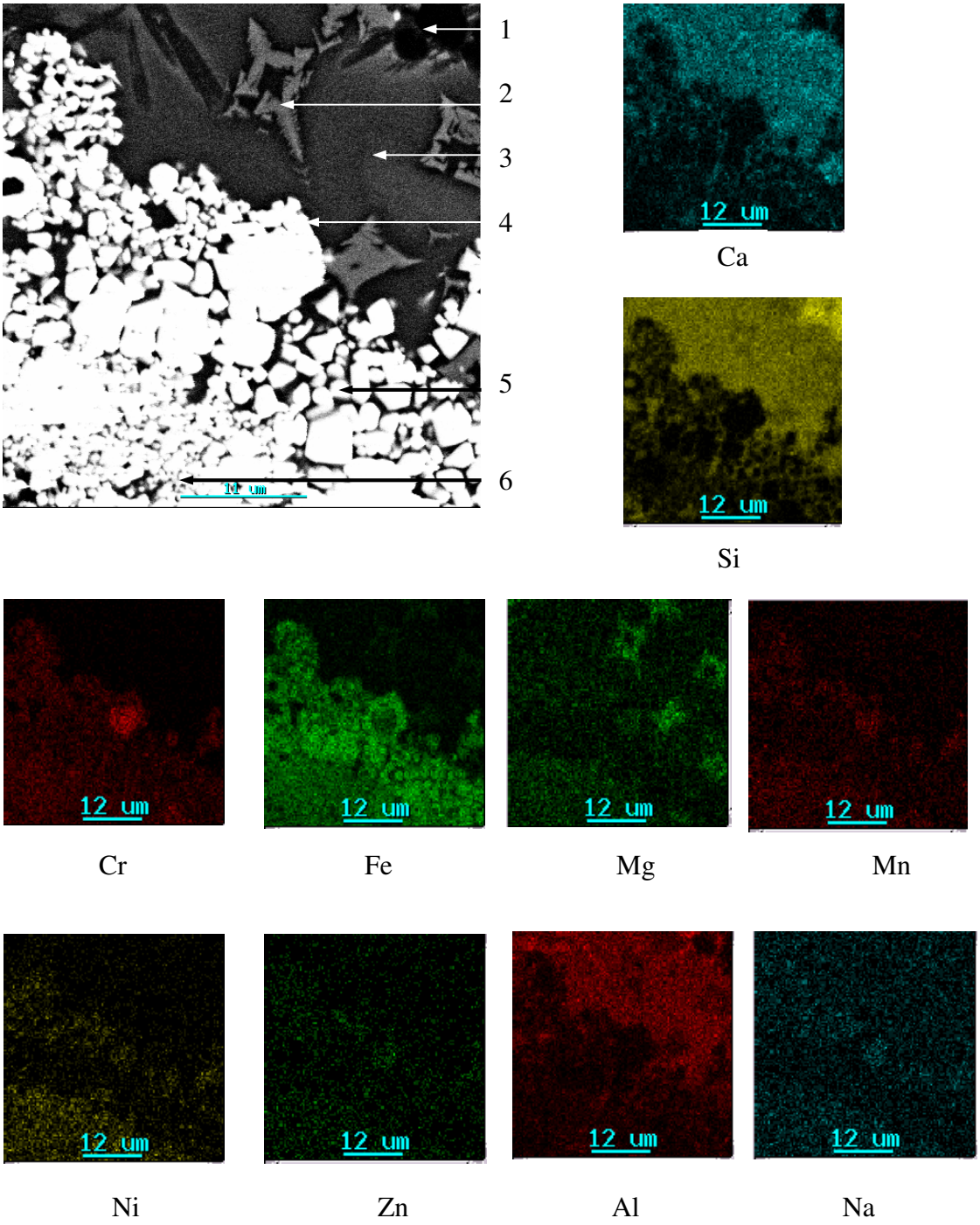

Figure 8.14 The microstructure of the sintered brick (1100°C, 5h and 50%AS-50% SPD) (1-Quartz; 2-Augite; 3- Glassy phase; 4- Cr-rich spinel; 5-Anorthite; 5-Hematite; 6-Fe-rich spinel)

8.3.8 Cr (VI) stabilisation in the sintered brick

Cr (VI) species can potentially exist in the forms of chromium trioxide, chromates and dichromates in the wastes. For this reason, CrO_3, $K_2Cr_2O_7$ and K_2CrO_4 were spiked into the mixture of 50%AS-50%SPD to investigate the Cr (VI) stabilisation. In addition, calcium chromate ($CaO{\cdot}CrO_3$), which can potentially be formed in the electric furnace dust during the sintering process due to the significant concentrations of free $Ca(OH)_2/CaCO_3$ in the stainless steel plant dust [182], was also spiked into the mixture of 50%AS-50%SPD. These mixtures were sintered in the tube furnace at 1100°C for 5 hours. The modified TCLP and modified ASTM D 3987-85 tests were used to evaluate the leachability of Cr (VI) in the sintered bricks.

Figure 8.15 shows the effect of the initial Cr (VI) concentration on the leachability of Cr (VI). It indicates that the Cr (VI) leachability only slightly increases when Cr (VI) is spiked into the 50%AS-50%SPD mixture. The amount of leachable Cr (VI) is 0.134 mg/l even though the brick was spiked with 10 wt% CrO_3.

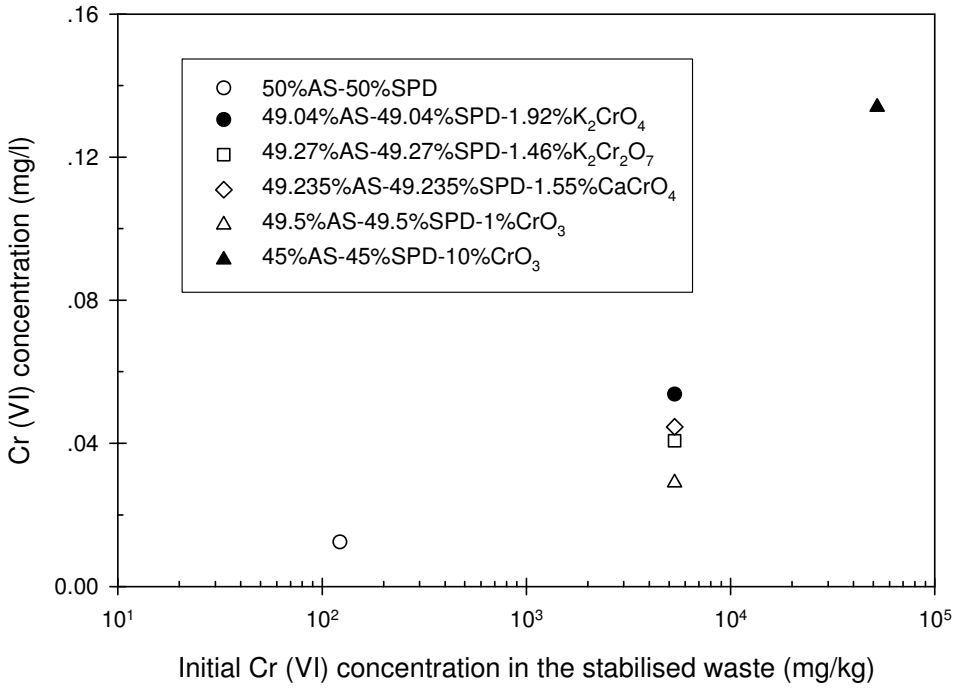

Figure 8.15 The influence of the initial Cr (VI) content on the leachability of Cr (VI)

The Cr (VI) leached ratio when the 50%AS-50%SPD mixtures were spiked with Cr (VI) species was calculated using the following equation:

$$\text{Cr (VI) leached ratio (\%)} = \frac{\text{Cr(VI)}_{\text{sintered brick}}}{\text{Cr (VI)}_{\text{green mixture}}} * 100$$

Where Cr (VI) $_{\text{green mixture}}$ is the total leachable Cr (VI) which was present in the mixture that was spiked with Cr (VI), i.e., the sum of the Cr (VI) present in the spiked Cr (VI) containing species and leachable Cr (VI) in the SPD, and Cr (VI) $_{\text{sintered brick}}$ is the leachable Cr (VI) from the sintered brick.

The results are shown in Table 8.4. It indicates that Cr (VI) in the sintered bricks are significantly stabilised (the leached ratios of Cr (VI) < 0.2%). This indicates that sintering the mixture of SPD and clay is an effective method whereby Cr (VI)-containing electric furnace dust can be treated.

Table 8.4 Calculated Cr (VI) leached ratios in the 50%AS-50%SPD mixture which were sintered at 1100°C for 5 hours and spiked with Cr (VI) species (%)

Mixtures	**Initial Cr (VI) conc. (mg/kg)**	**Cr (VI) leached ratio (%)**
50%AS-50%SPD	122.3	0.20
49.04%AS-49.04%SPD-1.92% K_2CrO_4	5321	0.02
49.27%AS-49.27%SPD-1.46%$K_2Cr_2O_7$	5321	0.02
49.235%AS-49.235%SPD-1.55%$CaCrO_4$	5321	0.02
49.5%AS-49.5%SPD-1%CrO_3	5321	0.01
45%AS-45%SPD-10%CrO_3	52110	0.005

XRD patterns of the stabilised SPD that was spiked with Cr (VI) species and sintered at 1100°C for 5 hours are shown in Figure 8.16. It was found that the major phases that were present in these samples were quartz, cristobalite, anorthite, hematite, augite and spinel. No Cr (VI) containing phases could be detected by XRD, even though one of the mixtures was spiked with 10 wt% CrO_3. It also shows that the hematite and spinel

contents of the sintered brick that was spiked with 10%CrO_3 is higher than in any of the other samples which were spiked with Cr(VI).

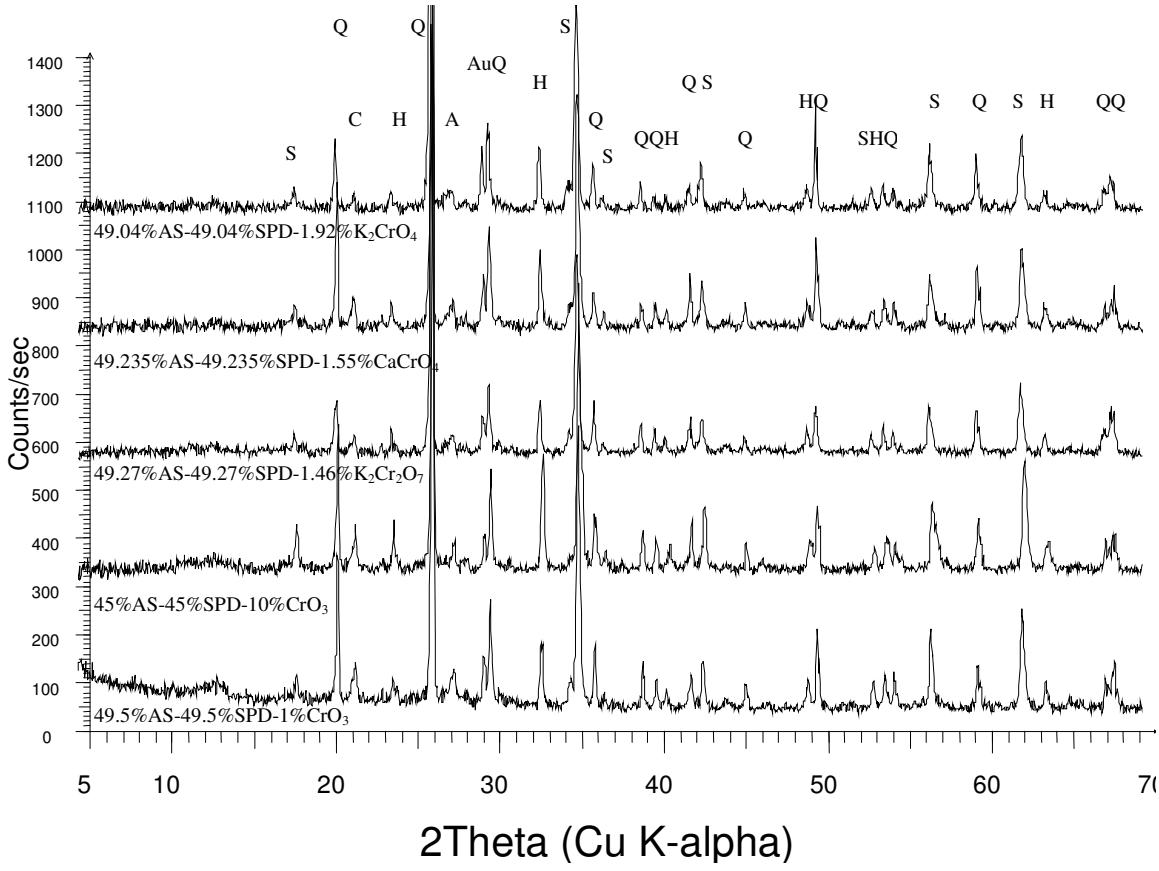

Figure 8.16 XRD patterns of the stabilised SPD that was spiked with Cr(VI) and sintered at 1100^{o}C for 5h(Q-quartz; C-cristobalite; A-anorthite; H-hematite; Au-augite and S-spinel)

The typical microstructures of the stabilised wastes that were spiked with Cr (VI) and were sintered at 1100^{o}C for 5h are shown in Figure 8.17. It shows that most of the chromium exists in the hematite [$(Fe,Cr,Al,Mn)_2O_3$] and spinel phases [$(Fe,Mn,Mg,Ni,Zn,Cr,Al)_3O_4$]. It was also found that large Cr_2O_3 particles were present in the 50%AS-50%SPD mixtures which were spiked with CrO_3, K_2CrO_4 and $K_2Cr_2O_7$ (Figure 8.17). It is possibly due to the decomposition of the spiked Cr (VI) species [184-186]. Cr_2O_3 particles could not be found in the sintered brick which was spiked with $CaCrO_4$ (Figure 8.18).

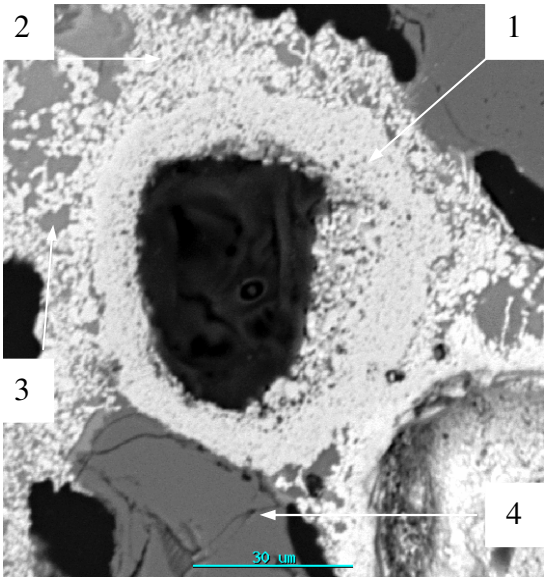

(a) Spiked with 10%CrO_3

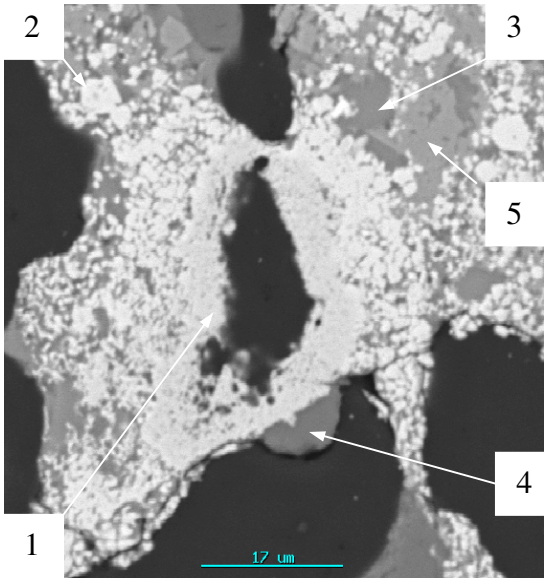

(b) Spiked with 1%CrO_3

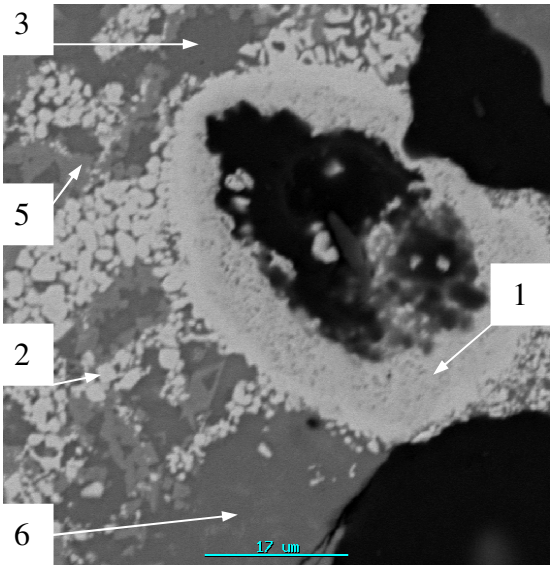

(c) Spiked with 1.46% $K_2Cr_2O_7$

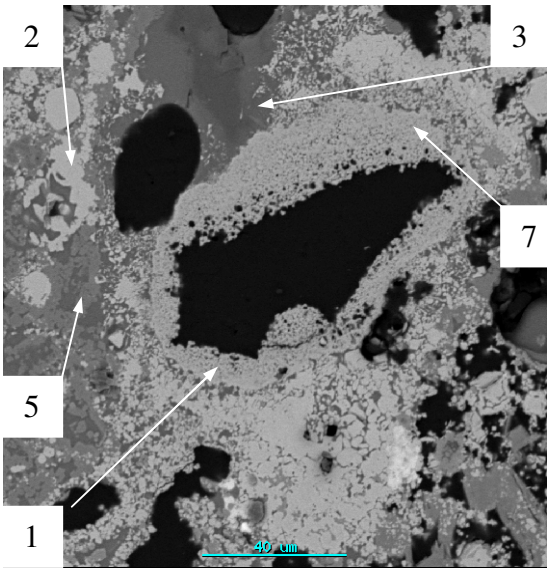

(d) Spiked with 1.92% K_2CrO_4

Figure 8.17 The typical microstructure of the stabilized SPD that was spiked with Cr (VI) and sintered at 1100°C for 5h [1-Cr_2O_3; 2-spinel $(Fe,Mn,Mg,Ni,Zn,Cr,Al)_3O_4$; 3-glassy phase; 4-unreacted quartz; 5-Augite $Ca(Mg,Fe)(Si,Al)_2O_6$; 6-Anorthite $Ca(Al,Fe)_2Si_2O_8$; 7-Hematite $(Fe,Cr,Mn)_2O_3$]

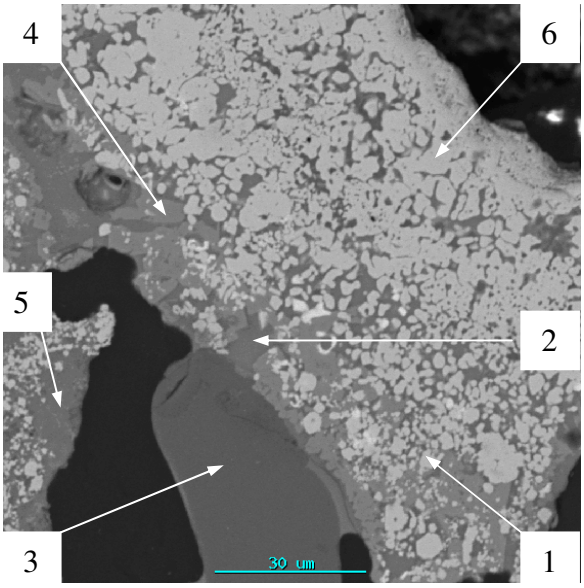

Figure 8.18 The typical microstructure of the stabilized SPD that was spiked with 1.55%$CaCrO_4$ and sintered at 1100°C for 5h [1-spinel $(Fe,Mn,Mg,Ni,Zn,Cr,Al)_3O_4$; 2-glassy phase; 3-unreacted quartz; 4-Augite $Ca(Mg,Fe)(Si,Al)_2O_6$; 5-Anorthite $Ca(Al,Fe)_2Si_2O_8$; 6-Hematite $(Fe,Cr,Mn)_2O_3$]

In order to verify the association between the formation of Cr (VI) and the presence of lime and/or alkali oxides, the sintered pure stainless steel plant dust (~4,000 mgCr(VI)/kg sintered waste) was also examined phase chemically (Figure 8.19). It indicates that the main crystalline phases are dicalcium silicate, spinel, hematite and a glassy phase (Table 8.5). Small amounts of calcium and alkali oxides were found to be present in the spinel and glassy phases of this sample, which was not the case in the samples to which clay was added. It is presumed that CaO and alkali oxides can form Cr (VI) species in the sintered wastes via reactions 8.5 and 8.6. This increases the extractable Cr (VI) from the sintered SPD.

Figures 8.20 and 8.21 summarises the influences of the mass %CaO/mass %SiO_2 ratio and the mass % K_2O in the mixtures on the leachability of Cr (VI) under different initial Cr (VI) concentrations [5321 mg Cr(VI)/kg mixture added as 1 wt% CrO_3, 1.46 wt% K_2CrO_4, 1.92 wt% $K_2Cr_2O_7$ and 1.55%$CaCrO_4$, and 245.6mg Cr(VI)/kg mixture added as

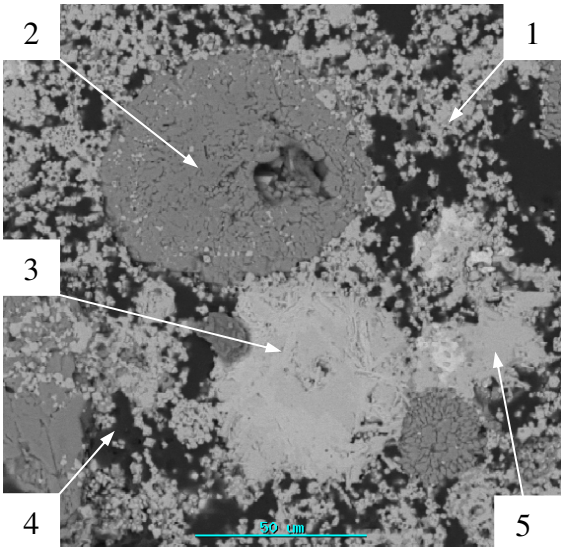

Figure 8.19 The microstructure of the sintered SPD (1100°C, 5h and 100% SPD) (1-Spinel; 2-Dicalcium silicate ($2CaO \cdot SiO_2$); 3- Hematite; 4- Pore; 5-glassy phase)

Table 8.5 Typical EDS analyses of the phases present in the brick (100%SPD, sintered at 1100°C for 5h) (mass%)

Phases	Fe_2O_3	Cr_2O_3	CaO	Al_2O_3	SiO_2	MgO	MnO	NiO	Na_2O
Spinel	55.3	21.2	2.5	0	0	5.7	7.0	5.2	3.1
Hematite	88.1	8.1	0	1.6	0	0	2.2	0	0
Dicalcium silicate	1.1	0.9	66.2	0	31.8	0	0	0	0
Glassy	33.1	9.5	28.8	0	23.3	1.0	1.0	0.8	1.0

K_2CO_3 (2.07wt% and 4.07wt%), CaO]. It indicates that the leachability of Cr (VI) increases with increasing mass %CaO/mass % SiO_2 ratio and the mass % K_2O in the mixtures. It implies that the contents of lime and alkali metal oxide content play important roles in the leachability of Cr (VI), due to the formation of Cr (VI)-containing phases, such as $CaCrO_4$ and alkali chromates [182,183]. Figures 8.20 and 8.21 also indicate that increasing initial Cr (VI) contents increase the leachability of Cr (VI).

8.3.9 Stabilisation of Cr (VI) in ferrochrome fine dust and filter cake by sintering

The mixtures that consist of 50wt% AS-50wt% waste (ferrochrome fine dust or filter cake) were sintered in a tube furnace at 1000°C for 5 hours. The leachability of Cr (VI)

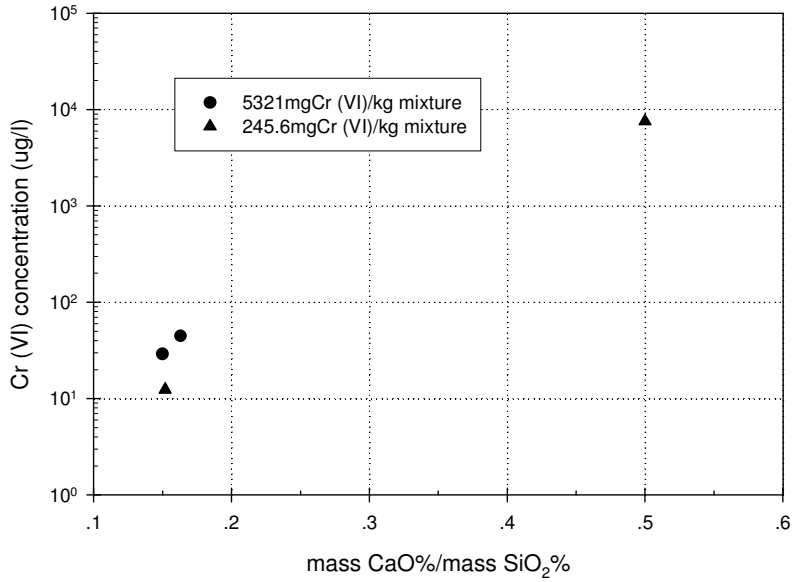

Figure 8.20 The influence of mass %CaO/mass %SiO_2 ratio on the leachability of Cr(VI) [5321mg Cr(VI)/kg mixture - 1 wt% CrO_3 and 1.55%$CaCrO_4$, and 245.6mg/kg –50%AS-50%SPD and CaO spiked 50%AS-50%SPD, 1100°C and 5 hours]

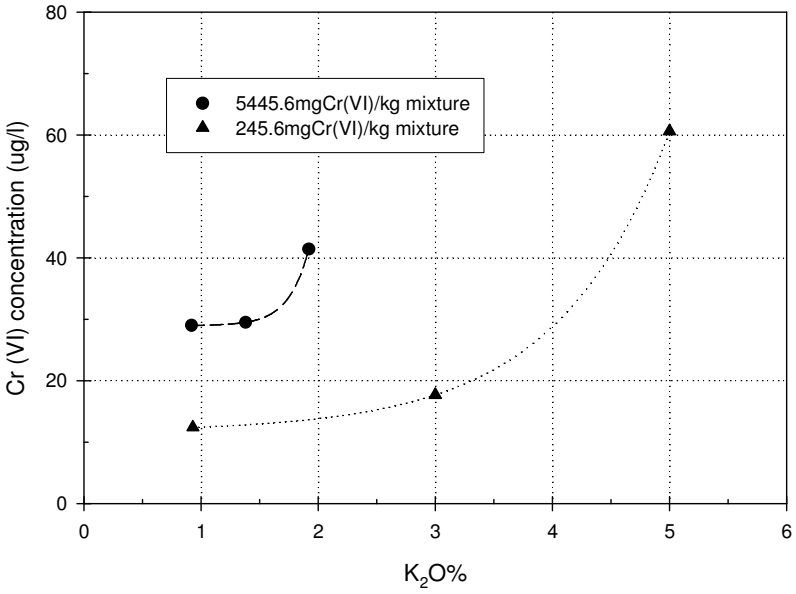

Figure 8.21 The influence of mass % K_2O in the mixture on the leachability of Cr(VI) [5321 mg Cr(VI)/kg mixture-1 wt% CrO_3, 1.46 wt% K_2CrO_4 and 1.92 wt% $K_2Cr_2O_7$, and 245.6mg/kg–50%AS-50%SPD and 2.07wt%, 4.07wt% K_2CO_3 spiked, 1100°C and 5 h]

from the different types of stabilised wastes is shown in Figure 8.22. It indicates that the stabilised FCD1 can meet the regulation limits for Cr (VI), while Cr (VI) concentrations in the leachate from the stabilised FCD2 and FC exceed the regulation limits on Cr (VI). The significant levels of Cr(VI) from the stabilised filter cake is presumably due to high concentrations of $CaO/CaCO_3$ and CaF_2 in the mixture.

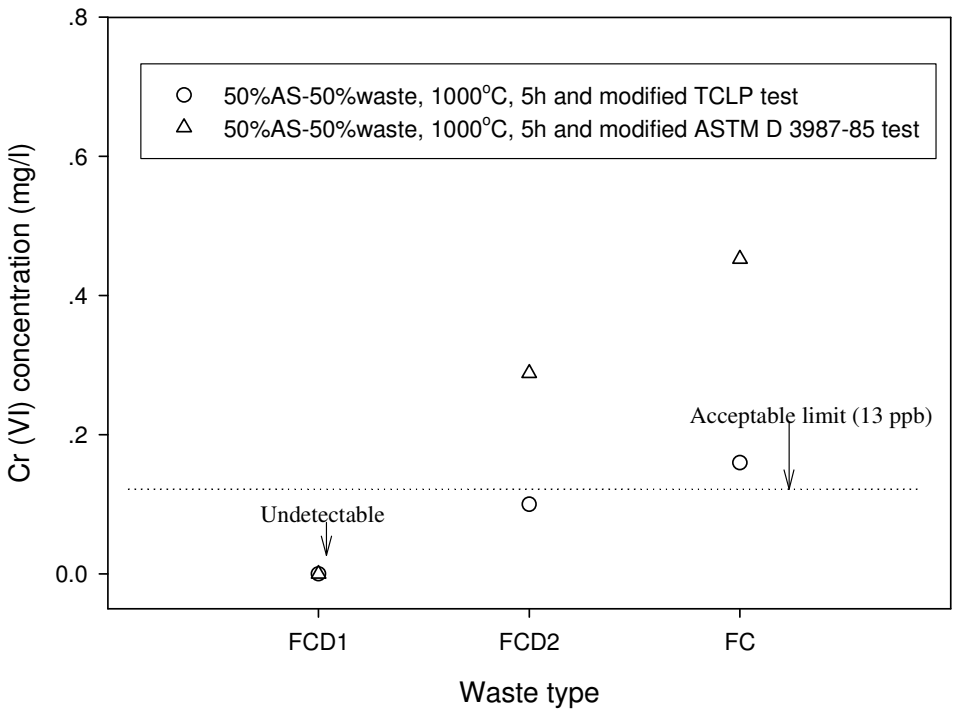

Figure 8.22 The leachability of Cr (VI) from the stabilised wastes (50%AS-50%FCD1, FCD2 or FC) that were sintered at 1000°C for 5 hours

The leachability of selected toxic substances from the leachates of the modified TCLP test is reported in Table 8.6. It indicates that zinc concentrations in the leachate of the modified TCLP test exceed the acceptable risk level. This is due to the significant contents of zinc oxide in the original ferrochrome dust, which can be extracted under the slightly acidic conditions associated with TCLP solution 1. The concentration of calcium in the leachate from the stabilised FC is 938 mg/l, which is presumably due to the significant contents of calcium in the filter cake. The concentrations of arsenic, chromium

Table 8.6 Concentrations of selected elements in the leachates of the modified TCLP tests from the stabilised FCD1, FCD2 and FC (ppm)

Elements	As	Al	Ca	Cd	Cr	Fe	Mg	Ni	Pb	Si	V	Zn
FCD1	<0.1	2.29	60.3	<0.05	0.09	1.22	29.4	<0.05	<0.05	33.5	<0.05	95.3
FCD2	<0.1	1.10	25.6	<0.05	0.34	0.14	40	<0.05	<0.05	23.1	<0.05	9.34
FC	<0.1	1.10	938	<0.05	0.33	0.23	5.04	0.13	<0.05	234	1.01	0.56
ARL *[15]	0.43	na	na	0.031	4.7**	na	na	1.14	0.1	na	1.3	0.7

Note: *: Acceptable Risk Level; **: ARL of Cr (III); na-not available.

and nickel are lower than the acceptable risk level, while the cadmium content is possibly above the acceptable risk level.

The stablisation of ferrochrome dust and filter cake in a sinter process at 1000°C for 5 hours using 50% clay AS is therefore not successful, as the acceptable risk levels of Cr(VI) (20ppb) or zinc (0.7ppm) for South Africa cannot be met.

8.3.10 Chromium emission during the sinter process

Chromium can be vaporised at high temperatures mostly through the formation of Cr (VI) species via the following reaction [173-175]:

$$1/2Cr_2O_3\ (s) + 3/4\ O_2\ (g) \leftrightarrow CrO_3\ (g)$$

The effects of different parameters on chromium emission are shown in Figure 8.23. It shows that chromium emission from the mixture of 50%AC-50%SPD is lower than that from the mixtures of 50%MR-50%SPD and 50%AC-50%SPD (Figure 8.23a). The total chromium emission factors from the stabilised waste during the sinter process is approximately 0.5 to 1.8 g/ton brick produced at 1100°C for 5 hours. It is lower than the emission factors from steel plants (4.0-36.1 g/t steel) and sewage sludge incineration (10g/t) [177], while it is similar to the cement industry (approximately 1.6g/t cement produced [176]). It indicates that under current experimental conditions the sinter process

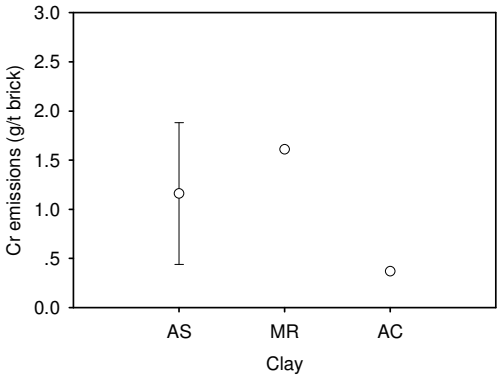

(a) Effect of clay type on Cr emission (1100°C, 50wt%SPD and 5 h)

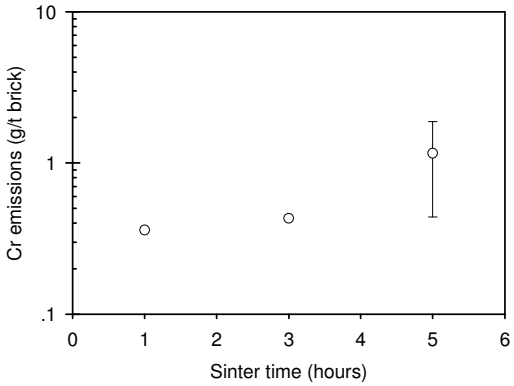

(d) Effect of sinter time on Cr emission (AS, 50wt% and 1100°C)

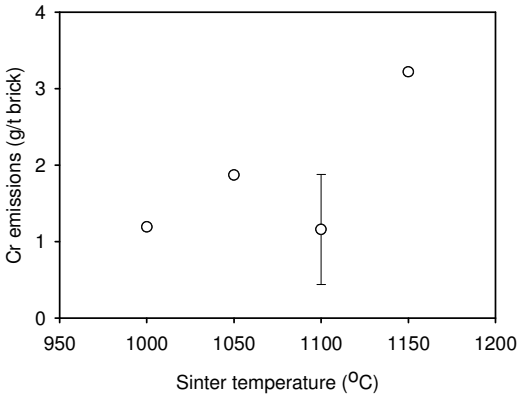

(b) Effect of sinter temperature on Cr emission (AS, 50wt%SPD and 5h)

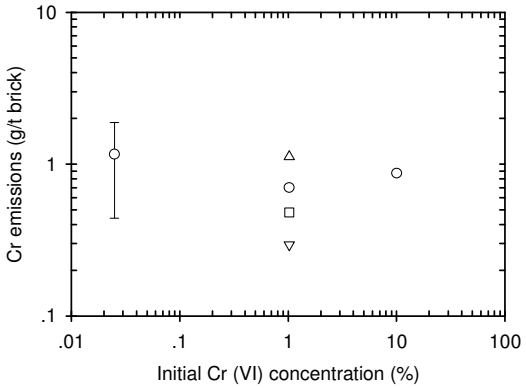

(e) Effect of initial Cr (VI) concentration on Cr emission (AS, 1100°C and 5h)

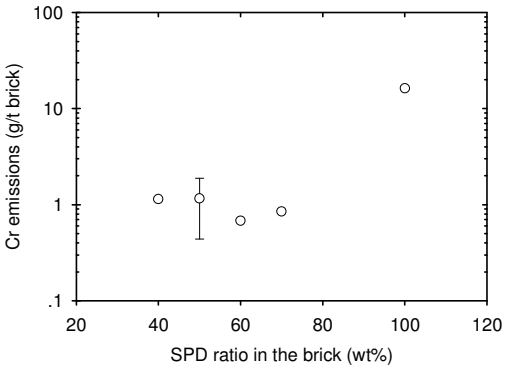

(c) Effect of wastes content on Cr emission (AS, 1100°C and 5 h)

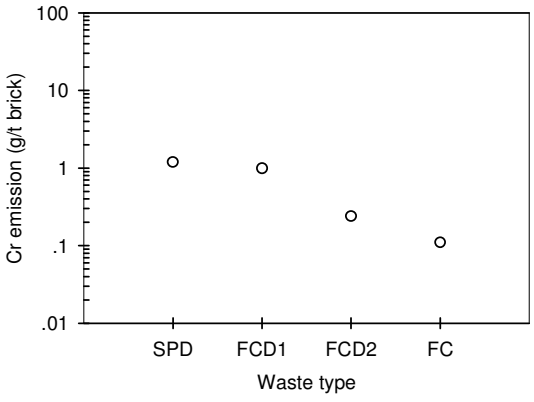

(f) Chromium emission of different wastes (1000°C and 5h)

Figure 8.23 Chromium emission during the sinter process

can be considered a safe process to treat SPD. In addition, increasing sinter temperature, waste ratio in the brick and sinter time increase the chromium emissions. However, increasing initial Cr (VI) concentration has no significant influence on chromium emission. A mass balance on the waste mixture (50%AS-50%SPD) which was sintered at 1100^{o}C for 5 hours confirmed that chromium was stabilised in the brick (see Appendix III).

Chromium emission from stabilised ferrochrome fine dust 2 and filter cake that was sintered at 1000^{o}C is lower than the emission factor of the stabilised stainless steel plant dust and stabilised ferrochrome fine dust 1 (Figure 8.23 f).

8.4 Conclusions

Bricks were produced by mixing wastes (stainless steel plant dust, ferrochrome dust and filter cake) and clay. The leachability of Cr (VI) from the stabilised wastes were investigated. The following conclusions can be drawn:

(1) When the bricks were sintered at 1100^{o}C for 5 hours with a 50 wt% SPD content in the brick, Cr (VI) in the stainless steel plant dust can be significantly stabilised.

(2) Decreasing sinter temperature, increasing waste content in the brick and reducing sinter time increase the leachability of Cr (VI) from the stabilised stainless steel plant dust.

(3) Clay AS has the best stabilisation capacity of Cr (VI) in stainless steel plant dust, while clay AC has the worst. This is presumably due to the higher mass %CaO/mass %SiO_2 ratio in the AC-SPD mixtures.

(4) When Cr (VI) in the stainless steel plant dust is stabilised with clay in a sinter process, other toxic substances such as As, Zn and Pb are also stabilised. A sinter process whereby SPD is mixed with clay is therefore considered to be an effective process to stabilise toxic substances in stainless steel plant dust.

(5) Cr (VI) recovery decreases with increasing leaching time. This is due to the fact that the spiked Cr (VI) was reduced or transformed into Cr (III) during the leaching period.

(6) The leachability of Cr(VI) is influenced by the mass%CaO/mass%SiO_2 ratio and alkali metal oxides content in the raw materials.

(7) Ferrochrome dust and filter cake that were sintered with 50% clay AS at 1000^{o}C for 5 hours could not be stabilised as the concentrations of zinc and/or Cr (VI) from the stabilised wastes in the modified TCLP and ASTM D 3987-85-tests exceed the regulation limits.

(8) The emission factors from the stabilised wastes (SPD, FCD1, FCD2 and FC) are similar to those reported for the cement industry.

Chapter 9 Stabilisation of Cr (VI) through sintering using silica-rich clay, Part III: Leaching behaviour of chromium from the stabilised wastes

9.1 Introduction

Stabilisation treatment processes are effective technologies through which pyrometallurgical wastes can be disposed. It can both immobilise the toxic substances and transform the wastes into non-hazardous commercial products such as construction materials [5,14,17,43,44,56,57].

The controlling leaching mechanisms of the toxic substances from the stabilised waste products have been investigated by several workers. Shin et al. studied the leaching behaviour of Si, Ca, Sr and Cs from vitrified radioactive incineration ash, using the International Organization for Standardisation (ISO)-6961-1982 leaching test [187]. Based on more than 820 days of leaching experiments, it was proven that the dominant leaching mechanisms of these elements are dissolution and diffusion. According to Andres et al. [188], leaching of Pb and Zn from steel foundry dusts which were stabilised by cement and anhydrite ($CaSO_4$) as binders were controlled by an initial wash-off followed by the diffusion process. TCLP tests showed that the stabilised products meet the regulatory limits on Zn, Pb, Cr and Cd. The treated products are therefore environmentally acceptable and can be used in the construction industry [188].

In the present chapter, the predominant leaching mechanisms of chromium species from the stabilised electric furnace dust and filter cake, using a semi-dynamic leaching test, are reported on. Two empirical models were used to evaluate the major leaching mechanisms of the chromium species. The values of the semi-empirical model parameters were used to evaluate the controlling leaching mechanisms of the chromium species from the stabilised products.

9.2 Background

Different leaching tests have been developed to evaluate the leaching behaviour of toxic substances from wastes. These include the Toxicity Characteristics Leaching Procedure (TCLP) test [21], the DIN 38414 (4) test [189], the ASTM D 3987-85 test [146] and the semi-dynamic leaching test [190-194]. The TCLP, DIN 38414 (4) and ASTM D 3987-85 tests, which are also called availability tests [192], are often used to assess the leachability of the toxic substances from the wastes.

A semi-dynamic leaching test can be used to study the controlling leaching mechanisms of toxic substances from the stabilised/solidified products. The leaching models which can be used to evaluate the leaching mechanisms of the toxic substances from the stabilised/solidified wastes are well documented [192-195]. The leaching mechanisms of the toxic substances from the products are schematically shown in Figure 9.1. [192]. It shows that leaching of the toxic substances from the stabilised/solidified wastes can be controlled by surface wash-off (interface reaction kinetics), matrix diffusion and dissolution or corrosion [192-195]. The initial wash-off is often due to the soluble components on the surface of the product, while matrix diffusion occurs when the components leach through the matrix of the stabilised/solidified product. The dissolution process dominates if toxic substances dissolve at a higher rate from the edge of the stabilised product than due to diffusion through the matrix of the stabilised product [192].

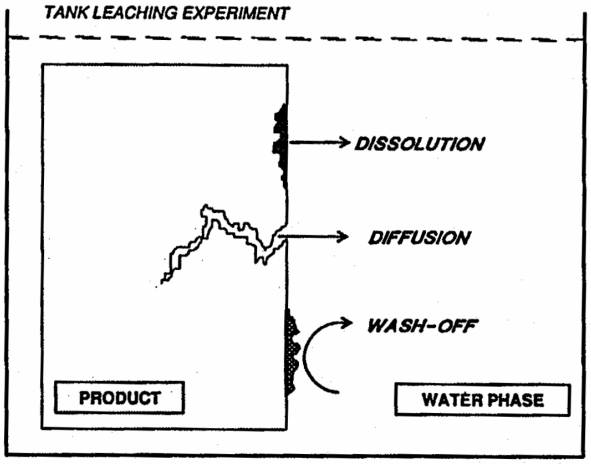

Figure 9.1 Leaching mechanisms of toxic elements from the stabilised product [192]

9.2.1 Leaching model based on initial wash-off or interface reaction kinetics

This model describes the mass exchange between the surface of the stabilised wastes and the aqueous solution [192,193,195]. It is relevant during the initial period of the leaching process and is also called initial surface wash-off. It can be described in terms of the exchange kinetics of a species "j" on the surface of the solid.

$$\text{species "j" } (s) \underset{k_d}{\overset{k_l}{\rightleftharpoons}} \text{species "j" } (w)$$

Where k_l and k_d are the rate constants describing the kinetics of releasing a species ("j") from the surface of the solid (s) and attaching a species ("j") from the aqueous solution (w).

The leach rate of a species from the stabilised waste can be expressed as an exponential function of the rate constants [192,193,195]:

$$L(t) = f\ \{\exp\ [-(k_l + \frac{S}{V_l} k_d)t\ ]\}\} \qquad (9.1)$$

Where S is the surface area of the stabilised waste form and V_l is the volume of the leachant.

The leaching process can also be expressed in terms of the cumulative fraction leached, $F(t)$, which is related to the leaching rate $L(t)$:

$$L(t) = \frac{M_0}{S} \frac{dF(t)}{dt} \qquad (9.2)$$

Where M_0 is the initial amount of a species in the stabilised waste and S is the surface area of the stabilised waste.

Replacing $L(t)$ in equation (9.1) into equation (9.2) and integrating with time, the cumulative fraction leached of a species can be expressed as an exponential function [192,193,195], i.e.,

$$F(t) = k_1\ \{1\text{-}\exp\ [-(k_l + \frac{S}{V_l} k_d)\ t]\} \qquad (9.3)$$

Where k_1 is a constant term. If the rate of the initial surface wash off is fast enough, the equation (9.3) can be further simplified as F (t) = k_1, which is the initial fraction leached.

9.2.2 Leaching model based on matrix diffusion

A species which is transported from the stabilised waste to the solution through diffusion can be described using Fick's second law:

$$\frac{\partial C}{\partial t} = D_e \frac{\partial^2 C}{\partial^2 x} \tag{9.4}$$

Where C is the concentration of the diffusing species and D_e is an average effective diffusion coefficient. In this study, the leaching behaviour of a species from the cylinder products can be assumed as a semi-infinite medium (x>0). Furthermore, a species in the stabilised waste is postulated to have a zero surface concentration and a constant effective diffusion coefficient [190-193,195]. In this case, the leaching rate of a species, which is a solution of equation (9.4), can be expressed as [190-193,195,196]:

$$L\,(\mathrm{t}) = \mathrm{C}_0 \left(\frac{\mathrm{D_e}}{\pi t}\right)^{\frac{1}{2}} \tag{9.5}$$

Where C_0 is the initial concentration of the species in the stabilised waste.

Therefore, replacing L (t) in equation (9.2), the cumulative leached fraction of a species that has been leached at time t can be derived as:

$$F\,(\mathrm{t}) = 2\frac{S}{V}\left(\frac{\mathrm{D_e t}}{\pi}\right)^{\frac{1}{2}} \tag{9.6}$$

Where S is the surface area of the stabilised waste and V is the volume of the sample.

It shows that the leached fraction has a linear relationship with the square root of the leaching time. It can therefore be written that:

$$\mathrm{Log}\ F\,(\mathrm{t}) = \frac{1}{2}\log\,(\mathrm{t}) + \log\left(2\frac{S\sqrt{\mathrm{D_e}}}{V\sqrt{\pi}}\right) \tag{9.7}$$

9.2.3 Leaching model based on dissolution or corrosion

According to Cote et al., the leaching rate of a species from the stabilised waste can be expressed as [193]:

$$L\,(\mathrm{t}) = L_0\,[1 - \frac{C^{(w)}(t)}{C^{(w)}_{sat}}] \tag{9.8}$$

Where L_0 is the maximum leaching rate, $C^{(w)}(t)$ is the concentration of a species in the aqueous solution and $C^{(w)}_{sat}$ is the concentration of a species at saturation in the aqueous solution.

This process can also be expressed using the network dissolution velocity u, if the matrix breakdown due to the leaching of a species from the stabilised waste:

$$u\,(\mathrm{t}) = \frac{L(t)}{C_0} \tag{9.9}$$

Where C_0 is the initial concentration of a species in the stabilised waste. Replacing equation 9.8 into equation 9.9 gives:

$$u\,(\mathrm{t}) = \mathrm{u}_0\,[1 - \frac{C^{(w)}(t)}{C^{(w)}_{sat}}] \tag{9.10}$$

In the case where the concentration of a species is much less than the saturation concentration of a species in aqueous solution, i.e., $C^{(w)}_{sat} >> C^{(w)}(t)$, it follows that $u\,(\mathrm{t}) = u_0$. Thus a linear function exists between the cumulative fraction of a released species and leaching time is [193]:

$$F\,(\mathrm{t}) = \frac{S}{V}\,u_0\mathrm{t} \tag{9.11}$$

The cumulative leached fraction of the toxic substances from the stabilised wastes can be therefore expressed as a function of leaching time, i.e.,

$$F\,(\mathrm{t}) = k_1[1\text{-}\exp\{-(\mathrm{k}_l + \frac{S}{V_l}\,\mathrm{k}_d)\mathrm{t}\}] + 2\frac{S}{V}\,(\frac{\mathrm{D_e t}}{\pi})^{\frac{1}{2}} + \frac{S}{V}\,u_0\mathrm{t} \tag{9.12}$$

Equation (9.12) can also be simplified as:

$$F(t) = k_1[1-\exp(-k_2 t)] + k_3 t^{\frac{1}{2}} + k_4 t \qquad (9.13)$$

Where $k_1[1-\exp(-k_2 t)]$ is the term contributed by initial surface wash-off, $k_3 t^{\frac{1}{2}}$ is based on matrix diffusion from the porous product media and $k_4 t$ is the leached fraction due to the dissolution or corrosion of the matrix.

The dominant leaching mechanisms of a species from the stabilised waste can also be obtained by empirically analysing the slope of the logarithm of the cumulative fraction released versus the logarithm of the leaching time [192]. Figure 9.2 shows the theoretical curves of the different leaching mechanisms [192]. It shows that the controlling mechanism is surface wash off if the slope of the logarithm of cumulative fraction release versus the logarithm of leaching time is zero. If it is 0.5, the major leaching mechanism is diffusion. Dissolution controls the leaching process if the slope is 1.

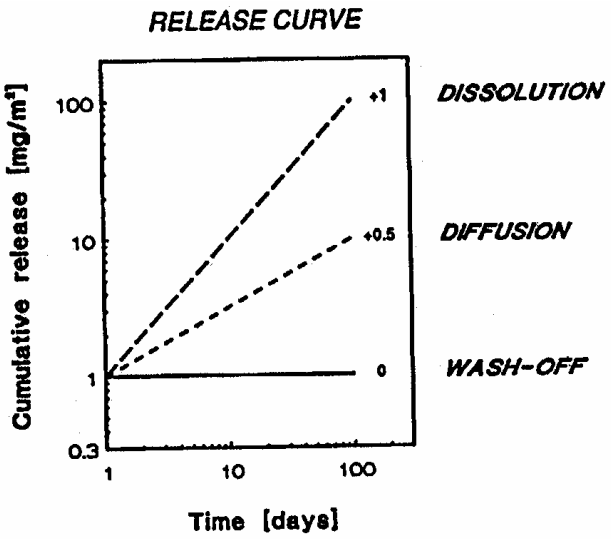

Figure 9.2 The theoretical curves of the different leaching mechanisms [192]

From the slope of the different leaching mechanisms, De Groot et al. derived that if the slope is below 0.4, the release of a species is controlled by initial surface wash-off [192]. The diffusion of a species from the solid matrix is the controlling mechanism when the

slope is between 0.4 and 0.6, while dissolution or corrosion of the network can control the leaching process with a slope of more than 0.6 [192].

9.3 Experimental

9.3.1 Sample preparation

Approximately 40 g mixtures with different ratios of clay and waste were well mixed and pressed into cylinders with diameters of 2.5 cm and 4.0±0.36 cm in height. These cylinders were dried at 110°C for 48 hours. Thereafter, they were sintered at 1000 or 1100 °C in a Muffle furnace for 5 hours in order to obtain a dimensionally stable product. The heating rate of the furnace was ~4°C/min and the furnace was cooled down to room temperature at a rate of ~1.6°C/min. The different types of samples and the experimental conditions are listed in Table 9.1.

Table 9.1 Samples and experimental conditions

Sample	Composition (wt.%)	Sinter temp. (°C)	Sinter time (h)
M1	50%SPD+50%AS	1100	5
M2	50%SPD+50%MR	1100	5
M3	20%FCD1+80%AS	1000	5
M4	20%FCD2+80%AS	1000	5
M5	20%FC+80%AS	1000	5

9.3.2 Leaching test

Duplicated sintered samples were immersed into distilled water at 25±1°C after being stored for approximately 2 days in a desiccator. The ratio of the surface area of the cylindrical specimens to the volume of leachant (distilled water) was 1:10 (cm^{-1}). The distilled water was replaced at designed intervals according to [192]:

$$t_n = n^2 t_1 \ (\ n = 1,3,5,7,9,\ldots)$$

Where t_n is the time at the end of the leaching period, t_1 is the time at the end of the first leaching period, where t_1 = 1 hour. The leaching setup of the semi-dynamic experiment is

shown in Figure 9.3. It shows that the cylindrical specimens were suspended using nylon wire in the centre of the leaching solution (distilled water).

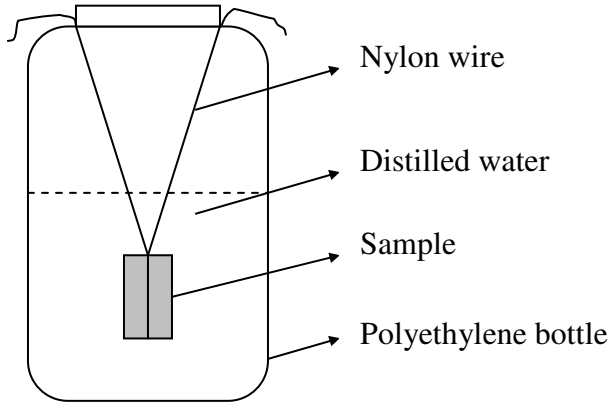

Figure 9.3 Experimental set-up of the leaching test

The Cr (VI) and total chromium concentrations in the leachates were analysed with the methods that are described in Appendix I. The pH of the leachate was also recorded.

9.4 Results and discussion

9.4.1 Leaching mechanisms of chromium from the stabilised product

The cumulative fraction of total chromium that leached from the stabilised waste as well as the model calculation results using function (9.13) is shown in Figure 9.4 (the data are shown in Appendix VI). It shows that the cumulative release fraction of total chromium from samples 50%SPD+50%AS (M1), 50%SPD+50%MR (M2), 20%FCD1+80%AS (M3), 20%FCD2+80%AS (M4) and 20%FC+80%AS (M5) are approximately 0.04%, 0.01%, 0.02% 0.07% and 1.9%, respectively. It indicates that chromium does not readily leach from stabilised wastes. The cumulative leached concentrations of total chromium from stabilised wastes M1, M2, M3 and M4 are 1.91, 0.58, 0.10 and 0.32 ppm respectively (Table VI.1), which are below the acceptable limits for chromium (the acceptable risk level of Cr (III) is 4.7 ppm in South Africa [15]). Sample M5 has an average cumulative leached concentration of 6.9 ppm, and therefore exceeds the acceptable risk level of chromium in South Africa.

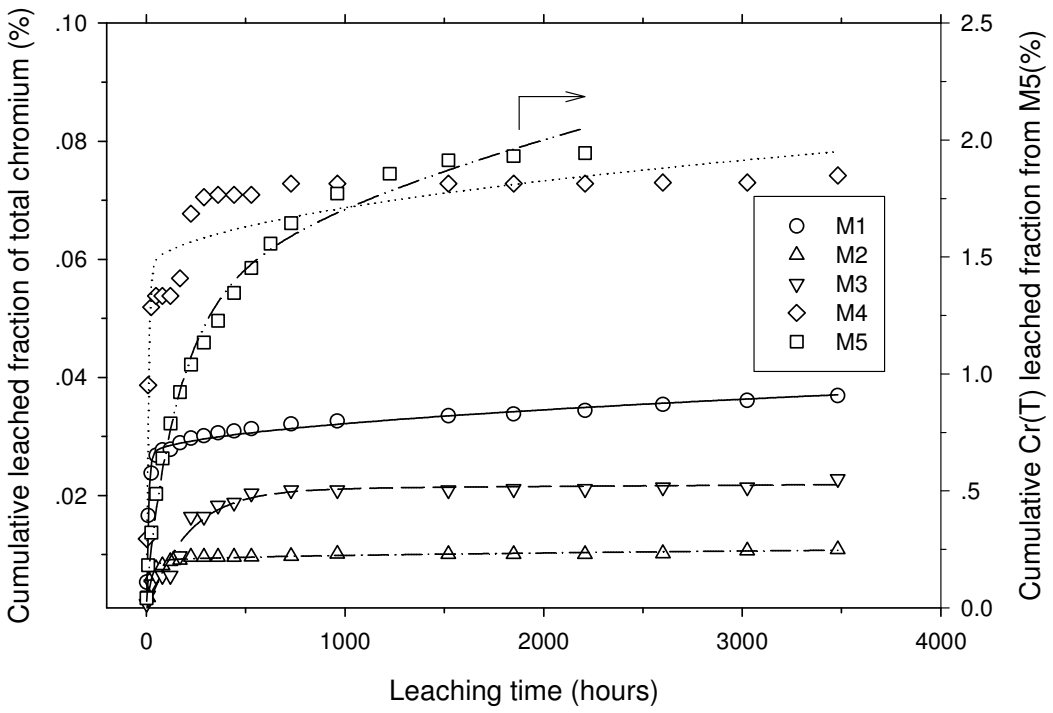

Figure 9.4 Cumulative Cr(T) release and modelling results from the stabilised wastes (M1-50%SPD+50%AS; M2-50%SPD+50%MR; M3-20%FCD1+80%AS; M4-20%FCD2+80%AS and M5-20%FC+80%AS)

By fitting the data to the leach model described by Cote et al. and Shin et al. (function 9.13), coefficients k_i, where i = 1, 2, 3, 4 and 5 were determined, and are listed in Table 9.2. It can be seen from Table 9.2 that the k_4 values are at least 9 orders of magnitude smaller than the k_1, k_2 and k_3 values. By comparing the values of the different terms in function (9.13), i.e., $k_1[1-\exp(-k_2 t)]$, $k_3 t^{\frac{1}{2}}$ and $k_4 t$, it is therefore clear that according to this model the predominant release mechanisms of total chromium are initial surface wash-off followed by matrix diffusion. It further indicates that the controlling leaching mechanisms of chromium from M1, M2, M3 and M4 change into diffusion control from initial wash off control after approximately 81h, 121h, 81h and 49h, respectively. The average effective diffusion coefficients of chromium from the solidified wastes can be calculated based on function (9.6). These were found to be, respectively, 2.52×10^{-10}, 9.73×10^{-12}, 3.43×10^{-12}, 9.46×10^{-10} and 3.98×10^{-6} m^2/s for M1, M2, M3, M4 and M5. The

correlation coefficients (R^2) of the cumulative release fraction as calculated from the model and the experimental values for leaching experiments M1, M2, M3, M4 and M5 are 0.99, 0.99, 0.96, 0.89 and 0.99, respectively.

Table 9.2 Controlling leaching mechanisms of total chromium from the stabilised wastes

Sample	k_1	k_2	k_3	k_4	Controlling leaching mechanisms
M1	2.65E-02	1.01E-01	1.79E-04	1.68E-14	Wash-off and diffusion
M2	8.82E-03	4.02E-02	3.25E-05	3.49E-15	Wash-off and diffusion
M3	2.06E-02	4.98E-03	2.09E-05	6.55E-15	Wash-off and diffusion
M4	5.77E-02	1.14E-01	3.47E-04	1.89E-13	Wash-off and diffusion
M5	9.94E-01	5.97E-03	2.25E-02	5.74E-12	Wash-off and diffusion

The logarithm of cumulative total chromium release versus logarithm of leaching time of the stabilised wastes are shown in Figure 9.5. It shows that the slopes for samples M1, M2, M3, M4 and M5 are 0.17, 0.28, 0.35, 0.17 and 0.49, respectively. According to De Groot, it means that the controlling leaching mechanisms of samples M1, M2, M3 and M4 are initial surface wash-off because the slope of the regression line is lower than 0.4 [192]. Matrix diffusion controls chromium that leaches from sample M5 since the slope of the regression line is 0.49 which is in the range of 0.4-0.6 [192]. This does not fully agree with the results of the model of Cote et al. and Shin et al. [187,193] (Table 9.2). The deviations from the model results are due to the fact that the latter model can only identify one major leaching mechanism of a species, while the former model can identify the leaching mechanisms of a species during different stages of the leaching process. It is, therefore, recommended that the model of Cote et al. and Shin et al. is used if the leaching process of a species is controlled by two or three different mechanisms.

9.4.2 Leaching mechanisms of Cr(VI) from the stabilised wastes

The cumulative Cr (VI) releases from the solidified wastes (expressed in mg/m^2) as a function of leaching time, as calculated from equation 9.13 are presented in Figure 9.6

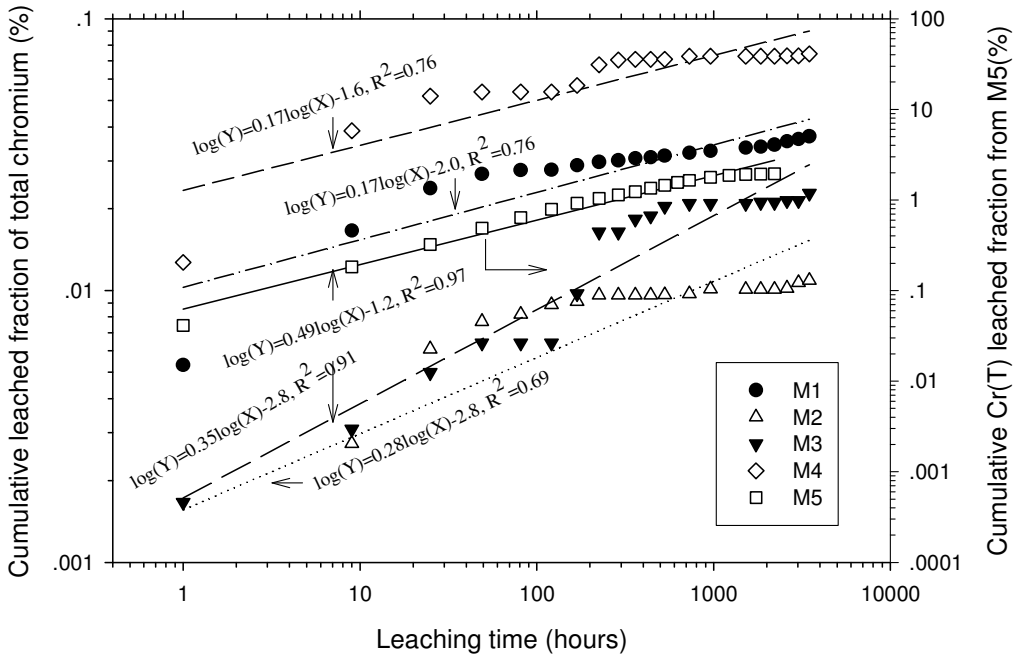

Figure 9.5 Logarithm of cumulative Cr (T) release vs. logarithm of leaching time

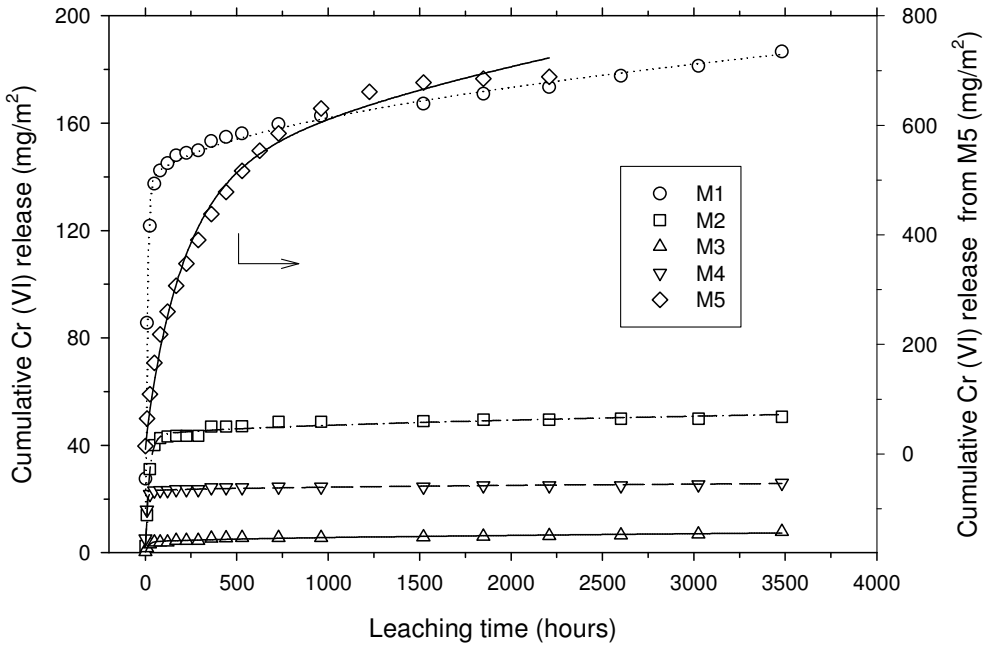

Figure 9.6 Cumulative Cr (VI) release from the solidified wastes (M1-50%SPD+50%AS; M2-50%SPD+50%MR; M3-20%FCD1+80%AS; M4-20%FCD2+80%AS and M5-20%FC+80%AS)

(the data are shown in Appendix VI). Coefficients k_1, k_2, k_3 and k_4 of this model are given in Table 9.3. It can be seen from Table 9.3 that the k_4 values are at least 7 orders of magnitude smaller than the values for k_1, k_2 and k_3. Cr (VI) therefore leaches from the stabilised wastes through initial wash-off and matrix diffusion. The large amounts of Cr (VI), which leached during the initial stage, are due to wash-off from the surface of the stabilised waste samples. The leaching of Cr (VI) slows down after approximately 81h, 121h, 81h and 49h for samples M1, M2, M3 and M4, respectively. The controlling leaching mechanism of Cr (VI) therefore changes to matrix diffusion. The correlation coefficients (R^2) of the cumulative release fraction between model predicted and experimental values for all the leaching experiments are more than 0.97.

Table 9.3 Controlling leaching mechanisms of Cr (VI) from the stabilised wastes

Sample	k_1	k_2	k_3	k_4	Controlling leaching mechanisms
M1	1.35E+02	1.05E-01	8.62E-01	5.13E-11	Wash-off and diffusion
M2	4.28E+01	4.71E-02	1.46E-01	2.38E-11	Wash-off and diffusion
M3	3.67E+00	6.26E-02	6.15E-02	1.09E-12	Wash-off and diffusion
M4	2.28E+01	1.42E-01	5.02E-02	7.25E-12	Wash-off and diffusion
M5	3.88E+02	4.84E-03	7.12E+00	2.52E-09	Wash-off and diffusion

The cumulative leached concentration of Cr (VI) from the stabilised wastes (samples M1, M2, M3, M4 and M5) are 1.87, 0.50, 0.08, 0.26 and 6.80 mg/l, respectively (Table VI.1). According to Kim et al., the solubility of the leaching components influences the cumulative release of the toxic substances [195]. By comparing the cumulative total chromium that leached from the stabilised wastes with the amount of Cr (VI) that leached, it is clear that more than 97.9%, 86%, 80%, 81% and 98.5% of the leachable chromium is in the oxidation state of Cr (VI) for M1, M2, M3, M4 and M5 respectively. This is due to the lower solubility of Cr (III)-containing species (below 0.0026g/l [192,193]), while the Cr (VI)-containing components, such as K_2CrO_4 (629g/l), $K_2Cr_2O_7$ (49g/l), Na_2CrO_4 (873g/l) and $CaCrO_4$ (163g/l) [197], are highly soluble.

It is noted that the leachable Cr (VI) concentrations from the stabilised wastes which were sintered in a Muffle furnace are higher than the Cr(VI) that leached from the sintered waste that were sintered in the tube furnace. The leachable Cr (VI) from the stabilised mixture of 50%AS-50%SPD is higher than that from the stabilised mixture of 50%MR-50%SPD. It is also found that the leachable Cr (VI) concentrations from the stabilised wastes exceed the acceptable limits. These are not fully in agreement with the results in Chapter 8. This is possibly due to the variations of the experimental conditions, such as the usage of the purge gas, different heating and cooling rates, leaching time and kinetics conditions.

Figure 9.7 shows the logarithm of cumulative Cr (VI) release versus the logarithm of leaching time of the stabilised wastes. The slopes from linear regressions for samples M1, M2, M3, M4 and M5 are 0.17, 0.27, 0.28, 0.13 and 0.50, respectively. It means that leaching of Cr (VI) from samples M1, M2, M3 and M4 is controlled by initial wash-off, while in sample M5 it is controlled by matrix diffusion. It can also be seen from Figure 9.7 that the leachable Cr (VI) from sample M5 is substantially higher than that from the other stabilised wastes. This might be due to the reformation of Cr (VI) during the sinter process since the filter cake contains significant concentrations of calcium oxide, which can react with Cr(III) under oxidizing conditions to form $CaCrO_4$ [182].

As discussed in Chapters 7 and 8, the Cr (VI)-containing species can possibly form during the sinter process via oxidation by air or reaction with lime, alkali oxides and oxygen. Cr (III)-containing species, which are close to the surface of the sample, can readily react with oxygen and reform Cr (VI). These Cr (VI)-containing species can easily leach out when they come in contact with the leachant (distilled water). This explains why surface wash-off is the controlling leaching mechanism during the initial leaching period from the stabilised wastes.

The cumulative releases of species, such as chromium, might also be influenced by the pH of the leaching solution [193]. The average pH values of the leachate during the leaching experiments on the stabilised wastes are shown in Figure 9.8. The pH values

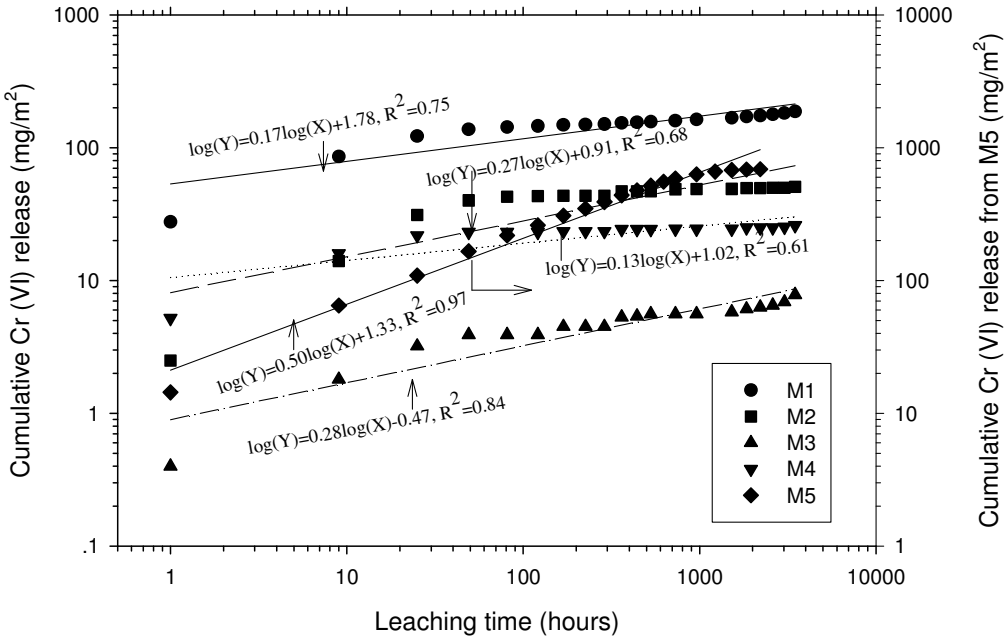

Figure 9.7 The logarithm of cumulative Cr (VI) release versus logarithm of leaching time of the stabilised wastes

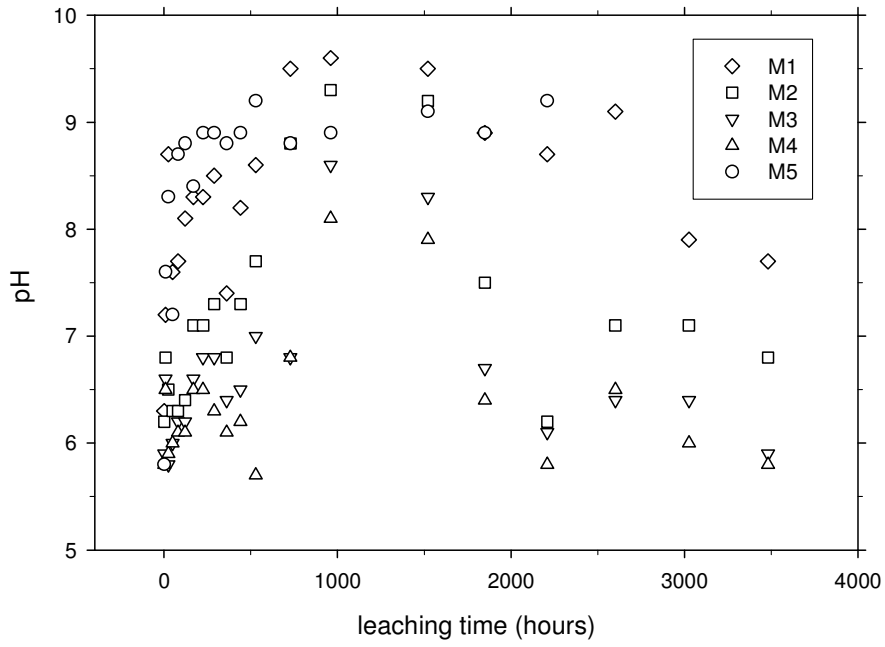

Figure 9.8 The pH profile of the leachant vs. time during the leaching process

range from 5.8 to 9.6. The pH values of the leachates of samples M1, M2, M3 and M4 initially increased, after which it decreased as the leaching process proceeded. The pH of the sample M5 remained constant after approximately 81 h of leaching.

Figure 9.9 shows the solubility diagrams of chromium species calculated using STABCAL-W32 [181]. It shows that Cr (III) precipitates in the pH range of approximately 5.5 to 12.5, while Cr (VI) would not precipitate in the whole pH range and only change from $HCrO_4^-$ and H_2CrO_4 to CrO_4^{2-}. The pH of the leachate during the semi-dynamic leaching test was in the precipitation range of Cr(III) (Figure 9.8). It therefore indicates that it can influence the leachable total chromium concentration in the leachate, but not the leaching mechanisms of total chromium. It can also explain that more than 80% of chromium in the experiment is Cr(VI).

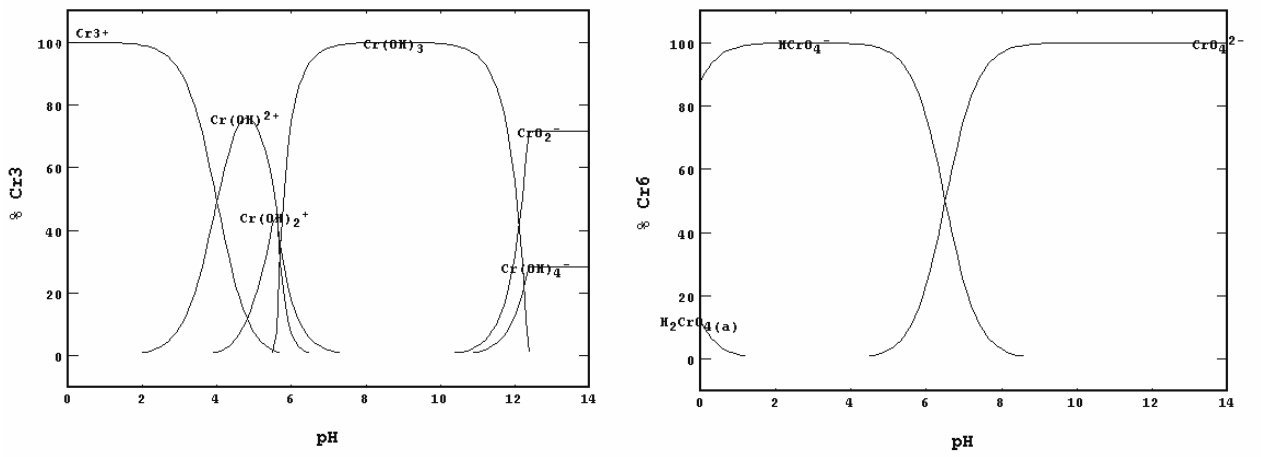

(a) Cr(III) (b) Cr (VI)

Figure 9.9 The solubility diagrams of chromium species calculated using STABCAL-W32 at 25°C with a concentration of 10^{-6} M [181].

9.5 Conclusions

Semi-dynamic leaching tests were conducted in order to understand the leaching mechanisms of the chromium species from the stabilised waste forms. Semi-empirical

models from the literature were used to evaluate the dominant leaching mechanisms of the chromium species.

1) It shows that the predominant leaching mechanisms of chromium species are initial surface wash-off followed by matrix diffusion.
2) Only very small amounts of chromium leaches out from the solidified products. The cumulative release fractions of chromium from the solidified wastes are lower than 2% over a period of approximately 5 months.
3) The cumulative leached concentrations of total chromium from stabilised wastes M1, M2, M3 and M4 are less than the acceptable limits for chromium, while the leachable chromium from sample M5 exceeds the acceptable risk level of chromium.
4) More than 80% of the leachable chromium from the stabilised products is Cr (VI) species due to the high solubility of Cr (VI) in distilled water.
5) The leachable Cr (VI) concentrations from the stabilised wastes which were sintered in a Muffle furnace exceed the acceptable limits, and are higher than from the stabilised wastes that were sintered in a tube furnace. This is possibly due to the variations of the experimental conditions, such as purge gas, heating and cooling rates, leaching time and leaching solution.

Chapter 10 Summary and Conclusions

The Cr (VI)-containing pyrometallurgical wastes (stainless steel plant dust, ferrochrome dust and filter cake from the waste acid treatment plant) potentially pose a threat to the environment and human health. In South Africa, the ferrochromium industry and the stainless steel industry produces approximately 100,000 t and 24,000 t of Cr (VI)-containing dust per year, respectively [17,39]. It is therefore of great importance to investigate the problem comprehensively and develop an appropriate treatment process.

A number of problems currently hamper the treatment of these wastes, such as the variation in composition of the stainless steel plant dust, significant contents of volatile substances in the ferrochrome dust and sulphur content in the filter cake.

The characteristics and microstructures of these wastes were therefore first investigated in order to fully understand the behaviour of these wastes, and to postulate the formation mechanisms of them. Suggestions are also given on how to reduce the amounts of wastes. The leachability and the aging behaviour of these wastes were then studied in order to further understand the toxic properties of these wastes.

It has been proven that stabilisation/solidification processes are effective technologies, whereby electric furnace dusts can be cemented, glassified and sintered into value added products. In the present thesis, the stabilisation of Cr (VI) in these wastes with silica-rich clay was studied, as well as the leaching behaviour of chromium species from the stabilised wastes. A summary of the results are given and the following conclusions can be drawn:

10.1 Summary

10.1.1 Stainless steel plant dust (SPD)

The stainless steel plant dust is chocolate-brown in colour, and consists of very fine particles. It has a bulk density of 1.39gcm^{-3} and low moisture content (0.40%). On leaching in water the examined stainless steel plant dust produces alkaline solutions.

The SPD is iron oxide, chromium oxide and CaO rich, but also contains some MgO, MnO, SiO_2, ZnO and nickel. The main phases that are present in the SPD are the $(Mg,Fe,Mn,Cr)_3O_4$ spinel phase, quartz, $Ca(OH)_2$ and nickel. TG/DTA analysis in air indicated that mass losses and gains occur during heating of SPD due to reactions in which H_2O and CO_2 are driven off, and metallic particles oxidize.

A microstructural examination of the SPD showed that the stainless steel plant dust contains particles that are irregular in shape, spherical or near spherical particles and particles coated with slag or oxides.

TCLP and ASTM 3987-85 tests show that stainless steel plant dust is a hazardous material due to the fact that the leachable Cr(VI) from SPD exceeds the limit of South Africa on Cr(VI). It is therefore pose a potential threat to the environment. Distilled water leaching experiments on the stainless steel plant dust showed that approximately 65% of the Cr (VI) leaches out within 5 min, but that the Cr (VI) leaches out more easily in acidic and basic solutions than in distilled water. Furthermore, it can be concluded that the Cr (VI) leaching reaction is most probably controlled by the diffusion of Cr(VI) inside the Cr (VI) leached layer and the rate of the chemical reactions whereby Cr (III) is transformed into Cr (VI).

Aging experiments on the SPD show that the extractable amount of Cr (VI) from the SPD decreases with increasing aging time, possibly due to the reduction reaction of Cr (VI) into Cr (III) by Fe (II)-containing phases. The extractable amount of Cr (VI) from the SPD increases with decreasing particle size. Higher water vapour content in the atmosphere tends to increase the extractable amounts of Cr (VI) from the SPD.

Cr (VI) in the stainless steel plant dust can be stabilised by mixing stainless steel plant dust with clay, and sintering it at 1100^{o}C for 5 hours. Decreasing sinter temperature, increasing waste content in the brick and reducing sinter time increase the leachability of Cr (VI) from the stabilised stainless steel plant dust. Increasing mass %CaO/mass %SiO_2 ratios and alkali oxides contents in the SPD-clay mixtures significantly increase the leachable Cr(VI) from the brick due to the formation of Cr (VI)-containing phases, such as $CaCrO_4$ and alkali chromates. The spiked Cr (VI) recovery decreases with increasing leaching time in the modified TCLP test, probably due to the fact that Cr (VI) is reduced into Cr (III) by Fe^{2+} and organic components.

In South Africa, the TCLP test is generally used to evaluate whether hazardous wastes are environmentally acceptable. The Cr (VI) concentrations in the leachate when the sintered bricks were examined with the modified TCLP test are below 10 ppb in this study, which is environmentally acceptable in South Africa. However, the leachable Cr (VI) in the leachates of the modified ASTM D 3987-85 test is higher than that in the modified TCLP test and still considered to be a potential threat to the environment and human health. This is due to the effects of redox potential and pH of the leachates, Fe^{2+} and organic components.

When Cr (VI) in the stainless steel plant dust is stabilised with clay in a sinter process, other toxic substances such as As, Zn and Pb are also stabilised. The emission factor from the stabilised SPD mixtures is similar to that of the cement industry.

The semi-static leaching experiment showed that the predominant leaching mechanisms of chromium species from the stabilised SPD are initial surface wash-off followed by matrix diffusion. Only very small amounts of chromium leaches out from the solidified SPD, and it is less than the acceptable limits for chromium. Approximately 98% of the leachable chromium from the stabilised SPD is Cr (VI). However, the leachable Cr (VI) concentrations from the stabilised SPD which was sintered in a Muffle furnace exceed the acceptable limits. This must be due to variations in the experimental conditions, such

as type of purging gas, heating and cooling rates, leaching time and type of leaching solution.

10.1.2 Ferrochrome plant dust (FCD1, FCD2 and FCD3)

The ferrochrome dusts are fine particles, have bulk densities that vary between 0.49 and 2.42gcm^{-3}, and have low moisture contents. Ferrochrome fine dusts (FCD1 and 2) generate slightly basic solutions (pH≈8), while ferrochrome coarse dust (FCD3) produces strong basic solutions (pH≈11).

The FCD1 and 2 contain significant concentrations of SiO_2, ZnO, MgO and alkali metal oxides, but also some sulphur and chlorine, while FCD3 is SiO_2-chromium oxide-iron oxide-Al_2O_3-MgO-C-based. The main phases present in the coarse fraction of ferrochrome dust are chromite, partly altered chromite, quartz and carbon, while the main components of the fine fractions include chromite, SiO_2, ZnO, NaCl and Mg_2SiO_4. TG/DTA analysis in air indicated that mass losses occur during heating of ferrochrome dusts due to the combustion of carbon, loss of crystalline water and vaporisation.

Ferrochrome fine dusts consist of clusters which contain charge materials, slag droplets as well as very fine SiO_2-MgO-ZnO-$(Na,K)_2O$ based particles. The coarse particles consist of reductant, slag droplets and chromite particles. It is also assumed that Cr (VI)-containing species in ferrochrome dust are generated at the top of the SAF or in the off-gas duct, as Cr (VI) is found on the surface of the dust.

TCLP and ASTM 3987-85 tests show that ferrochrome fine dusts are also hazardous materials according to South African legislation. They therefore pose a potential threat to the environment and human health. Static distilled water and nitric acid leaching experiments show that the ferrochrome fine dust particles have a core of SiO_2 with an outer layer of vaporisation substances such as ZnO and NaCl. Distilled water leaching experiments on ferrochrome dusts show that Cr (VI) is easily leached by distilled water.

Cr (VI) in ferrochrome fine dusts that were sintered with 50% clay AS at 1000^{o}C for 5 hours could not be stabilised, as the concentrations of zinc and/or Cr (VI) from the stabilised wastes in the modified TCLP and ASTM D 3987-85-tests exceed the regulation limits. The emission factors from the stabilised ferrochrome fine dusts (FCD1 and FCD2) are however very low (0.2-1g/t brick), and below the chromium emission factors from the cement industry.

The predominant leaching mechanisms of chromium species from the stabilised ferrochrome fine dusts are initial surface wash-off followed by matrix diffusion. The cumulative release fraction of total chromium from the solidified products are lower than 0.1% and less than the acceptable limits for chromium.

10.1.3 Filter cake (FC)

The original filter cake consists of very fine particles, and typically has a moisture content of 50%. Filter cake produce alkaline solutions when leached in water. The concentrations of calcium, fluorine, iron and sulphur are high in the filter cake. The major phases present in the filter cake is CaF_2, $CaSO_4$, $CaCO_3$ and a metal rich (Fe, Cr and Ni) amorphous oxide phase. TG/DTA analysis in air indicated that mass losses and gains occur during heating of these waste materials due to reactions in which H_2O, CO_2, SO_2, SO_3, fluorine, calcium and silicon are driven off.

TCLP and ASTM 3987-85 tests showed that filter cake is a hazardous material according to South African legislation. Distilled water leaching experiments on the filter cake showed that Cr (VI) is easily leached by distilled water.

By examining the aging behaviour of Cr (VI) in the filter cake it is clear that increasing temperature favours the oxidation of Cr (III) into Cr (VI). However, the extractable amount of Cr (VI) from the FC decreases with increasing aging time, possibly due to the reduction of Cr (VI) into Cr (III) by trace amounts of Fe (II)-containing phases. The extractable amount of Cr (VI) from FC increases with increasing particle size. The water

vapour and oxygen content in the atmosphere has no significant effect on the amount of extractable Cr (VI) from the filter cake.

An attempt was made to stabilise Cr(VI) in the filter cake by sintering a 50wt% AS-50wt% filter cake mixture at 1000^{o}C for 5 hours. The modified TCLP test indicated that the FC could not be stabilised with clay, presumably due to significant levels of $CaO/CaCO_3$ and CaF_2 in the mixture.

A semi-dynamic leaching test on the stabilised filter cake showed that the predominant leaching mechanisms of chromium species are initial surface wash-off followed by matrix diffusion. The cumulative release fractions of total chromium and chromium (VI) exceed the acceptable limits.

10.2 Conclusions

- Stainless steel dust is postulated to form by the entrainment of charge materials, evaporation or volatilisation of elements and ejection of slag and metal by spitting or the bursting of gas bubbles.
- Ferrochrome dusts are formed by the ejection of slag and metals droplets from the electrode hole, the entrainment of charge materials, vaporisation as well as the formation and precipitation of compounds from vaporised species in the off-gas duct.
- The crystalline phases (CaF_2 and $CaSO_4$) are generated in the neutralisation and reduction steps of the production process due to super saturation, while the metal rich amorphous phases are generated in the precipitation step.
- Due to the significant concentrations of Cr(VI) in the ferrochrome fine dust, it should not come in contact with water before being processed. The coarse ferrochrome dust is suitable to be recycled back to the SAF, as it contains low concentrations of volatile substances, but also usable carbon, quartz and chromite particles.
- Cr (VI) in the stainless steel plant dust can be stabilised by mixing stainless steel plant dust with clay, and sintering it at 1100^{o}C for 5 hours.

- Sintering temperature, sintering time, sinter atmosphere, initial Cr(VI) concentration, waste:clay ratio, mass %CaO/mass %SiO_2 ratios and alkali oxides contents in the bricks influence the Cr(VI) formation. It is postulated that Cr (VI) form when the $(Mg,Fe,Mn,Cr)_3O_4$ spinel phase, alkali oxides, Ca-containing phases such as $Ca(OH)_2$, CaO, $CaCO_3$ and CaF_2 react both at ambient and at high temperatures (1100°C).
- The filter cake could not be stabilised with clay at high temperature (1000°C), presumably due to significant levels of CaO/$CaCO_3$ and CaF_2 in the mixture.
- It is recommended that ASTM D 3987-85 test is used to evaluate the degree of toxicity of the sintered bricks.
- A semi-dynamic leaching test on the stabilised wastes showed that the predominant leaching mechanisms of chromium species are initial surface wash-off followed by matrix diffusion.

10.3 Recommendations for future work

10.3.1 Modelling of the formation mechanisms of Cr (VI)

The formation mechanisms of Cr (VI) species in the steelmaking and ferrochrome-making processes are still not completely understand as these processes are complex. Since Cr (VI) cannot form in the furnace where reducing conditions prevail, it would be meaningful to model the behaviour of the off-gases from the furnace to the baghouse filter by using thermodynamic calculation software such as FACTSage. Such a model could predict where and how Cr (VI) and other toxic substances form, but also assist in the design of the off-gas duct.

10.3.2 Simultaneous treatment of stainless steel plant dust and pickling acid

By minimising waste generation in a steelmaking plant, one waste material is often used to treat another waste. In the present project, it was found that the pH of the stainless steel plant dust is approximately 12, while the waste pickling acid has a pH of approximately 1. In addition, the stainless steel plant dust has a reduction capacity for Cr (VI) species, and it is expected that the concentration of Fe^{2+} would increase if the SPD is dissolved in the waste pickling acid. For the waste pickling acid, SPD might therefore be a potential

neutraliser and act as a reductant of Cr (VI). Less lime and ferrous sulphate would then be required to neutralise the acid and reduce Cr (VI) in the pickling acid. Furthermore, less sulphur would be introduced into the process due to the fact that no or less ferrous sulphate is added to reduce Cr (VI). The current filter cake production process can be used to treat the reaction product between the stainless steel plant dust and waste pickling acid. The precipitate of the process can then further be treated by either recovery or a stabilisation process. Such a simultaneous treatment process needs to be evaluated in detail.

10.3.3 Properties of the bricks

In this study, bricks were produced from mixtures of stainless steel dust and clay. These bricks can potentially be used for low cost housing, as the leachability of Cr (VI) from the bricks is under the regulatory limits. However, other properties of the bricks, such as density, apparent porosity, shrinkage during firing and cold crushing strength, need to be evaluated in order to determine whether these bricks can be used for such an application.

References

1. Ma, G. and Garbers-Craig, A.M., Cr (VI)-containing electric furnace dusts and filter cake from a stainless steel waste treatment plant, Part II: Formation and leachability, accepted by *Ironmaking and Steelmaking*, 2005.
2. Cox, X.B. and Linton, R.W., Determination of chromium speciation in environmental particles: Multitechnique study of ferrochrome smelter dust, *Environ. Sci. Technol*., Vol. 19, 1985, pp. 345-352
3. Zunkel, A. D., Electric arc furnace dust management: A review of technologies, *Iron and Steel Engineer*, No.3, 1997, pp. 33-38.
4. Nolasco-Sobrinho, P.J., Espinosa, D.C.R. and Tenorio, J.A.S., Characterisation of dusts and sludges generated during stainless steel production in Brazilian industries, *Ironmaking and Steelmaking*, Vol. 30, No.1, 2003, pp. 11-17.
5. Geldenhuis, J.M.A. and Horne, A.W., Recovery of valuables and stabilisation of chromium (VI) in stainless steel flue dust fines, *Steelmaking Conference Proceedings,* Nashville, USA, ISS, 2002, pp. 661-668.
6. Cowx, P.M. and Roddis, B., The recovery of alloy elements from EAF/AOD fume in the Tetronics plasma system, *Steelmaking Conference Proceedings*, Washington D.C., April 6-9, 1986, pp. 443-450.
7. Mukherjee, A.B., Chromium in the environment of Finland, *The Science of the Total Environment*, Vol. 217, 1998, pp. 9-19.
8. Niemela, P., Krogerus, H. and Oikarinen, P. Formation, characteristics and utilisation of CO-gas formed in ferrochromium smelting, *Tenth International Ferroalloys Congress*, 1-4 Feb., Cape Town, South Africa, 2004, pp. 68-77.
9. Private Communication with plant personnel.
10. Rodriguez-Pinero, M., Pereira, C.F., Francoy, C.R.E. and Parapar, J.F.V. Stabilisation of a chromium-containing solid waste: immobilization of hexavalent Chromium, *J. Air & Waste Manage. Assoc.*, Vol. 48, 1998, pp. 1093-1099.
11. ICDA, *Health Safety and Environment Guidelines for Chromium*, Paris, France, 2001, pp. 26-27.

12. Pelino, M., Karamanov, A., Pisciella, P., Crisucci, S. and Zonetti, D., Vitrification of electric arc furnace dusts, *Waste Management*, Vol. 22, 2002, pp. 945-949.
13. Karamanov, A., Pisciella, P. and Hreglich, A. Sinter glass-ceramics from municipal solid waste-incinerator fly ashes-part I: the influence of the heating rate on the sinter-crystallisation, *J. Euro. Cer. Soc.*, Vol. 23, No. 6, 2003, pp. 827-832.
14. Dusing, D.C., Bishop, P.L. and Keener, T.C., Effect of redox potential on leaching from stabilized/solidified waste materials, *J. Air Waste Manage. Assoc.*, Vol. 42, 1992, pp. 56-62.
15. Department of Water Affairs and Forestry (DWAF), *Minimum Requirements for the Handling, Classification and Disposal of Hazardous Waste*, South Africa, 2nd edn, 1998.
16. Giesekke, E.W., Smit, J.P., Viljoen, E.A., Kruger, A.W., Kruger, S.J. and Maine, C.F., Evaluation of solid-stabilised products made from Cr (VI)-containing ferrochrome bag-filter dust, *Waste Materials in Construction Conference*, Harrogate, England, United Kingdom, 31 May to 2 June, 2000.
17. Maine, C.F., Smit, J.P. and Giesekke, E.W. Report to the Water Research Commission on the project "*Solid Stabilization of Soluble Waste in the Ferro-alloy Industry*", 2000.
18. Bailey, D., Recycling of pickling liquor with diffusion dialysis, *Stainless Steel*, No. 11-12, 2003, pp. 10-11.
19. Stephenson, J.B., Hogan, J.C. and Kaplan, R.S., Recycling and metal recovery technology for stainless steel pickling liquors, *Environmental Progress*, Vol. 3, No. 1, 1984, pp. 50-53.
20. Brown, C.J., Productivity improvements through recovery of pickling liquors with the APU processes, *Iron and Steel Engineer*, No.1, 1990, pp. 55-60.
21. US EPA, *Toxicity Characteristic Leaching Procedure*, USA code of federal regulations, 40th edition, Part 261.
22. Finley, B.L., Kerger, B.D., Katona, M.W., Gargas, M.L., Corbett, G.C. and Paustenbach, D.J., Human ingestion of chromium (VI) in drinking water: Pharmacokinetics following repeated exposure, *Toxicology and Applied Pharmacology*, Vol. 142, 1997, pp. 151-159.

23. Huber, J.C., Rocabois, P., Faral, M., Birat, J.P., Patisson, F. and Ablitzer, D., The formation of EAF dust, *Electric Furnace Conference Proceedings,* ISS, Orlando, 2000, pp. 171-181.
24. Delhaes, C., Hauck, A. and Neuschutz, D., Mechanisms of dust generation in a stainless steelmaking converter, *Steel Research*, Vol. 64, No. 1, 1993,pp. 22-27.
25. Ohno, T., Ono, S. and Okajima, M., Experimental results on dust formation by small melting furnace, *Transactions ISIJ*, Vol. 26, 1986, pp. B-312.
26. Nedar, L., Dust formation in a BOF converter, *Steel Research*, Vol. 67, No. 8, 1996, pp. 320-327.
27. Schmitt, R.J., Kusik, C.L., O'Neil, R., Cowx, P.M. and Schade, C.T., Minimizing electric arc furnace dust generation, *Electric Furnace Conference Proceedings*, ISS, Chicago, 1997, pp. 567-580.
28. Li, C.L. and Tsai, M.S., Mechanism of spinel ferrite dust formation in electric arc furnace steelmaking, *ISIJ International*, Vol.33, No.2, 1993, pp. 284-290.
29. Huber, J.C., Patisson, F., Rocabois, P., Birat, J.P. and Ablitzer, D., *Proceedings of the "REWAS"99 Global Symposium on Recycling, Waste Treatment and Clean Technology*, San Sebastian, Spain, 1999, pp. 1483-1492.
30. Badger, S.R. and Kneller W.A., The characterization and formation of electric arc furnace (EAF) dusts, *Electric Furnace Conference Proceedings*, ISS, Chicago, 1997, pp. 95-98.
31. Stubbles, J.R., The formation and suppression of EAF dust, *Electric Furnace Conference Proceedings*, ISS, Nashville, 1994, pp. 179-185.
32. Muller, K.T., Holappa, L. and Neuschutz, D., Control of ejections caused by bubble bursting in steelmaking processes, *Steel Research*, Vol. 74, No.2, 2003, pp. 61-69.
33. Nedar, L., Lindblom, B. and Bjorkman, B., Mechanisms of dust formation in LD-converter, *Steelmaking Conference Proceedings*, ISS, Warrendale, 1996, pp. 755-762.
34. Tsujino, R., Hirai, M., Ohno, T., Ishiwata, N. and Inoshita, T., Mechanisms of dust generation in a converter with minimum slag, *ISIJ International*, Vol. 29, No.4, 1989, pp. 291-299.

35. Chigwedu, C., Kempken, J., Ploch, A. and Pluschkell, W., Numerical simulation model for exhaust gas transportation of dust in the BOF, *Steel Research*, Vol. 66, No.8, 1995, pp. 341-348.
36. Gritzen, A. and Neuschutz, D., Rates and mechanisms of dust generation in oxygen steelmaking, *Steel Research*, Vol. 72, No.9, 2001, pp. 324-330.
37. Sumi, I., Kawabata, R., Kikuchi, Y., Kohira, S. and Isawa, T., Technique of controlling dust generation during oxygen top blowing in BOF, *Steel Research*, Vol. 74, No.1, 2003, pp. 14-18.
38. Petersen, J., *Assessment and Modelling of Chromium Release in Minerals Processing Waste Deposits*, PhD thesis, University of Cape Town, 1998.
39. Geldenhuis, J.M.A., Recovery of valuables from flue dust fines, *Minerals Engineering*, Vol. 15, 2002, pp. 95-98.
40. Eksteen, J.J., Frank, S.J. and Reuter, M.A., Dynamic structures in variance based data reconciliation adjustments for a chromite smelting furnace, *Minerals Engineering*, Vol. 15, 2002, pp. 931-943.
41. McDonnell, C.E., Triger, D.R. and Argent, B.B., Characteristics of steelworks dusts. *Ironmaking and Steelmaking*, Vol. 16, No. 6, 1989, pp. 435-445.
42. Vinals, J., Balart, M.J. and Roca, A., Inertization of pyrite cinders and co-inertization with electric arc furnace flue dusts by pyroconsolidation at solid state, *Waste Management*, Vol. 22, No.7, 2002, pp. 773-782.
43. Cheng, T.W., Combined glassification of EAF dust and incinerator fly ash, *Chemosphere*, Vol. 50, 2003, pp. 47-51.
44. Peng, B., Zhang, C. and Peng, J., Treatment of steelmaking dust in electric arc furnace by vitrification, *J. Cent. South Univ. Technol.*, Vol. 31, No. 2, 2000, pp. 124-126.
45. Peng, B., Lobel, J., Kozinski, J.A. and Bourassa, M., Non-isothermal reduction kinetics of EAF dust-based pellets, *CIM Bulletin*, Vol. 94, No. 4, 2001, pp. 64-70.
46. Lobel, J., Peng, B., Kozinski, J.A. and Bourassa, M., Pilot-scale direct recycling of flue dust generated in electric stainless steelmaking, *Iron and Steelmaker*, No.1, 2000, pp. 41-45.

47. Matway, R.J., Deferrari, N.L. and Deszo, R.L., On-site recycling of flue dust and other waste streams by briquetting, *Electric Furnace Conference Proceedings*, ISS, Orlando, 1989, pp. 661-668.
48. McCrea, J. and Pickles, C.A., Agglomeration and recycling of electric arc furnace dust, *Electric Furnace Conference Proceedings*, ISS, Orlando, 1995, pp. 159-170.
49. Li, C.L. and Tsai, M., A crystal phase study of zinc hydroxide chloride in electric-arc-furnace dust, *Journal of Materials Science*, Vol. 28, 1993, pp. 4562-4570.
50. Karamanov, A., Pisciella, P., Cantalini, C. and Pelino, M., Influence of Fe^{3+}/Fe^{2+} ratio on the crystallization of iron-rich glasses made with industrial wastes, *J. Am. Ceram. Soc.*, Vol. 83, No.12, 2000, pp. 3153-3157.
51. Schoukens, A.F.S., Shaw, F. and Chemaly, E.C., The Enviroplas process for the treatment of steel-plant dusts, *J. S. Afr. Inst. Min. Metall.*, Vol. 93, No.1, 1993, pp. 1-7.
52. Stegemann, J. A., Roy, A. Caldwell, R.J., Schilling, P.J. and Tittsworth, R., Understanding environmental leachability of electric arc furnace dust, *Journal of Environmental Engineering*, No.2, 2000, pp. 112-120.
53. Goff, T.J. and Dento, G.M., Direct smelting of stainless steel plant dust, *Tenth International Ferroalloys Congress*, SAIMM, Cape Town, South Africa, 2004, pp. 687-692.
54. Strobos, J.C. and Friend, J.F.C., Zinc recovery from baghouse dust generated at ferrochrome foundries, *Hydrometallurgy*, Vol. 74, 2004, pp. 165-171.
55. Kornelius, G., Dust from air pollution control operations in the ferro-alloy industry: Problems and opportunities, *S A Journal of Chemical Engineering*, Vol. 7, No.1, 1995, pp. 28-38.
56. Cohn, B and Petrie, J.G., Containment of chromium and zinc in ferrochromium flue dusts by cement-based solidification, *Canadian Metallurgical Quarterly*, Vol. 36, No.4, 1997, pp. 251-260.
57. Gericke, W.A., Environmental solutions to waste products from ferrochrome production, *The Proceedings of INFACON 8*. Beijing, China, 1998, pp. 51-58.
58. Giesekke, E.W., Mineral-based treatment strategies for wastes and effluents, *South African Journal of Science*, Vol. 95, 1999, pp. 367-371.

59. Braun, E., How to improve pickling of stainless steel strip, *Iron and Steel Engineer*, April 1980, pp. 79-81.
60. Lindblom, B. and Ma, P., Characterisation and reduction studies of the waste pickling sludge of stainless steel, *REWAS'99 Global Symposium on Recycling, Waste Treatment and Clean Technology*, Sebastian, Spain, 5-9 September, 1999, pp. 1493-1501.
61. Reisenhofer, K. and Losch, H., Erfahrungen bei der behandlung von chromhaltigen spulwassern und altsauren im durchlaufverfahren, *Stahl und Eisen*, Vol. 111, No.3, 1991, pp. 67-70.
62. Ito, M., Yoshioka, M., Seino, Y., Suzuki, M., Sakuta, M., Maki, Y. and Kawabata, Y., Development of recycling system for sludge from the stainless steel nitric-hydrofluoric acid pickling process, *ISIJ International*, Vol. 37, No.4, 1997, pp. 391-398.
63. Lindblom, B., Samuelsson, C., Sandstrom, A. and Ye, G., Fine-particle characterization - An important recycling tool, *JOM*, December 2002, pp. 35-38.
64. Hahn, I. and and Neuschutz, D., Ejection of steel and slag droplets from gas stirred steel melts, *Ironmaking and Steelmaking*, Vol. 29, No.3, 2002, pp. 219-223.
65. Beukes, P., Cr^{6+} and the pyrometallurgical industry, *Pyrometallurgy: Current Issues and Future Trends*, Mintek, Randburg, South Africa, 2001.
66. Peckner, D. and Bernstein, I.M. (Edi.), *Handbook of Stainless Steel*, McGraw-Hill, USA, pp. 35-1-35-16.
67. Weast, R.C. and Astle, M.J. (eds), *CRC Handbook of Chemistry and Physics*, CRC Press, Boca Raton, Florida, USA, 1982, pp. B 87-B 89.
68. Barrera-Godinez, J.A., O'Keefe, T. J. and Watson, J.L., Effect of ultrasound on acidified brine leaching of double-kiln treated EAF dust, *Minerals Engineering*. Vol. 5, No. 10-12, 1992, pp. 1365-1373.
69. Wu, K., Yang, T. and Gudenau, H.W., Treatment of recycling fine dust formed in ironmaking and steelmaking processes with injecting method, *Iron and Steel*, Vol. 34, No. 12, 1999, pp. 60-66.
70. Jensen, J.T. and Wolf, K., Reduction of EAF dust emissions by injecting it into the furnace, *MPT International*, No. 3, 1997, pp. 58-62.

71. Evans, L.G. and Hogan, J.C., Recycling of EAF dust by direct injection, *Electric Furnace Conference Proceedings*, ISS, Dallas, 1985, pp. 367-372.
72. Gudenau, H.W., Stoesser, K., Denecke, H. and Schemann, V., Environmental aspects and recycling of filter dusts by direct injection or use of agglomerates in shaft furnaces, *ISIJ International*, Vol. 40, No.3, 2000, pp. 218-223.
73. Wang, M. and Cheng, W., EAF dust recycling into the furnace for slag foaming, *Journal of University of Science and Technology Beijing*, Vol. 23, No.1, 2001, pp. 15-17.
74. Zhao, Y. and Stanforth, R., Extraction of zinc from zinc ferrites by fusion with caustic soda, *Minerals Engineering*, Vol. 13, No.13, 2000, pp. 1417-1421.
75. Xia, D. K. and Pickles, C. A., Caustic roasting and leaching of electric arc furnace dust, *Canadian Metallurgical Quarterly*, No. 3, 1999, pp. 175-186.
76. Xia, D. K. and Pickles, C. A., Microwave caustic leaching of electric arc furnace dust, *Minerals Engineering*, No. 1, 2000, pp. 79-94.
77. Frenay, J., Ferlay, S. and Hissel, J., Zinc and lead recovery from EAF dusts by caustic soda process, *Electric Furnace Conference Proceedings*, ISS, Dallas, 1986, pp. 417-421.
78. Jarupisitthorn, C., Pimtong, T. and Lothongkum, G., Inverstigation of kinetics of zinc leaching from electric arc furnace dust by sodium hydroxide, *Materials Chemistry and Physics*, Vol. 77, 2002, pp. 531-535.
79. Zhao, Y. and Stanforth, R., Integrated hydrometallurgical process for production of zinc from electric arc furnace dust in alkaline medium, *Journal of Hazardous Materials*, Vol. 80B, 2000, pp. 223-240.
80. Leclerc, N., Meux, E. and Lecuire, J.M., Hydrometallurgical recovery of zinc and lead from electric arc furnace dust using mononitrilotriacetate anion and hexahydrated ferric chloride, *Journal of Hazardous Materials*, Vol. 91B, 2002, pp. 257-270.
81. Corsini, T., Treatment of EAF dust by a leachant process, *Steel Times*, No.10, 1994, p. 400.

82. Baik, D.S. and Fray, D.J., Recovery of zinc from electric-arc furnace dust by leaching with aqueous hydrochloric acid, plating of zinc and regeneration of electrolyte, *Trans. Instn Min. Metall.*, Vol. 109, No.9-12, 2000, pp. C121-127.
83. Antrekowitsch, J. and Antrekowitsch, H., Hydrometallurgically recovering zinc from electric arc furnace dusts, *JOM*, No.12, 2001, pp. 26-28.
84. Hilber, T., Marr, R., Siebenhofer, M. and Zapfel, W., Solid/liquid extraction of zinc from EAF-dust, *Separation Science and Technology*, Vol. 36, No.5-6, 2001, pp. 1323-1333.
85. Leclerc, N., Meux, E. and Lecuire, J.M., Hydrometallurgical extraction of zinc from zinc ferrites, *Hydrometallurgy*, Vol. 70, 2003, pp. 175-183.
86. Cruells, M., Roca, A. and Nunez, C., Electric Arc Furnace flue dusts: characterization and leaching with sulphuric acid, *Hydrometallurgy*, Vol.31, 1992, pp. 213-231.
87. Dreisinger, D.B., Peters, E. and Morgan, G., The hydrometallurgical treatment of carbon steel electric arc furnace dusts by the UBC-Chaparral process, *Hydrometallurgy*, Vol. 25, 1990, pp. 137-152.
88. Ghoreshy, M. and Pickles, C.A., Microwave processing of electric arc furnace dust, *Electric Furnace Conference Proceedings*, ISS, Nashville, 1994, pp. 187-196.
89. Palencia, I., Romero, R., Iglesias, N. and Carranza, F., Recycling EAF dust leaching residue to the furnace: a simulation study, *JOM*, No.8, 1999, pp. 28-32.
90. Unger, T.W., Waelz kiln recovery process for electric arc furnace dust, *Electric Furnace Conference Proceedings*, ISS, Dallas, 1986, pp. 413-415.
91. Thomas, S.S. and Clifton, E.D., Economic evaluation of the HTR process for treatment EAF dust, *Electric Furnace Conference Proceedings*, ISS, Chicago, 1987, pp.413-419.
92. Maczek, H. and Kola, R., Recovery of zinc and lead from electric-furnace steelmaking dust at Berzelius, *JOM*, January 1980, pp. 53-58.
93. Pargeter, J.K. and Lehmkuehler, H.J., Recycling of waste and flue dust from the steel industry into hot metal using the INMETCO process, *Steelmaking Conference Proceedings*, 1986, pp. 403-408.

94. Chapman, C.D. and Cowx, P.M., Treatment of EAF dust by the Tetronics plasma process, *Steel Times*, No. 6, 1991, pp. 301-304.

95. Schoukens, A.F.S., Abdelatif, M.A., Freeman, M.J. and Barcza, N.A., The Environplas process for the recovery of Zinc, Chromium and Nickel from steel-plant dust, *Electric Furnace Conference Proceedings*, Dallas, ISS, 1996, pp. 341-351.

96. Eriksson. S., Herlitz, H.G. and Santen, S.O., Operation experience with the plasmadust process, *Electric Furnace Conference Proceedings*, ISS, Dallas, 1986, pp. 425-429.

97. Guorgi, G.A., Lightfoot, B.W. and Short, W.E., Processing EAF dust with Ausmelt technology, *Steel Times*, No.12, 1993, pp. 520-521.

98. Pusateri, J.F., Chew, R. and Stanze, A.E., On-site treatment of EAF dust via the ST. Joe flame reactor, *Electric Furnace Conference Proceedings,* ISS, Dallas, 1986, pp. 397-401.

99. Hanewald, R.H. and Dombrowski, D.E., Recovery of metals from steel wastes and production of DRI by the INMETCO process, *Iron and Steel Engineer*, No. 3, 1985, pp. 62-67.

100. Hara, Y., Ishiwata, N., Itaya, H. and Matsumoto, T., Smelting reduction process with a coke packed bed for steelmaking dust recycling, *ISIJ International*, Vol. 40, No.3, 2000, pp. 231-237.

101. Yamada, S., Itaya, H. and Hara, Y., Simultaneous recovery of zinc and iron from electric arc furnace dust with a coke-packed bed smelting-reduction process, *Iron and Steel Engineer*, No.8, 1998, pp. 64-67.

102. Mantovani, M.C., Takano, C. and Buchler, P.M., Electric arc furnace dust-coal composite pellet: effects of pellet size, dust composition, and additives on swelling and zinc removal, *Ironmaking and Steelmaking,* Vol. 29, No.4, 2002, pp. 257-265.

103. Wang, J.C., Hepworth, M.T. and Reid, K.J., Recovering Zn, Pb, Cd and Fe from electric furnace dust, *JOM,* No.4, 1990, pp. 42-45.

104. Lee, J.J., Lin, C.I. and Chen, H.K., Carbothermal reduction of zinc ferrite, *Metallurgical and Materials Transactions B*, Vol. 32, No.12, 2001, pp. 1033-1040.

105. Lopez, F.A., Medina, F., Medina, J. and Palacios, M.A., process for recovery of non-ferrous metals from steel mill dusts involving pelletising and carbothermic reduction, *Ironmaking and Steelmaking*, Vol. 18, No. 4, 1991, pp. 292-295.
106. Mantovani, M.C. and Takano, C., The strength and the high temperature behaviors of self-reducing pellets containing EAF dust, *ISIJ International*, Vol. 40, No. 3, 2000, pp. 224-230.
107. Donald, J.R. and Pickles, C.A., Reduction of electric arc furnace dust with solid iron powder, *Canadian Metallurgical Quarterly*, Vol. 35, No. 3, 1996, pp. 255-267.
108. Gudenau, H.W., Lukat, B. and Stoesser, K., Recycling of agglomerated dusts of the iron and steel industry with embedded carbon, *Steel Research*, Vol. 69, No. 10+11, 1998, pp. 391-397.
109. Wu, L. and Themelis, N.J., The flash reduction of electric arc furnace dusts, *JOM*, No.1, 1992, pp. 35-39.
110. Matsuoka, T., Hurozu, S. and Koyabu, Y., New technology for treating electric arc furnace dust, *Iron and Steel Engineer,* No.2, 1991, pp. 37-40.
111. Nishioka, K., Maeda, T. and Shimizu, M., Dezincing behaviour from iron and steelmaking dusts by microwave heating, *ISIJ International,* Vol. 42, Supplement, 2002, pp. S19-S22.
112. Schaffner, B., Hoffelner, W., Sun, H. and Steinfeld, A., Recycling of hazardous solid waste material using high-temperature solar process heat: 1. Thermodynamic analysis, *Environ. Sci. Technol.,* Vol. 34, 2000, pp. 4177-4184.
113. Freeman, H.M.(Edi), *Standard Handbook of Hazardous Waste Treatment and Disposal* (2nd ed.), McGraw-Hill, New York, USA, 1997.
114. Zunkel, A. D. and Schmitt, R.J., Review of electric arc furnace dust treatment processes and environmental regulations, *Electric Furnace Conference Proceedings*, Orlando, ISS, 1995, pp. 147-158.
115. Stone, J.N., Treatment of electric furnace dust in combination with other wastes, *Electric Furnace Conference Proceedings*, ISS, Dallas, 1986, pp. 409-412.
116. Stone, J.N. and Marasco, G.F., Integrated treatment of wastes at Atlas Steels, *Iron Steel Eng.,* April 1986, pp. 43-47.

117. Jones, R.D., O'Donnell, F.J. and Buddemeyer, J., Transformation of EAF dust into commercial products, *Electric Furnace Conference Proceedings*, 1997, ISS, Chicago, pp. 583-588.

118. Gress, L., Recycling vitrification process for electric arc furnace dust, *Iron and Steel Engineer*, No.8, 1993, pp. 38-40.

119. Ek, R.B. and Schlobohm, J.E., Glassification of electric arc furnace dust, *Iron and Steel Engineer*, No.4, 1993, pp. 82-84.

120. Skvara, F., Kastanek, F., Pavelkova, I., Scolcova, O., Maleterova, Y. and Schneider, P., Solidification of waste steel foundry dust with Portland cement, *Journal of Hazardous Materials,* Vol. 89 B, 2002, pp. 67-81.

121. Pereira, C.F., Rodriguez-Pinero, M. and Vale, J., Solidification/stabilisation of electric arc furnace dust using coal fly ash: Analysis of the stabilisation process, *Journal of Hazardous Materials*, Vol. 82 B, 2001, pp. 183-195.

122. Ionescu, D., Meadowcroft, T.R. and Barr, P.V., Glassification of EAF dust: The limits for Fe_2O_3 and ZnO content and an assessment of leach performance, *Canadian Metallurgical Quarterly*, Vol. 36, No. 4, 1997, pp. 269-281.

123. Lopez, F.A., Sainz, E., Lopez-Delgado, A., Pascual, L. and Fernandez Navarro, J.M., The use of blast furnace slag and derived materials in the vitrification of electric arc furnace dust, *Metallurgical and Materials Transaction B*, Vol. 27, No.6, 1996, pp. 379-384.

124. Ay, N., Caki, N. and Kara, A. Ferrochromium fly ash used as a pigment in ceramic glaze, *Am. Cer. Soc. Bull.*, Vol. 73, No.12, 1994, pp. 47-48.

125. Webber, M.D., The potential for agricultural use of EAF dusts in Canada, *Environ. Technol. Lett.,* Vol. 8, No.3, 1987, pp. 113-120.

126. American Society for Testing and Materials, *Screening apparent specific gravity and bulk density of waste,* Method D 5057-90, ASTM, PA, USA.

127. American Society for Testing and Materials, *Screening of pH in waste*, Method D 4980-89, ASTM, PA, USA.

128. *NIST X-ray Photoelectron Spectroscopy Database Version 2.0*, US Secretary of Commerce, 1989.

129. Brasier, M.D., Green, O.R., Jephcoat, A.P., Kleppe, A.K., van Kranendonk, M.J., Lindsay, J.F., Steele, A. and Grassineau, N.V., Questioning the evidence for Earth's oldest fossils, *Nature*, Vol. 416, 7 March 2002, pp. 76-81.

130. Malezieux, J.M. and Piriou, B., Relation entre la composition chimique et le comportement vibrationnel de spinelles de synthese et de chromites naturelles en microspectrometrie Raman, *Bull. Mineral.*, Vol. 111, 1988, pp. 649-669.

131. National Institute of Advanced Industrial Science and Technology, *Database of Mineral Raman Spectra*, Nagoya, Japan.

132. Nyquist, R. A. and Kagel, R.O., *Infrared Spectra of Inorganic Compounds (3800-45cm^{-1})*, Academic Press, New York, 1973.

133. Nasdala, L., Witzke, T., Ulrich, B. and Brett, R., Gordaite [$Zn_4Na(OH)_6Cl.6H_2O$]: Second occurrence in the Juan de Fuca Ridge, and new data, *American Mineralogist*, Vol. 83, 1998, pp. 1111-1116.

134. Mikhail, S. A., Turcotte, A. M. and Aota, J., Thermoanalytical study of EAF dust and its vitrification product, *Thermochimica Acta*, Vol. 287, 1996, pp. 71-79.

135. Haugsrud, R., On the high-temperature oxidation of nickel, *Corrosion Science*, 45 (1), 2003, pp. 211-235.

136. Matsuno, M., Tomoda, K. and Nakamura, T., Volatilization mechanism of Pb from fly ash in municipal waste incinerator, *Materials Transactions*, 44 (12), 2003, pp. 2481-2488.

137. Chen, Y., Mori, S. and Pan, W.P., Studying the mechanisms of ignition of coal particles by TG-DTA, *Thermochimica Acta*, Vol. 275, 1996, pp. 149-158.

138. Bear, I.J., Grey, I.E., Newnham, I.E. and Rogers, L.J., The $ZnSO_4 \cdot 3Zn(OH)_2$-H_2O system. I. Phase formation, *Aust. J. Chem.*, Vol. 40, 1987, pp. 539-56.

139. Nyirenda, R.L. The processing of steelmaking flue-dust: A review, *Minerals Engineering*, Vol. 4, Nos 7-11, 1991, pp. 1003-1025.

140. Calder, L. M., Chromium contamination of groundwater, In: *Chromium in the Natural and Human Environments*, (ed. J.O. Nriagu and E. Nieboer), John Wiley & Sons, New York, 1988, pp. 215-229.

141. *FACT Sage 5.1*, Centre for Research in Computational Thermochemistry, Ecole Polytechnique, Montreal, Quebec, Canada, 2002.

142. Yang, Y., Xiao, Y. and Reuter, M. A., Analysis of transport phenomena in submerged arc furnace for ferrochrome production, *Tenth International Ferroalloys Congress*, Cape Town, South Africa, Feb. 2004, SAIMM, pp. 15-25.
143. Furimsky, E. and Zheng, L., Quantification of chlorine and alkali emissions from fluid bed combustion of coal by equilibrium calculations, *Fuel Processing Technology*, Vol. 81, 2003, pp. 7-21.
144. Wei, X., Schnell, U., Han, X. and Hein, K.R.G., Interactions of CO, HCl, and SOx in pulverized coal flames, *Fuel*, Vol. 83, 2004, pp. 1227-1233.
145. Gericke, W.A., Environmental aspects of ferrochrome production, *INFACON 7*, Trondheim, Norway, June 1995, pp. 131-140.
146. American Standards Tests for Materials, *Shake extraction of solid waste with water*, Method D 3987-85, ASTM, PA, USA.
147. Cohen, B., Lewis, A., Petersen, J., Von Blottnitz, H., Drews, S.C. and Mahote, S. I., The TCLP and its application for the characterisation of worst case leaching of wastes from mining and metallurgical operations, *Advances in Environmental Research*, Vol. 3, No. 2, 1999, pp. 152-165.
148. Levenspiel, O., *Chemical Reaction Engineering (3rd edition)*, John Wiley & Sons, New York, 1999, pp. 566-586.
149. US EPA, *Test methods for evaluating solid waste, physical/chemical method*, SW-846.
150. Jackson, E., *Hydrometallurgical Extraction and Reclamation*, John Wiley & Sons, New York, 1986, pp. 155-158.
151. Bartlett, R.J. and James, B.R., Mobility and bioavailability of chromium in soils, In: *Chromium in the Natural and Human Environments*, (ed. Nriagu, J.O. and Nieboer, E.), John Wiley & Sons, New York, 1988, pp. 267-304.
152. Hwang, I., Batchelor, B., Schlautman, M.A. and Wang, R., Effects of ferrous iron and molecular oxygen on chromium (VI) redox kinetics in the presence of aquifer solids, *Journal of Hazardous Materials*, Vol. 92B, 2002, pp. 143-159.
153. White, A.F. and Peterson, M., Reduction of aqueous transition metal species on the surfaces of Fe (II)-containing oxides, *Geochimica et Cosmochimica Acta*, Vol. 60, No.20, 1996, pp. 3799-3814.

154. Peterson, M.L., Brown, G.E., Parks, G.A. and Stein, C.L. Differential redox and sorption of Cr (III/VI) on natural silicate and oxide minerals: EXAFS and XANES results, *Geochimica et Cosmochimica Acta*, Vol. 61, No.16, 1997, pp. 3399-3412.

155. Zouboulis, A.I., Kydros, K.A. and Matis, K.A., Removal of hexavalent chromium anions from solutions by pyrite fines, *Water Research*, Vol. 29, No. 7, 1995, pp. 1755-1760.

156. Kiyak, B., Ozer, A., Altundogan, H.S., Erdem, M. and Tumen, F., Cr (VI) reduction in aqueous solutions solutions by using copper smelter slag, *Waste Management*, Vol. 19, 1999, pp. 333-338.

157. Hattori, M., Yaku, K. and Nagaya, K. Treatment of the sludge containing chromium and calcium by heating with silica, *Environmental Science and Technology*, Vol. 12, No.13, 1978, pp 1431-1434.

158. Pillay, K., von Blottnitz, H. and Petersen, J., Aging of chromium (III)-bearing slag and its relation to the atmospheric oxidation of solid chromium (III)-oxide in the presence of calcium oxide, *Chemosphere*, Vol. 52, 2003, pp. 1771-1779.

159. Schroeder, D.C. and Lee, G.F., Potential transformations of chromium in natural waters, *Water, Air and Soil Pollution*, Vol. 4, 1975, pp.355-36.

160. Lee, Y. and Nassaralla, C.L., Formation of hexavalent chromium by reaction between slag and magnesite-chrome refractory, *Metallurgical and Materials Transactions*, Vol. 29B, No.4, 1998, pp. 405-410.

161. Beszedits, S., Chromium removal from industrial wastewaters, In: Nriagu, J.O. and Nieboer, E., *Chromium in the Natural and Human Environments*, John Wiley & Sons, 1988, pp. 231- 265.

162. Huang D., Drummond, C.H., Wang, J. and Russell, D.B., Incorporation of chromium (III) and chromium (VI) oxides in a simulated basaltic, industrial waste glass-ceramic, *J. Am. Ceram. Soc.*, Vol. 87, No. 11, 2004, pp. 2047-2052.

163. Imai, A. and Gloyna, E.F., Effects of pH and oxidation state of chromium on the behaviour of chromium in the activated sludge process, *Water Research*, Vol. 24, No.9, pp. 1143-1150.

164. Ball, J.W. and Izbicki, J.A., Occurrence of hexavalent chromium in ground water in the western Mojave Desert, California, *Applied Geochemistry*, Vol. 19, 2004, pp. 1123-1135.

165. Johnson, S.M., Pask, J.A. and Moya, J.S., Influence of impurities on high-temperature reactions of kaolinite, *J. Am. Ceram. Soc.*, Vol. 65, No.1, 1982, pp. 31-35.

166. Brindley, G.W. and Nakahira, M., The Kaolinite-mullite reaction series: III, The high-temperature phases, *J. Am. Ceram. Soc.*, Vol. 42, No.7, 1959, pp 319-324.

167. Chakraborty, A.K., DTA study of preheated kaolinite in the mullite formation region, *Thermochimica Acta*, Vol. 398, 2003, pp 203-209.

168. Brindley, G.W. and Nakahira, M., The Kaolinite-mullite reaction series: II, Metakaolin, *J. Am. Ceram. Soc.*, Vol. 42, No.7, 1959, pp 314-318.

169. Guggenheim, S., Chang, Y.H., van Groos, A.F.K., Muscovite dehydroxylation: High-temperature studies, *American Mineralogist*, Vol. 72, 1987, pp 537-550.

170. James, B.R., Petura, J.C., Vitale, R.J. and Mussoline, G.R., Hexavalent chromium extraction from soils: A comparison of five methods, *Environ. Sci. Technol.*, Vol. 29, 1995, pp. 2377-2381.

171. Vitale, R.J. and Mussoline, G.R., Rinehimer, K.A., Petura, J.C. and James, B.R., Extraction of sparingly soluble chromate from soils: Evaluation of methods and Eh-pH effects, *Environ. Sci. Technol.*, Vol. 31, 1997, pp. 390-394.

172. Pettine, M. and Capri, S., Digestion treatments and risks of Cr(III)-Cr(VI) interconversions during Cr (VI) determination in soils and sediments- a review, *Analytica Chimica Acta*, Vol. 540, 2005, pp. 231-238.

173. Caplan, D. and Cohen, M., The volatilisation of chromium oxide, *Journal of the Electrochemical Society*, No. 5, 1961, pp. 438-442.

174. Stearns, C.A., Kohl, F.J. and Fryburg, G.C., Oxidative vaporization kinetics of Cr_2O_3 in oxygen from 1000^o to 1300^{o}C, *J. Electrochem. Soc.: Solid-State Science and Technology*, Vol. 121, No.7, 1974, pp. 945-951.

175. Fryburg, G.C., Kohl, F.J. and Stearns, C.A., Enhanced oxidative vaporization of Cr_2O_3 and chromium by oxygen atoms, *J. Electrochem. Soc.: Solid-State Science and Technology*, Vol. 121, No.7, 1974, pp. 952-959.

176. Pacyna, J.M. and Nriagu, J.O., Atmospheric emissions of chromium from natural and anthropogenic sources, In: Nriagu, J.O. and Nieboer, E., *Chromium in the Natural and Human Environments*, John Wiley & Sons, 1988, pp. 105-123.
177. Pacyna, J.M., Emission factors of atmospheric elements, In: Nriagu, J.O. and Davidson, C.I., *Toxic Metals in the Atmosphere*, John Wiley & Sons, 1988, pp. 1-32.
178. Abbas, Z., Steenari, B.M. and Lindqvist, O., A study of Cr (VI) in ashes from fluidised bed combustion of municipal solid waste: leaching, secondary reactions and the applicability of some speciation methods, *Waste Management*, Vol. 21, 2001, pp. 725-739.
179. Allan, M.L. and Kukacka, L.E., Blast furnace slag-modified grouts for *in situ* stabilization of chromium-contaminated soil, *Waste Management*, Vol. 15, No.3, 1995, pp. 193-202.
180. White, A.F. and Peterson, M.L., Reduction of aqueous transition metal species on the surface of Fe(II)-containing oxides, *Geochimica et Cosmochimica Acta*, Vol. 60, No. 20, 1996, 0pp. 3799-3814.
181. *STABCAL-W32*, Huang, H.H., Montana Tech., USA.
182. Lee, Y. and Nassaralla, C.L., Minimization of hexavalent chromium in magnesite-chrome refractory, *Metallurgical and Materials Transactions*, Vol. 28B, No.10, 1997, pp. 855-859.
183. Xu, H.B., Zhang, Y., Li, Z.H., Zheng, S.L., Wang, Z.K., Qi, T., Li H.Q., Development of a new cleaner production process for production chromic oxide from chromite ore, *Journal of Cleaner Production*, 2004, Article in Press.
184. Abadir, M.F., Gadalla, A.M. and El-Agamawi, Y.M., Equilibrium relationships in the system chromium-oxygen, *Transactions and Journal of the British Ceramic Society*, Vol. 75, No.4, 1976, pp. 74-76.
185. Sekiya, T. and Okuda, H., Growth of Cr_2O_3 crystals by the decomposition of a $K_2Cr_2O_7$ melt, *Journal of Crystal Growth*, Vol. 46, 1979, pp. 410-414.
186. Brittain, R.D., Lau, K.H. and Hildenbrand, D.L., Mechanism and thermodynamics of the vaporization of K_2CrO_4, *Journal of the Electrochemical Society: Solid-State Science and Technology*, No. 11, 1987, pp. 2900-2904.

187. Shin, H.S., Kim, I.T., Yoo, J.H., Shon, J.S., Kim, J.H. and Seo, Y.C., Leaching of glass components and surrogate nuclides from glassy waste forms for radioactive incineration ash, *Journal of Radioanalytical and Nuclear Chemistry*, Vol. 253, No.1, 2002, pp. 121-128.

188. Andres, A., Ortiz, I., Viguri, J.R. and Irabien, A., Long-term behaviour of toxic metals in stabilized steel foundry dusts, *Journal of Hazardous Materials*, Vol. 40, 1995, pp. 31-42.

189. Deutsches Institut fur Normun, *DIN 38414 (4)*, Berlin, Germany, 1984.

190. Dutre, V. and Vandecasteele, C., An evaluation of the solidification/stabilisation of industrial arsenic containing waste using extraction and semi-dynamic leach tests. *Waste Management*, Vol. 16, No. 7, 1996, pp. 625-631.

191. Cheng, K.Y. and Bishop, P.L., Leaching boundary movement in solidified/stabilized waste forms, *J. Air Waste Manage. Assoc.*, Vol. 42, No.2, 1992, pp. 164-168.

192. De Groot, G.J. and van der Sloot, H. A., Determination of leaching characteristics of waste materials leading to environmental product certification, In: *Stabilisation and Solidification of Hazardous, Radioactive and Mixed Wastes*, Gillian, T.M. and Wiles, C.C. (eds), American Society for Testing and Materials, Philadelphia, 1992, pp. 149-169.

193. Cote, P.L., Constable, T.W. and Moreira, A., An evaluation of cement-based waste forms using the results of approximately two years of dynamic leaching, *Nuclear and Chemical Waste Management*, Vol. 7, pp 129-139.

194. Cote, P.L. and Isabel, D., Application of a dynamic leaching test to solidified hazardous wastes, In: *Hazardous and Industrial Waste Management and Testing*, L.P. Jackson. A.R. Rohlik and R.A. Conway (eds), American Society for Testing and Materials, Philadelphia, 1983, pp. 49-60.

195. Kim, I.T., Kim, J.H., Lee, K.S., Seo, Y.C. and Koo, J.K., Leaching characteristics of glassy waste forms containing two different incineration ashes, *Waste Management*, Vol. 20, 2000, pp. 409-416.

196. Geankoplis, C.J., *Mass Transport Phenomena*, Holt, Rinehart and Winston, Inc., New York, 1972, pp. 143-192.

197. Dean J.A., *Lange's Handbook of Chemistry*, New York, MaGraw-Hill, 1985.

198. Clark, R.P., Blucher, R.L. and Goldsmith, H.J., Phase diagram of the system LiCl-KCl-$CaCrO_4$, *Journal of Chemical and Engineering*, Vol. 14, No.4, 1969, pp. 465-470.

Appendix I Cr (VI) and total chromium determination using spectrophotometer

I.1 Cr (VI) determination

I.1.1 Reagents

I.1.1.1 Colour reagent

Dissolve 0.4 g s-diphenyl carbazide (AR) in 100 ml 95% ethanol. Add 120 ml 85% phosphoric acid and dilute to 500 ml using distilled water.

I.1.1.2 Standard Cr (VI) solution

Dissolve 0.1414g $K_2Cr_2O_7$ in 1 l distilled water. Use different dilutions to prepare the calibration curve.

I.1.2 Determination procedure

I.1.2.1 Sample handing

The leaching mixture were shaken and filtered before a representative leachate sample is taken. The pH of the solution must be acidic (pH< 2) for the colour compound to form.

I.1.2.2 Prepare standards and calibration curves

Prepare two sets of standards (7 standards per set), ranging from 0.5 to 10mg/l (standard set 1) and from 0.02 to 0.5 mg/l (standard set 2) in 100 ml volumetric flasks. Transfer 5 ml standards solution for standard set 1 and 20 ml standards solution for standard set 2 into 25ml volumetric flasks, and pipette 3 ml of colour reagent and add distilled water to the mark. Set the solutions 20 minutes for the colour development of the mixture. Prepare a blank solution as the methods of standards just without the Cr (VI) solution. Prepare a calibration curve for the two different sets of standards at 542 nm.

I.1.2.3 Cr(VI) concentration determination

Transfer 5 ml leachate sample into 25ml volumetric flask, add 3 ml of colour reagent, and add distilled water to mark, set 20 minutes. Prepare a blank solution in exactly the same

as the leachate sample without adding 5 ml of the leachate sample. Use the calibration curve to determine the Cr (VI) concentration in the unknown sample. If the Cr (VI) concentration is higher than that in the calibration curve, the leachate sample was diluted and the Cr (VI) concentration is measured again. If the Cr (VI) concentration is lower than that in the calibration curve, prepare the sample as the lower concentrations calibration curve (standard set 2) as the following procedure: Transfer 20 ml leachate sample into 25ml volumetric flask, add 3 ml of colour reagent, and add distilled water to mark, set 20 minutes. Prepare a blank solution in exactly the same as the leachate sample without adding 20 ml of the leachate sample.

I.2 Total Cr concentration determination

I.2.1 Regents

I.2.1.1 H_2SO_4 and H_3PO_4 solution (V/V=1:1)

I.2.1.2 $KMnO_4$ solution (0.4%)

I.2.1.3 Urea solution (20%)

I.1.2.4 Sodium nitrite solution (2%)

I.1.2.5 Colour reagent and stock Cr (VI) standards solution (as I.1)

I.2.2. Analytical procedure

I.2.2.1 Standards preparation

Transfer 20ml standards solution for standards set of 0.02~0.5mg/l and 5ml for standards set of 0.5~15mg/l into 150ml flask and adjust pH value (approximately 7) by NH_3OH or H_2SO_4, then add 0.5ml H_2SO_4 and 0.5ml H_3PO_4 and shake. Add 4 drops $KMnO_4$ solution into the solution, if the purple in the solution disappear soon. Add it again to keep the purple. Vaporise the solution to 20ml.

Cool the solution down to room temperature and add 1ml urea solution. Pipette the sodium nitrite solution into the solution until the purple colour disappears. Transfer the solution to 50ml volumetric flask and dilute up to mark, and add 3 ml colour reagent, give 15 min to develop colour, use the absorption value to develop a calibration curve.

I.2.2.2 Concentration determination

The procedure is exactly same with that in I.2.2.1 only change the standards solution into the leachate samples.

Appendix II Thermal characteristics of clays

The thermal characteristics of the clays are shown in Figure II.1 a-c, in which the weight loss (TG), differential weight loss (DTG) and differential thermal analysis (DTA) of the clays, when they are heated from room temperature up to 1300°C, are reported.

Figure II.1a shows the continuous weight loss of the clay from room temperature to approximately 900°C. The initial weight loss of the clay is mostly due to the vaporisation of the hygroscopic water in the samples (an endothermic peak at about 70°C on the DTA curve). The dehydroxylation of kaolinite at 540°C to metakaolinite, contributes to most of the weight loss (about 4%): which is associated with an endothermic peak,

$$Al_2Si_2O_5(OH)_4\ (s) \rightarrow Al_2Si_2O_7\ (s) + 2H_2O\ (g) \qquad (II.1)$$

The DTA curve shows that there are several exothermic peaks at 960 °C, 980 °C, 1010 °C and 1110°C, although the weight of the sample remains stable above 900°C. According to Johnson et al. and Brindley et al., it is associated with the mullitisation of the metakaolinite [165,166], which can be expressed as:

$$3Al_2Si_2O_7\ (s) \rightarrow Al_6Si_2O_{13}\ (s) + 4SiO_2\ (s) \qquad (II.2)$$

XRD analysis of the residue from the thermal experiments confirms the presence of mullite (Figure II.2). Figure II.2 also shows that cristobalite present in the residue, which is related to the polymorphic transformation of quartz during heating.

Figure II.1b shows the thermal characteristics of clay MR from room temperature to 1300 °C. The DTG curve shows that four weight loss peaks exist at approximately 75, 290, 520 and 580 °C. It is owing to the loss of absorbed water, dehydration of muscovite and dehydration of kaolinite, respectively [167-169]. The DTA curve also shows that the exothermic peaks about 980 °C and 1110°C which are associated with the mullitisation of the kaolinite in the sample.

Figure II.1c shows the same tendency with clay AS. It shows the vaporisation of the absorbed water (at 90°C), dehydration of muscovite, dehydration of kaolinite (at 570°C), and the mullitisation of the sample at approximately 1000°C and 1110°C.

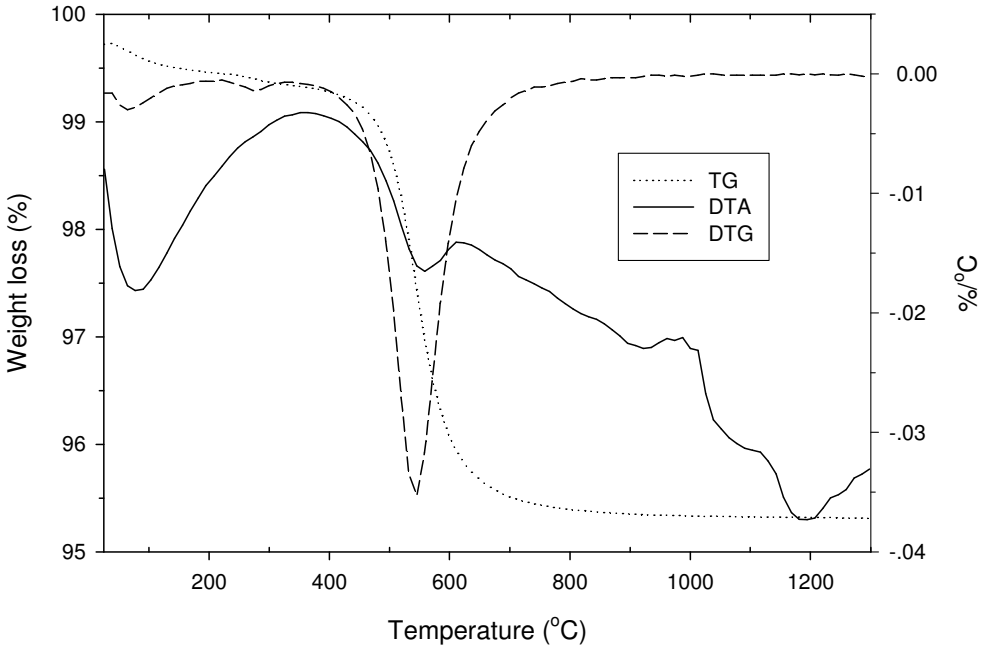

(a)AS

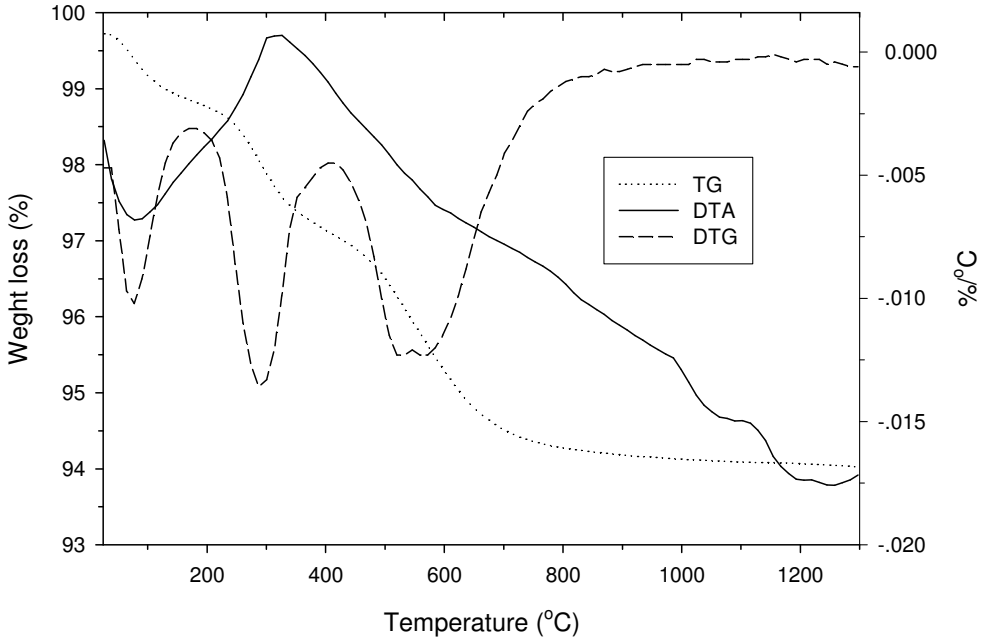

(b)MR

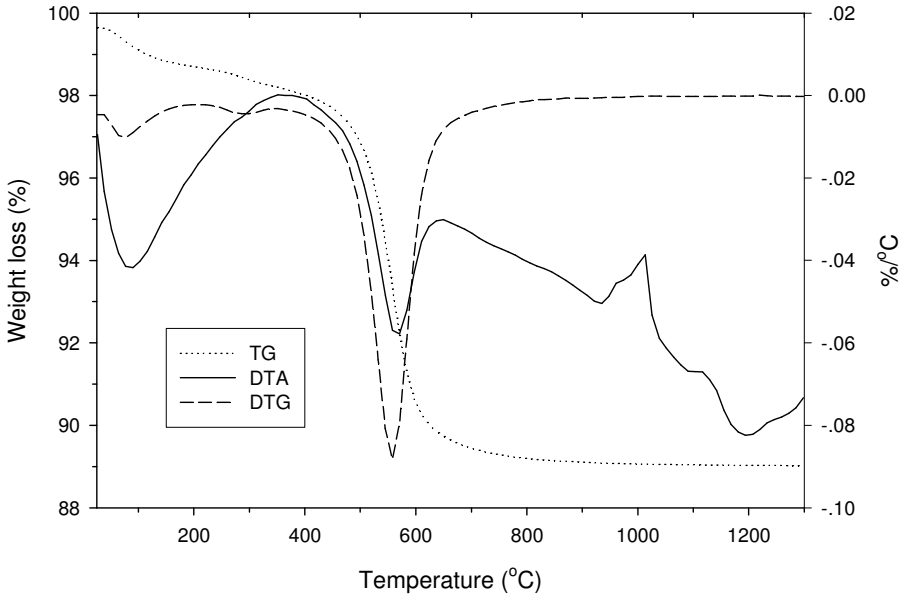

(c)AC

Figure II.1. The thermal characteristics of the clays (a)AS, (b)MR and (c)AC

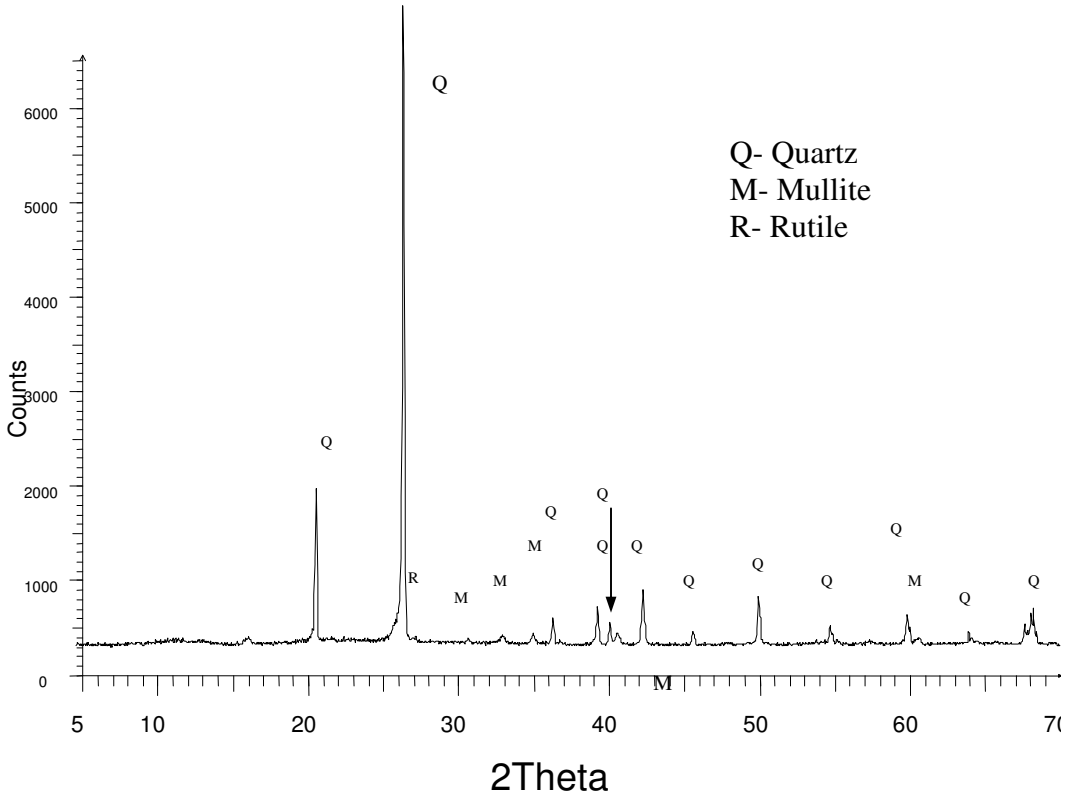

Figure II.2. XRD pattern of the residue of TG/DTA experiment (AS)

Appendix III Mass balance of the sintered brick

Table III.1 Mass balance of the synthetic sample
(AS spiked with 0.0636gCrO_3, 1200^oC and 5 hours)

%	AS	AS+CrO_3 (calculated)	Brick (analysed)
SiO_2	80.68	80.68	82.82
TiO_2	0.78	0.78	0.81
Al_2O_3	12.20	12.20	12.68
Fe_2O_3	0.99	0.99	1.08
MnO	0.02	0.02	0.00
MgO	0.06	0.06	0.02
CaO	0.00	0.00	0.00
Na_2O	0.06	0.06	0.03
K_2O	0.87	0.87	0.9
P_2O_5	Nd	Nd	0.02
Cr_2O_3	0.02	**0.117**	**0.095**
NiO	Nd	Nd	0.00
V_2O_5	Nd	Nd	0.01
PbO	Nd	Nd	0.002
LOI	3.84	3.84	0.03
Total	99.45	99.55	98.50

Table III.2 Mass balance of the sintered 50%AS-50%SPD (1100°C and 5 hours)

%	SPD	AS	50%AS-50%SPD (calculated)	Brick (analysed)
SiO_2	4.81	80.68	43.04	43.53
TiO_2	0.08	0.78	0.43	0.49
Al_2O_3	0.40	12.20	6.34	7.17
Fe_2O_3	43.4	0.99	24.52	23.96
MnO	5.08	0.02	2.59	2.73
MgO	5.44	0.06	2.79	2.28
CaO	12.9	0.00	6.55	6.12
Na_2O	0.60	0.06	Nd	Nd
K_2O	0.97	0.87	0.93	0.73
P_2O_5	0.04	Nd	Nd	Nd
Cr_2O_3	14.6	0.02	**7.42**	**7.86**
NiO	2.79	Nd	1.42	1.80
V_2O_5	0.09	Nd	Nd	0.06
ZnO	4.49	Nd	2.28	2.14
MoO_3	1.35	Nd	Nd	Nd
PbO	0.39	Nd	Nd	0.06
LOI	-0.21	3.84	1.82	0.07
Total	98.55	99.45	100.13	99.01

Table III.3 Mass balances of the sintered bricks that contained 50%AS and 50% ferrochrome dust or filter cake (1000°C and 5 hours)

%	50AS+50FCD1 (calculated)	Brick (analysed)	50AS+50FCD2 (calculated)	Brick (analysed)	50AS+50FC** (calculated)	Brick (analysed)
SiO_2	57.59	61.14	60.69	63.08	41.41	47.03
TiO_2	0.44	0.47	0.43	0.46	0.42	0.48
Al_2O_3	8.55	8.84	8.09	8.52	6.44	7.35
Fe_2O_3	1.86	1.91	1.60	1.67	10.28	11.28
MnO	0.22	0.21	0.27	0.28	0.49	0.64
MgO	5.76	6.03	9.56	9.97	0.62	0.46
CaO	0.25	0.25	0.19	0.14	19.38	22.92
Na_2O	4.96	4.18	3.29	2.26	0.20	0.26
K_2O	1.71	2.57	2.39	2.93	0.45	0.50
P_2O_5	0.01	0.02	0.01	0.02	0.02	0.04
Cr_2O_3	**1.59**	**1.67**	**1.72**	**1.80**	**1.55**	**1.70**
NiO	0.01	0.01	0.01	0.01	0.73	0.80
V_2O_5	0.01	0.02	0.01	0.02	0.01	0.02
ZnO	7.30	7.99	4.78	4.65	0.20	0.12
Cl*	1.60	0.84	0.47	0.03	0.03	0.01
SO_3*	1.63	3.98	1.18	0.88	3.55	1.6
F*	0.39	0.29	0.02	0.01	11.01	10.54
LOI	5.98	1.60	5.16	0.95	8.87	3.54
Total	99.86	102.2	99.87	97.68	105.66	109.29

: Elements that are indicated with an "" should be considered semi-quantitative;
**: It is assumed that calcium in the filter cake is present as CaF_2, the total content of the filter cake is therefore not calculated using 113.49% but 102.18% (Table 3.2).

Appendix IV Calculations on the acceptable Cr (VI) concentration in the leachate

Due to the fact that the stainless steel plant can generate approximately 2,000 t stainless steel dust monthly, the total amount of bricks that can be produced by mixing stainless steel plant dust and clay would amount to $\frac{2\times10^8}{R_{SPD}}$ (kg/month) by assuming that all the stainless steel dust are treated, where R_{spd} is the ratio of stainless steel plant dust in the brick (%).

Since the mass of one sintered brick is approximately 125 grams and it has a dimension of approximately 28mm×20mm×100mm, the surface area of one sintered brick can be calculated as:

Surface area (m^2) = $2\times(28\times20+20\times100+28\times100)\times10^{-6}$

= 0.01072 m^2

The quantity of the stabilised stainless steel plant dust bricks which can be made from these wastes is $\frac{2\times10^8}{R_{SPD}*0.125}$.

Thus the total surface area of these bricks is:

Total surface area (ha/month) = $0.01072\times10^{-4}\times\frac{2\times10^8}{R_{SPD}*0.125}$ (ha/month)

Furthermore, the amount of Cr (VI) in one sintered brick can be calculated as:

The amount of Cr (VI) in one sintered brick (mg)

$$=C_{Cr\,(VI)}\times\frac{\text{volume of the leachate (l)}}{\text{mass of the sintered brick in one leaching test (kg)}}\times\text{mass of one brick (kg)}$$

$$=C_{Cr\,(VI)}\,(\text{mg/l})\times\frac{0.8\,\text{l}}{0.04\,\text{kg}}\times0.125\text{kg}$$

Where $C_{Cr\,(VI)}$ is the Cr (VI) concentration in the leachate (mg/l).

Assuming that the total area of the dumping site is the same as the total surface area of the bricks, the total amount of Cr (VI) on this site per month would be:

Total Cr (VI) load on the dumping site (mg/month)

$$= C_{Cr(VI)} \times \frac{0.8}{0.04} \times 0.125 \times \frac{2\times10^{8}}{R_{SPD} * 0.125}$$

Then the EEC value can be calculated using the following function [15]:

EEC (ppb) = dose (g/ha/month) × 0.66[1)]

$$= [C_{Cr(VI)} \times \frac{0.8}{0.04} \times 0.125 \times 10^{-3} \times \frac{2\times10^{8}}{R_{SPD} * 0.125}] \Big/ [0.01072 \times 10^{-4} \times \frac{2\times10^{8}}{R_{SPD} * 0.125}] \times 0.66$$

$$= 1539.2\ C_{Cr(VI)}\ (ppb)$$

The stainless steel plant dust containing bricks can only be used when the EEC is lower than 0.02 ppm (20ppb). Therefore,

EEC (ppb) = 1539.2 $C_{Cr(VI)}$ < 20 ppb

That is, the Cr (VI) concentration in the leachate ($C_{Cr(VI)}$) should be less than 0.013 mg/l.

[1)] 0.66 is calculated from the ratio of the toxic substance in a weight of underground body of water [15].

Appendix V The production process of synthetic calcium chromate

The process whereby $CaCrO_4$ was prepared is similar to that described by Clark et al. [198]. 30 g of lime (AR grade) was slowly added into 59.6 ml hydrochloric acid (AR grade, 32% and 1.15g/ml) with vigorous stirring using a glass rod. The solution was heated to boil. 100 ml Na_2CrO_4 solution which was made by dissolving 70.2 g $Na_2CrO_4 \cdot 2H_2O$ in distilled water (approximately 3 mol/l) was then added in the solution slowly with vigorous stirring. The mixture was stirred for about 1 hour. The obtained precipitate was washed with boiling water 6 times and filtered using filter paper. It was then dried at 110°C for 18 hours, after which it was heated to 400°C for 2 hours. The powder product was examined using XRD. The XRD pattern confirmed that the product is calcium chromate (Figure V.1).

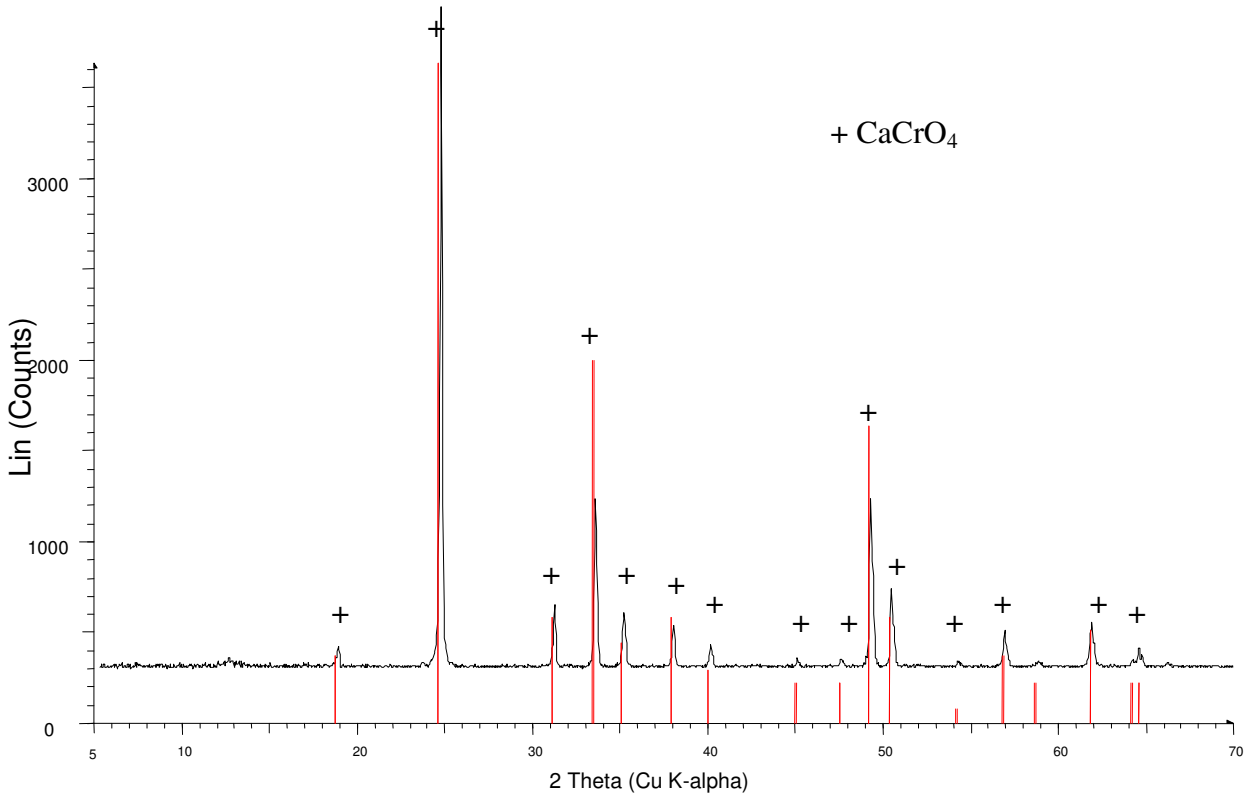

Figure V.1 The XRD pattern of calcium chromate

Appendix VI Details of experiments on leaching behaviour of chromium from the stabilised wastes

Table VI.1 Average experimental values for the concentrations of Cr (VI) and Cr (T) in the leachate

Cumulative leach time (h)	Cr (VI) (mg/l)					Cr (T) (mg/l)				
	M1	**M2**	**M3**	**M4**	**M5**	**M1**	**M2**	**M3**	**M4**	**M5**
1	0.275	0.025	0.004	0.052	0.144	0.275	0.026	0.007	0.055	0.144
9	0.581	0.115	0.014	0.108	0.505	0.583	0.120	0.006	0.112	0.496
25	0.361	0.171	0.014	0.058	0.441	0.371	0.179	0.007	0.057	0.492
49	0.157	0.090	0.007	0.013	0.571	0.155	0.085	0.006	0.008	0.579
81	0.049	0.026	0	0.001	0.522	0.047	0.026	0	0	0.538
121	0.027	0.006	0	0	0.419	0.015	0.037	0	0	0.521
169	0.030	0.002	0.006	0.003	0.474	0.046	0.013	0.014	0.013	0.472
225	0.009	0	0	0	0.403	0.043	0.027	0.028	0.047	0.418
289	0.009	0	0	0	0.427	0.019	0	0	0.012	0.329
361	0.035	0.025	0.008	0.008	0.398	0.026	0	0.008	0.002	0.407
441	0.015	0	0.001	0	0.4	0.017	0	0.002	0	0.419
529	0.013	0.001	0.002	0	0.389	0.021	0.001	0.007	0	0.376
625	nd	nd	nd	nd	0.365	nd	nd	nd	nd	0.367
729	0.035	0.016	0	0.002	0.317	0.038	0.004	0.002	0.008	0.309
961	0.031	0.001	0	0	0.452	0.030	0.022	0	0	0.442
1225	nd	nd	nd	nd	0.305	nd	nd	nd	nd	0.300
1521	0.045	0.002	0.002	0	0.17	0.042	0	0	0	0.199
1849	0.037	0.006	0.003	0.005	0.068	0.018	0	0.001	0	0.062
2209	0.025	0	0.002	0	0.037	0.032	0	0	0	0.047
2601	0.042	0.003	0.002	0	nd	0.048	0.006	0.001	0.001	nd
3025	0.037	0	0.004	0.003	nd	0.041	0.023	0	0	nd
3481	0.053	0.007	0.009	0.007	nd	0.040	0.012	0.006	0.005	nd

Note:nd-not determined.

Experimental conditions:

Mass of the sample: ~ 40g

Shape of the sample: Cylinder (Φ25mm×40±0.36mm)

Furnace: Muffle furnace

Sinter temperature: 1100^{o}C for 50%SPD+50%AS (M1) and 50%SPD+50%MR (M2), 1000^{o}C for 20%FCD1+80%AS (M3), 20%FCD2+80%AS (M4) and 20%FC+80%AS (M5)

Sinter time: 5 hours

Heating rate: ~4^{o}C/min

Cooling rate: ~1.6^{o}C/min

Leaching temperature: 25^{o}C